LUND UNIVERSITY

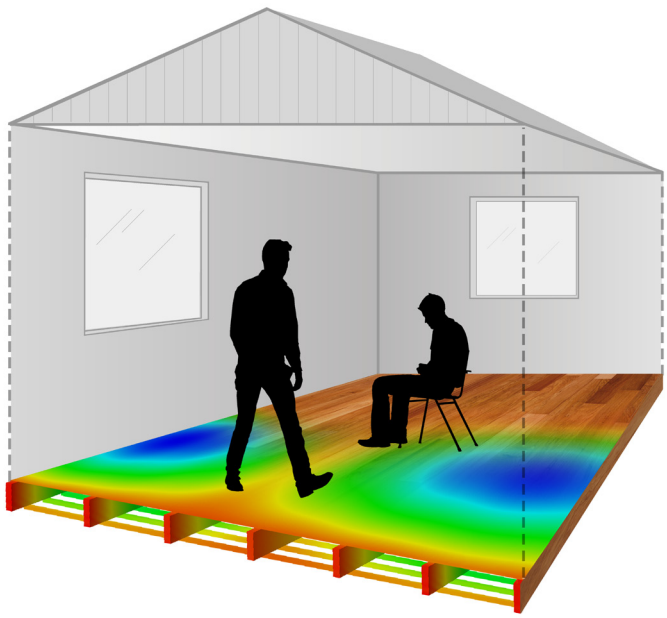

VIBROACOUSTIC PERFORMANCE OF WOODEN BUILDINGS
Prediction and Perception

JUAN NEGREIRA

Engineering Acoustics

Doctoral Thesis

DEPARTMENT OF CONSTRUCTION SCIENCES

DIVISION OF ENGINEERING ACOUSTICS

ISRN LUTVDG/TVBA--16/1013--SE (1-280) | ISSN 0281-8477

ISBN 978-91-7623-642-0 (print) | ISBN 978-91-7623-643-7 (pdf)

DOCTORAL THESIS

VIBROACOUSTIC PERFORMANCE OF WOODEN BUILDINGS

Prediction and Perception

JUAN NEGREIRA

Online version available at: http://bit.ly/1UYMLhp

Printed by Media-Tryck LU, Lund, Sweden, May 2016 *(Pl)*.

For information, address:

Division of Engineering Acoustics,
Faculty of Engineering LTH, Lund University, Box 118, SE-221 00 Lund, Sweden.

Homepage: www.akustik.lth.se

Acknowledgements

The work presented in this PhD thesis was carried out at the Department of Construction Sciences of Lund University (Division of Engineering Acoustics), with Dr. Delphine Bard as my main supervisor, and Professor Per-Erik Austrell as my co-supervisor. The research reported on here was funded by the *Silent Spaces* project, a part of the EU program Interreg IV-A, by the Vinnova and Formas project *AkuLite* and by the WoodWisdom-Net project *Silent Timber Build*. The author highly appreciates the financial support provided. The simulations carried out in the frame of the PhD project were performed on resources provided by the Swedish National Infrastructure for Computing (SNIC) at Lunarc, which is also acknowledged.

First, I would like to thank my supervisor Dr. Delphine Bard for her continuous support and encouragement. Likewise, I am grateful to Professor Göran Sandberg for giving me the opportunity to join the department as a master thesis student back in 2010. I am also pleased to extend my greetings to all my colleagues at the Department of Construction Sciences for the nice moments spent together during *fika* breaks. Amongst all, my officemates and friends Peter Persson and Ola Flodén are especially acknowledged (thank you guys, without you I would have probably finished the PhD much earlier, but the journey would not have been as pleasant). Mr. Bo Zadig is also acknowledged for his invaluable help with the design of certain pictures included in the thesis. A word of thanks to my co-authors Arnaud Trollé, for nice talks, his very hard work and inestimable aid in matters related to statistics; and Anders Sjöström, for his help in general and with measurement related issues in particular. I would also like to express my gratitude to Håkan Hansson, my *skånska* teacher during my PhD project.

My time is Sweden has been filled not just with knowledge but also with unforgettable experiences. However, living abroad is not always easy. Ups and downs kick in more frequently due to the closest ones being far away. These difficulties would never be possible to overcome without my family and my mates. Thanks so much to my Swedish family of friends, who have always been understanding and supportive, at the same time as sharing daily experiences here with me. Likewise, my friends from back home have also kept me going straight when needed. I am deeply grateful to my *brother* Alberto, for having walked all this way with me.

Deserving of special mention are my parents Juan and Mariluz, for their endless love, patience, support and understanding throughout all my life. They have always unconditionally stood behind the cause. Nothing would be as it is if they didn't encourage me to fight for what I am capable of, plus a little bit extra.

Juan Negreira
Lund, April 2016

Abstract

When the Swedish building regulations in 1994 allowed wooden multi-storey buildings to be built, this type of lightweight construction became popular due to its low cost and ease of construction, as well as wood being a plentiful resource in Sweden. However, complaints amid inhabitants are often reported due to nuisances caused by disturbing vibrations and noise propagating in the building. Still in 2016, no vibration limits are given in any international standard due the complexity involved. Certain guidelines and guide values have simply been suggested instead. The vibrational response of wooden buildings has therefore become an issue to be tackled during their design phase. Accordingly, the aims of the research presented in this thesis can be divided into two basic categories: (i) development of prediction tools for the verification of vibratory and acoustic performance before a building is constructed and (ii) the development of indicators of human exposure to floor vibrations.

As of today, there still exist no accurate and reliable methods for predicting the vibroacoustic performance of wooden buildings. Product development is carried out on an empirical basis, involving both observations and the experience of engineers. Time and costs could be reduced by addressing issues of vibration during the design phase, for instance by using numerical methods (e.g. finite element simulations) as prediction tools; since experiments on prototypes and existing buildings are both time consuming and expensive. Development of such accurate finite element prediction tools is the major objective of the research dealt with in this work. In line with this, finite element models of a prefabricated timber volume element based building were created in the investigations presented, and specifically the flanking transmission occurring was analysed. On the basis of the conclusions drawn in that study, other investigations aiming at improving the accuracy of numerical prediction tools were performed. Thus, the question of whether or not air and insulation in cavities of multi-storey wooden buildings affect the transmission of structural vibrations was investigated. The conclusions showed that acoustic media must be considered when predicting low frequency vibroacoustic behaviour of such buildings by use of numerical models. Likewise, a method for extracting the properties of elastomers, frequently used in timber buildings at the junctions as a vibration-reduction measure, was also developed in order to have reliable assessments of the material properties involved as input for the finite element models employed. This was done through performing analytical calculations, and carrying out finite element simulations and mechanical testing in a uni-axial testing machine. Moreover, modelling guidelines on how to model different types of beam-plate connections (both glued and unglued together with screws) when creating predictive models, are presented. The guidelines were drawn by comparing measurements to their calibrated numerical models. In addition, a time-efficient frequency domain method to implement the tapping machine into predictive models of impact sound insulation, is presented.

Regarding the perception part of the thesis, the investigations performed aimed at supplementing the lack of existing studies addressing human response to floor vibrations. In order to obtain a better estimate of an acceptable level of vibrations in dwellings, measurements on real floors while people walked on the them, as well as when they sat down while another person was walking, were performed. The accelerations, velocities and deflections they were exposed to during the test were measured. Indicators of human response to vibrations were extracted by determining relationships between people's answers to questionnaires about their perception and experience of the vibrations, and different parameters as determined by measurements. Several indicators were found to describe people's answers to questions both regarding vibration annoyance and vibration acceptability.

The measurements performed in the thesis were carried out using transducers developed and calibrated in-house within the frame of the project; all the construction processes, calibrations, accuracy and justification of their use to the applications dealt with here, are also thoroughly described in the thesis.

In summary, adequate knowledge of the vibrational performance of wooden buildings such as that obtained here by use of measurements and of finite element simulations is seen as paving the way for further development in this area. The conclusions drawn in the thesis will ultimately entail time and cost savings for the industry as well as help dwellers to feel more comfortable in their homes.

Keywords: Prediction tools; Low frequency vibrations; Vibroacoustics; Wooden buildings; Impact sound insulation; Finite element method; Vibration measurements; Flanking transmission; Elastomers; Design indicators; Vibration acceptability; Vibration annoyance; MEMS accelerometers.

Populärvetenskaplig sammanfattning

Fram till 1994 var det förbjudet att bygga flervåningshus i trä i Sverige på grund av ett stort antal stadsbränder under 1800-talet. Efter att förbudet lyftes har dessa byggnader stadigt ökat i popularitet. På grund av sin låga vikt är dessa hustyper känsligare för störande buller och vibrationer jämfört med mer traditionella typer såsom betonghus. Att uppnå akustisk komfort i flervåningshus i trä är det långsiktiga målet med forskningen som presenteras i avhandlingen.

Undersökningar har utförts med målet att utveckla indikatorer på människors uppfattning av golvvibrationer. I en serie tester fick personer gå på träbjälklag och genom frågeformulär beskriva hur de upplevde vibrationerna. Samtidigt utfördes mätningar av vibrationerna i bjälklagen. Testpersonerna fick även sitta på en stol när andra personer gick på bjälklagen och beskriva hur de upplevde vibrationerna. Genom statistiska jämförelser mellan svaren i frågeformulären och resultaten från vibrationsmätningarna togs indikatorer fram som beskriver människors uppfattning av golvvibrationer. Sådana indikatorer kan användas till att analysera huruvida ett träbjälklag kan betraktas som tillfredsställande eller ej med hänsyn till vibrationer.

Metoder för uppskattning av vibrationsnivåer har också behandlats i avhandlingen. Det finns flera faktorer som bidrar till att det är svårt att göra sådana uppskattningar. Exempelvis har trä som material stora variationer i sina materialegenskaper. Dessutom är det komplicerat att beskriva beteendet för kopplingar och infästningar i byggnaderna. I avhandlingen har riktlinjer tagits fram för hur man med hjälp av datorberäkningar kan uppskatta vibrationsnivåer i flervåningshus i trä. Detta gjordes genom att kalibrera datormodeller med mätningar. Med riktlinjerna kan man i ett tidigt skede i konstruktionsfasen minska risken för störande vibrationer och buller. Dessutom innebär användandet av sådana verktyg tids- och kostnadsbesparingar för industrin eftersom det undviker behovet av att bygga fysiska modeller och testbyggnader.

Slutsatserna som beskrivs i avhandlingen bidrar till möjligheterna att konstruera flervåningshus i trä med en bättre ljudmiljö än idag. Slutsatserna i avhandlingen kan även ligga till grund för förbättringar av nuvarande byggstandarder och tillgängliga utvärderingsmetoder för att dessa ska korrelera bättre med hur människor uppfattar ljud och vibrationer.

Popular abstract

Wooden multi-storey buildings have steadily increased their market share in Sweden since 1994, the year in which their construction was reintroduced after a century-old-ban (due to numerous urban fires during the 1800s) was lifted. However, there are unfortunately few examples of acoustically successful multi-storey wooden buildings due to noise and disturbing vibrations. To enable vibroacoustic comfort for dwellers is the main aim of this thesis.

Investigations on how people perceive vibrations were carried out to establish design indicators of human response to floor vibrations. To that end, psycho-vibratory tests were performed in a laboratory. People were asked to either walk on floors or be seated in a chair while the test leader was walking on it. Measurements of the vibrations they produced were recorded during the test. After the experiment, the test subjects were given a questionnaire where they described their perception and experiencing of the vibrations. By statistically analysing the vibratory measurements and the responses obtained in the questionnaires, design indicators for vibration acceptability and vibration annoyance were developed so that newly manufactured floors can be regarded as satisfactory.

In addition, matters of vibration prediction were dealt with in the thesis. Unlike for concrete buildings, where the vibroacoustic performance can be predicted through the use of e.g. computer models, prediction tools for wooden multi-storey buildings are still lacking. The variability of a natural material such as wood, the complexity of the junctions between structural parts and external factors such as workmanship, makes it difficult to accurately predict vibroacoustic performance. In the thesis, guidelines on how to set up numerical prediction tools are given. The latter was done by calibrating numerical models with measurements. In this way, simplified but accurate prediction tools can be created. Such tools can, during the design phase of the construction, ensure that acoustic comfort is met once the building is constructed as well as predict the influence of structural modifications. The development of such prediction tools will entail time and cost savings for the building industry, because it avoids the need of mock-ups and test buildings.

All together, the conclusions drawn in the thesis pave the way towards vibroacoustic comfort to be met in wooden framed buildings. As a result, improvements to the existing building standards and evaluation methods, which correlate better with how humans perceive sound and vibrations, can be proposed.

Contents

Paper C
Characterisation of an elastomer for noise and vibration insulation in lightweight timber buildings.
J. Negreira, P-E. Austrell, O. Flodén, D. Bard.
Building Acoustics, 21(4): 251–276, 2014.

Paper D
Low frequency vibroacoustic investigation of wooden T-junctions.
J. Negreira, A. Sjöström, D. Bard.
Applied Acoustics, 105:1–12, 2016.

Paper E
Modelling of the tapping machine for finite element prediction tools: Preliminary parametric studies
J. Negreira, D. Bard.
Submitted to ICA 2016, Buenos Aires, Argentina (September 2016).

Paper F
Psycho-vibratory evaluation of timber floors – Towards the determination of design indicators of vibration acceptability and vibration annoyance.
J. Negreira, A. Trollé, K. Jarnerö, L-G. Sjökvist, D. Bard.
Journal of Sound and Vibration, 340: 383–408, 2015.

Paper G (Attachment G)
Construction and in-house calibration of MEMS-based vibration transducers.
R. Darula, A. Sjöström, J. Negreira, D. Bard.
Report TVBA-3131, Division of Engineering Acoustics, Lund University, 2016.

Nomenclature

BBR National board of housing, building and planning.

BC Boundary conditions.

CEN European Standardization Organization.

CLF Coupling loss factor.

CLT Cross-laminated timber.

CO_2 Carbon dioxide.

DOF Degree of freedom.

EU European Union.

EWP Engineered wood products.

FE Finite element.

FFT Fast Fourier transform.

FSI Fluid-structure interaction.

HVAC Heating, ventilation, and air conditioning.

ISO International Organization for Standardization.

LSL Laminated strand lumber.

LVL Laminated veneer lumber.

MAC Modal assurance criterion.

MDOF Multi degree of freedom.

MEMS Micro electro mechanical system.

MIMO Multiple input multiple output.

MOR Model order reduction.

MWR Methods of weighted residuals.

NRFD Normalised relative frequency difference.

OMA Operational modal analysis.

OSB Oriented strand board.

PCA Principal component analysis.

PSL Parallel strand lumber.

SDOF Single degree of freedom.

SEA Statistical energy analysis

SIMO Single input multiple output.

SIS Swedish Standards Institute.

SVD Singular value decomposition.

TVE Timber volume element.

WHO World Health Organization.

Part I

Introduction and overview

1
Introduction

The World Health Organization (WHO) defines health as "a state of complete physical, mental and social well-being and not merely the absence of disease or infirmity" [1]. Thus, matters related to sound should not just be considered when problems stemming from noise exposure arise[1], but also when the well-being is disturbed. Along those lines, acoustical comfort (in particular applied to building environments) can be characterised as [2]: (i) absence of unwanted sound, (ii) presence of desired sounds with the right level and quality, and (iii) opportunities for activities without being heard by other people or annoying them. The latter implies that acoustic comfort, as perceived by a subject, involves not only the individual as a receiver, but also the person themself as a source of sound. Hence, it could potentially be equally annoying for someone to be subjected to sound as well as to feel a lack of privacy due to other people listening to the activities performed by him/herself. Neighbour noise is unfortunately still a highly underestimated risk factor for health and it should be of priority for the construction business [2]. The previous statement triggers the general motivation for the research presented in the thesis.

1.1 WOODEN BUILDINGS – VIBROACOUSTIC ISSUES

As a consequence of numerous urban fires that occurred during the 1800s, a Swedish law prohibiting the use of wooden frames in multi-storey constructions was passed in the year 1874[2]. This century-old ban was revoked in 1994, the year in which Swedish building regulations were revised with the aim of their harmonisation with the building rules of the European Union (EU). Since then, there has been a rapid growth in constructions of these types due to wood being a plentiful resource in Sweden[3], and considerable research concerning such buildings has being carried out within recent years.

[1] Hearing impairment, hypertension, cardiovascular and cognitive adverse effects, annoyance, sleep disturbance.
[2] The document containing this law corresponds to the first building regulations in the country's history [3].
[3] Sweden is the 3rd largest country by area in the EU, and 70% of it (28 million hectares) is forest [4].

Wooden constructions have many advantages [5], some of these being related to matters of sustainability such as wood's property of storing carbon dioxide (CO_2), its use resulting in reduced amounts of waste at construction sites, relatively little energy being required for wooden buildings to be produced, and wood being a renewable raw material. Other advantages are of pragmatic character, such wood being light in weight, the high degree of attainable prefabrication, the ease of assembly of the building parts involved, the possibility of the thermal insulation being improved without the facade walls needing to be thickened, and the foundations being simpler, cheaper and lighter than the corresponding ones in traditional concrete constructions. Current architectural trends, due to wood being considered by many to be aesthetically appealing, have also contributed to the use of wood. Accordingly, lightweight timber frame constructions have been steadily increasing their market share in several countries[4], to the detriment of heavy constructions, such as concrete buildings.

Nevertheless, there are many problems to overcome in the use of timber as a construction material in multi-storey buildings. Achieving a high level of acoustic quality, especially in the low frequency range (defined in this thesis as up to 200 Hz) is a major challenge, with various problems in connection with this being a major drawback in the use of lightweight timber structures. The differences in weight, stiffness, density and repartitioning as compared with more traditional materials have repercussions on how sound propagates throughout the structures. This triggers problems with sound insulation that can make acoustic comfort difficult to attain; and which, in turn, is very hard to predict before the building is constructed due to the variability in the properties of a natural material such as wood.

In most European countries, sound requirements are a remnant from the past and are not adapted to the current development of new systems. The standards for acoustic approval of a building have been developed on the basis of the performance of traditional heavy constructions, the principles applying there being extrapolated directly to lightweight timber buildings, in spite of their different behaviours. Due to this, there are unfortunately not particularly many examples of acoustically successful multi-storey wooden framed constructions. Even when buildings comply with current regulations, complaints by inhabitants often arise due to the occurrence of low frequency noise which is outside the scope of the standards. Accordingly, solutions for successfully achieving acoustic comfort, regarding both sound and vibration, as well as improvement of the standards that presently exist, are called for.

There remains a great deal to investigate before the vibrational behaviour of wooden structures can be regarded as readily predictable and satisfactory for dwellers. Although Sweden is undoubtedly a pioneering country in matters of lightweight timber constructions[5], convincing the market and the industry that wood is a natural structural material adequate for use in multi-level buildings is still a challenge. To achieve this, further knowledge is needed, in particular regarding the acoustic and vibrational behaviour of such timber structures.

[4] In Sweden, the market share for wood multi-storey buildings increased from 1% in 2000 up to 15% in 2012 [6], and according to [3], the intention is that it amounts at least 30% by the year 2020.

[5] In the last years, national research funding and promoting programmes continuously foster wood as a an alternative construction material for public buildings from an economic and environmental point of view.

1.2 AIM AND OBJECTIVE

The authorisation for the construction of wooden multi-storey buildings in Sweden brought with it an increase in the demand for open planning of both residential and office buildings that involved use of long-span floor structures. Wood is high in both strength and stiffness in relation to its weight. This makes it possible to build very long spans, especially with use of glue-laminated (glulam) timber. However, slender floor constructions involving long spans have low resonance frequencies that, in combination with a low degree of damping, are easily excited by such human activities as walking, running and jumping. Since people tend to be sensitive to the vibrations thus produced, floors of this sort are often regarded as annoying. Accordingly, obtaining adequate indicators of **human response to vibrations** in lightweight structures dynamically excited by human activities can contribute very much to obtaining better estimates of what can be regarded as acceptable levels of vibrations in dwellings. Attempting to develop such indicators is one objective of the research presented in the thesis.

Today, there are still no methods that have been clearly shown to be reliable and have come into any sort of general use for predicting the vibratory and acoustic performance of wooden buildings. At the same time, predictive tools based on numerical methods, such as the finite element (FE) method can be conceived as being promising in this respect. In order to construct large wooden buildings of adequate vibroacoustic performance, reliable predictive tools are needed in order for appropriate structural adjustments to be made before such a building is erected. By addressing vibration issues during the design phase of the building, time and costs can be markedly reduced, as experiments on prototypes and existing buildings can be time-consuming and expensive. **Developing FE tools for predictive purposes** is the main objective of the investigations reported in the thesis.

All together, it is known that the evaluation methods in use today substantially underrate the effects of low frequency impact sound, which hinders the achievement of acoustic comfort in wooden dwellings. Hence, there is a definite need of research to increase knowledge within this area and ultimately improve the evaluation methods employed, which should better correlate with human perception. Gaining knowledge of the impact sound in the low frequency range on timber structures, both from a prediction and a perception point of view through making use of both measurements and numerical simulations is thus sought after in the thesis. The latter will enable the **aim of achieving acoustic comfort in dwellings.**

Research limitations and assumptions applied

The investigations presented in the thesis intend to ultimately enable the use of numerical models for predicting and mimicking the behaviour of real structures. In doing so, the first step should aim at gaining knowledge about the physical phenomena occurring in these structures. Consequently, the objective of some of the publications presented in the thesis (viz. **Paper A**, **Paper B** and **Paper E**), was to compare relative differences between models, rather than trying to mimic absolute values from measurements, thus striving to assess and understand different phenomena and uncertainties at the time. This will eventually reduce unknown sources of error when creating predictive tools for complete buildings. Likewise, the conclusions drawn

from **Paper D** are limited to the types of wooden junctions investigated there, although many junctions in the market resemble those connections studied, thus the outcomes are quite general and applicable to other types of connections. Lastly, the perception studies presented in **Paper F** are promising and pave the way for further studies to be performed using the same methods developed. However, a larger number of floors would be needed to generalise the conclusions drawn, since test were performed on five floor structures. The studies presented in the thesis are limited to the evaluation of impact sound caused by vibrations in the low frequency range, i.e. up to 200 Hz, which, in turn is where the most severe problems related to acoustic comfort for wooden buildings are. No frequencies beyond that limit are analysed.

The loads dealt with are of low magnitude (linked to serviceability matters), which generate a linear elastic material response. Likewise, the assumption of long wavelengths in relation to heterogeneities in the materials is assumed, allowing materials to be modelled as homogeneous.

1.3 OUTLINE

The thesis is divided into two parts: **Part I** is an extended summary of the different topics dealt with in the papers that are appended; its aim being to provide a broad and theoretical overview of the topic. It is, in turn, structured as follows: after presenting in the current **Chapter 1** the introduction and the aim and objectives of the thesis, **Chapter 2** provides an overview of building with wood, describing various lightweight materials commonly used in timber buildings, while also touching upon such topics as building techniques, the current building regulations and problems concerned with acoustics and vibrations in buildings of the sort described. An extensive review of literature concerning wooden buildings (in terms of both existing serviceability criteria as well as in the field of prediction tools) is also presented. **Chapter 3** considers floor vibrations in detail, presenting the theoretical background of the topic in question as well as touching upon the experimental side of it. **Chapter 4** addresses the main core of the thesis. It first presents several existing methods to address vibroacoustic issues, and then delves deeper into the FE method from a theoretical point of view; this being the main tool used here in developing the aforementioned prediction tools. A scheme to calibrate computer models using measurement results as input, so as to enable predictive tools, is also presented. **Chapter 5** briefly introduces the theoretical background of the statistical methods employed in one of the papers that are appended, methods involved in relating subjective responses concerned with how people experienced vibrations on the floors of the sort studied, to objective measurements performed on those floors at the same time people walked or sat on them. **Chapter 6** summarises all of the appended papers, the conclusions drawn there as well as the specific contributions of the author to each of them. Finally, **Chapter 7** discusses the conclusions of the present work as a whole and suggests paths for further research.

Part II, in turn, compiles all the appended publications. A schematic summary of the publications that are appended together with their field of research, their aims and conclusions as well as the connections between them, is presented in Figure 1.1. Likewise, the investigations presented in the thesis are graphically summarised in Figure 1.2.

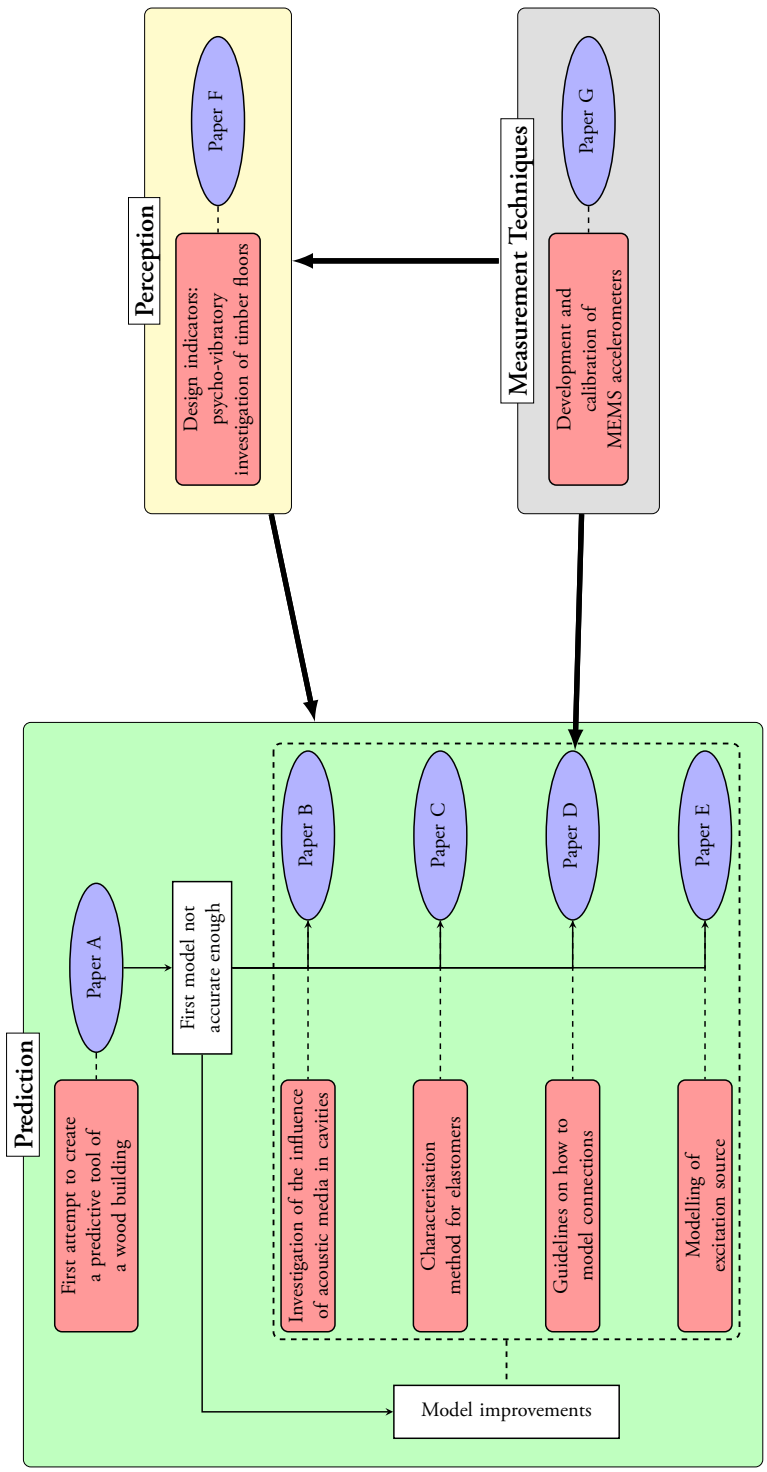

Figure 1.1: Flowchart showing the appended publications, their research field, aims and conclusions as well as the connections between them.

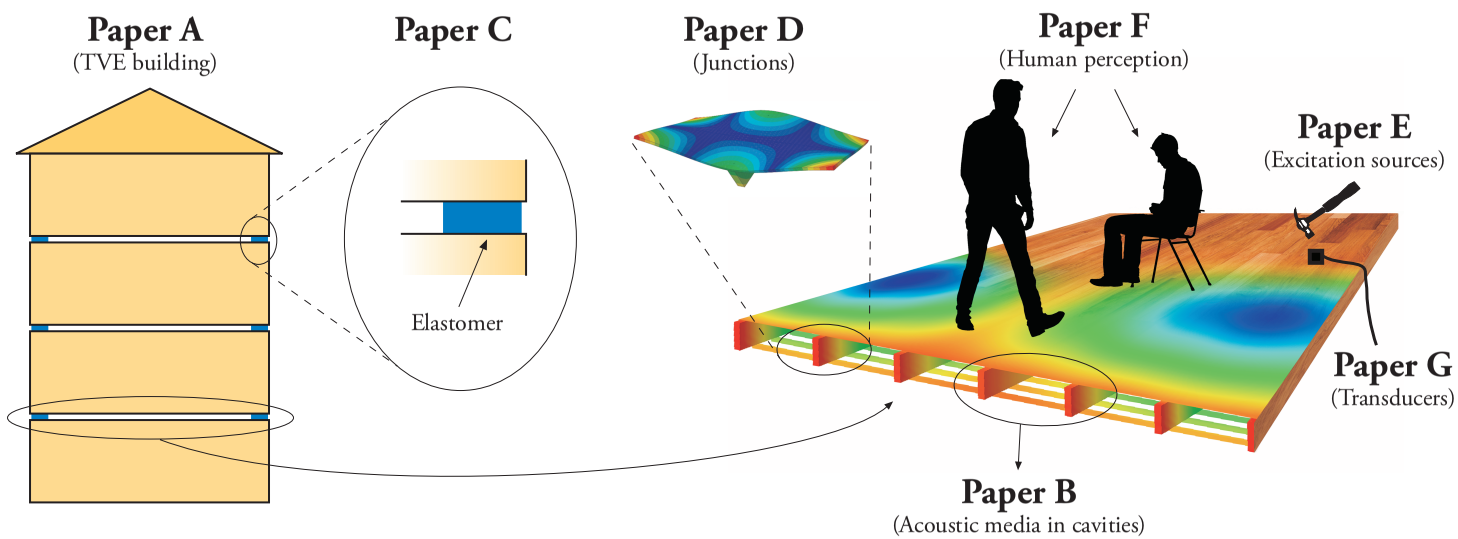

Figure 1.2: *Graphical summary of the different aspects dealt with in the thesis. Three main areas in the development of prediction tools are dealt with: (i) the impact source, (ii) the modelling of the vibration transmission through the floor and its parts and (iii) the psycho-vibratory response.*

2

Building in wood

The dwindling share of single-family houses in the construction market, in deference to wooden multi-storey constructions in Sweden since 1994 [5, 6], has led to the regulations regarding both impact and airborne sound insulation becoming more stringent due to complaints of noise disturbances by the occupants of such buildings. Accordingly, new materials and new building techniques have been developed. In this chapter, a general overview about wood and its mechanical properties as well as a description of the main engineered products manufactured from wood nowadays is given. Likewise, the existent building methods when using wood as load bearing material and the existing building regulations, serviceability criteria and prediction methods apropos vibrations and acoustics are presented.

2.1 MECHANICAL PROPERTIES OF WOOD

Wood is a natural structural material that generally has a high strength-to-weight ratio. Due to its anisotropy, strength and stiffness, its properties can vary considerably with different load orientations. Wood is generally both strong and stiff when loaded parallel to the grain, but is relatively weak when loaded perpendicular to it. Its mechanical behaviour is affected by, for example, duration of load, moisture content and temperature [7]. The characteristics of the material may be described and modelled as a continuous media at different scales (i.e. macro-scale, meso-scale and micro-scale), ranging from the components of the cells walls to massive structural members [8]. For the applications reported in the thesis, however, only modelling at the macro-scale level is necessary.

Regarding mechanical/acoustic modelling on the macro-scale, wood is often regarded as a homogeneous material, and its behaviour at low-to-moderate stress levels can be considered as linear elastic orthotropic [7]. The mechanical behaviour and properties of wood may thus be characterised, at each point, using different properties with respect to three perpendicular symmetry planes. Hence, three orthogonal directions are often considered: longitudinal (L), radial (R) and tangential (T) directions (see Figure 2.1). The R- and T-directions are defined

from the growth ring orientation, whereas the L-direction is considered as being aligned with the direction of the wood fibres, i.e. in the direction of the grain. The L-direction is, however, not necessarily fully aligned with the longitudinal direction of the tree stem, due to possible log taper and spiral growth [7]. Hence, a transformation of the stiffness matrix must be made in order to determine the material stiffness with reference to the global directions, as depicted in Figure 2.1b. If the wood sample studied is small, however, and for global deformation patterns which make it possible to assume the in-plane properties to be equal, the L-, R-, T-coordinate system can be regarded as a Cartesian coordinate system.

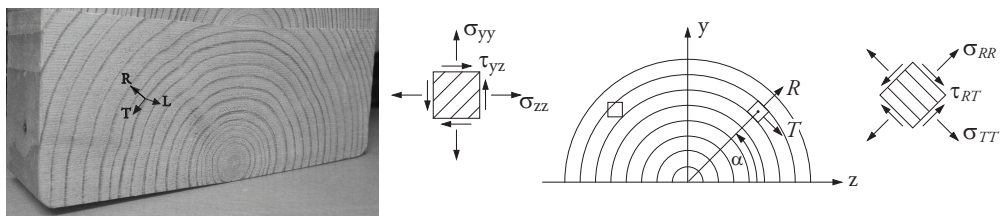

(a) Growth ring pattern present in the Norway spruce (Picea abies).

(b) Local and global stress components in the plane perpendicular to grain.

Figure 2.1: *Illustration of coordinate systems and stress components.*

Wood's constitutive behaviour, assuming small enough strains, can be described by Hooke's generalised law as a linear elastic orthotropic material by use of matrix notation as

$$\boldsymbol{\varepsilon} = \mathbf{C}\boldsymbol{\sigma}; \quad \text{i.e.} \quad \begin{bmatrix} \varepsilon_{\mathrm{LL}} \\ \varepsilon_{\mathrm{RR}} \\ \varepsilon_{\mathrm{TT}} \\ \gamma_{\mathrm{LR}} \\ \gamma_{\mathrm{LT}} \\ \gamma_{\mathrm{RT}} \end{bmatrix} = \begin{bmatrix} \frac{1}{E_L} & \frac{-\nu_{RL}}{E_R} & \frac{-\nu_{TL}}{E_T} & 0 & 0 & 0 \\ \frac{-\nu_{LR}}{E_L} & \frac{1}{E_R} & \frac{-\nu_{TR}}{E_T} & 0 & 0 & 0 \\ \frac{-\nu_{LT}}{E_L} & \frac{-\nu_{RT}}{E_R} & \frac{1}{E_T} & 0 & 0 & 0 \\ 0 & 0 & 0 & \frac{1}{G_{LR}} & 0 & 0 \\ 0 & 0 & 0 & 0 & \frac{1}{G_{LT}} & 0 \\ 0 & 0 & 0 & 0 & 0 & \frac{1}{G_{RT}} \end{bmatrix} \begin{bmatrix} \sigma_{LL} \\ \sigma_{RR} \\ \sigma_{TT} \\ \tau_{LR} \\ \tau_{LT} \\ \tau_{RT} \end{bmatrix} \tag{2.1}$$

or as the inverse relation

$$\boldsymbol{\sigma} = \mathbf{D}\boldsymbol{\varepsilon} \qquad \text{with} \qquad \mathbf{D} = \mathbf{C}^{-1}, \tag{2.2}$$

where $\boldsymbol{\varepsilon}$ is the elastic strain vector, $\boldsymbol{\sigma}$ the vector containing the stresses and $\mathbf{D}$ the material stiffness matrix. The parameters of the material stiffness matrix $\mathbf{D}$ are three moduli of elasticity (namely E_L, E_R and E_T), three shear moduli (G_{LR}, G_{LT} and G_{RT}) and six Poisson's ratios (ν_{LR}, ν_{LT}, ν_{RL}, ν_{RT}, ν_{TL} and ν_{TR}). For uniaxial cases, the first index of the Poisson's ratio denotes the loading direction, whereas the second one indicates the strain direction. For the applications addressed in the thesis (i.e. vibrations of small amplitude), the material is assumed to be linear elastic. The material stiffness matrix $\mathbf{D}$ is symmetric, i.e.

$$\frac{\nu_{RL}}{E_R} = \frac{\nu_{LR}}{E_L}; \qquad \frac{\nu_{TL}}{E_T} = \frac{\nu_{LT}}{E_L}; \qquad \frac{\nu_{TR}}{E_T} = \frac{\nu_{RT}}{E_R}. \tag{2.3}$$

Due to this symmetry, there are nine independent parameters (engineering constants) describing the stiffness of the orthotropic material. This is the way wood was modelled in the FE commercial software used (*Abaqus* [9]) to carry out the simulations that are reported in the thesis.

Owing to the fact that the fibres in the stem are oriented mostly along the longitudinal direction, the parallel to grain stiffness E_L is far greater than the two perpendicular directions. In fact, E_R and E_T are of similar magnitude, albeit E_R is, in general, higher than E_T (about 1.5 times [7]). The difference between the longitudinal and the perpendicular directions implies that for certain applications, wood can be modelled as a transversely isotropic material, i.e. just the parallel to grain direction and the perpendicular to grain direction being considered. Another characteristic intrinsic to softwoods is the very low rolling shear stiffness G_{RT} [8]. For more information about wood mechanics, see [7, 8, 10–12].

Natural imperfections such as knots, growth ring irregularities, resin pockets and other defects that develop in the tree during the growth process are generally contained in the wood specimens of the size of those treated in the work presented here. Likewise, wood generally displays considerable variation in its mechanical properties not only between different species, but also between different logs of the same species and even within a single log. This variability, which may be random or structured, can be accounted for by use of probabilistic approaches such as Weibull theory or Monte Carlo simulations [8]. Matters of that sort are already well addressed in the areas of e.g. wood mechanics and timber engineering.

2.2 ENGINEERED WOOD PRODUCTS

Engineered wood products (EWPs) represent a broad class of materials intended for structural applications and commonly used in timber constructions. In contrast to lumber or solid sawn timber, which is obtained by sawing logs or cants into individual solid elements, EWPs are typically manufactured from wood which has been reduced to smaller pieces by sawing, peeling, chipping, slicing or defibration. EWPs are comprised of such constituents as sawn laminations, veneers, strands, flakes, and sawdust that are bonded together by use of adhesives and/or through application of heat and pressure to form panel-like, or timber-like elements of differing size or shape to create structural products of different kinds. One type of EWP, that of glulam, is manufactured in a different manner, being made by simply gluing either sawn timber or laminates into larger units. EWPs are, in general, more expensive per weight than sawn timber, but have distinct advantages [12]:

- The possibility of producing products of virtually any size.
- Better and more efficient utilisation of the raw wood material.
- The strength-reducing inhomogeneities present in solid wood such as knots, growth ring irregularities, and resin pockets, are neutralised in part; the extent to which this occurs depending upon the type of EWP involved.
- The dimensional stability and tolerances they possess are significantly better, in general, than those of sawn timber. A wooden beam, for example, will likely suffer, after pro-

duction, larger deformations than an EWP due to its adaptation to the environmental conditions it will be exposed to.
- Their ready adaptation to market requirements (in terms of customised sizes, the specific properties sought, and the like).

EWPs can be found on the market in many different forms, the most prominent types of these being the following: structural wood panels (plywood, particleboard, oriented strand board –OSB–, and cross-laminated timber –CLT–), structural composite lumber (laminated veneer lumber –LVL–, parallel strand lumber –PSL–, laminated strand lumber –LSL–, glulam, and wood I-joists), etc. Figure 2.2 show, as an example, sketches of some of these EWPs commonly used in the prefabricated constructions of the sort dealt with in the thesis. Accounts of the properties of each of the aforementioned materials, as well as further information regarding them, can be found in the literature, e.g. [10–12].

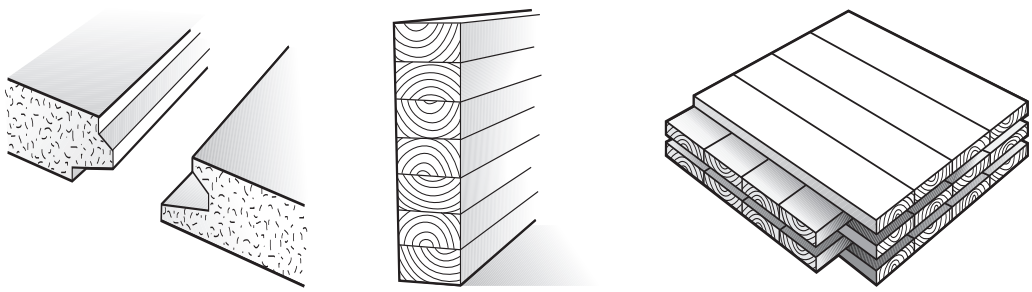

(a) Particleboard. *(b) Glulam.* *(c) CLT.*

Figure 2.2: *Different EWPs.*

2.3 BUILDING METHODS

Although lightweight timber frame buildings can be put up completely on-site, the tendency leans towards them being erected by assembling prefabricated elements at the building site. The higher the degree of prefabrication is, the less weather-dependent the building process becomes, the time spent at the construction site being reduced and moisture problems thus also being avoided to a considerable degree. In addition, the level of quality control (for example, in terms of the degree of accuracy with regard to size) is higher indoors, in a factory, due to optimisation of the production techniques there. Moreover, prefabrication can improve production economy, in terms both of reducing the working time required and the material waste, all of this resulting in less expensive tenements [13, 14]. Only prefabricated structures are dealt with in the thesis, due to the fact that the market is moving towards prefabricated constructions for the most part and also because buildings with massive wooden floors do not have such severe problems with regard to low frequency sound insulation (owing to their higher mass). At the present time, three main prefabricated building methods can be distinguished in Europe [5]:

1. **Balloon-frame method:** with use of this method, also known as the Chicago method, the walls are continuous over many storeys with the floors hanging between the walls. Although this method provides advantages in terms of better air tightness of the building, its use is not widespread and has fallen out of favour, due to the construction problems it results in, such as limitations in the height of the building, prefabrication issues and difficulties in the on-site mounting of the construction in question. The method has been superseded by the platform-frame construction, or by some mixed balloon and platform-frame methods, in which the floors are fixed to notches in the walls.
2. **Platform-frame method:** the floor elements here are fixed on top of the walls of the lower level and are most often continuous from one room to another on the same floor, thus becoming a working platform for construction of the next building layer. This is the standard approach in lightweight frame construction in Europe.
3. **Box-assembly:** in this method, also called timber volume element (TVE) based constructions, prefabricated box-like elements are stacked together to assemble the complete building (see Figure 2.3). Each box can be regarded as a closed three-dimensional structure built up by the floor, ceiling and walls together with electrical, heating, water, sanitation and ventilation installations. The degree of prefabrication performed at the factory is considerable so that the work on-site required is held to a strict minimum. In fact, with prefabricated wood modules, savings of up to 20-25% of the total cost can be achieved, as the time spent at the building site can be reduced as much as 80% compared to on-site construction [6]. Particularly in Sweden, this method has been gaining popularity lately. The costs and the difficulties in transportation can be the main drawbacks of this building approach.

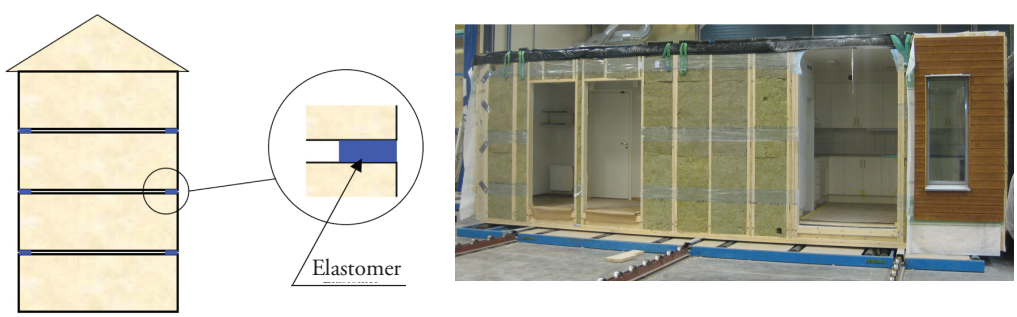

(a) Sketch of a TVE-based building, [13]. *(b) TVE during manufacturing process.*

Figure 2.3: *Box-assembly construction method.*

A distinct advantage often present in this type of building system, as regards vibrations and acoustic performance, is that, for any two volumes placed above the other, the upper volume contains the upper part of the flooring system to it, being the ceiling comprised in the lower volume. An elastomer is usually inserted in between the two volumes. The only mechanical contact between two adjacent TVEs is by means of some metallic tie plates that assure horizontal stability and through these elastomers that are placed on the flanks (either shaped as blocks separated a certain distance, as strips, etc.). If correctly

used, they can markedly reduce the flanking transmission; see Figure 2.3. Considerable research on lightweight timber buildings has been carried out. According to [13], however, there is still a lack of systematic studies dealing specifically with volume based element buildings. It is still a question, therefore, to what extent the knowledge regarding traditional lightweight buildings attained thus far is directly applicable to volume systems. Different investigations of buildings constructed following this method, will be taken up in the thesis, more specifically in **Paper A**, **Paper B** and **Paper C**.

Placing various construction elements (e.g. floor, walls, and whole rooms) on top of a resilient layer, with the intention of reducing low frequency noise, is a recent method often employed not only when using the box-assembly method, but also when other building systems are involved. In using resilient strips in-between parts of lightweight buildings, it is very important to design and select the appropriate stiffness for the material so that the degree of isolation desired can be achieved, since a load higher than the recommended one can compress the elastomer to such an extent that its isolating properties are greatly reduced. The latter statement was proven in [15], where it was shown (after measuring 31 nominally identical TVE-based buildings) that the sound reduction obtained was better the higher up one examined in the building. This highlighted that nowadays, those elastomers are still sometimes not properly installed, since a stiffness lower than the recommended one was used in the lower levels of the building, the mechanical coupling between the parts being increased and thus compressing the elastomers excessively to such a level that the sound insulation was worsened. A method for characterising elastomers so as to have reliable assessments of their material properties when modelling them using FE software, together with a literature review on the topic, is presented in the appended **Paper C**.

2.4 SOUND TRANSMISSION

Disturbing sounds (noise) or vibrations in a building environment can stem from sounds or vibrations travelling from one part of it to another. On the basis of the noise source, one can distinguish between:

1. **Airborne sound transmission:** when sound waves travel through the air and reach a building element they cause it to vibrate. The vibrations produced travel throughout the element in question and radiate out to the other side of it through creating pressure differences that propagate and create noise. Typical airborne transmission sources are speech, HiFi systems (such as speakers), and appliances. The sound transmission path here is one in which the energy is carried for the most part by the air, and only to a minor extent via structural-borne waves [16]; see Figure 2.4a. Airborne sound propagation is outside the major scope of the thesis and will thus not be specifically dealt with.
2. **Structure-borne sound transmission:** the direct impact of an object in striking a separating surface of a building, such as a floor, causing both sides of the building element involved to vibrate, and generating waves that propagate through it and transmit the sound to adjacent rooms, is called structure-borne sound. Typical impact sources are footsteps and dropped objects; see Figure 2.4b. The “character” of such sources is of-

ten described by occupants of wooden buildings as “thuds”, “thumps”, and “booming” sounds [17]. Structure-borne sound, particularly in the low frequency range, is of central interest in the thesis, as it is believed to be the main source of annoyance for people living in multi-storey wooden dwellings, [17–26].

Both airborne and impact sources generate **direct** and **flanking transmission** to adjacent rooms; see Figure 2.4. A typical example of flanking transmission is when the vibrations of a floor spread to the load-bearing walls and result in sound radiation from the walls, which sometimes is greater than that from the floor. Indeed, flanking transmission is often one of the main acoustic problems in lightweight constructions, especially as regards impact sounds. With use of suitable devices for suppressing flanking transmission, sound insulation can be improved by approximately 15 dB. Theoretically, it can be reduced in line with [18]:

- Reduction of low frequency noise (airborne or impact) transmitted into the plate-like structures in the source room, the reduction being achieved, for example, by increasing the surface weight of the upper part of the floors by means of an extra layer of heavy material, or also by a resilient floor[1].
- Reducing the transmission of vibrations from the source room to the receiving room. Means of accomplishing this have been widely used in Sweden, especially in buildings made of TVEs, the noise transmission be lessened by use of elastic layers as previously described, if correctly used. Suspended ceilings are another possible measure[2].
- Reducing noise radiation from plate-like structures in the receiving room by use of walls made of plasterboard placed on top of wooden studs instead of massive wooden walls[3].

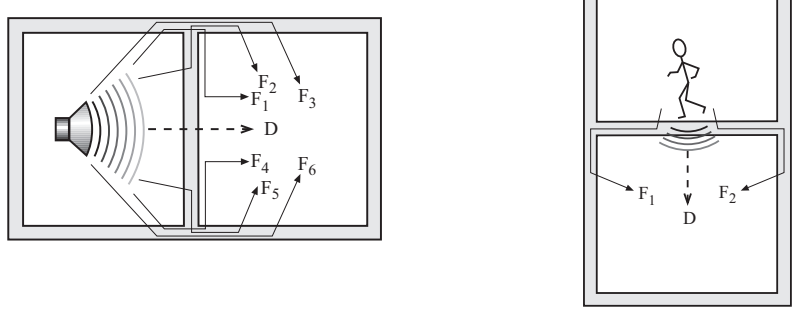

(a) Airborne sound transmission. *(b) Impact sound.*

Figure 2.4: *Sound transmission types. “D” denotes direct transmission whereas the “F_i” indicate the different flanking paths involved.*

In practice, splitting the construction frameworks of adjoining apartments or rooms (by e.g. use of elastomers or detaching structural elements) would be a safe solution in terms of redu-

[1]The efficiency of these methods is discussed in [5, 18, 19]. Particularly, in [26], it was concluded that for a floating floor, sound insulation improvements start around 100-200 Hz, getting better with increasing frequency.

[2]The benefit of a resilient ceiling was shown in [26] to start at 50 Hz, improving with increasing frequency.

[3]The radiation from plasterboards on studs is comparatively lower, especially at low frequencies [5, 18, 19].

cing flanking transmission, as acoustic bridges are partially eliminated, although the solutions adopted should be investigated for each individual case[4]. Yet this is often not a practicable approach due to factors of stabilisation affected by, for example, wind loads. All in all, structural parts should be decoupled as much as possible so as to improve the sound insulation while still withstanding static loads. A sort of catalogue illustrating state-of-the-art solutions for buildings using wood materials (both for terrace houses and apartment constructions) to achieve satisfactory sound insulation, is presented in [5]. Therein, discussions on practical solutions such the use of floating floors, suspended ceilings, and optimised party walls, floors and junctions so as to reduce flanking transmission, are discussed, with airborne and impact sound insulation measurements presented alongside.

2.5 REQUIREMENTS AND SUBJECTIVE JUDGEMENTS

Acoustics encompasses both sound and vibration. At the present time, proper acoustics (i.e. fulfilment of the current standards) serves as a performance characteristic for building with wood, being a prerequisite for the acceptance of timber constructions by the building industry, by building owners and by consumers [18]. Due to the high degree of variability of vibratory and acoustic behaviour that characterises wood as a load-bearing material, large uncertainties are always involved in assembling buildings of the types described in the thesis, the most important being that of ensuring acoustic comfort of their occupants. Greater knowledge in this regard concerning wood can reduce the risks of using it, enhance the positive qualities of choosing wood as a construction material and aid the industry in constructing these types of buildings. In line with this, improvements in the standardised prediction and evaluation methods employed as well as the development of new excitation sources representing realistic loads, are needed in order to better ensure the comfort of residents. In the following, a thorough overview of the acoustics and vibration criteria currently in force, applied to wooden multi-storey buildings, is presented.

2.5.1 Building acoustics regulations

In order for acoustic comfort to be met, international sound insulation regulations have been established since the 1940s in some countries (e.g. 1945 in Sweden). Those requirements have changed considerably over time, the current descriptors for evaluation of airborne and impact sound insulation being defined in the ISO 717:2013 [28, 29], referring to measurements performed according to the methods described in ISO 10140:2010 and ISO 16283:2014 [30–37], where also single-number quantities and the different spectrum adaptation terms are defined. The descriptors, however, involve different adaptations depending on the country of application, this causing problems as the building industry is no longer restricted to national boundaries [38].

A sound insulation requirement may be expressed either as the sum of a weighted value and a spectrum adaptation term, or solely as the weighted value. The weighted value is obtained from

[4] Occasionally, if wrongly used, elastomers could lead to vibration amplification at certain frequencies [27].

the frequency dependent performance of the structural element in question (e.g. wall or floor) assessed via measurements by procedures described in the ISO standards (i.e. [28] for airborne sound insulation and [29] for impact sound insulation). Roughly speaking, the weighted value summarises the performance of the structural element in one single figure, given in decibels [dB]. For airborne sound insulation, the weighted value expresses a sound reduction index or a level difference (i.e. the higher the value, the better the performance of the partition); whereas for impact sound, the performance is described by means of a single-number rating indicating impact sound level (i.e. the lower the value, the better the performance). The spectrum adaptation terms, in turn, account for different spectra of noise sources, namely highway traffic, road traffic, aircraft noise, standardised excitation sources (e.g. tapping machine), low frequency noise, etc. depending on the type of sound which is being evaluated.

One of the main obstacles nowadays is the high degree of diversity in the regulatory requirements across Europe (and worldwide). Different indicators and limit levels are used depending on the country of application (see Table 2.1 to check the existent descriptors).

Table 2.1: *Overview of ISO 717:2013 descriptors for evaluation of sound insulation in buildings (information retrieved from [2]). Definitions of the different descriptors as well as the spectrum adaptation terms used are found in the corresponding ISO standards [28, 29]. For the sake of simplicity, airborne sound insulation of facades is not included.*

ISO 717:2013 descriptors for evaluation of field sound insulation	Airborne sound insulation between rooms ISO 717-1 [28]	Impact sound insulation between rooms ISO 717-2 [29]
Basis descriptors (weighted quantities)	R'_w $D_{n,w}$ $D_{nT,w}$	$L'_{n,w}$ $L'_{nT,w}$
Spectrum adaptation terms	None C $C_{50-3150}$ $C_{100-5000}$ $C_{50-5000}$	None C_I $C_{I,50-2500}$
Number of descriptors	3×5=15	2×3=6

All in all, building regulations call for some sort of harmonisation of the international standards. The benefits that harmonising descriptors would bring include [2, 38]: (i) facilitating the exchange of construction data, knowledge and design details, (ii) presence of less complicated national adaptations that will (iii) encourage more cross-country trade, (iv) lower the risk of mistakes due to lack of awareness of the rules, (v) reduce the costs for the industry and (vi) initiate the development of design tools. According to [19, 38], however, harmonisation of sound insulation requirements seems unrealistic at the present time, as "jungles" have to be removed first; namely the variety of sound insulation descriptors (cf. Table 2.1), the complex national rules making it difficult to find limit values, and the national rules (i.e. local adaptations) in addition to standardised methods. Nevertheless, it would be a great benefit if, initially, similar descriptors could be agreed upon. Along those lines, several single-number figures have been suggested as potential harmonised values [2, 19], those being:

- For airborne sound insulation: $D_{nT,w} + C_{50-3150}$
- For impact sound insulation: $L'_{nT,w} + C_{I,50-2500}$

The reason why $D_{nT,w}$ and $L'_{nT,w}$ are chosen as single-number descriptors is because the properties D_{nT} and L'_{nT} correlate better with the performance of airborne and impact sound insulation, respectively, as perceived by the occupant than any other quantity in Table 2.1 [20].

Lightweight constructions: low frequency issues and dwellers' perception

Whereas heavy constructions do not present problems in regard to sound insulation at low frequencies due to the large mass they possess, many lightweight wooden constructions are prone to suffer low acoustic and vibratory quality at lower frequencies. High frequency problems in wooden buildings are, in general, easier to palliate; those normally being related to e.g. duct-noise or leakages.

Statistical methods developed based on the assumption of the presence of a diffuse field are often employed in the existent predictive calculations. These methods are not appropriate to use for low frequencies, due to the lightweight elements being exposed to non-diffuse conditions because of the internal damping being greater than that for heavy elements. This produces a high degree of uncertainty and variability in the measurement results obtained. Persons walking, running or jumping, as well as appliances, traffic, airplanes, fans and other heating, ventilation, and air conditioning (HVAC) systems, etc. need to be dealt with properly if acoustic comfort (both in terms of buildings complying with regulations and providing comfort for the occupants) is to be achieved.

The current requirements to acoustically approve a building are, in most countries, based on evaluations of the acoustic performance from the 100 Hz third octave band and upwards. At the same time, an increasing need has been felt to look carefully at the performance of buildings at levels below 100 Hz, especially as regards lightweight buildings, since complaints often arise amid people living in those dwellings. Their discontent has been found to be caused mainly by the frequencies left outside the scope of the standards [17–26]. Consequently, the frequency range of evaluation was enlarged down to 50 Hz in the year 1999 in Sweden, the requirements thus currently demanding measurements and evaluations in the so-called extended frequency range 50-3150 Hz. Up to date, low frequency spectrum adaptation terms have been implemented in the regulatory minimum requirements only in Sweden for residential buildings [19]. However, research indicates that the introduction of this adaptation term does not necessarily prevent bad constructions from entering the market, at least for impact sound [2, 18, 38]. As previously mentioned, results of the evaluation procedures currently employed often fail to adequately correlate measurements of impact sound insulation with acoustic quality as perceived by residents[5], despite the building having been classified as fulfilling higher than the minimum (Swedish) demands according to the corresponding standardised procedure employed [18]. Since a great part of the vibration energy of a floor is contained in the first few modes (up to approximately 30 Hz), these are believed to be the vibrations that cause most of the annoyance,

[5] In [39], different evaluation methods (in terms of proposed reference curves) are discussed.

yet since such low frequencies are outside the scope of the standards, they are not accounted for in the weighted descriptors obtained in accordance to the norms. Reformulation of the standards and the evaluation methods employed is thus needed and encompassing frequencies even below the lower limit of the extended frequency range, i.e. 50 Hz.

In line with this, in one of the articles stemming from the measurements performed in the project frame of the Swedish project *AkuLite* [21], it is highlighted the importance of extending the frequency range of analysis down to 20 Hz, especially for impact sound insulation. Therein, statistical analyses between objective measured parameters (accelerations, deflections, etc.), and subjective ratings of people living in the apartments that were measured, were performed. A total of 10 newly constructed buildings (less than 10 years) were measured; four of them having a traditional wooden framework and flooring boards, one having a cold-formed thin-walled steel framework, four being made of CLT and one having walls and floors made of massive concrete cast in-situ. Regarding airborne sound insulation, the rating $R'_w + C_{l,50\text{-}3150}$ [28] was proven to be adequate as compared with subjective perception, yet being important that the frequency of analysis starts at 50 Hz, as the correlation given by the statistical parameter R^2 decreased considerably from 73% to 58% when starting at 100 Hz. No further improvement in the correlation was found when including frequencies down to 20 Hz. When analysing the impact sound, however, including frequencies down to 20 Hz improved the correlation of measurements to occupants' rating of annoyance from 32% using $L'_{n,w} + C_{l,50\text{-}2500}$ [29] to 85% when including a new proposed spectrum adaptation term $L'_{n,w} + C_{l,Akulite,20\text{-}2500}$. The latter highlights the importance of including low frequencies in the evaluation of such problems and paves the way for more research to be carried out in, for example, other type of buildings, and also preferably from different countries (i.e. not just Sweden) [21]. Moreover, it is emphasised that the standardised single number evaluation of sound insulation should not be considered as neutral with respect to building technique and materials due to the different behaviours involved. Other references stressing the need of addressing low frequency issues when dealing with lightweight buildings and for impact sound insulation can be found in, amongst many others [2, 5, 17–26, 40]. Likewise, the *WoodWisdom-Net* project *Silent Timber Build* [41] is continuing the work of the aforementioned project *AkuLite* mainly on the development of low frequency vibroacoustic prediction tools. The goal must then be a high correlation between prediction, field measurement results and subjective evaluation.

Classification schemes

As aforementioned, the fact that the standards and legal requirements currently in force are met does not necessarily guarantee sufficient acoustic comfort. Due to the latter and aiming at reflecting levels of acoustic comfort, several countries have introduced classification schemes, enabling specification of better acoustic conditions than required by the legal minimum requirements. In particular in Sweden, a classification system is presented in the national building regulations (BBR) for both airborne and impact sound. It stems from two Swedish Standards: SS 25267:2015 [42] for dwellings and SS 25268:2007 [43] for premises of other types, each of which involves four sound classes, denoted as A, B, BBR (previously called class C) and D. Sound class BBR is the minimum requirement for the acceptance of a building, classes

A and B being recommended for the achievement of a good sound climate, at the same time as class D, despite its limitations, may be regarded as acceptable in certain rebuilding projects. For classes A, B and BBR, the extended frequency ranges 50-3150 Hz for impact sound, and 50-5000 Hz for airborne sound, apply. For class D, however, the traditional frequency range of analysis (starting from 100 Hz), is still used (cf. Table 2.2).

Table 2.2: *Sound classes proposed in SS 25267:2015 in terms of the minimal sound insulation from spaces outside the dwelling to spaces inside the dwelling. There are a few exceptions, however, depending of the type of the space outside the dwelling; see [42].*

Sound Class	A [dB]	B [dB]	BBR [dB]	D [dB]
Air-borne sound insulation ($D'_{nT,w} + C_{50-3150}$)	60	56	52	48
Impact sound insulation ($L'_{nT,w} + C_{I,50-2500}$)	48	52	56	60

2.5.2 Prediction standards

The standards EN 12354:2000[6] [44–49] predict the acoustic performance of buildings from the standpoint of the performance of individual building elements. They can be seen as an approach where theoretical calculations can be combined with empirical data, which in turn facilitates the free trade of products due to the universality of the results obtained [50]. Specifically, they describe a simplified statistical energy analysis (SEA) model to predict the apparent sound reduction index and the impact sound level between two rooms including contributions from the flanking paths. The input performance data of each individual element taking part in the structure or of the junction itself (e.g. radiation factor, vibration reduction index, structural reverberation time...) may be determined by calculations (applying construction and material characteristics) or by laboratory measurements, carried out according to ISO 10140:2010 [30–34] (for the direct transmission) as well as following ISO 10848:2006 [51–54] (for flanking transmission). Nevertheless, lightweight elements typically do not meet the hypotheses that SEA relies on (at low frequencies, the prediction uncertainty of SEA-like models increases due to the lower modal density found there) and unfortunately, the existing prediction models for sound transmission appear to be reliable only for monolithic weakly-damped building elements made of concrete or brickwork [55]. Accordingly, applying the EN 12354:2000 model to wood elements may result in inaccurate predictions. Several investigations have led to corrections factors for applying these prediction standards to lightweight buildings [56], although there is still a long way to go before the prediction models can be expected to be accurate and reliable enough.

[6]The parts 1 to 4 of these European standards have each an identical international version contained in the series ISO 15712:2005. The European Standardization Organization (CEN) has just revised the first 4 parts of the EN 12354:2000, closing and publishing a first draft on March 28th 2016. The decision thus far seems to lean towards merging those parts into the EN ISO 12354:2016 series, which has to be approved by means of a ballot by April 28th 2016. Although ISO will have the right to decide on revisions eventually, they are likely to stay under CEN leads. In case the EN ISO 12354:2016 are published, the first edition of ISO 15712:2005 will be superseded by the revised standards. No corresponding discussion has taken place yet regarding parts 5 and 6 of EN 12354:2000.

Numerical prediction models

In order to overcome the aforementioned shortcomings in the existing standardised procedures, use of numerical models as prediction tools may be the way to proceed so as to gain insight into the behaviour of such types of structures and eventually develop better evaluation methods and prediction standards to assess low frequency performance of wooden buildings. The substitution of measurements by easy-to-use numerical predictive models during the design phase of the building, however, must take place only after those have proven to possess enough accuracy for the predictions carried out. The FE method has proven to be a powerful tool and is therefore employed in the investigations reported in the thesis to develop numerical prediction tools. In Chapter 4, a thorough theoretical background of the FE method is given.

Nonetheless, mimicking measurement values by use of FE simulations is still a daunting and challenging task. The uncertainty related to a building system encompasses not just the building system itself (structural parts, material properties, connections), but also the standard of workmanship and the measurement procedure. It is generally accepted that the variation of craftsmanship needs to be considered when assessing sound and vibration transmission in wooden structures [15, 57–62], some of the previous references indicating that the variations in sound insulation decrease with the amount of work necessary in the field. Accordingly, work on how to handle and account for such uncertainties has been performed, amongst others, in [50, 63]. Modelling of wood gross defects and material variations is feasible, although such an approach is not utilised within the work presented here, as modelling insight was most times gained through studying relative differences between different models rather than seeking for absolute correlation to measurements. With the knowledge stemming from such a strategy, it will eventually be easier to handle the modelling of wooden buildings and hence match measurement results by means of numerical models.

A broad literature review about work performed up to now using the FE method in matters related to predictive numerical models is given in the appended papers, and thus not reported again here in this chapter. More specifically, issues related to vibration reduction measures, prediction of flanking transmission, modelling of connections and junctions (with especial focus put on connections involving elastomers) as well as work done on material parameters' uncertainties, are presented **Paper C** and **Paper D**. Moreover, in **Paper B**, a theoretical background of porous material models for including acoustic media in numerical FE models, is described.

2.5.3 Floor vibration standards and serviceability criteria

Not only the prediction of vibrations in buildings entails difficulties, but also the understanding of the reason behind the acceptance (or not) of those vibrations by the occupants, when they actually occur, is a highly complicated issue, due to the numerous factors affecting their perception; see Figure 2.5. The complexity involved in matters related to floor vibrations is well illustrated by the fact that despite years of research and product development, no common standardised design rules exist as of today, but rather some national regulations or guidelines. Extensive research in the area of human perception of whole-body vibration and human re-

sponse to such vibration has been carried out and many design criteria stemming proposed based on those outcomes, yet still complains from inhabitants arise in timber buildings due mainly to low frequency noise [2, 5, 17–26, 40].

According to [64], human response to whole-body vibration can be divided into five categories: (i) degraded comfort, (ii) interference with activities, (iii) impaired health, (iv) occurrence of motion sickness and (v) perception of low-magnitude vibration. In the case of building vibrations, human response to it can be said to consist of annoyance and of a reduction in comfort.

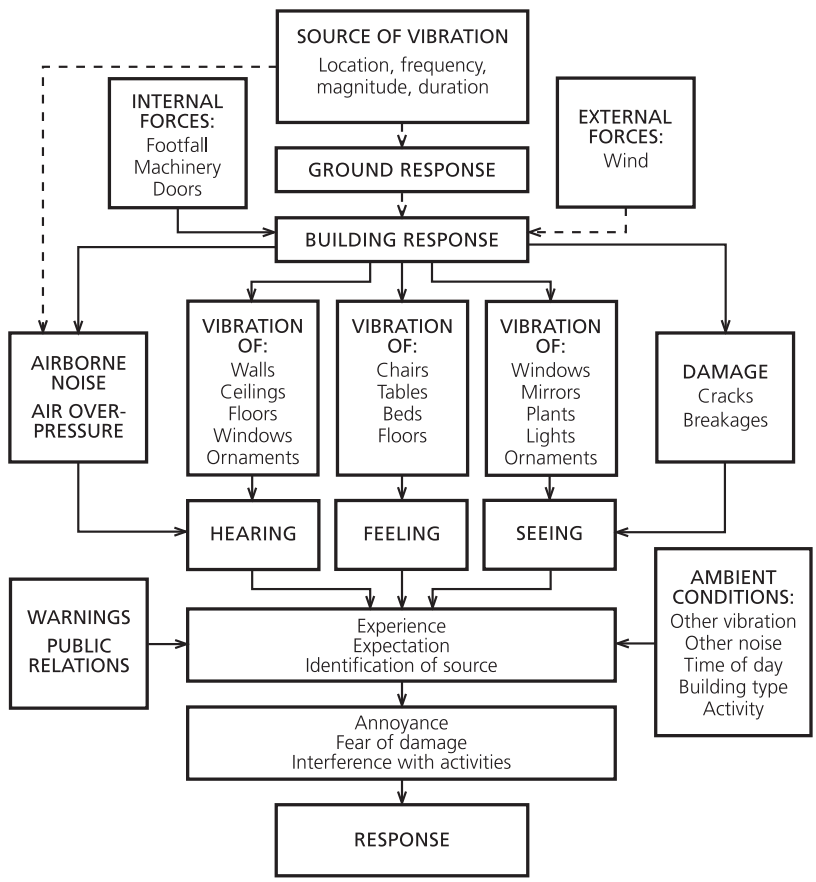

Figure 2.5: *Factors affecting the acceptability of building vibrations, [64].*

Due to the complexity, sensitivity and variability of the human body, there are no clearly stated limits for acceptable vibration levels that are used in buildings nowadays but simply certain guidelines that have been developed. The response of a human to vibration not only depends upon a large number of variables but is also highly subjective. For instance, people differ in how they react in response to what are nominally the same vibration levels (reflecting inter-subject differences in this respect), and a given person may respond differently to a particular level or type of vibration under differing circumstances (intra-subject differences) [65].

More specifically, one can say that human response to whole-body vibration depends both on psychological and on physiological variables. Thus, characteristics of the vibration, i.e. its amplitude, frequency, duration and direction, may very well influence the perception of it as much as age, gender, posture, fitness, type of activity being performed, attitude, expectations, context or motivation [65].

If humans are subjected to vibrations for too long a time, there is the risk of health problems being involved. According to ISO 2631-1:2003 [66], long-term high-intensity whole-body vibrations can result in an increased health risk for the lumbar spine and the connected nervous system of the segments affected. The digestive system, the genital/urinary system, and the female reproductive organs are also assumed to be affected, although the probability of this can be regarded as being lower. Such effects have only been investigated in the case of seated persons, no corresponding research having been carried out on standing or recumbent persons thus far. It has also been found that it normally takes several years for the health changes involved to occur.

The previous mentioned ISO 2631-1:2003 [66] and the ISO 2631-2:2007 [67] concern human exposure to whole-body vibration and shock in buildings in the frequency range 1-80 Hz with respect to the comfort and annoyance of the occupants. They specify a method for measurement and evaluation; however, no acceptable magnitudes of vibration are stated. Based on the latter two norms and for the same frequency range, the Swedish standard SS 4604861:2004 [68] proposes some contour plots, in addition to the perception thresholds given in [66, 67], with limits for accelerations and velocities labelled as "moderate disturbance" and "probable disturbance". Methods for measuring the latter quantities are also stated alongside. Furthermore, the standard ISO 10137:2007 [69] gives recommendations on the evaluation of serviceability against vibrations in buildings and in walkways (their being either located within a building, connecting separate constructions or serving as an exit pathway).

Regarding vibration requirements, the Eurocode standards [70] provide common structural design rules for the design of whole structures and of component products. The Eurocodes are a set of harmonised technical rules developed by the European Standardization Organization (CEN) for the structural design of construction work carried out within the European Union. Specifically, the design of timber structures is dealt with in EC5-1-1, and for matters related to the research reported in the thesis, the reader is referred to the section of the serviceability limit state design guidelines regarding floor vibration performance. Calculations in accordance with Eurocode 5, as well as further explanation of the procedures in question can be found in the appended **Paper F**. There is still concern nowadays, however, regarding the guidelines proposed in [70], due to the complexity that vibration issues involve. It is stated in [71], for example, that the design criteria currently contained in EC5-1-1 do not adequately address issues concerning the dynamic response of timber flooring systems and associated vibrational problems. Reconsideration of the design criteria is thus called for.

An extensive literature review is presented **Paper F** and hence the reader is referred to there. It focuses on: (i) human perception of structural vibrations and (ii) current serviceability criteria to minimise annoying vibrations in floor systems, applicable to timber constructions.

2.6 CHALLENGES

At the present time, the existing standards, prediction methods and serviceability criteria are still not properly adapted to wooden buildings. Results of the evaluation procedures currently employed often fail to correlate closely enough measured impact sound insulation with perceived acoustic quality, in particular due to increased low frequency noise. Gaining knowledge about the behaviour of wooden multi-storey buildings will:

- Enable predictive tools so that vibroacoustic issues can be dealt with before the construction of the building, the latter saving time and costs for the industry.
- Pave the way for the development of new standards more adapted to this type of constructions in terms of evaluation methods and excitation sources.
- Improve building design so that the approval of such structures for residence is linked at all times with human acoustic comfort inside them.

In order to reach the previous goals, Nordic and international standardisation groups, the Swedish Standards Institute (SIS), researchers working in the field and the business-related industry have pointed out problems to be tackled [5, 18, 19, 72]:

- The acoustic requirements for buildings are often based on various judgements of highly uncertain character and on doubtful background data.
- New products and combinations of these are often approved on the basis of principles of evaluation that are out of date and should be reconsidered.
- Measurement repeatability and reproducibility must be improved.
- Accurate transfer of results and knowledge gained from theory to practice.

Although the number of investigations concerned with vibrations in lightweight buildings has increased in the recent years, paving the way for providing greater acoustic comfort for their inhabitants, there is still a long way to go before the performance of lightweight buildings can be adequately predicted and be approved amid occupants of these buildings.

3
Floor vibrations

In this chapter, a thorough background on floor vibrations is given. First, a theoretical overview of structural dynamics is presented, due to its importance for understanding the vibroacoustic behaviour of wood structures. More specifically, the concepts of eigenfrequencies and eigenmodes of a system and the closely related phenomenon of resonance for harmonic vibrations are addressed. Furthermore, it is discussed how the dynamic behaviour of structures is affected by the introduction of damping. Only free vibration and the response to harmonic excitation are considered here as it suffices for providing a basic understanding. Finally, concepts of measurement techniques in terms of both excitation sources and extraction methods are discussed.

3.1 INTRODUCTION

In broad strokes, floor vibrations can be divided into two types [73]: local deflection and resonant vibration. Local deflection, only experienced by the active person or another person relatively close to the former, appears in the direct vicinity of the occupant when an induced force is applied, its value increasing with decreasing stiffness. It is typical of lightweight constructions. Resonant vibration, in turn, generally occurs as a result of a lack of damping, force at hand generating a long-lasting vibration of the floor, its magnitude being larger the lower the damping is. The parameters that affect the dynamic behaviour of a floor are the following [73]:

- Stiffness, which determines the springiness[1] of the floor. The higher the stiffness the better it is, since the deflection due to a force that is applied is lower. Albeit increasing the stiffness of the floor might seem preferable, this would counteract the main advantages of lightweight buildings, those of being light and cheap (since in principle an increase in stiffness could only be achieved by either increasing the existing physical dimensions or by making the material of which is composed stronger, which would mean an increase in mass density). A representative Swedish wood flooring system (see Figure 3.1) is com-

[1] Defined in [74] as a disturbing sensation due to floor deflection/vibration at the point of application of a load.

posed of joists along the load bearing direction on top of which a sheathing of structural boards is placed (a so-called subfloor often made of any of the EWPs described in Section 2.2). Due to this, the stiffness is orthotropic, since it is much larger in the load bearing direction than along its transverse direction. One arising problem with clustering of eigenmodes[2] which can, in turn, yield to poor vibration performance [75–77] is due to the low transversal stiffness. In order to partially solve this, bridging between joists and/or strapping can be performed. In doing so, any load applied will be distributed to adjacent joists. The load sharing is being beneficial in terms of vibration performance, as the stiffness is increased without a marked increase of mass.

- Damping, an increase in it being generally beneficial since vibrations would die out quicker. Although any given material has its own internal damping, the damping of a structure is not straightforward or easy to assess, due to the joints, couplings, screws etc. present in it. Damping will be dealt with further in Section 3.2.3.
- Mass: low mass being economically desirable, allowing supporting walls to be slimmer and foundations to be simpler. On top of that and from a pragmatic point of view, low mass permits a higher degree of prefabrication to be achieved, since transportation from the factory to the construction site can be done in lorries; the latter not being possible in the case of analogous heavier elements, e.g. those made of concrete. Regarding floor vibrations, however, it can be stated as a general rule that the greater the mass, the better vibroacoustic performance, since the response of the floor to an impact force is lower in amplitude. Further analyses would nevertheless be needed when adding mass, as the fundamental frequency of the floor would change, resulting in the floor being excited by other types of loads present.
- Fundamental frequency, which is a function of the mass, the stiffness and, to some extent, the damping. Human response to floor vibrations is often assumed to be a result of the first natural frequency (referred here to as fundamental frequency). The description of criteria regarding serviceability in wooden buildings is presented in Section 2.5.3.

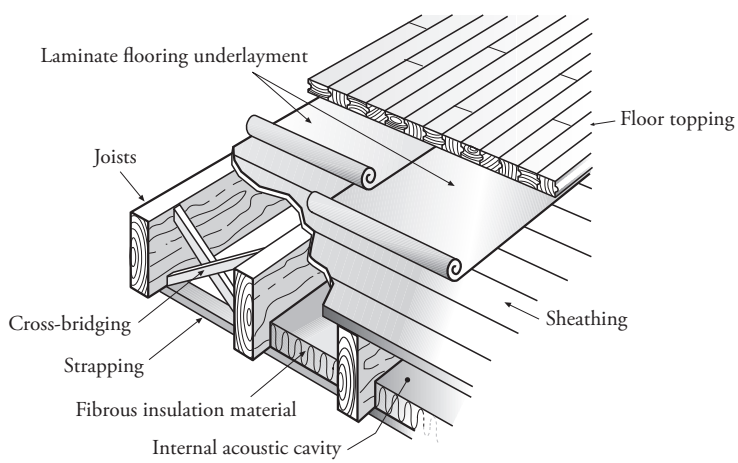

Figure 3.1: *Representative Swedish wood flooring system together with its main components.*

[2]A theoretical explanation of this matter is given in Section 3.2.2.

3.2 STRUCTURAL DYNAMICS – GOVERNING THEORY

Vibrations normally appear in systems subjected to time-varying forces, such as produced by people walking, jumping or running, which is often the case in dwellings. When analysing and dealing with such dynamic events, the magnitude of the force may not be as important as its frequency. Thus, it is of utmost importance to describe and analyse a vibratory signal both in the time domain (a magnitude being plotted versus the time), and in the frequency domain (a magnitude being plotted versus the frequency); see Figure 3.2. Fourier analysis methods, such as the Fast Fourier Transform (FFT), can readily make the shift from the time domain to the frequency domain, the opposite being done by applying the inverse FFT [78].

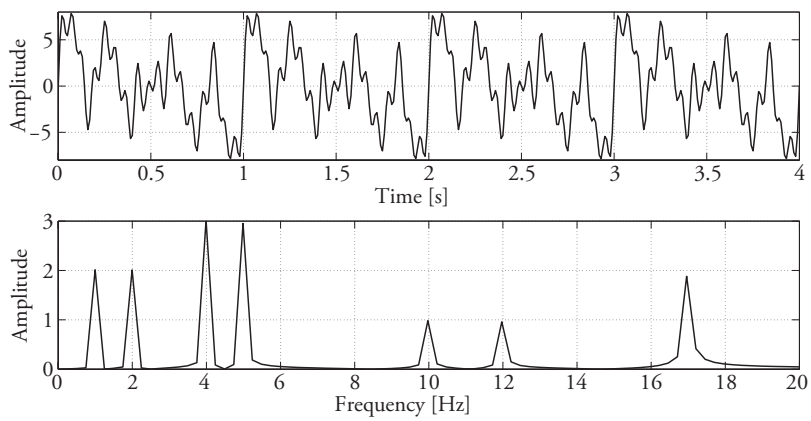

Figure 3.2: *Time series (above) and its representation in the frequency domain (below).*

In studying a structure, a modelling simplification can be made by discretising it, when possible. The degrees of freedom (DOFs) involved can be defined as the number of independent displacement components required to define the exact position of the system at any given time. Hence, it is straightforward to make the distinction between discrete systems, in which a finite number of DOFs is needed to describe them completely, and continuous systems, for which an infinite number of DOFs are needed for defining their position at any given time. Discrete systems lead to a system of ordinary differential equations, whereas continuous systems yield a system of differential equations with partial derivatives, often solved by use of the FE method, as it will be taken up further in Chapter 4. The theory presented hereafter is summarised from the account of it found in [79, 80], and only free vibration and the response to harmonic excitation are considered, as it suffices for providing a basic understanding. Furthermore, the herein presented theory assumes linearity, neglecting any non-linear behaviour of the structures[3]; such assumptions being valid for loads having magnitudes that are sufficiently low for the system in question (e.g. vibrations in buildings related to serviceability, as the ones dealt with in the thesis).

[3]Non-linearities could be present in the close vicinity of the application of the load, e.g. where the foot strikes the floor when walking, but they would not affect the global dynamic behaviour of the structure in question.

3.2.1 Single-degree-of-freedom systems

The easiest way to describe a dynamic system is by use of a single-degree-of-freedom (SDOF) system. The classical SDOF system is a mass-spring-damper system, which can be seen as representing a simplified floor structure subjected to human walking (i.e. a dynamic force). Considering the spring and the damper to both be massless, the mass to be a lumped mass and all the motions to be in the vertical direction, as shown in Figure 3.3, Newton's second law of motion represents the differential equation that describes the motion of the system:

$$m\ddot{u}(t) + c\dot{u}(t) + ku(t) = f(t), \tag{3.1}$$

$f_s(t) = ku(t)$ being the elastic force, $f_d(t) = c\dot{u}(t)$ the damping force (related to the velocity of the structure), c the viscous damping coefficient given in [N·s/m], $f(t)$ the time-dependent external force applied, $f_I(t) = m\ddot{u}(t)$ the inertial force of the mass, and u the only DOF necessary to describe the system. The displacements of the system, $u(t)$, can be easily obtained by solving Equation (3.1), supplementing it with the initial conditions that are involved.

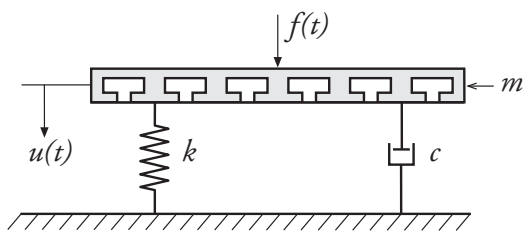

Figure 3.3: *Mass-spring-damper SDOF system.*

Undamped SDOF system

Although real structures always having damping effects, the solution to the undamped system has an important value theoretically. The solution to the undamped ($c = 0$) equation

$$m\ddot{u}(t) + ku(t) = f(t), \tag{3.2}$$

consists in a particular solution in which the system is subjected to harmonic loading, $u_p(t)$, and in a homogeneous solution in which no load is involved, $u_h(t)$, i.e.

$$u(t) = u_p(t) + u_h(t). \tag{3.3}$$

- The particular solution is arrived at through solving the equation

$$m\ddot{u}_p(t) + ku_p(t) = f_0 \cos(\omega t). \tag{3.4}$$

  The response of a system subjected to a harmonic force is also harmonic, and because of linearity and superposition, the response is the sum of the responses of the harmonic

components of the original forces, expressed as:

$$u_p(t) = \frac{u_{qs}}{1 - \left(\frac{\omega}{\omega_n}\right)^2} \cos(\omega t) = \frac{u_{qs}}{1 - \beta^2} \cos(\omega t) = u_{qs} R_d \cos(\omega t), \tag{3.5}$$

with $\beta = \omega/\omega_n$, $u_{qs} = f_0/k$ being the quasi-static displacement, $R_d = 1/(1 - \beta^2)$ referred to as the deformation response factor (or amplitude response) for an undamped SDOF, and $\omega_n = \sqrt{k/m}$ the undamped natural angular frequency involved.

- The homogeneous part of the solution stems from solving

$$m\ddot{u}_h(t) + ku_h(t) = 0, \tag{3.6}$$

its having the form

$$u_h(t) = A_1 \cos(\omega_n t) + B_1 \sin(\omega_n t). \tag{3.7}$$

Hence, by use of Equations (3.5) and (3.7), Equation (3.3) can be rewritten as

$$u(t) = u_{qs} R_d \cos(\omega t) + A_1 \cos(\omega_n t) + B_1 \sin(\omega_n t). \tag{3.8}$$

The constants A_1 and B_1 are determined by the initial conditions, i.e. the initial displacement and velocity of the SDOF system. Note that if the excitation frequency ω coincides with one of the natural frequencies of the system, infinite displacements are obtained (seen by substituting $\omega = \omega_n$ in R_d), i.e. resonance occurs, as it will be explained later on; see Figure 3.7.

Damped SDOF system

The solution to the damped ($c \neq 0$) SDOF, stemming from Equation (3.1), is

$$m\ddot{u}(t) + c\dot{u}(t) + ku(t) = f_o \cos(\omega t), \tag{3.9}$$

being also composed of both a particular and a homogeneous solution; see Equation (3.3).

- The particular solution is given as

$$u_p(t) = u_{qs} R_d(\omega) \cos(\omega t - \alpha) = u_{qs} \frac{1}{\sqrt{(1 - \beta^2)^2 + (2\zeta\beta)^2}} \cos(\omega t - \alpha), \tag{3.10}$$

$R_d(\omega)$ being the amplitude response for a damped SDOF, u_{qs} the quasi-static displacement, $\beta = \omega/\omega_n$, and α the phase response given by

$$\alpha(\omega) = \tan^{-1}\left(\frac{2\zeta\beta}{1 - \beta^2}\right), \tag{3.11}$$

where ζ, the viscous damping ratio, is defined as

$$\zeta = \frac{c}{c_{cr}} = \frac{c}{2m\omega_n}. \tag{3.12}$$

The critical damping c_{cr} is defined as the lowest level of viscous damping, one in which the mass exhibits no oscillation when displaced from the equilibrium; ζ is dimensionless and is usually expressed as a percentage. A system is classified as underdamped if $\zeta < 1$, as critically damped if $\zeta = 1$, and as overdamped if $\zeta > 1$.
One can then define the frequency response function (FRF) as the non-dimensional complex relationship of a system's input to its output. Some common FRFs that depend upon the input and the output considered are referenced to as follows: compliance (displacement/force), mobility (velocity/force), accelerance (acceleration/force), and mechanical impedance (applied force/velocity).

- The homogeneous part of the solution can be written as

$$u_h(t) = e^{-\zeta\omega_n t}\left[A_2\cos(\omega_D t) + B_2\sin(\omega_D t)\right], \tag{3.13}$$

the damped natural frequency being given as

$$\omega_D = \omega_n\sqrt{1-\zeta^2}. \tag{3.14}$$

The total response thus becomes

$$u(t) = u_{qs}R_d\cos(\omega t - \alpha) + e^{-\zeta\omega_n t}\left[A_2\cos(\omega_D t) + B_2\sin(\omega_D t)\right]. \tag{3.15}$$

The constants A_2 and B_2 are again determined by the initial conditions, i.e. the initial displacement and velocity of the damped SDOF. Note that the particular solution is controlled by the ratio $\beta = \omega/\omega_n$ (contained in R_d). Thus, if the loading frequency ω approaches the natural frequency of the system, ω_n, the solution is dominated by the damping in accordance with $u_p(t) \approx u_{qs}/(2\zeta)$ (see Section 3.2.2). The homogeneous solution, in turn, vanishes with increasing time, the system response being defined by just the particular solution after some time has passed, i.e. $u(t) \approx u_p(t)$; cf. Figure 3.4.

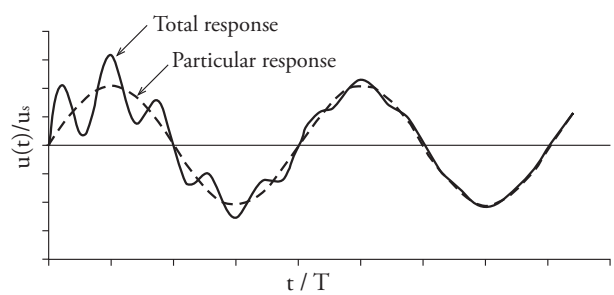

Figure 3.4: *Total response of a damped system subjected to a harmonic force, [79].*

3.2.2 Multi-degree-of-freedom systems

More than one DOF is normally needed in fact to describe a structure completely. It is possible, however, to create an approximate model of it, referred to as multi-degree-of-freedom

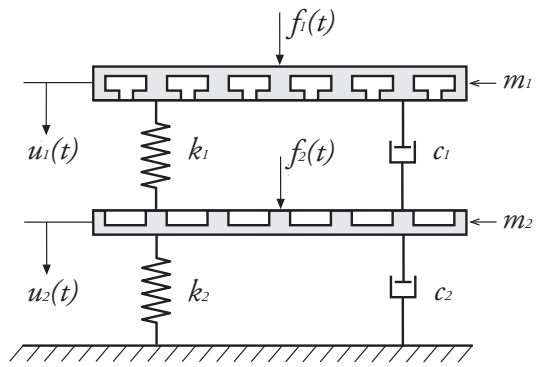

Figure 3.5: *A two-DOF system: a mass-spring-damper MDOF system.*

system (MDOF) with a finite number of DOFs by considering a finite number of massless elements and a finite number of node displacements, the mass being lumped on these nodes (see Figure 3.5, which can be seen as a floor-floating ceiling system).

Newton's second law of motion equation here yields the differential equation for an n-degree-of-freedom discrete system subjected to small displacements

$$\mathbf{M}\ddot{\mathbf{u}}(t) + \mathbf{C}\dot{\mathbf{u}}(t) + \mathbf{K}\mathbf{u}(t) = \mathbf{f}(t), \tag{3.16}$$

where n is the number of DOFs, $\mathbf{M} \in \mathbb{R}^{n\times n}$ is the mass matrix (symmetric and positive-definite), $\mathbf{C} \in \mathbb{R}^{n\times n}$ is the damping matrix, $\mathbf{K} \in \mathbb{R}^{n\times n}$ is the stiffness matrix (symmetric and whether positive or semi-positive-definite), $\mathbf{f}(t)$ is the external load vector containing the dynamic external forces and having the dimensions $\mathbb{R}^{n\times 1}$ and $\mathbf{u}(t)$ being the displacement vector with the dimensions $\mathbb{R}^{n\times 1}$. Equation (3.16) (both for the damped and undamped case) can be solved, for example, by means of the FE method, and comprises, as well as in the SDOFs, a part of the solution stemming from the homogeneous equation and another one from the particular, depending on the type of loading.

- Particular solution: the load and the corresponding displacements can be expressed, if harmonic (i.e. steady-state) loading is applied, as the following complex functions

$$\mathbf{f} = \hat{\mathbf{f}}e^{i\omega t} \qquad \text{and} \qquad \mathbf{u} = \hat{\mathbf{u}}e^{i\omega t}, \tag{3.17}$$

  $\hat{\mathbf{f}}$ and $\hat{\mathbf{u}}$ denoting the complex load and the displacement amplitude, respectively. The equation of motion can be expressed in the frequency domain, by just inserting Equations (3.17) into Equation (3.16), as

$$\mathbf{D}(\omega)\hat{\mathbf{u}} = \hat{\mathbf{f}}, \tag{3.18}$$

  $\mathbf{D}(\omega)$ being the frequency-dependent dynamic stiffness matrix given as

$$\mathbf{D}(\omega) = -\omega^2\mathbf{M} + i\omega\mathbf{C} + \mathbf{K}. \tag{3.19}$$

  For the sake of simplicity (as it gets too cumbersome), and also because the analysis is somewhat similar to the corresponding one of an SDOF, the step-by-step solution of the previous equations will be omitted here.

- Homogeneous solution: the undamped MDOF homogeneous solution of the undamped MDOF is extensively presented next, due to its theoretical value.

Undamped system: natural frequencies and modes of vibration

Modal analysis can be used to determine natural frequencies (those of free vibration) and the vibrational mode shapes (the spatial pattern of free vibration) of a structure. By taking the undamped system ($\mathbf{C} = \mathbf{0}$) described by Equation (3.16) and particularising it for the free vibrational case ($\mathbf{f}(t) = \mathbf{0}$), results in

$$\mathbf{M}\ddot{\mathbf{u}}(t) + \mathbf{K}\mathbf{u}(t) = \mathbf{0}, \tag{3.20}$$

with the initial conditions of $\mathbf{u}(0) = \mathbf{u}_0$ and $\dot{\mathbf{u}}(0) = \mathbf{v}_0$. The undamped modes satisfy an orthogonality relationship (i.e. they form an orthogonal basis) over the mass and stiffness matrices and thus uncouple the equations of motion, i.e. $\Phi^T\ \mathbf{M}\ \Phi$ and $\Phi^T\ \mathbf{K}\ \Phi$, with Φ being the modal matrix and $\mathbf{M}$ and $\mathbf{K}$ being diagonal matrices. This simplifies the dynamic analysis of MDOFs, since they can be effectively treated as a collection of SDOFs oscillators. The latter implies that the solution to Equation (3.20) can be expressed as a sum of the eigenmodes for its free vibration case as

$$\mathbf{u}(t) = \sum_{j=1}^{n} q_j(t)\phi_j, \tag{3.21}$$

with the amplitude deflected shape of the j-th mode ϕ_j being constant over time. The time variation of the displacements is described by the harmonic function

$$q_j(t) = A_n \cos(\omega_n t) + B_n \sin(\omega_n t), \tag{3.22}$$

A_n and B_n being constants of integration determined on the basis of the initial conditions. Equation (3.21) is referred to as the modal decomposition of $\mathbf{u}$(t). Combining Equations (3.21) and (3.22) and substituting them in Equation (3.20) yields

$$\left[-\omega_n^2\mathbf{M}\phi_j + \mathbf{K}\phi_j\right] q_j(t) = \mathbf{0}. \tag{3.23}$$

Equation (3.23) can be satisfied in two ways, either by the trivial solution $q_j(t) = 0$, meaning there to be no motion of the system, or through the natural angular frequencies ω_n and the modes of vibration ϕ_j satisfying the matrix eigenvalue problem

$$\left[\mathbf{K} - \omega_n^2\mathbf{M}\right] \phi_j = 0, \tag{3.24}$$

the quantities to determine being ω_n and $\phi_j(t)$, as the matrices $\mathbf{K}$ and $\mathbf{M}$ are known. This system of equations is homogeneous, its coefficient matrix being singular. Hence, it has a solution different from the trivial zero (no-motion), one of

$$\left|\mathbf{K} - \omega_n^2\mathbf{M}\right| = 0. \tag{3.25}$$

A polynomial of n order in ω_n^2 is obtained in expanding the determinant (called the characteristic equation or frequency equation), with n being the number of DOFs necessary to describe the system, its having n positive and real roots since both **M** and **K** are symmetric and positive-definite. The positive-definite property of **K** is assured for all structures supported in a way preventing rigid-body motion, and for **M** making sure that all masses are non-zero in each of the DOFs.

In solving the frequency equation, the n roots ω_n^2 determine the n natural frequencies ω_n of vibration. When a natural frequency ω_n is known, Equation (3.24) can then be solved to obtain the corresponding vector ϕ_j to within a multiplicative constant, referred to as the natural mode of vibration or the natural shape of vibration. Note that the eigenvalue problem does not fix the absolute amplitude of the vectors but simply the shape of the vector given by the relative displacements ϕ_j ($j = 1, 2, \ldots, n$). As many eigenvectors (ϕ_j) as eigenvalues (ω_n^2) exist.

In summary, when a structure is disturbed from its static equilibrium position and is allowed to oscillate without any external dynamic excitation, it vibrates with certain frequencies ω_n, i.e. the natural frequencies. Associated with each natural frequency is a modal shape of the structure, which can be defined as the deformed shape of the structure at the specific frequency involved (cf. Figure 3.6). A structure has an unlimited number of natural frequencies, these being a property of the structure, their in principle depending upon the mass and the stiffness as well as on their distribution. If the FE method is used to model the structure, it will have as many natural frequencies and corresponding mode shapes as there are DOFs. The natural frequencies of a damped system differ somewhat from the natural frequencies of the same system without damping. For lightly damped structures (which is normally the case for lightweight timber structures), however, the natural frequencies of the damped vibrations are approximately the same as the natural frequencies of the structure without damping [79]; cf. Equation (3.14).

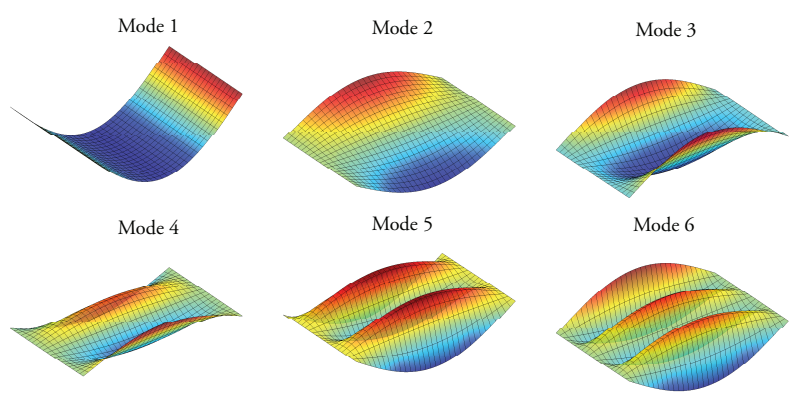

Figure 3.6: *Example of calculated modes of vibration (using the FE Matlab toolbox CALFEM [81]) of one of the floors dealt with in* ***Paper F****.*

Resonance: if a structure is subjected to a dynamic force having a frequency close to one of its natural frequencies, the response can be strongly enhanced, increasing its amplitude. Both the amplitude and the acceleration become very high then. This phenomenon is that of resonance. Without the presence of any damping, this amplitude gradually increases towards infinity. Some damping is, however, always present in structures (e.g. joints and micro-cracks) preventing both this crescent and uncontrolled oscillations from occurring [79].

It is of paramount importance to be aware and address accordingly the presence of resonances in the low frequency range, since the first few modes of vibration contain almost all of the vibration energy of the floor[4], making it vibrate excessively, and hence being most likely the cause for annoyance of inhabitants. Those resonance frequencies should ideally thus be considered in the design phase together with the usage the building will be built for, i.e. having in mind which loads will most often take place, so as to avoid their excitation. In Figure 3.7, the effects of various damping ratios on the resonant response in terms both of the amplitude response and the phase response are depicted. The amplitude response $R_d(\omega)$ shown on the vertical axis of the plot at the left is the ratio of the dynamic deformation to the quasi-static deformation, whereas the horizontal axis shows the ratio of the current excitation frequency to the natural angular frequency. As one can see, damping needs to be incorporated into the structure in order for resonant vibrations to be minimised.

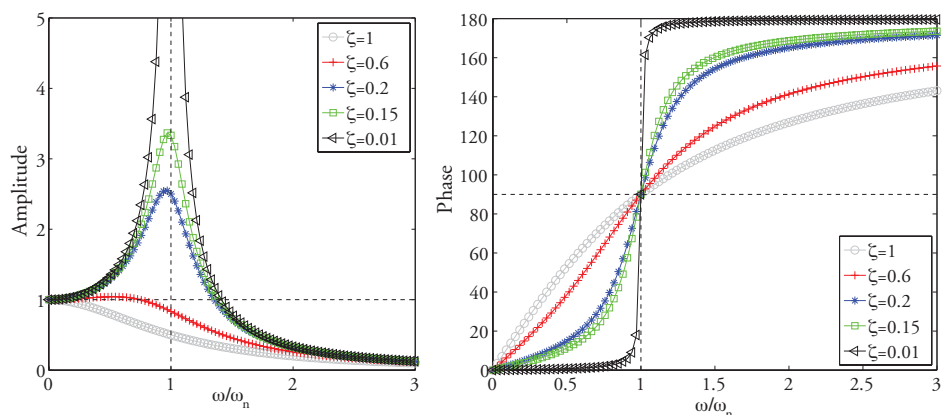

Figure 3.7: Amplitude response (left) and phase (right) of a resonant structure.

3.2.3 Damping

In many areas of civil engineering, wood is not considered to be a linear elastic material. In earthquakes analyses, for example, strains can be of such magnitude that non-linearities cannot be neglected. In the case under study of human-made vibrations or serviceability loads, however, strains are usually at a level such that an assumption of linear elasticity applies. Damping,

[4]These first modes of vibration typically lie below 50 Hz, where the extended frequency range of the building acoustic regulations start (see Section 2.5.1) and hence their effect is rarely accounted for in the norms.

since it generally plays an important role in terms of dynamic responses that occur, is thus usually applied to the linear elastic material under such conditions.

In order to have a floor which is light in weight, provides open-space and yet is not that prone to vibration, damping needs to be incorporated into its makeup[5]. Damping is, in general terms, the reduction of a vibration response due to the irreversible conversion of mechanical energy into other forms of energy. It arises not only from the internal material damping itself, but also from other sources such as friction in cracks and joints. The complexity of the physical phenomena involved and the mechanisms that cause damping, makes damping difficult to describe by means of an accurate unique model. Damping itself may be described and introduced into models either via mathematical models[6], physical mechanisms[7], or else rheological models[8]. Likewise, although certain analytical models exist to evaluate damping, so as to be able to include it in the overall calculations, damping parameters are generally estimated on the basis of measurement data from similar existent structures or by carrying out new measurements on similar structures[9]. Albeit damping mechanisms are non-linear, linear damping models often suffice for small oscillations and slight damping [83], which are the types of cases under study in the present thesis. Herein, a brief explanation account of the mathematical way of modelling damping used in **Paper A**, **Paper B** and **Paper C** is provided.

Rayleigh damping

In **Paper B**, **Paper C** and **Paper E**, damping is modelled, for the wooden parts involved, by use of Rayleigh damping, which can be used for both transient and steady-state analyses. It is an appropriate idealisation if the assumption that both the mass and the stiffness are evenly distributed throughout the structure. Hence, in determining the classical damping matrix, damping ratios are used considering that the damping matrix is a linear combination of the mass matrix and the stiffness matrix (see Figure 3.8), in accordance with

$$\mathbf{C} = a_o\mathbf{M} + a_1\mathbf{K}\,, \tag{3.26}$$

the damping ratio (see Equation (3.12)) for the n-th mode being given by

$$\zeta_n = \frac{a_0}{2}\frac{1}{\omega_n} + \frac{a_1}{2}\omega_n. \tag{3.27}$$

[5]For example, inclusion of rubber-like materials such elastomers in the junctions is a common technique used in junctions of wooden buildings. In Section 2 of **Paper C**, a literature review about the use of these elastomers in timber buildings is compiled, whereas in Section 3, the governing theory of linear viscoelasticity is presented.

[6]Viscous, hysteretic, proportional (Rayleigh) and visco equivalent damping [82].

[7]Material (inherent materials of a structure have different damping characteristics and contribute in varying degrees to the total damping of the structure), structural (arising from connections between surfaces of different materials and in the junctions due to friction) or fluid damping (masses vibrating in fluid media) [82].

[8]Kelvin-Voigt, Maxwell, Biot model, etc. [82].

[9]Estimation of damping via measurements either in the time domain or the frequency domain can be done using several methods [82], namely logarithmic decrement, envelope fitting, phase plot diagrams, resonant amplification, half-power bandwidth, resonant energy loss per cycle, identification of damping parameters from the FRF, phase angle methods, laboratory viscoelastic methods, acoustic methods, amid others.

This damping ratio is shown to not be constant for all modes of vibration. If the damping ratios ζ_i and ζ_j for the i-th and j-th modes, respectively, can be assumed to have the same value, the constants a_0 and a_1 can be calculated as

$$a_0 = \zeta \frac{2\omega_i \omega_j}{\omega_i + \omega_j} \qquad \text{and} \qquad a_1 = \zeta \frac{2}{\omega_i + \omega_j}, \tag{3.28}$$

In applying this procedure to a practical problem, i and j with specified damping ratios should be chosen so as to ensure that reasonable values for the damping ratios are obtained for all modes that contribute significantly to the response [79]. The latter is due to the fact that for practical engineering analyses, it would be practical to consider simplifying assumptions in selecting constant damping ratios for all significant modes for the structure under study, but modal mass participation normally decreases with increasing mode number.

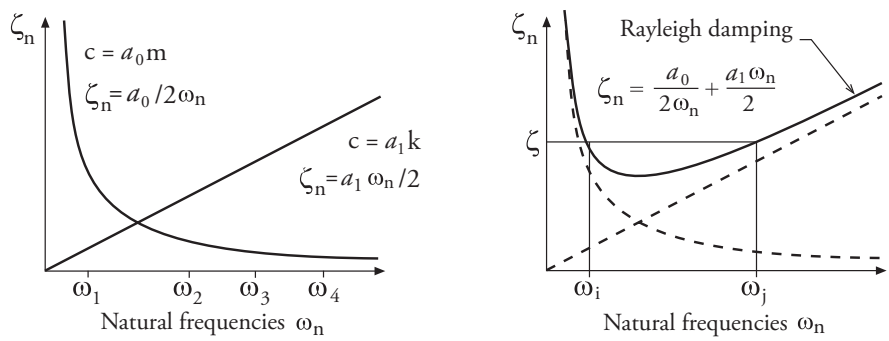

Figure 3.8: *(Left) Mass and stiffness proportional damping, (right) Rayleigh damping, [79].*

Although the assumption that the damping is proportional to the mass and to the stiffness matrices has no rigorous physical basis, it has been shown to provide fairly good approximations. Also, in practice, the damping distribution is rarely known in sufficient detail to warrant use of any other, more complicated model [9]. In general, it is more important to damp the lower frequencies due to their being more difficult to damp, and also because the annoyance in lightweight buildings is mostly caused by low frequencies. As stated in the formula, a_0 is more important for lower modes, whereas a_1 is important mainly for the higher frequencies (i.e. the lower frequencies being damped by the mass, whereas the higher frequencies are damped by the stiffness).

Structural damping

A loss factor that takes account of propagating waves in steady-state analyses can be used to introduce rate-independent linear damping into the system. Accordingly, in **Paper A**, structural damping was assigned to the elastomer blocks in the form of a loss factor due to the lack

of material properties at that point[10]. It is defined [79] as

$$\eta = \frac{1}{2\pi}\frac{E_D}{E_{S_0}} = \frac{1}{2\pi}\frac{\pi c\omega u_o^2}{k\frac{u_0^2}{2}} = \frac{c\omega}{k}, \tag{3.29}$$

where in a steady-state analysis, the energy dissipated in the form of viscous damping in a given cycle of harmonic vibration, is denoted as $E_D = \pi c\omega u_o^2$ and the strain energy as $E_{S_o} = ku_0^2/2$, c being the damping constant and u_o the amplitude of motion. The relationship between structural damping and Rayleigh damping in steady-state analyses can be expressed as

$$\eta = 2\zeta\frac{\omega}{\omega_n}, \tag{3.30}$$

and when the exciting frequency is equal to the natural angular frequency, it reads

$$\eta = 2\zeta. \tag{3.31}$$

For the general case of an MDOF, Equation (3.29) can be written as:

$$\mathbf{K}\eta = \omega\mathbf{C}, \tag{3.32}$$

And by inserting Equation (3.32) into Equation (3.19), it results in

$$\mathbf{D}(\omega) = -\omega^2\mathbf{M} + (1 + i\eta)\mathbf{K}. \tag{3.33}$$

The imaginary part of the latter equation is referred to as the structural damping matrix. The limitation of this damping model is that it cannot be used in the time domain, for which the Rayleigh damping can be employed instead.

3.3 FLOOR VIBRATION MEASUREMENTS

As pointed out in previous chapters, product development in wooden buildings is mainly done based on engineers' experience and knowledge gained through analysing measurements performed in already existent constructions. In this section, a brief overview of the most prominent excitation methods, as well as measurement techniques, used nowadays in floor vibratory measurements, is presented.

3.3.1 Excitation sources

When performing vibratory measurements, different excitation sources can be employed to set the structure into movement and thus vibrations to propagate. The most common excitation sources utilised to perform vibration measurements are listed next.

[10]The latter approach of adding structural damping and employing a linear elastic material model was found in **Paper A** to not be accurate enough in the case of the elastomers. Accordingly, in **Paper C**, a method for characterising the resilient strips often used at the junctions of wooden buildings, in terms of their frequency dependent linear viscoelastic material properties, was developed.

Standardised sources

ISO tapping machine: the device (see Figure 3.9c) consists of five steel hammers, each of them hitting the floor with two taps per second, which gives it ten taps per second altogether. This means one hit every 0.1 second. The machine was developed before 1994, when the construction of wooden multi-storey houses in Sweden was still prohibited. In [17], however, it was pointed out that the shape of the low frequency spectrum produced by the tapping machine closely resembled that of a live walker on a timber floor; the latter conclusions agreeing also with those drawn in [84, 85], where it was stated that there is no need to abandon the use of the ISO tapping machine as excitation source in the norms, but rather to modify both the test procedures as well as enlarge the frequency range of analysis towards the lower end. Nevertheless, other investigations [26, 86–90] highlighted that in wood flooring systems, the amplitude of the input force of the tapping machine, in the low frequency range, is lower than that produced by daily activities, such as people walking and heel impacts; see Figure 3.9a. The latter highlights the need for the norms to be revisited. It should be ensured that the sources employed have a realistic frequency content and that the evaluation methods correlate better with subjective judgements. To that end, it would be beneficial to include in the evaluation methods the sound pressure level peaks in the room below (their often occurring in the third-octave band containing the first natural frequency of the structural system in question [17]) and which are normally outside the frequency range of analysis nowadays.

Nevertheless and until new methods are developed and other excitation sources introduced in the standardised evaluation procures, there is a need for accurate modelling this excitation source if reliable predictions according to the norms are to be achieved. First attempts to do so, both from an analytical point of view as well as making use of the FE method, have been presented in [91–96]; however not enough accurate results being achieved yet. In the appended **Paper E**, preliminary guidelines on how to implement the tapping machine into commercial FE software using a developed time-efficient frequency domain method are presented, as well as a literature review on the topic.

Japanese ball: this hollow heavy-soft spherical impact source (cf. Figure 3.9d) is made of natural rubber and polybutadiene and is described in terms of the Japanese standard [97]. It weights 2.55 kg and is 183 mm in diameter. Its properties when it is dropped from a height of 1 meter are similar to those of the relevant human impacts (cf. Figure 3.9b), allowing it to be used for floor vibration measurements for frequencies below approximately 70 Hz [90].

Rubber tire: the Japanese standard [98] describes a method in which a 3 kg rubber tire (see Figure 3.10a) is dropped from a height of 300 to 900 mm, producing a peak force of 1250 to 2400 N. This method was adopted to simulate children jumping and to study the impact sound insulation in thin concrete floor constructions. For further information, see [99].

The lack of standardised vibration requirements is closely coupled with the sparseness of systematised measuring methods and sources. Certain non-standardised methods for assessing vibrations in floors aiming at obtaining knowledge of various types have come about in the recent years, the most prominent of these being those listed in the following.

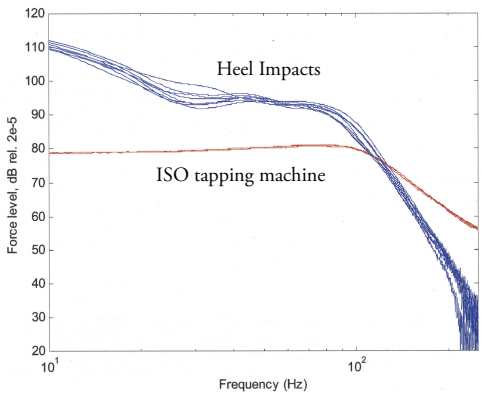

(a) Force spectra of repeated heel impacts and repeated impacts produced by the tapping machine, [90].

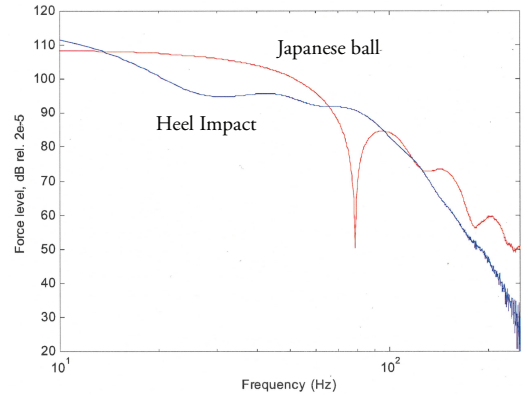

(b) Force spectra of the Japanese ball and a heel impact, [90].

(c) Tapping machine.

(d) Japanese ball.

Figure 3.9: *ISO tapping machine and Japanese ball. A plot of their force spectra against that of a heel impact is also shown.*

Non-standardised sources

Shaker: producing a continuous excitation is sometimes preferred in order to study the result spectrum with a high degree of resolution, the applied load of which can be measured by means of force transducers. In broad terms, a shaker (see Figure 3.10b) consists of a loudspeaker which is fed with a signal and is connected to the floor by a connecting rod (called a stinger), which in turn sets the floor into motion when it starts playing the signal and setting the membrane into motion. The stinger possesses a high degree of axial stiffness and a low bending stiffness, so that it can be considered to represent a point load on the floor, without there being any rotatory loading. The attachment needs to be carefully made so that no reaction forces from the main body of the shaker will be transmitted and so no reaction forces from the floor are transmitted back. An electro-mecanical shaker, that can generate a broad range of different types of signals (sine, stepped sine, pure random, pseudo-periodic random, burst random and chirp [100–102]), depending upon the needs that arise, gives a better (higher) signal-to-noise ratio than a tapping machine or an impact hammer do. A shaker is commonly used for modal analysis measurements, the equipment involved being expensive, the time for its installation being normally high, and typically needing a skilled operator to implement it [101]. Specific-

ally, shaker excitation was used in the appended **Paper F** to get the dynamic properties of the wooden floors dealt with there and in **Paper G** to perform the back-to-back calibration of the accelerometers developed.

Impact hammer: this consists basically of a hammer with a force transducer placed on its tip; see Figure 3.10c. The tip can be changed depending upon the material being tested (using tips of differing stiffness), since different tips provide different frequency contents of the excitation. Hammer testing is commonly employed for modal analysis measurements, since it is quick, easy to use and relatively cheap. The convenience of this technique is attractive, its requiring very little hardware (the impact hammer itself and a single accelerometer suffice) and the measurements it provides are not time-consuming at all. Hammer testing is decried mainly because of its lack of repeatability, its low signal-to-noise ratio, the relative low control over the frequency content of the excitation and also because local damage and non-linearities due to the hammer blows could also occur. Moreover, the signal post processing techniques involved in hammer testing are more complex than the corresponding ones for the shaker excitations [82, 101]. In **Paper D**, a hammer excitation was performed to get the dynamic properties of the T-junctions under investigation.

(a) Rubber tire.

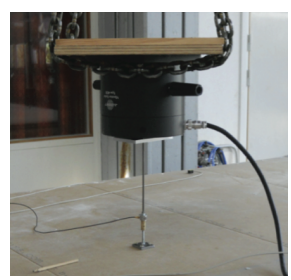

(b) Shaker.

(c) Impact hammer.

Figure 3.10: *Various excitation sources.*

3.3.2 Measurement techniques

Experimental modal analysis (EMA)[11]**:** when studying the vibroacoustic behaviour of a structure, EMA is a technique often used to obtain its dynamic properties (namely those of eigenfrequencies, eigenmodes and damping ratios). In the appended **Paper D**, EMA was employed during the process of setting up the numerical predictive tools for the T-junctions under study there. Measurements were done in the real specimens in order to get accurate input data for subsequent calibration of the FE models. Likewise, EMA was also carried out in **Paper F** so as to get reliable dynamic properties of the wooden floors under study. In practice, EMA measurements could be divided into three main phases:

[11] Do not confuse with operational modal analysis (OMA), a different technique which aims at identifying the modal properties of a structure based on vibration data collected when the structure is under its operating conditions, i.e. without any applied artificial initial excitation.

1. Experiments: design of the experimental setup. EMA involves measuring and analysing the dynamic response of a structure when excited by a load (either a continuous one created by a shaker or an impact one induced by a modal hammer). The response to the load created by the excitation source in question is recorded by sensors, which generally are accelerometers; these being placed strategically at one or more spots for registering the vibrations. Likewise, issues like boundary conditions (BC) and acquisition parameters (viz. frequency band and resolution, number of records and averaging to reduce leakage and non-linearities, window selection, etc.) must be thoroughly addressed here.
2. Processing of the measured data: the FRFs obtained for each excitation point measurement location pair, give the structure's magnitude and phase response over the frequency range of interest. After the measurements are finished, the signals are post-processed with data acquisition hardware and software that are adequate for the purpose in question. To that end, a variety of extraction algorithms are used to identify the modal parameters from the FRF data, through fitting the measurement data to appropriate mathematical expressions. This is done by minimising the squared error (or squared difference) between an analytical function and the measured data[12]. Since EMA is a linear theory, the FRFs obtained are also linear. Hence, the validity of the FRFs is assessed by the coherence function, γ^2; the closer its value is to 1, the better the match between the input and output signals is. Values lower than 0.75 are normally considered poor, due to this being a sign of noise in the measured input or output signal, such values thus being disregarded [82].
3. Validating the model: the extracted modal model must be assessed for its physical representation of the dynamical behaviour of the structure in the studied frequency band.

Thus, the relationship (i.e. FRF) between the input **F** (excitation force) and the output **X** (vibration response[13]) of a linear system is given by

$$\mathbf{X} = \mathbf{H} \cdot \mathbf{F} \qquad \text{i.e.} \qquad \begin{bmatrix} X_1 \\ X_2 \\ \vdots \\ X_n \end{bmatrix} = \begin{bmatrix} H_{11} & H_{12} & \dots & H_{1n} \\ H_{21} & H_{22} & \dots & H_{2n} \\ \vdots & \vdots & \vdots & \vdots \\ H_{n1} & H_{n2} & \dots & H_{nn} \end{bmatrix} \begin{bmatrix} F_1 \\ F_2 \\ \vdots \\ F_n \end{bmatrix} \tag{3.34}$$

the H_{ij} terms of the full frequency response matrix, $\mathbf{H}(\omega)$, being defined as

$$H_{ij}(\omega) = \frac{X_i(\omega)}{F_j(\omega)} \tag{3.35}$$

where $X_i(\omega)$ is the Fourier transform of the time response $x_i(t)$ at location (i.e. DOF) i, and $F_j(\omega)$ is the Fourier transform of the time excitation $f_j(t)$ at location j.

In the EMA measurements performed in the frame of this project, the SIMO protocol was used, in terms of which the single input was that of the excitation (impact hammer in **Paper D** and shaker in **Paper F**) and the multiple output was that of the MEMS accelerometers

[12] For more information regarding modal parameter extraction algorithms, see e.g. [100, 103].

[13] As advanced in Section 3.2.1, the FRF is called accelerance if the vibration response is measured in terms of acceleration, mobility if the velocity is used and compliance if the displacement is considered instead.

employed (those developed as described in **Paper G**). When obtaining the FRFs for SIMO[14], different calculation schemes (estimators) are available in order to optimise the quality in the given measurement situation of a system in the frequency domain (presence of noise, frequency resolution, etc.). In situations where the output of the system is expected to be noisier than the input, a so-called FRF H_1 (the most common estimator) is used, defined as the ratio of the cross-spectral density in the frequency domain of the input $f(t)$ and the output $x(t)$ –denoted as S_{fx}[15]– by the auto-spectral density in the frequency domain of the input $f(t)$ –denoted as S_{ff}–. In turn, if the input is believed to be noisier (i.e. it is necessary to eliminate, by averaging, the influence of uncorrelated noise at the input), the so-called FRF H_2 is utilised instead, its being defined as the ratio of the input auto-spectra of the output response S_{xx} and the cross-spectrum between output and input S_{xf}. Other less common estimators for the applications dealt with here are H_v, H_{eV}, H_{iV}. For more information regarding this issue, see [103].

Theoretically, it does not matter whether the FRFs come from an impact test or a shaker test, due to reciprocity. The only difference is that an impact test generates one of the rows of the FRF matrix $\mathbf{H}(\omega)$, whereas the shaker test yields the columns instead. Likewise, from a theoretical point of view, only one row or one column of the FRF matrix is required to establish a modal model; however it does seldom suffice from a practical standpoint, since that would imply that the chosen reference DOF has information for all excited modes in the frequency range of interest (i.e. it is never a nodal point). Bare in mind that in order to eventually calibrate (scale) the modal model, the driving-point measurement (i.e. the measurement where both the excitation and the response is at the same DOF), needs to be included. All in all, in order to assure that all modes are properly included in the information contained in $\mathbf{H}(\omega)$ and that quality data is acquired, more measurements considering several reference DOFs are normally performed.

[14] The estimation of the FRFs in the case of MIMO -multiple inputs multiple outputs- is a little less straightforward due to the coupling between the different excitations employed, [104].

[15] The formulation for cross-spectrum between input and output used here is: $S_{fx} = (1/N) \cdot \sum(F^* X)$, with F* being the complex conjugate of the input spectrum, X the spectrum of the output and N the number of averages (observations). The other cross-spectra and auto-spectra are defined in the same fashion accordingly.

4

Prediction tools

The costly process of using test buildings is common, however the measurement results obtained are not directly applicable to buildings of slight different construction [18]. Likewise, product development based on engineers' experience remains a common way to deal with vibroacoustic issues. Prediction models, despite being highly useful for the designing of new buildings with regards to preventing the need of severe and costly changes in the aftermath of construction, are still very much lacking today. Gaining an adequate understanding of the dynamic behaviour of multi-storey lightweight buildings, especially at low frequencies, requires the use numerical models that represent the geometry of the buildings in great detail. This is due to the fact that small structural modifications can have strong effects on the vibration transmission paths. In the present chapter, an overview of existing methods for prediction of vibroacoustic problems is discussed first. The chapter then delves deeply into the FE method, the tool used in the publications contained in the thesis to gain knowledge and develop predictive models.

4.1 PREDICTIVE METHODS IN VIBROACOUSTICS

Depending on the problem at hand, different methods for solving the equations describing the dynamic phenomena involved can be distinguished. The choice of one or another lies in various factors including the complexity of the system, the boundary conditions (BC) involved or the frequency of interest, as sketched in Figure 4.1.

4.1.1 Analytical algorithms and multibody oscillators

Analytical algorithms in form of equations with exact solution have been developed and exist to solve specific well-defined (and most often, fairly simple) problems. Likewise, when a structure can be simplified resembling a calculation model that involves discrete springs (either tension, compression, torsional or bending springs), dashpots and individual rigid bodies (characterised by their position, mass and moments of inertia and centrifugal moments), one is creating

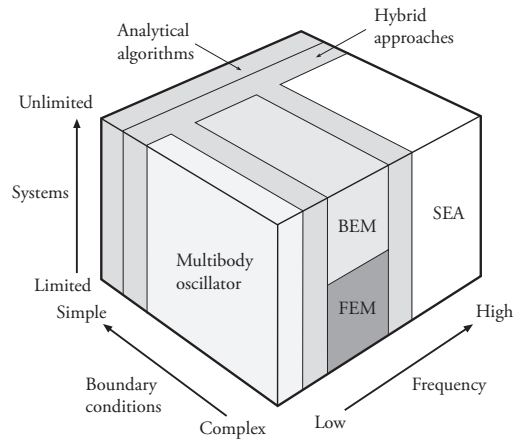

Figure 4.1: *Prediction Methods [105].*

the so-called multibody oscillator[1]. The way to handle these systems and solve the equations governing the problem at hand can be seen, for example, in [79].

4.1.2 Boundary element method

The boundary element method (BEM) has lately emerged as a powerful alternative to the FE method in certain applications. As opposed to FEM, where all the domain is discretised, the partial differential equations (PDE) defining the problem in question are approximated, using BEM, by use of integral equations only at its boundaries (for linear problems). This makes it especially suitable for problems with infinite or semi-infinite domains. However, even though only the finite surface of the infinite domain has to be discretised, the solution at any arbitrary point of the interior domain can eventually be retrieved after having determined the unknown boundary data. The dimension of the problem applying BEM is hence reduced one order; consequently, there is less unwanted information and the computer calculation time and storage required are also reduced when compared to FEM. BEM is particularly useful for problems that require re-meshing, as it is easier to change the mesh than when using FEM. Furthermore, BEM is advantageous for problems where stresses change rapidly, since the calculations involved are accurate, as there are no approximations imposed on the solution in the interior domain points. One of its main drawbacks, however, is the need of knowing "fundamental solutions" (i.e. Green's functions) to the application being dealt with, in order to solve the integral equations. These solutions must be developed beforehand. Moreover, the accuracy of BEM is poor compared to FEM for analyses of three-dimensional thin shell-like structures, due to the large surface-to-volume ratio and the close proximity of nodal points on either side of the structure thickness. This causes inaccuracies in the numerical integrations. Its application is mostly restricted to the lower end of the spectrum. For more information about BEM, see [106–109].

[1] SDOFs and MDOFs have been addressed thoroughly in Chapter 3.

4.1.3 Statistical energy analysis

Statistical energy analysis (SEA), introduced in the 1960s [110], is another method for predicting the transmission of sound and vibration through complex structural acoustic systems by means of statistical approaches using energy as the primary variable. In order to predict vibroacoustic behaviour using SEA, a system is divided and represented in terms of two or more smaller, simply identifiable and interconnected subsystems (typically plates, shells, beams and acoustic cavities characterised by the type of waves expected to propagate within them). Having broken down the complete system into smaller units, SEA relies on the fact that the mean power exchanged between two subsystems is proportional to the difference of modal energies. The aforementioned proportionality constant, in a way describing the energy flow between subsystems, is described by the coupling loss factor (CLF). Knowing the power input to the system, a set of equations can be derived from the power balances of the subsystems, such that the only unknowns of the problem are their averaged energies. These power flow equations are valid if the subsystems are reverberant, and therefore the pressure or vibration field in them can be considered to be diffuse. The hypotheses SEA must satisfy in order to analyse systems with more than two subsystems are [111]: (i) the forces applied must be statistically independent in order to have uncorrelated modes of vibration (i.e. the external forces do not excite a particular mode as the excitation has components at all frequencies), (ii) there is equal probability of modes occurring within a certain frequency range (this guaranteeing the assumption of the presence of a diffuse field), (iii) equipartition of modal energy in a subsystem as well as incoherent modal response between modes in the coupled subsystems (i.e. no dominance of any mode in particular) and (iv) weak (or light) coupling between the different subsystems involved (i.e. the exchanged energy is small as compared with the internal dissipation).

Solving vibroacoustic problems with SEA has many advantages [112], such as low computational cost, robustness against small parameter changes and working directly with the averaged energy, which is often required for eventually computing the quantity of interest (accelerations, velocities...). However, the hypotheses listed above in which SEA rely on are not always satisfied in real problems, and are definitely not fulfilled in the low frequency range, where the interest lies regarding wooden buildings. The absence of a diffuse field due to low modal density makes SEA only applicable to mid and high frequency problems, where the modal density is high and the wavelengths are small when compared to the characteristic length of the problem[2]. Hence, SEA was not used in the investigations reported in the thesis. For more information about SEA, see [91, 110, 111, 113].

4.1.4 Hybrid methods

Hybrid methods combining FEM-BEM ([106, 114]) or FEM-SEA ([115–117]) can also be found to extend the frequency range of prediction by combining the strengths of both methods, which has proven powerful for the applications that were developed. However, the FEM-SEA combination has not been thoroughly investigated yet for application to wooden

[2] As mentioned in Section 2.5.2, the prediction standards EN 12354:2000 are based on SEA, but they often result in inaccurate predictions for wooden elements.

buildings. In line with this, the *WoodWisdom-Net* project *Silent Timber Build* [41] ultimately aims at combining both methods to create predictive tools over the whole frequency range.

In the present thesis, intensive use of the FE method was made in efforts to seek and develop prediction tools for timber buildings, specifically as provided by the FE package *Abaqus*, a software for FE analysis commercialised by *Dassault Systèmes* [9]. The main reason behind this choice with respect to other methods was that the FE method is more established and commercially developed. And since the prediction tools to be developed are ultimately intended to be used by engineers and consultants, they are more prone to use a well-established computer program rather than venture into new, more cumbersome methods (such as BEM at this stage of development). Furthermore, the FE method has proven to be a robust method to address low frequency problems of the sort of those dealt with herein (as aforementioned, the accuracy of BEM is poor compared to FEM for analyses of three-dimensional thin shell-like structures). In the subsequent sections, a thorough theoretical background of the FE method is presented.

4.2 FINITE ELEMENT METHOD

PDEs arise in the mathematical modelling of many engineering problems. The analytical solutions of PDEs are often either impossible or impracticable to obtain by use of classical analytical methods. The FE method is a numerical approach by which boundary value differential equations, both linear and non-linear, can be solved in an approximate manner.

In broad strokes, one can say that the differential equation, or equations describing the physical problems considered, are assumed to hold over a particular region of the structure under study (1D, 2D or 3D regions). This region is divided into smaller parts (finite elements), and what is usually a polynomial approximation of the solution for each such element (as regards acceleration, velocity, temperature, etc.) is then sought. The assembly of all the elements involved is called a FE mesh. The correct choice of elements for a particular simulation is essential if accurate results at a reasonable computational cost are to be obtained. The elements are assembled according to the geometry using a topological description of element connections to obtain a solution for the entire region, which eventually enables one to obtain an approximate solution for the body as a whole [118]. This procedure will be explained in theoretical terms in the sections that follow. For a broader discussion of the FE method, see [118, 119].

FE formulation of linear elasticity: the differential equations defining the problem under study, together with the BCs applying to the region of validity, or what is termed as strong formulation of the problem, is first transformed into a finite set of algebraic equations that hold across the region of interest, this being called the weak formulation of the problem in question. The algebraic approximations of all the small regions involved (the finite elements) are assembled by use of certain mathematical manipulations, so as to obtain the FE formulation of the problem, as explained in the following. First, derivations are done for the structural domain, and then for the acoustic domain, the coupling between both domains also being described.

4.2.1 Structural domain

Strong formulation

For 3D problems and assuming small deformations, the differential equations of motion of a body as given by Newton's second law, are

$$\tilde{\boldsymbol{\nabla}}^T \boldsymbol{\sigma} + \mathbf{b} = \rho \frac{\partial^2 \mathbf{u}}{\partial t^2}, \tag{4.1}$$

where $\boldsymbol{\sigma}$ is the vector representing the stresses, $\mathbf{b}$ the body force vector, ρ the material density, $\mathbf{u}$ the displacement vector, t the time, and $\tilde{\boldsymbol{\nabla}}^T$ a differential operator matrix, given as

$$\tilde{\boldsymbol{\nabla}}^T = \begin{bmatrix} \frac{\partial}{\partial x} & 0 & 0 & \frac{\partial}{\partial y} & \frac{\partial}{\partial z} & 0 \\ 0 & \frac{\partial}{\partial y} & 0 & \frac{\partial}{\partial x} & 0 & \frac{\partial}{\partial z} \\ 0 & 0 & \frac{\partial}{\partial z} & 0 & \frac{\partial}{\partial x} & \frac{\partial}{\partial y} \end{bmatrix}; \quad \boldsymbol{\sigma} = \begin{bmatrix} \sigma_{xx} \\ \sigma_{yy} \\ \sigma_{zz} \\ \sigma_{xy} \\ \sigma_{xz} \\ \sigma_{yz} \end{bmatrix}; \quad \mathbf{b} = \begin{bmatrix} b_x \\ b_y \\ b_z \end{bmatrix}; \quad \mathbf{u} = \begin{bmatrix} u_x \\ u_y \\ u_z \end{bmatrix}. \tag{4.2}$$

Carrying out the matrix multiplications yields the three differential equations of motion:

$$\begin{aligned} \frac{\partial \sigma_{xx}}{\partial x} + \frac{\partial \sigma_{xy}}{\partial y} + \frac{\partial \sigma_{xz}}{\partial z} + b_x &= \rho \frac{\partial^2 u_x}{\partial t^2} \\ \frac{\partial \sigma_{yx}}{\partial x} + \frac{\partial \sigma_{yy}}{\partial y} + \frac{\partial \sigma_{yz}}{\partial z} + b_y &= \rho \frac{\partial^2 u_y}{\partial t^2} \\ \frac{\partial \sigma_{zx}}{\partial x} + \frac{\partial \sigma_{zy}}{\partial y} + \frac{\partial \sigma_{zz}}{\partial z} + b_z &= \rho \frac{\partial^2 u_z}{\partial t^2}. \end{aligned} \tag{4.3}$$

At the surface boundary of the body ($\mathbf{n}$ being a normal vector pointing outwards the body), the traction vector $\mathbf{t}$ must fulfil the natural BCs along a surface Γ_h, as well as the essential BCs (the prescribed displacements $\mathbf{g}$) along the boundary, denoted as Γ_g, where

$$\mathbf{t} = \boldsymbol{\sigma}\mathbf{n} = \begin{bmatrix} \sigma_{xx} n_x + \sigma_{xy} n_y + \sigma_{xz} n_z \\ \sigma_{yx} n_x + \sigma_{yy} n_y + \sigma_{yz} n_z \\ \sigma_{zx} n_x + \sigma_{zy} n_y + \sigma_{zz} n_z \end{bmatrix} \quad \text{on } \Gamma_h, \tag{4.4}$$

$$\mathbf{u} = \mathbf{g} = \begin{bmatrix} g_x \\ g_y \\ g_z \end{bmatrix} \quad \text{on } \Gamma_g. \tag{4.5}$$

The differential equations (4.3) together with the BCs given in Equations (4.4) and (4.5), and the region of interest in which the equations hold, represent the so-called strong formulation of the problem in question.

Weak formulation

In order to derive the weak formulation of the FE problem, a time independent weight vector $\mathbf{v}$ is introduced. The weak form is a variational statement of the problem in which one integrates against the test function $\mathbf{v}$. This has the effect of relaxing the problem, where instead of finding an exact solution everywhere, a solution that on the average satisfies the strong formulation over the domain in question is sought. A solution of the strong form also satisfies the weak form, the two being identical [118]. The weight function has the following form:

$$\mathbf{v} = \begin{bmatrix} v_x & v_y & v_z \end{bmatrix}^T . \tag{4.6}$$

Multiplying the Equations (4.3) in the order stated by v_x, v_y and v_z respectively, and integrating the expressions over the volume V, yields

$$\underbrace{\int_V \mathbf{v}^T \rho \ddot{\mathbf{u}} \mathrm{d}V}_{\text{(I)}} = \underbrace{\int_V \mathbf{v}^T \tilde{\boldsymbol{\nabla}}^T \boldsymbol{\sigma} \mathrm{d}V}_{\text{(II)}} + \underbrace{\int_V \mathbf{v}^T \mathbf{b} \mathrm{d}V}_{\text{(III)}} . \tag{4.7}$$

Integrating by parts through applying the Green-Gauss theorem to term (II), the traction vector emerges, giving

$$\int_V \mathbf{v}^T \tilde{\boldsymbol{\nabla}}^T \boldsymbol{\sigma} \mathrm{d}V = \underbrace{\int_S \mathbf{v}^T \mathbf{t} \mathrm{d}S}_{\text{(IV)}} - \underbrace{\int_V \left(\tilde{\boldsymbol{\nabla}} \mathbf{v}\right)^T \boldsymbol{\sigma} \mathrm{d}V}_{\text{(V)}} . \tag{4.8}$$

Inserting terms (IV) and (V) into Equation (4.7) gives the weak formulation

$$\underbrace{\int_V \mathbf{v}^T \rho \ddot{\mathbf{u}} \mathrm{d}V}_{\text{(I)}} = \underbrace{\int_S \mathbf{v}^T \mathbf{t} \mathrm{d}S}_{\text{(IV)}} - \underbrace{\int_V \left(\tilde{\boldsymbol{\nabla}} \mathbf{v}\right)^T \boldsymbol{\sigma} \mathrm{d}V}_{\text{(V)}} + \underbrace{\int_V \mathbf{v}^T \mathbf{b} \mathrm{d}V}_{\text{(III)}} . \tag{4.9}$$

The advantages of the weak formulation as compared with the strong formulation are [118]:

- The FE equations are based on the weak formulation.
- The strong formulation presents a second derivative, whereas the weak formulation has only the first derivative, due to the integration that is performed. It is thus much better to deal with approximating functions which are differentiable once (whereas if the strong formulation had been considered instead, the approximating functions would have to be differentiable twice).
- Whereas the strong formulation varies when discontinuities in the problem are present, the weak form retains its form, its thus being invariant.

Establishing the FE equations

The weak form, as given in Equation (4.9), involves the displacements **u** and the arbitrary weight function **v**, certain approximations being needed in order to achieve the FE formulation.

Choice of approximating functions: the region is now to be divided into finite elements, a piecewise-approximation across these elements being carried out first, and then, on the basis of these results, established for the entire region. The approximations over each of the elements can be selected from a variety of different types (exponential functions, trigonometrical, etc.), the use of polynomial functions being especially advantageous and convenient to use due to their simplicity.

Obviously, the smaller the elements considered over the region are, the more accurate the final solution will be, at the same time the computational cost increasing as the number of elements increases. In the limiting case in which the elements are infinitely small, the approximate solution is infinitely close to the exact solution (this is the so-called convergence requirement). The convergence requirement is fulfilled if and only if the two following conditions are met:

- The approximations of the vector **u** must be able to represent an arbitrary constant rigid-body motion and an arbitrary constant strain state (completeness requirements).
- The approximations of the displacement vector **u** must vary in a continuous manner over the boundaries of the elements (compatibility or conforming requirement).

Although in some cases the compatibility requirement may be relaxed and convergence still be achieved (in the case of non-conforming elements), the fulfilment of completeness is a necessary condition for convergence to be satisfied.

Irrespective of the particular type of element selected, the approximation of the unknown function, i.e. the displacement field within each element in this case, is carried out as an interpolation between the displacement of the nodal points of the element (the superscript *e* denoting element-wise quantities), expressed as

$$\mathbf{u} = \mathbf{N}^{\mathrm{e}}\mathbf{a}^{\mathrm{e}}, \tag{4.10}$$

where $\mathbf{a}^{\mathrm{e}}$ contains the nodal displacements of all the nodal points n_e in an element, and $\mathbf{N}^{\mathrm{e}}$, the element shape functions, given by

$$\mathbf{u} = \begin{bmatrix} u_x \\ u_y \\ u_z \end{bmatrix};\ \mathbf{N}^{\mathrm{e}} = \begin{bmatrix} N_1^{\mathrm{e}} & 0 & 0 & N_2^{\mathrm{e}} & 0 & 0 & \dots & N_{n_e}^{\mathrm{e}} & 0 & 0 \\ 0 & N_1^{\mathrm{e}} & 0 & 0 & N_2^{\mathrm{e}} & 0 & \dots & 0 & N_{n_e}^{\mathrm{e}} & 0 \\ 0 & 0 & N_1^{\mathrm{e}} & 0 & 0 & N_2^{\mathrm{e}} & \dots & 0 & 0 & N_{n_e}^{\mathrm{e}} \end{bmatrix};\ \mathbf{a}^{\mathrm{e}} = \begin{bmatrix} u_{x1} \\ u_{y1} \\ u_{z1} \\ \vdots \\ u_{xn_e} \\ u_{yn_e} \\ u_{zn_e} \end{bmatrix}. \tag{4.11}$$

Note that the polynomial forms of the shape functions N_i^{e} vary for each type of element (tetrahedral, quadrilateral, etc.) and node (i.e. their depending upon the coordinates), here

simply the general notation being given. The particularisation to a specific type of element is explained, for example, in [118, 119]. The vector $\mathbf{a}^e$ has the dimension $\mathbb{R}^{3n_e \times 1}$. The matrix $\mathbf{N}^e$ has as many rows as there are displacement components for each node (three components in the case presented here, in the x-, y- and z-directions) and as many columns as there are DOFs in all of the nodes.

All N_i^e, regardless of the order of the approximation assumed (i.e. linear, quadratic, etc.) must possess the following property:

$$N_i^e = \begin{cases} 1 & \text{at nodal point } i \\ 0 & \text{at all other nodal points} \end{cases} \tag{4.12}$$

In addition, one should recall that an element shape function related to a specific nodal point is zero along its element boundaries, which do not contain the nodal point in question. Also, the element shape functions must also comply with the following property:

$$\sum_{i=1}^{n_e} N_i^e = 1. \tag{4.13}$$

Moreover, one should note that the interpolation scheme matches that of the adjacent elements since they share common nodes, the function varying (linearly for linear elements, quadratically for quadratic elements, and so on) between those nodes. To illustrate the latter relationships, the linear shape functions for a triangular 2D element are shown in Figure 4.2.

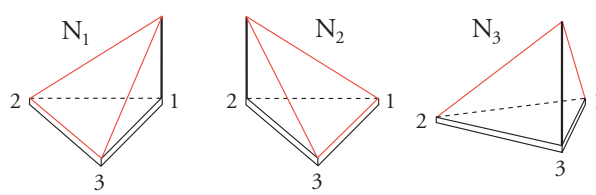

Figure 4.2: *Example of linear shape functions for a triangular 2D element.*

Choice of a weight function v: different methods of weighted residuals (MWR) exist for solving differential equations approximately, namely the collocation method, the sub-domain method, the method of moments, and the least squares method. The differences between then lie in the way the solution is approximated. It is not required that the weight functions be approximated by use of the same interpolants that are used for the trial solutions, although, for most problems it is advantageous. The method that possesses the latter distinguishing feature is called the Galerkin method. Use of the Galerkin method (cf. [118, 119] for more information), and knowing that $\mathbf{c}$ is a vector with arbitrary constants, allows one to state that

$$\tilde{\boldsymbol{\nabla}}\mathbf{v} = \mathbf{B}^e\mathbf{c} \qquad \text{or} \qquad \mathbf{v} = \mathbf{N}^e\mathbf{c}. \tag{4.14}$$

Once the displacements have been interpolated, the strains within each of the elements can also be obtained according to

$$\boldsymbol{\varepsilon} = \mathbf{B}^{\mathrm{e}}\mathbf{a}^{\mathrm{e}} \qquad \text{where} \qquad \mathbf{B}^{\mathrm{e}} = \tilde{\boldsymbol{\nabla}}\mathbf{N}^{\mathrm{e}}, \tag{4.15}$$

the dimension of $\mathbf{B}^{\mathrm{e}}$ being $\mathbb{R}^{6\times 3n_e}$ and

$$\boldsymbol{\varepsilon}^T = \begin{bmatrix} \varepsilon_{xx} & \varepsilon_{yy} & \varepsilon_{zz} & \gamma_{xy} & \gamma_{xz} & \gamma_{yz} \end{bmatrix}. \tag{4.16}$$

FE equations: the FE approximations given in Equations (4.10) and (4.15) are then inserted into the terms (I), (III), (IV) and (V) as indicated in Equation (4.9).

$$\begin{aligned}
(I) \qquad & \int_V \mathbf{v}^T \rho \ddot{\mathbf{u}} \mathrm{d}V = \mathbf{c}^T \underbrace{\int_V \mathbf{N}^{\mathrm{eT}} \rho \mathbf{N}^{\mathrm{e}} \mathrm{d}V}_{\text{mass matrix } \mathbf{M}^{\mathrm{e}}} \ddot{\mathbf{a}}^{\mathrm{e}} \\
(III) \qquad & \int_V \mathbf{v}^T \mathbf{b} \mathrm{d}V = \mathbf{c}^T \underbrace{\int_V \mathbf{N}^{\mathrm{eT}} \mathbf{b} \mathrm{d}V}_{\text{body forces } \mathbf{f}_b^{\mathrm{e}}} \\
(IV) \qquad & \int_S \mathbf{v}^T \mathbf{t} \mathrm{d}S = \mathbf{c}^T \int_S \mathbf{N}^{\mathrm{eT}} \mathbf{t} \mathrm{d}S = \mathbf{c}^T \underbrace{\int_{\Gamma_h} \mathbf{N}^{\mathrm{eT}} \mathbf{h} \mathrm{d}S}_{\text{applied force } \mathbf{f}_s^{\mathrm{e}}} + \mathbf{c}^T \underbrace{\int_{\Gamma_g} \mathbf{N}^{\mathrm{eT}} \mathbf{t} \mathrm{d}S}_{\text{reaction force } \mathbf{f}_r^{\mathrm{e}}} \\
(V) \qquad & \int_V \left(\tilde{\boldsymbol{\nabla}}\mathbf{v}\right)^T \boldsymbol{\sigma} \mathrm{d}V = \mathbf{c}^T \int_V \left(\tilde{\boldsymbol{\nabla}}\mathbf{N}^{\mathrm{e}}\right)^T \boldsymbol{\sigma} \mathrm{d}V = \mathbf{c}^T \int_V \mathbf{B}^{\mathrm{eT}} \boldsymbol{\sigma} \mathrm{d}V.
\end{aligned} \tag{4.17}$$

Finally, summing all of the terms and cancelling $\mathbf{c}$ due to its arbitrary nature,

$$\begin{aligned}
\mathbf{c}^T \mathbf{M}^{\mathrm{e}} \ddot{\mathbf{a}}^{\mathrm{e}} + \mathbf{c}^T \int_V \mathbf{B}^{\mathrm{eT}} \boldsymbol{\sigma} \mathrm{d}V = \mathbf{c}^T \left(\mathbf{f}_s^{\mathrm{e}} + \mathbf{f}_r^{\mathrm{e}} + \mathbf{f}_b^{\mathrm{e}}\right) \Rightarrow \\
\mathbf{M}^{\mathrm{e}} \ddot{\mathbf{a}}^{\mathrm{e}} + \int_V \mathbf{B}^{\mathrm{eT}} \boldsymbol{\sigma} \mathrm{d}V = \mathbf{f}^{\mathrm{e}},
\end{aligned} \tag{4.18}$$

which is the FE formulation valid for any constitutive relationship. Particularising for the linear elastic solid dynamic case and under conditions of zero initial strains, where $\boldsymbol{\sigma} = \mathbf{D}\boldsymbol{\varepsilon} = \tilde{\boldsymbol{\nabla}}\mathbf{N}^{\mathrm{e}}\mathbf{a}^{\mathrm{e}} = \mathbf{B}^{\mathrm{e}}\mathbf{a}^{\mathrm{e}}$, yields

$$\begin{aligned}
\mathbf{M}^{\mathrm{e}} \ddot{\mathbf{a}}^{\mathrm{e}} + \underbrace{\int_V \mathbf{B}^{\mathrm{eT}} \mathbf{D} \mathbf{B}^{\mathrm{e}} \mathrm{d}V}_{\text{stiffness matrix } \mathbf{K}^{\mathrm{e}}} \mathbf{a}^{\mathrm{e}} = \mathbf{f}^{\mathrm{e}} \Rightarrow \\
\mathbf{M}^{\mathrm{e}} \ddot{\mathbf{a}}^{\mathrm{e}} + \mathbf{K}^{\mathrm{e}} \mathbf{a}^{\mathrm{e}} = \mathbf{f}^{\mathrm{e}},
\end{aligned} \tag{4.19}$$

which is the element-wise FE formulation of a dynamic undamped problem, in which

$$\begin{aligned}
\mathbf{M}^{\mathrm{e}} = \int_V \mathbf{N}^{\mathrm{eT}} \rho \mathbf{N}^{\mathrm{e}} \mathrm{d}V; \qquad \mathbf{K}^{\mathrm{e}} = \int_V \mathbf{B}^{\mathrm{eT}} \mathbf{D} \mathbf{B}^{\mathrm{e}} \mathrm{d}V; \\
\mathbf{f}_b^{\mathrm{e}} = \int_V \mathbf{N}^{\mathrm{eT}} \mathbf{b} \mathrm{d}V; \qquad \mathbf{f}_s^{\mathrm{e}} = \int_{\Gamma_h} \mathbf{N}^{\mathrm{eT}} \mathbf{h} \mathrm{d}S; \qquad \mathbf{f}_r^{\mathrm{e}} = \int_{\Gamma_g} \mathbf{N}^{\mathrm{eT}} \mathbf{t} \mathrm{d}S.
\end{aligned} \tag{4.20}$$

If damping is present in the system, the term $\mathbf{C}^e\dot{\mathbf{a}}^e$ is added to the the left-hand side of Equation (4.19) to account for the damping forces present in the structure, the damping matrix $\mathbf{C}^e$ being easily created by assuming Rayleigh damping, for example, as explained in Section 3.2.3. The equation of the dynamic damped problem in its complete form looks like the one given in Equation (3.16).

Equation of motion of the whole system: the equilibrium equation obtained for each finite element can be applied to all of the finite elements in the structure. Once all the matrices have been created for each of the elements, the assembly process must be carried out according to

$$\bigcup_e \mathbf{M}^e\ddot{\mathbf{a}}^e + \bigcup_e \mathbf{K}^e\mathbf{a}^e = \bigcup_e \mathbf{f}^e, \tag{4.21}$$

where $\bigcup_e$ is used here in order to indicate the assembly (union) of the magnitudes in question in accordance with the topology of the structure. This yields the equation of motion for the system as a whole.

One can readily see that the size of the global stiffness, mass and damping (if present) matrices $\mathbf{K}$, $\mathbf{M}$ and $\mathbf{C}$, respectively, is $n_{\mathrm{DOF}_{\mathrm{total}}} \times n_{\mathrm{DOF}_{\mathrm{total}}}$, whereas the size of the correspondent element matrices $\mathbf{K}^e$, $\mathbf{M}^e$ and $\mathbf{C}^e$ is $n_{\mathrm{DOF}_{\mathrm{el}}} \times n_{\mathrm{DOF}_{\mathrm{el}}}$. The global and element force vectors, in turn, have the dimensions $n_{\mathrm{DOF}_{\mathrm{total}}} \times 1$ and $n_{\mathrm{DOF}_{\mathrm{el}}} \times 1$, respectively.

Finally, the BCs must be applied in the corresponding positions of the matrix, i.e. in the DOF in question, in order to reduce the order of the resultant system and allow its calculation. For further information regarding the assembly process, see [118, 119].

4.2.2 Fluid-structure interaction

Vibrating structures can interact with surrounding fluids, inducing acoustic pressure waves, and vice versa. For heavier structures, the influence of the acoustic pressure waves on the structural vibrations is usually negligible. For lightweight structures, however, it is more likely to have a two-way interaction between the domains, demanding simultaneous analyses of the domains to yield realistic results, as it was proved in **Paper B**. The FE method can also be employed for analysing structure-acoustic problems, i.e. fluid-structure interaction (FSI), calculating both the structural response and the acoustic pressure field in a fluid. By imposing conditions of continuity for the displacements and the pressures at boundaries separating the two domains, they can be coupled to form an interacting FE system of equations, as it is hereafter presented.

Structural domain

In the derivations below, a subscript F is adopted for quantities in the acoustic fluid domain Ω_F, whereas the subscript S is used for quantities in the structural domain Ω_S. Having stated that, Equation (4.19) can be rewritten, for the whole structural domain, as

$$\mathbf{M}_S\ddot{\mathbf{a}}_S + \mathbf{C}_S\dot{\mathbf{a}}_S + \mathbf{K}_S\mathbf{a}_S = \mathbf{f}_{l,S} + \mathbf{f}_{b,S} = \mathbf{f}. \tag{4.22}$$

The procedure for determining the FE formulation for the acoustic domain is similar to the one used for the structural domain seen in Section 4.2.1, although in this section some of the steps will be skipped for the sake of brevity. For more detailed information, see [120].

Acoustic fluid domain

Apart of the already mentioned assumption of small displacements, the governing equations of the acoustic fluid are derived assuming the fluid to be irrotational and inviscid [120]. The motion of the fluid in the acoustic fluid domain Ω_F, is governed by the equation of motion and the continuity equation [120]:

$$\rho_0 \frac{\partial^2 \mathbf{u}_F}{\partial t^2} + R \frac{\partial \mathbf{u}_F}{\partial t} + \boldsymbol{\nabla} p_F = 0, \tag{4.23}$$

$$\frac{\partial p_F}{\partial t} + \rho_0 c_0^2 \boldsymbol{\nabla} \cdot \frac{\partial \mathbf{u}_F}{\partial t} = 0, \tag{4.24}$$

where ρ_0 is the static density, R is the flow resistivity, $\boldsymbol{\nabla}$ is the gradient operator, p_F is the acoustic pressure and c_0 is the speed of sound. By differentiating Equation (4.24) with respect to time and inserting Equation (4.23), the wave equation in the acoustic fluid domain choosing the acoustic pressure as the primary variable (other primary variables e.g. fluid displacements $\mathbf{u}_F$ could be employed too) is obtained as

$$\frac{1}{c_0^2} \frac{\partial^2 p_F}{\partial t^2} + \frac{R}{\rho_0 c_0^2} \frac{\partial p_F}{\partial t} - \boldsymbol{\nabla}^2 p_F = 0. \tag{4.25}$$

Performing again a FE discretisation and use of Galerkin's method results in a FE formulation in the acoustic fluid domain, given by

$$\mathbf{M}_F \ddot{\mathbf{p}}_F + \mathbf{C}_F \dot{\mathbf{p}}_F + \mathbf{K}_F \mathbf{p}_F = \mathbf{f}_{b,F}, \tag{4.26}$$

$$\begin{aligned} \mathbf{M}_F &= \frac{1}{c_0^2} \int_{\Omega_F} \mathbf{N}_F^T \mathbf{N}_F \, \mathrm{d}V; & \mathbf{C}_F &= \frac{R}{\rho_0 c_0^2} \int_{\Omega_F} \mathbf{N}_F^T \mathbf{N}_F \, \mathrm{d}V; \\ \mathbf{K}_F &= \int_{\Omega_F} (\boldsymbol{\nabla} \mathbf{N}_F)^T \boldsymbol{\nabla} \mathbf{N}_F \, \mathrm{d}V; & \mathbf{f}_{b,F} &= \int_{\partial \Omega_F} \mathbf{N}_F^T \mathbf{n}_F^T \boldsymbol{\nabla} p_F \, \mathrm{d}S, \end{aligned} \tag{4.27}$$

where $\mathbf{p}_F$ is the nodal pressure vector, $\mathbf{f}_{b,F}$ the boundary load vector, $\mathbf{N}_F$ the shape functions and $\mathbf{n}_F^T$ the boundary normal vector, pointing outwards from the acoustic fluid domain.

Coupling of domains

At the domain-separating boundaries connecting the structural to the acoustic fluid domain ($\partial \Omega_{SF}$), continuity conditions in terms of both displacements and pressures are prescribed as

$$\mathbf{u}_S \mathbf{n}_F = \mathbf{u}_F \mathbf{n}_F, \tag{4.28}$$

$$\boldsymbol{\sigma}_S|_{n_F} = -p_F, \tag{4.29}$$

where $\boldsymbol{\sigma}_S|_{n_F}$ is the stress normal to $\partial\Omega_{SF}$. The spatial coupling matrix is defined as

$$\mathbf{H}_{SF} = \int_{\partial\Omega_{SF}} \mathbf{N}_S^T \mathbf{n}_F \mathbf{N}_F \, \mathrm{d}S, \tag{4.30}$$

and the boundary load vectors at $\partial\Omega_{SF}$ can then be rewritten as

$$\mathbf{f}_{b,S} = \mathbf{H}_{SF}\mathbf{p}_F, \tag{4.31}$$

$$\mathbf{f}_{b,F} = -\rho_0 \mathbf{H}_{SF}^T \ddot{\mathbf{a}}_S - R\mathbf{H}_{SF}^T \dot{\mathbf{a}}_S. \tag{4.32}$$

Using Equations (4.31) and (4.32) in combination with Equations (4.22) and (4.26) results in the structure-acoustic system of equations

$$\begin{bmatrix} \mathbf{M}_S & \mathbf{0} \\ \rho_0 \mathbf{H}_{SF}^T & \mathbf{M}_F \end{bmatrix} \begin{bmatrix} \ddot{\mathbf{a}}_S \\ \ddot{\mathbf{p}}_F \end{bmatrix} + \begin{bmatrix} \mathbf{C}_S & \mathbf{0} \\ R\mathbf{H}_{SF}^T & \mathbf{C}_F \end{bmatrix} \begin{bmatrix} \dot{\mathbf{a}}_S \\ \dot{\mathbf{p}}_F \end{bmatrix} + \begin{bmatrix} \mathbf{K}_S & -\mathbf{H}_{SF} \\ \mathbf{0} & \mathbf{K}_F \end{bmatrix} \begin{bmatrix} \mathbf{a}_S \\ \mathbf{p}_F \end{bmatrix} = \begin{bmatrix} \mathbf{f}_{l,S} \\ \mathbf{0} \end{bmatrix} + \begin{bmatrix} \mathbf{f}_{b,S} \\ \mathbf{f}_{b,F} \end{bmatrix}, \tag{4.33}$$

where $\mathbf{f}_{b,S}$ and $\mathbf{f}_{b,F}$ contain contributions from the parts of the domain boundaries $\partial\Omega_S$ and $\partial\Omega_F$, respectively, that are separated from the interface boundary $\partial\Omega_{SF}$.

4.2.3 Finite elements

Different categories of finite elements can be distinguished depending on their dimension:

- Line elements: truss, beam and restriction elements.
- Area elements: plane stress, plain strain, axisymmetric, membrane, plate and shell.
- Volume elements: tetrahedral and hexahedral solid elements.

The criteria for selection of the proper element for each specific problem depends on many factors, such as the type of load applied (traction or compression, moment...), types of variables to be evaluated (displacements, rotations...), the geometry of the problem in question, etc. These need to be examined by the analyst prior to performing the calculations, see [118, 119].

Isoparametric elements

Normally, the sides of quadrilateral elements must be parallel to the coordinate axes in order for them to behave in a compatible manner. This restriction is very difficult to fulfil, however, when modelling bodies with arbitrary geometries. This can be done, nevertheless, with use of isoparametric elements, since the functions used for interpolating the geometry are coincident with those used for interpolating the displacements. Therefore, this was the type of elements used in the appended papers.

Consider a cubic domain bounded in a $\xi\eta\zeta$-coordinate system (parent domain) and also bounded by $\xi = \pm 1$, $\eta = \pm 1$ and $\zeta = \pm 1$. The transformation through which the parent domain is transformed into a global cartesian xyz-coordinate system, is called mapping, and occurs as follows:

$$x = x(\xi, \eta, \zeta); \qquad y = y(\xi, \eta, \zeta); \qquad z = z(\xi, \eta, \zeta). \tag{4.34}$$

This relationship is univocal, i.e. for every point given by its $\xi\eta\zeta$-coordinates in the parent domain there exists a unique point given by its xyz-coordinates in the global domain. Differentiating Equation (4.34) and using the chain rule, leads to an expression that allows the following transformation between two domains to occur,

$$\begin{bmatrix} dx \\ dy \\ dz \end{bmatrix} = \begin{bmatrix} \frac{\partial x}{\partial \xi} & \frac{\partial x}{\partial \eta} & \frac{\partial x}{\partial \zeta} \\ \frac{\partial y}{\partial \xi} & \frac{\partial y}{\partial \eta} & \frac{\partial y}{\partial \zeta} \\ \frac{\partial z}{\partial \xi} & \frac{\partial z}{\partial \eta} & \frac{\partial z}{\partial \zeta} \end{bmatrix} \begin{bmatrix} d\xi \\ d\eta \\ d\zeta \end{bmatrix} = \mathbf{J}^{-1} \begin{bmatrix} d\xi \\ d\eta \\ d\zeta \end{bmatrix}, \tag{4.35}$$

where the matrix $\mathbf{J}$, which is related to the mapping, is the so-called Jacobian matrix. Equation (4.35) requires $\det(\mathbf{J}) \neq 0$. It should be emphasised that, even when the mapping is unique, this does not necessarily imply that it is possible to invert Equations (4.34) and obtain explicit solutions in the form of $\xi = \xi(x, y, z)$, $\eta = \eta(x, y, z)$ and $\zeta = \zeta(x, y, z)$ [118]. If an element behaves in a conforming, i.e. compatible, manner in the parent domain, its isoparametric version also behaves in a conforming way, no mismatch between adjacent elements existing. The completeness criterion is satisfied with use of Equation (4.13).

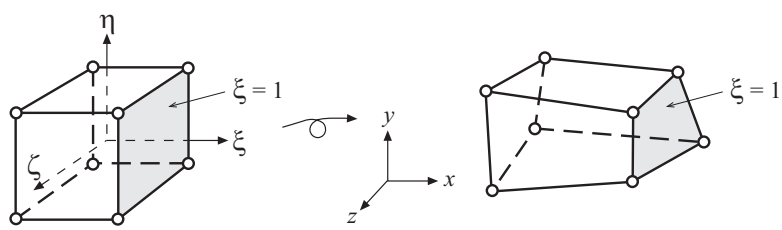

Figure 4.3: *An eight-node three-dimensional isoparametric element [118].*

4.2.4 Meshing

As a rule of thumb, one should always consider at least between 6 and 10 nodes per wavelength when dealing with dynamic problems. The latter implies that the element size must be chosen by taking into account the highest frequency of interest involved in the analysis, as the wavelength decreases with increasing frequency, its limiting the previous condition in terms of nodes per wavelength. This is, in fact, the main drawback of the FE method when using it in connection to dynamic analyses of the type of buildings dealt with here, since its frequency range of applicability is restricted to the low frequencies (up to approximately a couple of hundred Hz). As the response of the structure is requested for higher frequencies, shorter wavelengths must be resolved and smaller details in the geometry become increasingly important. The modelling of finer and smaller details is a challenging task. On top of that, it becomes practically impossible to perform the analyses due to the extensive size of the resulting FE models. For the issues dealt with here, nevertheless, low frequencies are of interest and the FE method is powerful for developing predictive tools of wooden buildings.

4.2.5 Substructure modelling

A major problem when requesting a higher upper limit for the frequency range of analysis and/or when models get larger and more detailed, is that the number of DOFs quickly increases to the point of exceeding the limits of the computer capacity available, at least for calculation times that are reasonable. Hence, reduction of such models is often sought to perform calculations within a feasible time. The methodology of substructure modelling consists on dividing the structure under investigation into separate, simpler components, or substructures, which are reduced in size and subsequently assembled to form reduced global models. Combination of full detailed models together with reduced models, and even experimental substructures described by their measured FRFs can be combined in the global model depending on the problem at hand.

Two main ways of reducing models can be performed [121, 122], model order reduction (MOR) and interface reduction. Substructure modelling has not been employed in the thesis, although once reliable prediction tools are achieved with help of the conclusions drawn in the thesis, its use will be needed; hence why a brief description is included.

Model order reduction

The efficiency of the reduced order models obtained depends on the choice of the MOR method, which, in turn, depends on the application under study. In general matters, in order to reduce the size of certain substructure, a vector $\mathbf{u}_{S,R} \in \mathbb{R}^{m\times 1}$ being the reduced state vector and a so-called transformation matrix $\mathbf{T} \in \mathbb{R}^{n\times m}$ are introduced, where $\mathbf{u}_{S,R} = \mathbf{T}\mathbf{a}$ and $m \ll n$. The latter allows Equation (4.22) to be rewritten in the following form:

$$\mathbf{M}_{S,R}\ddot{\mathbf{u}}_{S,R} + \mathbf{C}_{S,R}\dot{\mathbf{u}}_{S,R} + \mathbf{K}_{S,R}\mathbf{u}_{S,R} = \mathbf{f}_{S,R}, \tag{4.36}$$

where $\mathbf{M}_{S,R} = \mathbf{T}^T\mathbf{M}_S\mathbf{T} \in \mathbb{R}^{m\times m}$, $\mathbf{C}_{S,R} = \mathbf{T}^T\mathbf{C}_S\mathbf{T} \in \mathbb{R}^{m\times m}$ and $\mathbf{K}_{S,R} = \mathbf{T}^T\mathbf{K}_S\mathbf{T} \in \mathbb{R}^{m\times m}$ are the reduced mass, damping and stiffness matrices respectively, and $\mathbf{f}_{S,R} = \mathbf{T}^T\mathbf{f} \in \mathbb{R}^{m\times 1}$ the reduced load vector. The different MOR methods available in the literature differ in the procedures involved to establish the transformation matrix as well as the reduced state vector. For a more thorough review about these matters, see e.g. [121].

Interface reduction

The efficiency of the reduced order models depend to a great extent upon the number of interface DOFs at the interface surfaces connecting the substructures involved. Several methods to reduce those DOFs are available in the literature. Some of them are explained and investigated for a specific case of TVE-based building in [122], where interface reduction between the elastomer blocks and the building parts was performed (see Figure 2.3).

4.3 CALIBRATION OF FE PREDICTION TOOLS

In order to unerringly predict the real behaviour of the types of construction under study, a calibration procedure of the FE models with experiments must be carried out. More specifically, a calibration procedure based on [123], was developed and applied in some of the appended publications. In general terms, one could see [123] as a scheme which aims to fulfil four different objectives. First, a FE model of the structure to be studied is set up and analysed by performing several sensitivity analyses. Secondly, the latter model is calibrated until its response matches the measurement's output. Subsequently, effort is put into making the FE model numerically efficient so it can be used as a predictive tool. Finally and once the prediction tool is created, design improvements of the structure in question can be carried out by modifying features in the model.

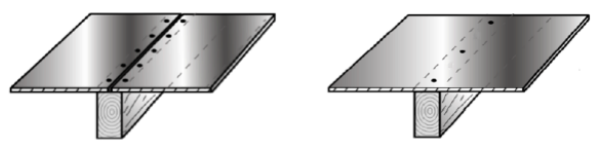

Figure 4.4: *Dual-plate junction (left) and single-plate junction (right).*

In the following, an adaptation of the method described in [123] in connection to the predictive tools for the wooden T-junctions developed in **Paper D** (see Figure 4.4) is described. More specifically, the procedure can be divided into 12 steps:

1. **Pre-analysis**. The first step deals with the partition of the structure into several dissimilar components or substructures, always being mindful of their performance requirements, both individually and when considered included in the structure they pertain to. In doing so, one must thoroughly understand the behaviour of the whole structure first. For the case of the T-junctions under study here, the natural way to go is by identifying and partitioning the structure into load bearing beams and plates (chipboards).
2. **Free-free analyses.** It is believed that vibration modes and mode shapes of free-free states yield the most of each substructure as well as the total structure, as local-global interactions could be unrevealed utilising constrained models [123]. Thus, models of the load bearing beams and plates were created and analysed in a free-free state. Eigenvalue analyses were performed with different FE mesh sizes following a convergence analysis to ensure that the behaviour of the constructive element in question was properly caught, at least up to the highest frequency of interest, i.e. 200 Hz.
3. **Sequential BC applications**. The influence of the BCs on the dynamic response of each substructure (load bearing beams and boards) was individually checked by sequentially introducing different BCs, e.g. simply supported, clamped. Knowledge of their behaviour was gained, allowing to easily identify possible sources of error when assembling all parts into the whole structure.
4. **BC and connection uncertainties**. After the substructures comprising the whole structure (load bearing beams and boards here) were correctly modelled and their behaviour

fully understood, the construction elements were assembled (including now the screws and the glue) to form the different parts involved in the junctions. Boundary uncertainties (e.g., not fully fixed) between the parts were introduced and vibration sensitivity analyses were performed so as to see how these modelling conditions would influence the dynamic characteristics of the structure. This was done in terms of eigenvalue analyses. This was a crucial step, as experience indicates that mismatches between analytical models and test results are often due to inaccurate BCs or substructure interactions [123].

5. **Substructure modelling**. Procedures as the ones described in Section 4.2.5 could be used here to speed up the simulations. No reduction procedures were carried out in the case of the T-junctions, since the models dealt with were not large enough to do so.
6. **Pre-test analysis**. Simulations should be carried aiming at maximising the richness of the data that will be subsequently acquired during measurements. By adjusting the location of the loads and evaluation points in the simulations, optimal positioning for the accelerometers and excitations can be found.
7. **Pre-test setup**. Measurements come here into play by running preliminary tests and adjusting instrumentation locations, if necessary. Signal processing is to be performed in order to see whether or not expected frequency contents are captured.
8. **Modal test**. Somewhat connected with the previous step, the aim here is to carry out a multitude set of vibration tests, performing system realisation (or some other method) to obtain modes, mode shapes and damping. To that end, EMA (already dealt with in Section 3.3.2) was performed on the T-junctions.
9. **Reconciliation**. Based on the experimental data, go back to the FE model and adjust boundary uncertainties, material properties, connection issues, etc. so as to match results from both simulations and measurements. The decision making parameters resolving whether a FE model is accurate enough to be valid as a prediction tool can be various depending on the application at hand (e.g. peak acceleration, RMS velocity, etc.), and should always be stated along with a tolerance. Specifically in **Paper D**, the models were validated in terms of eigenfrequencies and eigenmodes in line with:
    - **Modal assurance criterion (MAC):** the MAC-value [124] can be used to compare measured and simulated eigenmodes (or also two different FE models) denoted as cases Φ_i^{a} and Φ_i^{b} respectively, its being defined, for the i-th eigenmode, as

$$\mathrm{MAC} = \frac{\left|(\Phi_i^{\mathrm{a}})^{\mathrm{T}}(\Phi_i^{\mathrm{b}})\right|^2}{\left|(\Phi_i^{\mathrm{a}})^{\mathrm{T}}(\Phi_i^{\mathrm{a}})\right|\left|(\Phi_i^{\mathrm{b}})^{\mathrm{T}}(\Phi_i^{\mathrm{b}})\right|}. \tag{4.37}$$

      Equation (4.37) is the normalised scalar product of the eigenmodes from the measurements and the simulations (or from two FE models). The MAC-value is in the range 0-1, where 1 represents total correlation and 0 means no correlation at all.
    - **Normalised relative frequency difference (NRFD):** indicator used to check discrepancies in eigenfrequencies between two analysed cases "a" and "b":

$$\mathrm{NRFD}_i[\%] = \frac{\left|f_{\mathrm{a}_i} - f_{\mathrm{b}_i}\right|}{f_{\mathrm{b}_i}} \cdot 100, \tag{4.38}$$

where f_{a_i} is the eigenfrequency of the mode $i = 1, 2, \ldots n$ and the case under study "a", and f_{b_i} is the analogous eigenfrequency for the same mode number i in the other case, considered as reference, "b". Note that the MAC plots complete those of NRFD's (examples of both types of plots can be found in **Paper D**), since the former give the degree of correlation in terms of mode shapes and the latter the differences in the eigenfrequencies.

10. **Energy map**. Energy flow patterns can be analysed by use of the experiment-updated model in assessing how noise and vibration energy propagates through the structure. It has not been performed in the frame of this project, although it could potentially be a powerful tool to analyse, for example, flanking transmission paths in buildings.
11. **Synthesis**. Noise and vibration mitigation strategies can be synthesised based on the knowledge gained thus far when setting up the models. Once the FE prediction tools are calibrated, design modifications can be performed to optimise the structures.
12. **Iterations**. After a new design or improvement is proposed, steps 2-11 should be repeated as many times as necessary so as to meet the vibration requirements stipulated.

The previous 12-step scheme can be applied (slight modifications may be needed depending on the problem treated) to any dynamically loaded structure for which a numerical prediction model is sought.

4.4 ADVANCES PERFORMED FOR FE PREDICTIVE TOOLS

Three main areas in the development of prediction tools were dealt with in the thesis: (i) the impact source, (ii) the modelling of the vibration transmission through the floor and its parts and (iii) the psycho-vibratory response; see Figure 1.2. The first attempts of developing a prediction tool for a whole TVE building (described in **Paper A**) showed that details at a smaller scale needed to be addressed first. In doing so, sources of error are minimised by tackling issues individually before a global model is put together. The following issues have been investigated in the publications included in the thesis:

- The influence of acoustic media has been investigated to see whether or not air and insulation need to be modelled when performing low frequency predictions for wooden buildings (**Paper B**).
- A method for characterising elastomers commonly used in junctions, in order to get reliable material properties to use as input to FE models, was developed in **Paper C**.
- Guidelines on how to model plate-beam connections were established in **Paper D**.
- Guidelines and parametric studies aiming at accurately model the ISO tapping machine have been presented in **Paper E**.

A general structure of a numerical predictive tool of the sort sought in the thesis is presented in Figure 4.5, where it is also highlighted the parts that have been dealt with and those which are proposed as further work.

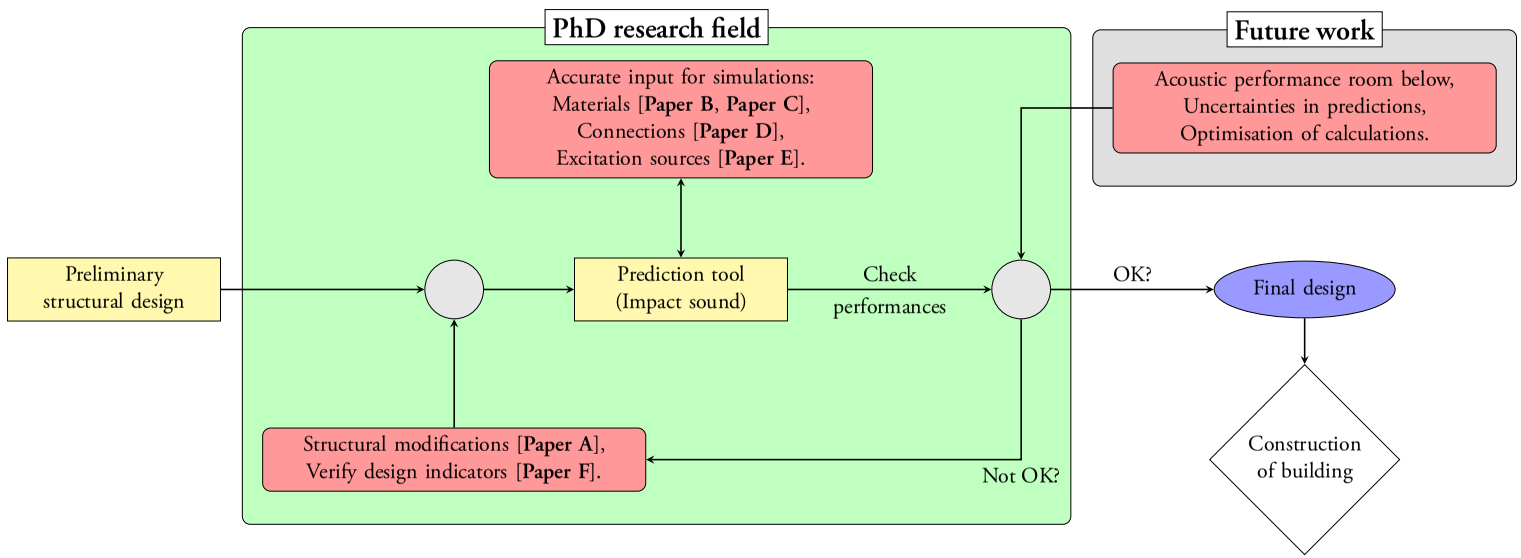

Figure 4.5: *Flowchart showing schematically the idea of a complete numerical prediction tool for impact sound insulation. The areas dealt with in the thesis (and the papers where they are treated) as well as proposals for further work are also highlighted.*

5

Analysis of subjective responses

In order to obtain greater insight into human response to sound and vibrations, specifically floor vibrations here, a technique often used is that of confronting data stemming from questionnaires handed in to test participants with objective measurements performed on the floors under study. Several statistical studies were performed in that manner in the thesis. Specifically, in the appended **Paper F**, the data analysis carried out (both in terms of objective dynamic properties of the floors as well as subjective judgements from people) aimed eventually at finding a satisfactory indicator for two subjective attributes -vibration annoyance and vibration acceptability-, in the form of an objective parameter that could best explain the subjective data. To this end, use was made of multilevel regression. Nevertheless, the large amount of non-subject-dependent objective parameters available made it impossible to determine by means of multilevel regression analysis the relationships between each and every one of these objective parameters, on the one hand, and the subjective data, on the other. Thus, a preliminary analysis based on use of principal component analysis (PCA) was carried out first, in order to select beforehand a small number of objective parameters that could be thought to best explain the subjective data. A brief review of the statistical methods employed in **Paper F** is presented in this chapter.

5.1 PRINCIPAL COMPONENT ANALYSIS

Principal component analysis (PCA) is a technique involving multivariate statistics, mainly descriptive, used for reducing the dimension of a set of multidimensional data. The technique is useful for finding the separate sources of variability in a set of data and ordering them in terms of importance. The mathematical procedures involved use an orthogonal transformation to convert a set of n observations over p variables that are possibly correlated with one another, into a set of linearly uncorrelated variables q (where $q \leq p$) termed principal components. The idea is that, if a variable is a function of one or more other variables, it contains redundant information and therefore the size of the data should be reduced. This transformation is defined in such a way that the first principal component has the largest possible variance (and thus

accounting for as much of the variability in the data as possible), and that each succeeding component, in turn, has the highest variance possible under the constraint that it be orthogonal to (i.e. uncorrelated with) the preceding components. After a reduction of this sort, the q new components (the number of new components to consider is up to the analyst) are obtained as linear combinations of the original variables. For further information concerning standard PCA, see e.g. [125, 126].

Two types of PCA were employed in **Paper F**: the so-called logistic PCA, suitable to binary data (De Leeuw's model being used specifically [127]) in order to deal with the vibration acceptability data, and the PCA for metric data (the MDPREF model being utilised [128,129]) to deal with the vibration annoyance data. Both types of PCA are explained in the following.

5.1.1 PCA of metric data – MDPREF

In this study, the annoyance scores uttered by the subjects on the five different floors involved were analysed by use of the MDPREF model. The analysis was carried out by use of the program *MDPREF* [128]. The model makes it possible to inspect inter-individual differences graphically. Furthermore, it is possible to go on then to identification of those vibratory features of the floors that can account for the vibration annoyance scores uttered by the subjects.

Theoretical framework: MDPREF is a multidimensional scaling model that belongs to the family of scalar product models [129]. It is commonly applied to metric data set up in a rectangular two-mode matrix. This matrix, termed $\mathbf{S}$, contains scores; in that which follows, it will be supposed that $\mathbf{S}$ contains vibration annoyance scores uttered by N subjects (arranged in rows) to a set of n stimuli (i.e. floors here, arranged in columns).

The aim of the model is to represent the stimuli and the subjects in a joint space. More precisely, MDPREF provides a configuration of n points representing the stimuli, and of N unit vectors passing through the origin representing the subjects. These entities are placed in the space in such a way that the orthogonal projections of the different points onto each vector are in maximal agreement with the annoyance scores uttered in response to the stimuli by the various subjects; see Figure 5.1. The vibration annoyance scores increase in continuous fashion along the subject vector. The further a stimulus is projected onto the vector for a given subject, the more it is judged to be annoying to the subject.

The MDPREF algorithm is based on the singular value decomposition (SVD) of the matrix $\mathbf{S}$ according to the Eckart-Young procedure [130]. In that sense, MDPREF strongly resembles PCA. Indeed, the algorithm determines by diagonalisation the eigenvalues of the major (i.e. the product $\mathbf{S}\mathbf{S}^t$) and the minor (i.e. the product $\mathbf{S}^t\mathbf{S}$) covariance matrices and their associated eigenvectors. The magnitude of the eigenvalues common to both covariance matrices makes it possible to estimate the number of principal factors, r, to be retained. In the r-dimensional space, the components of the subject vectors are determined by computing the product of the matrix of the r first eigenvectors of $\mathbf{S}\mathbf{S}^t$ and of the diagonal matrix of the r first eigenvalues; the coordinates of the stimulus points being given by the components of the r first eigenvectors of $\mathbf{S}^t\mathbf{S}$ [131].

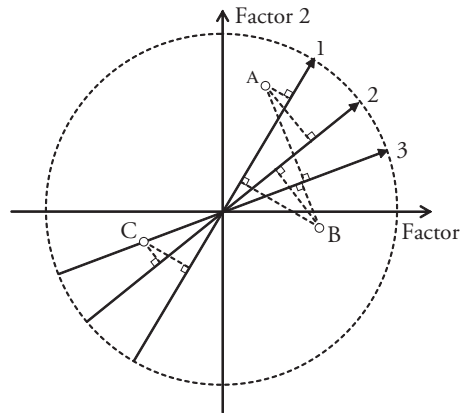

Figure 5.1: *llustration of a representation space provided by MDPREF. Let a 2-D space in which three stimuli A, B and C and three subjects 1, 2 and 3 are represented. In the example shown here, the respective projections of points A, B and C onto the vectors 1, 2 and 3 reproduce the annoyance scores given by the three subjects to the three stimuli.*

Data pre-processing: the respective row mean is substracted from each of the entries. This removes any effects due to the differences in the ranges of values used by the individual subjects.

Dimensionality selection: the number of principal components to be retained can be determined by means of the *scree test* method [132], used in PCA. The test applies to a plot of the eigenvalues of the covariance matrices $\mathbf{S}\mathbf{S}^t$ and $\mathbf{S}^t\mathbf{S}$ in terms of the number of the principal components associated with them (Figure 5.2). According to this method, the appropriate dimensionality can be estimated by the number of the principal factor the associated eigenvalue of which is located at the end of the line that can join up a maximal number of low eigenvalues "at one go". In Figure 5.2, for example, since a line going through eigenvalues 3 to 10 can be drawn, the number of components to be retained can be considered likely to be equal to 3.

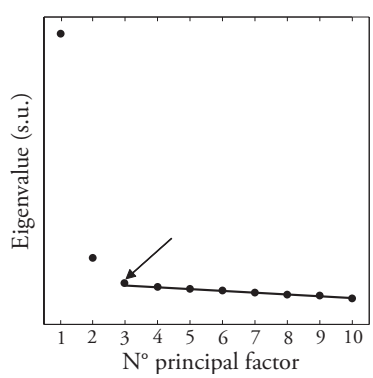

Figure 5.2: *Example of a plot of the eigenvalues obtained in relation to the number of associated principal components involved. The number of the principal factors to be retained can be considered likely to be equal to 3, since a line going through eigenvalues 3 to 10 can be drawn "at one go".*

Interpretation – General issues: from the MDPREF space produced, the inter-individual differences in rating involved can be assessed by inspecting the relative locations of the respective subject vectors. Indeed, the cosine of the angle between two subject vectors provides a measure of the extent of agreement there is between the scores uttered by two subjects. When both vectors are perfectly represented in the space, the cosine of the angle is equivalent to the correlation coefficient between the two series of scores, whereas when it is not the case that both vectors are perfectly represented in the space, the cosine of the angle is always lower than the correlation coefficient between the two series of scores [133].

The links between the subject vectors and the axes of the space are then examined. The direction in which a subject vector points gives an idea of how the subject combines the vibratory features of the floors to utter what, after the data analysis required, represent her/his vibration annoyance scores, this assuming that the factors have a psychological meaning and that they refer to vibratory features of the floors. The cosine of the angle between the subject vector and the axis also provides a measure of the importance the subject attaches to the factor in question [133]. If the subject vectors are closely related to an axis (i.e. are close to this axis), and are located on the same side of this axis, then the axis denotes a factor of consensus among the subjects. In contrast, if some of the subject vectors have a positive component along an axis whereas others have a negative component, this axis denotes a factor of inter-individual differences [134].

To investigate the assumption that the factors have a psychological meaning, the links between the factors, on the one hand, represented by the axes, and the vibratory indices, on the other, computed on the basis of the vibratory measurements obtained for the various floors, as represented in the vector space as vectors by use of PREFMAP procedure [133], are examined. An index vector points in a direction such that the projections of the stimulus points onto the vector are in maximal agreement with the index values, the non-normalised vector length being equivalent to the correlation coefficient between the projections and the index values, this indicating the quality of the representation of the index within the vector space [134].

Thus, an index vector very close to the axis in question suggests that the factor refers very clearly to the vibratory features described by the index, these vibratory features appearing rather clearly to be used by the subjects to utter their degree of annoyance as expressed in the annoyance scores. For further information regarding the analysis of the results, see also **Paper F**.

5.1.2 PCA of binary data – De Leeuw's model

In the investigations presented in the appended **Paper F**, the vibration acceptability responses were analysed by use of the De Leeuw's model, in practice the analysis being carried out by use of the *R* code that De Leeuw developed [127]. Just like the output of the MPREF model, it is possible, in inspecting the inter-individual differences in question graphically, to identify the vibratory features of the floors that can account for the vibration acceptability responses uttered by the subjects. The theoretical framework of this model will now be presented briefly, the general issues regarding the interpretation of the solution being basically the same as for MDPREF.

Suppose that $\mathbf{P} = p_{ij}$ is an $n \times m$ binary data matrix, a matrix of observed acceptability judgements in this case, the elements of which are equal to one or to zero (i.e. the vibrations being acceptable or non-acceptable respectively). The rows in $\mathbf{P}$ refer to the different subjects, whereas the columns refer to the floors. $\mathbf{P}$ is to be fitted to a predicted matrix $\mathbf{\Pi}(X, Y)$ (the acceptability matrix as given by the PCA). The predicted matrix is a function of X, an $n \times r$ matrix of row scores, and of Y, an $m \times r$ matrix of column scores. The parameter r is the dimensionality of the solution. The computational problem is that of minimising the distance between $\mathbf{P}$ and $\mathbf{\Pi}(X, Y)$ over X and Y, the distance being measured by the loss function

$$\mathscr{D}(X, Y) = -\sum_{i=1}^{n}\sum_{j=1}^{n}\left[p_{ij}\log\pi(x_i'y_j) + (1 - p_{ij})\log(1 - \pi(x_i'y_j))\right]. \tag{5.1}$$

Two different ways of specifying the function π, which maps the parameters in X and Y, to the zero-one scale of the outcomes are given in [127]. In the logit case, $\pi(x)$ is

$$\boldsymbol{\pi(x)} = \int_{-\infty}^{x}\psi(x)\mathrm{d}t = \frac{1}{1 + e^{-x}}, \tag{5.2}$$

where the standard logistic density function is given by

$$\psi(x) = \frac{e^{-x}}{(1 + e^{-x})^2}. \tag{5.3}$$

By defining a matrix $\mathbf{\Lambda} = \lambda_{ij}$ in terms of logits, i.e. $\lambda_f = \psi^{-1}(\pi(x', y_f))$, the basic relationship to be fitted can be written as $\mathbf{\Lambda} = XY'$. This shows that the problem being dealt with is a fixed-rank-approximation problem on the logit scale, a problem usually solved by PCA or, equivalently, by SVD in the linear case in which $\mathbf{\Lambda}$ is observed directly. Similarly, this model provides a multidimensional space consisting of a configuration of floor points and of subject vectors that pass through the origin. A vector endpoint represents the point of maximum acceptability for the subject in question. For further information regarding logistic PCA, see [127] and **Paper F**.

5.2 MULTILEVEL REGRESSION ANALYSIS

Multilevel regression has advantages over classical regression for the modelling of repeated measures data. Notably, a multilevel regression formulation complies strictly with the hierarchical structure of the repeated measures data involved, like that in **Paper F**, which consists of observations nested within individuals in question as the data is collected. It thus takes account of the fact that the observations are not independent. For an introduction to multilevel regression models, the reader can be referred to the textbooks [135, 136]. Although not a new idea, this conception of things has become much more popular as the growth of computing power and the availability of appropriate softwares have increased.

More generally, a multilevel model is considered to be a regression model (either a linear or a generalised regression model) in which the parameters, i.e. the regression coefficients, are

modelled at a second level. In modelling repeated measures data, the feature that distinguishes multilevel models from classical regression models is in the modelling of the variation between individuals [135]. Multilevel models can be used on data with many levels, although 2-level models are the most common. The dependent variable needs to be examined at the lowest level of analysis [137]. In what concerns repeated measures data, the lowest level of analysis is the occasion level.

Conceptually, such models are often viewed as representing hierarchical system of regression equations. Assume there to be data on J individuals, and also to be a different number of occasions N_j for each individual involved. On the occasion (the lowest) level, there is a set of dependent variables Y_{ij} and a set of explanatory variables X_{ij}, whereas on the individual level one has the explanatory variable Z_j. Thus, a separate regression equation can be applied to each individual in accordance with

$$Y_{ij} = \beta_{0j} + \beta_{1j}(X_{1ij}) + e_{ij}. \tag{5.4}$$

The β_j values are modelled by explanatory variables at the individual level:

$$\begin{aligned} \beta_{0j} &= \gamma_{00} + \gamma_{01}Z_j + u_{0j}, \\ \beta_{1j} &= \gamma_{10} + \gamma_{11}Z_j + u_{1j}. \end{aligned} \tag{5.5}$$

Substitution of Equations (5.5) in (5.4) gives

$$Y_{ij} = \gamma_{00} + \gamma_{10}X_{ij} + \gamma_{11}Z_jX_{ij} + u_{1j}X_{ij} + u_{0j} + e_{ij}. \tag{5.6}$$

There is generally more than one explanatory variable at the lowest level, and also more than one at the highest level. Let P be the number of explanatory variables X at the lowest level ($p = 1...P$) and Q be the number of explanatory variables Z at the highest level ($q = 1, ..., Q$). Equation (5.6) then becomes

$$Y_{ij} = \gamma_{00} + \sum_{p=1}^{P}\gamma_{p0}X_{pij} + \sum_{q=1}^{Q}\gamma_{0q}Z_{qj} + \sum_{p=1}^{P}\sum_{q=1}^{Q}\gamma_{pq}Z_{qj}X_{pij} + \sum_{p=1}^{P}u_{pj}X_{pij} + u_{0j} + e_{ij}. \tag{5.7}$$

Prior to the analysis to be carried out, the researcher must first decide, which predictors, if any, are to be included in it. Secondly, she or he must decide whether the parameter values (i.e. the elements that are to be estimated) are to be fixed or random. Fixed parameters are composed of a constant that applies to all the individuals, whereas a random parameter has a different value for each of the individuals [138]. The types of models to be selected between are the random-intercept model, the random-slope model and the random-intercept-random-slope model [138]. In **Paper F**, a random intercept and random-intercept-random-slope model were tested. The first of these is a model in which the intercepts are allowed to vary across individuals. This model assumes that the slopes involved are fixed (the same across each of the individuals included). The second model is a model in which both the intercepts and the slopes are allowed to vary across individuals. For further information regarding these models, see **Paper F**.

6
Appended publications

In this chapter, a summary of the publications that are appended in the thesis, together with the author's scientific contribution to each of them, is presented. Likewise, other publications not included in the thesis to which the author also contributed during the course of his PhD project are also listed at the end of the chapter.

6.1 SUMMARY OF THE APPENDED PAPERS

6.1.1 Paper A

Investigation of the vibration transmission through a lightweight junction with elastic layer using the finite element method.
J. Negreira, A. Sjöström, D. Bard.
Proceedings of Internoise 2012, New York, USA, 2012.

Summary: in this paper, a first attempt to create a model for flanking transmission prediction applied to a TVE-based building was performed. Likewise, efforts were put into investigating the differences in vibration transmission performance when different types of TVE configurations were considered. The main conclusion was that the model had to be further refined and developed, as non-realistic results, such as nearly total vibration reduction within a junction, were sometimes obtained. Thus, it was concluded that connections, material properties, BCs, etc. needed to be looked deeper into separately, before a global model was set up.

Contributions: in this publication, the author of the thesis performed all the work, both in terms of planning and developing the research tasks, the simulations and the writing. Anders Sjöström and Delphine Bard proofread the paper.

6.1.2 Paper B

The effect of modelling acoustic media in cavities of lightweight buildings on the transmission of structural vibrations.
O. Flodén, J. Negreira, K. Persson, G. Sandberg.
Engineering Structures, 83: 7–16, 2015.

Summary: accurately predicting the dynamic behaviour of wooden buildings by means of FE analyses requires models representing the geometry in great detail, resulting in models having many DOFs. It is hence important to investigate exhaustively what is essential to actually include in the models and the level of details required to capture the dynamic phenomena involved accurately. Herein, it was investigated whether or not air and insulation in cavities of multi-storey wooden buildings affect the transmission of low frequency structural vibrations. It was concluded, by means of numerical studies, that is not just the structural vibration transmission that is of importance, but also the acoustic resonant transmission. Thus, air and insulation in cavities, modelled as acoustic media, have to be considered when predicting the vibration transmission from a floor to the underlying ceiling and surrounding walls.

Contributions: Juan Negreira created the FE models used for the analysis of the structural transmission and was involved in the analysis and discussion of these results. Also, he took part in the discussions of the results when including acoustic media and proofread the paper.

6.1.3 Paper C

Characterisation of an elastomer for noise and vibration insulation in lightweight timber buildings.
J. Negreira, P-E. Austrell, O. Flodén, D. Bard.
Building Acoustics, 21(4): 251–276, 2014.

Summary: some building techniques using wood frequently utilise elastomers at junctions to reduce low frequency noise. FE simulations yield results which are very much dependent of the input material properties. Thus, the research reported on this paper concerns the characterisation of an elastomer, presenting an accurate method for extracting its material properties from the manufacturer's data sheet (properties there being often linked to such structural effects as shape factors and BCs of samples and tests). The properties were extracted by comparing results obtained by analytical calculations, FE simulations, and mechanical testing, separating geometry and material dependence. Ultimately, the properties obtained will serve as input to commercial FE software for setting up accurate numerical prediction tools.

Contributions: Juan Negreira planned and performed the research tasks, measurements, analytical derivations and FE simulations involved, together with their analyses, as well as he wrote the entire article. Per-Erik Austrell contributed with ideas about the methodology to be employed, and discussing the results. The other authors proofread the paper.

6.1.4 Paper D

Low frequency vibroacoustic investigation of wooden T-junctions.
J. Negreira, A. Sjöström, D. Bard.
Applied Acoustics, 105:1–12, 2016.

Summary: in this paper, an experimental investigation on the influence of glue on the low frequency vibroacoustic performance (up to 200 Hz) of wooden T-junctions is presented along with a discussion of modelling issues related to the junctions. The mock-ups studied represent cut-outs of full size timber floor assemblies typically used in Sweden. Their dynamic performance was first studied experimentally by means of modal analysis. Moreover, FE simulations of the T-junctions were carried out so as to establish reliable prediction tools, using the measurement data as calibration input. Modelling issues were addressed to investigate the influence of different features that must be taken into account when simulating the connections as part of larger structures. Guidelines for modelling these type of connections, when developing low frequency FE predictive tools, are presented.

Contributions: the author of the thesis performed the planning and developed the research tasks, the measurements as well as the FE simulations. The postprocessing and analysis of the data, as well as the writing part were also carried out by Juan Negreira. Anders Sjöström and Delphine Bard proofread the paper and helped discussing the results.

6.1.5 Paper E

Modelling of the tapping machine for finite element prediction tools – Preliminary parametric studies.
J. Negreira, D. Bard.
Submitted to ICA 2016, Buenos Aires, Argentina (September 2016).

Summary: the procedures to evaluate impact sound insulation performance described in the ISO 717-2:2013 involve the use of a standardised excitation source: the tapping machine. Even though considerable research concerning the modelling of wooden floor structures (e.g. connections, material properties) has been carried out within recent years, few investigations have been conducted in a way aiming at characterising and modelling the excitation source, its hindering the development of models which could foresee and mimic results stemming from standardised measurements. The study reported on the paper aims at suggesting improvements of low frequency tools for purposes of prognosis by gaining insight about the modelling of the tapping machine. The first results of a developed method to implement the tapping machine into FE commercial software are presented in this preliminary study.

Contributions: Juan Negreira took the main responsibility for the research presented in the paper by planning and developing the research tasks, as well as performing the writing bit. He developed the numerical strategies and the finite element models employed, and performed the calculations.

6.1.6 Paper F

Psycho-vibratory evaluation of timber floors – Towards the determination of design indicators of vibration acceptability and vibration annoyance.
J. Negreira, A. Trollé, K. Jarnerö, L-G. Sjökvist, D. Bard.
Journal of Sound and Vibration, 340: 383–408, 2015.

Summary: studies addressing human response to vibrations are needed in order to be able to better estimate what level of vibrations can be seen as acceptable in wooden dwellings. In the present study, measurements on five different wooden floors were performed in a laboratory environment. Acceleration measurements were carried out while a person either was walking on a particular floor or was seated in a chair placed there as the test leader was walking on the floor. These participants filled out a questionnaire regarding their perception and experiencing of the vibrations in question. Independently of the subjective tests, several static and dynamic characteristics of the floors were determined through measurements. Indicators of human response to floor vibrations were developed, specifically those regarding vibration acceptability and vibration annoyance, their being drawn based on relationships between the questionnaire responses obtained and the parameter values determined on the basis of the measurements carried out. To that end, use was made of multilevel regression (not widely used as yet), which also proved to be a valuable tool for modelling repeated measures data that involves substantial inter-individual differences in rating.

Contributions: Juan Negreira carried out all measurements and tests performed at Lund University and post processed them. Likewise, he made the merging of the data coming from both laboratories (Lund University and SP Technical Research Institute of Sweden), being also actively involved in discussing the selection of the statistical methods to be employed and in the analysis of the results stemming from those. The writing was also done by him.

6.1.7 Paper G

Construction and in-house calibration of MEMS-based vibration transducers.
R. Darula, A. Sjöström, J. Negreira, D. Bard.
Report TVBA-3131, Division of Engineering Acoustics, Lund University, 2016.

Summary: the calibration of the prediction tools for wooden buildings is carried out using measurement data as calibration input for the models. In line with the latter, having numerous transducers facilitates the acquisition of data as well as improves the richness of it and hence the quality of the predictions. A hindrance in having such an extensive measurement equipment with many transducers is the price of the apparatus involved. Thus, the idea of the research presented in this report was to built and develop accelerometers from scratch, by buying MEMS capacitive sensors (i.e. the inner-chip), mount the components and perform the calibration ourselves. The report presents and explains all the aforementioned steps thoroughly, proving that the accelerometers developed are accurate enough and hence valid for the

applications dealt with in the thesis. The ultimate aim of the research performed is, hence, to increase the accuracy and reliability of the measurements carried out using these MEMS capacitive accelerometers and eventually thus have calibration input of better quality for the low frequency vibroacoustic prediction tools that are to be developed.

Contributions: most of the measurements as well as writing and proofreading of the report were performed together by Radoslav, Anders and Juan, Delphine Bard being involved in the proofreading of the report.

6.2 LIST OF PUBLICATIONS NOT INCLUDED IN THE THESIS

Licentiate dissertation

- *Vibrations in lightweight buildings – Perception and prediction.*
  J. Negreira.
  Report TVBA-3130, Division of Engineering Acoustics, Lund University, 2013.

Conference papers

- *Numerical prediction tools for low-frequency sound insulation in lightweight buildings.*
  J. Negreira, D. Bard.
  Proceedings of IMAC XXXIII, Orlando, USA, 2015.
- *Modelling walking on a lightweight wooden floor.*
  A. Sjöström, J. Negreira, D. Bard.
  Proceedings of Internoise 2015, San Francisco, USA.
- *Determination of vibration acceptability and annoyance design indicators for human response to wooden-floor vibrations.*
  J. Negreira, A. Trollé, K. Jarnerö, L-G. Sjökvist, D. Bard.
  Proceedings of Internoise 2014, Melbourne, Australia.
- *Flanking transmission in three different lightweight wooden building types.*
  A. Sjöström, J. Negreira, D. Bard, G. Sandberg, C. Novak, H. Ule.
  Proceedings of Internoise 2014, Melbourne, Australia.
- *Challenges for acoustic calculation models in "Silent Timber Build"*
  D. Bard, G. Borello, C. Guigou, J. Negreira, J-L. Kouyoumji.
  Proceedings of ICSV 21st, Beijing, China, 2014.
- *Teaching and learning adaptation of international students in Sweden.*
  V. Sohrabpour, A. Pazirandeh, D. Bard, J. Negreira, J. Zhang.
  Proceedings of 41st SEFI Conference, Leuven, Belgium, 2013.
- *Reflection and transmission properties of a wall-floor building element: comparison between finite element model and experimental data.*
  J. Negreira, O. Flodén, D. Bard.
  Proceedings of Acoustics Hong Kong 2012.

- *Field measurements of vibrations in a wooden floor.*
  D. Bard, J. Negreira.
  Proceedings of BNAM, Odense, Denmark, 2012.
- *Vibration analysis of underground tunnel at high-tech facility.*
  J. Negreira, K. Persson, D. Bard, P-E. Austrell, G. Sandberg.
  Proceedings of the 23rd NSCM, Stockholm, Sweden, 2010.
- *Vibration analysis in high-tech facility: a Swedish light synchroton.*
  D. Bard, P. Persson, J. Negreira, K. Persson, P-E. Austrell, G. Sandberg.
  Proceedings of ICSV 17th, Cairo, Egypt, 2010.

Technical reports

- *Investigation of the acoustic properties of facade elements – Selected study cases of Swedish building constructions.*
  D. Bard, N-G. Vardaxis, J. Negreira.
  Report TVBA-3132, Division of Engineering Acoustics, Lund University, 2016.
- *Beräkningsmodell för sammansatta volymelement med FEM.*
  J. Negreira, D. Bard.
  Technical Report SP Report 2013:15, 2013.
- *Physical and psycho-vibratory testing of wooden floors.*
  J. Negreira, A. Trollé, K. Jarnerö, L-G. Sjökvist, D. Bard.
  Technical Report SP Report 2012:29, 2012.

Conference abstracts

- *Influence of air cavities on flanking transmission in lightweight building structures.*
  J. Negreira, O. Flodén, D. Bard, G. Sandberg.
  Proceedings of the V International Conference on Coupled Problems in Science and Engineering, Ibiza, Spain, 2013.
- *A component mode synthesis approach for vibration transmission analysis in a multi-storey wood building.*
  O. Flodén, J. Negreira, K. Persson, G. Sandberg.
  Proceedings of the V International Conference on Coupled Problems in Science and Engineering, Ibiza, Spain, 2013.
- *Finite element analysis of flanking transmission in a lightweight junction with elastic layers.*
  J. Negreira, D. Bard, K. Persson, G. Sandberg.
  Proceedings of the 25th NSCM, Lund, Sweden, 2012.
- *Characterisation of a rubber foam material for noise and vibration isolation in buildings by laboratory testing, material modelling, and finite element analysis.*
  J. Negreira, P-E. Austrell, A. Sjöström, D. Bard.
  Proceedings of 10th WCCM, São Paulo, Brazil, 2012.

7
Conclusions

Although research within the field of wooden buildings has increased in recent years, much is left to do with regards to investigating the vibroacoustic behaviour of such constructions. More investigations must be conducted before wooden buildings can be regarded as both predictable and as consistently satisfactory for those living in them. Two major goals connected with achieving this were the focus of the thesis:

1. Developing accurate prediction tools for use in connection with wooden buildings.
2. Gaining more adequate insight into human response and perception of floor vibrations.

7.1 MAIN SCIENTIFIC CONTRIBUTIONS

The research reported here aimed at being able to predict more accurately and better understand the low frequency sound. The results provided insight into three basic pillars of research in investigating vibrations in wooden buildings: (i) research concerned with the development of numerical prediction tools, (ii) research on human perception of floor vibrations and (iii) measurement techniques in connection with the development of vibration transducers. The scientific contributions can be summarised as:

- **Prediction**
    1. It was shown in **Paper B** that acoustic media (air and insulation) in cavities of multi-storey wooden buildings have to be considered when performing FE low frequency predictions. This is due to the fact that it is not just the structural vibration transmission that is of importance, but also the acoustic resonant transmission. FSI proved to affect the vibroacoustic behaviour due to the propagation of vibrations through the acoustic media from a floor to the underlying ceiling and surrounding walls.
    2. The novelty of the research presented in **Paper C** is the method that was developed (based on laboratory testing, material modelling and FE simulations) for characterising elastomers (in terms of their frequency-dependent linear viscoelastic

properties), which are often used in junctions in wooden buildings as vibration-reduction measure. Ultimately, this method allows the introduction of accurate material properties into FE software in a practical way.

3. The originality of the research reported on **Paper D** lies in the modelling guidelines that were developed for including, in an accurate but simplified way, different types of wooden T-junctions (i.e. beam-plate connections) as part of numerical prediction tools of larger structures.
4. Preliminary studies presenting guidelines on how to use a developed time-efficient frequency domain method to implement the ISO tapping machine into FE predictive models were drawn in **Paper E**.

- **Perception**
  1. Design indicators of human response to floor vibrations (viz. vibration annoyance and vibration acceptability) were developed in **Paper F** by carrying out psycho-vibratory tests of different floors in which a number of participants took part.
  2. Another novel finding reported in **Paper F** was proving that multilevel regression (not widely used as of yet) can be a valuable tool for modelling repeated measures data that involves substantial inter-individual differences in rating.
- **Measurement techniques**
  1. The novelty of the research reported in **Paper G** lies in the in-house development (i.e. construction and calibration) of MEMS-based vibration transducers. It was shown that the transducers were accurate in the frequency range of interest and hence valid for the applications under study in the thesis. Having a large number of transducers (at a reasonable price) when performing measurements, greatly increases the richness of data acquired, which is needed for calibration of the predictive models that are to be developed.

Nevertheless, problems still remain; despite the lightweight wooden buildings comply with the standardised criteria currently employed, subjective vibratory studies of modern timber framework buildings still show that the inhabitants of these buildings are frequently annoyed by vibrations. Thus, further work in the field is called for. The conclusions drawn pave the way for the further research discussed below.

7.2 PROPOSALS FOR FURTHER WORK

Prediction: particular efforts should be directed at the development of better prediction tools. One should be aware, however, that wooden frame constructions can be quite complex, showing strong variations both within each nominally identical floor and wall elements, as well as in the couplings, materials, etc. This makes the development of a general prediction tool difficult. At the same time, the steady increase in the industrial production of wood prefabricated buildings makes the development of appropriate prediction models seem more feasible than before. This is in part due to the standardisation of the building technique. The thesis has addressed several individual issues that will improve the quality of the predictions. The suggestions for future improvements of tools for purposes of prognosis are:

- Construction of mock-ups in laboratories to validate FE models against measurements performed in a controlled way should be prioritised. This is advised to gain further knowledge about modelling issues such as BCs and connections, which could influence to a great extent the results obtained.
- Based on the knowledge gained through laboratory experiments, FE models of real buildings should be set up. Relating the results provided by such models to specific in-situ measurements, in order to validate FE models, is of paramount importance.
- The room in the level below should also be dealt with adequately to be able to calculate its sound pressure level due to the excitation source applied on the floor above. In doing so, one could eventually apply the same evaluation methods as in the ISO standards and thus obtain the weighted values for impact sound insulation. Attempts in doing so have been addressed in [139, 140], yet more accurate results are still needed.
- Further development of substructure modelling to speed up calculations when assembling more building parts (resulting in larger models) is also advised.
- Uncertainties should be better handled and understood, both in terms of material properties, insulation materials, BCs, damping, connections as well as workmanship. To that end, statistical methods can be used so results are given alongside a level of confidence of the predictions carried out. A recent work performed along these lines is presented in [63].

Perception: the findings obtained concerning the psycho-vibratory tests were obtained in what can be considered a pilot study. This is with regards to the small sample size (five different wooden floors), although there were a sufficiently large number of subjects to provide clear statistical support for the conclusions drawn.

- The results can serve as a starting point to a follow up study involving a larger sample of floors, making it possible to extract power laws also concerning other design indicators.
- More studies regarding human perception of low frequency vibrations are advised to get reliable input for improvement of the evaluation methods existent in the current impact sound insulation standards, so they correlate better with people's perception of vibrations. Likewise, studies of the sort mentioned will enable new excitation sources to be proposed, whose spectra are closer to the ones wooden buildings are exposed to.

7.3 CLOSING REMARKS

It should be kept in mind that ideally, the tools developed should ultimately be used by the industry (they are, in a way, the "clients" of the academia). Hence, the predictive models should not only be accurate, but also easy to use and not too time consuming. Therefore, it is advised that researchers should not only think from an academic point of view, but also, from the perspective of a consultant. Guidelines with simplified ways of modelling wooden structures in an accurate way, enabling accurate predictions and therefore optimised constructions during the design phase of the buildings, should be the outcome of thorough research in the area.

References

[1] World Health Organization (New York, 19th-22nd June 1946; signed on July 22nd 1946 by the representatives of 61 States and entered into force on April 7th, 1948), *Preamble to the Constitution of the World Health Organization as adopted by the International Health Conference*.

[2] Rasmussen, B. (2010), *Sound insulation between dwellings – Requirements in building regulations in Europe*, Applied Acoustics **71**(4), 373–385.

[3] Näringsdepartementet (2004), *Mer trä i byggandet – Underlag för en nationell strategi att främja användning av trä i byggandet (in Swedish), [More wood in construction – Basis for a national strategy to promote use of wood in construction]*, Tech. Rep. Ds 2004:1, Ministry of Industry, Employment and Communications, Government of Sweden, Stockholm.

[4] *Swedish Wood*, `http://www.swedishwood.com`, Accessed: 2016-03-06.

[5] COST Action FP0702 (2012), *Net-Acoustics for timber based lightweight buildings and elements*, eBook (available online at `http://extranet.cstb.fr/sites/cost/ebook/Forms/AllItems.aspx`).

[6] Swedish Wood (2012), *Building with wood – Modern solutions for wood construction*, Tech. rep., Swedish Forest Industries Federation, Stockholm, Sweden.

[7] Persson, K. (2000), *Micromechanical modelling of wood and fibre properties*, Ph.D. thesis, Department of Construction Sciences, Division of Structural Mechanics, Lund University, Sweden.

[8] Danielsson, H. (2013), *Perpendicular to grain fracture analysis of wooden structural elements – Modeling and applications*, Ph.D. thesis, Department of Construction Sciences, Division of Structural Mechanics, Lund University, Sweden.

[9] Dassault Systèmes (2012), *Abaqus theory manual, Version 6.11*, Dassault Group, Vélizy-Villacoublay, France.

[10] Bucur, V. (2006), *Acoustics of wood*, Springer, Berlin, Germany.

[11] Forest Products Laboratory (United States Department of Agriculture) (2010), *Wood handbook – Wood as an engineering material*, Centennial Edition, Madison, Wisconsin, USA.

[12] Thelandersson, S., Larsen, H.J. (2003), *Timber engineering*, Wiley, Chichester, UK.

[13] Ljunggren, F., Ågren, A. (2011), *Potential solutions to improved sound performance of volume based lightweight multi-storey timber buildings*, Applied Acoustics **72**, 231–240.

[14] Ågren, A. (2010), *Acoustic highlights in Nordic light weight building tradition – Focus on ongoing development in Swedish*, in: *Proceedings of Baltic-Nordic Acoustic Meeting (BNAM)*, Bergen, Norway.

[15] Öqvist, R., Ljunggren, F., Ågren, A. (2010), *Variations in sound insulation in nominally identical prefabricated lightweight timber constructions*, Building Acoustics **17**(2), 91–103.

[16] Morfey, C.L. (2001), *Dictionary of acoustics*, Academic Press, Trowbridge, UK.

[17] Blazier, W.E., DuPree, R.B. (1994), *Investigation of low-frequency footfall noise in wood-frame, multifamily building construction*, The Journal of the Acoustical Society of America **96**(3), 1521–1532.

[18] Forssén, J., Kropp, W., Brunskog, J., Ljunggren, S., Bard, D., Sandberg, G., Ljunggren, F., Ågren, A., Hallström, O., Dybro, H., Larsson, K., Tillberg, K., Sjökvist, L.G., Östman, B., Hagberg, K., Bolmsvik, Å., Olsson, A., Ekstrand, C.G., Johansson, M. (2008), *Acoustics in wooden buildings. State of the art 2008. Vinnova project 2007-01653*, Technical Research Institute of Sweden. Report 2008:16, Stockholm, Sweden.

[19] COST Action TU0901 (Integrating and harmonizing sound insulation aspects in sustainable urban housing constructions) (2014), *Building acoustics throughout Europe. Volume 1: Towards a common framework in building acoustics throughout Europe*, DiScript Preimpresion S.L.

[20] Rasmussen, B., Rindel, J.H. (2010), *Sound insulation between dwellings – Descriptors applied in building regulations in Europe*, Applied Acoustics **71**(3), 171–180.

[21] Ljunggren, F., Simmons, C., Hagberg, K. (2014), *Correlation between sound insulation and occupants' perception – Proposal of alternative single number rating of impact sound*, Applied Acoustics **85**, 57–68.

[22] Einarsson, S. (1983), *Low frequency impact sound from timber joist floors*, in: *Proceedings of Internoise 1983*, Edinburgh, Scotland.

[23] Hveem, S. (2000), *Nordic multi-storey timber buildings for residential housing*, in: *Proceedings of Internoise 2000*, Nice, France.

[24] Bradley, C.W. (1990), *Sound performance of wood floor/ceiling assemblies*, Tech. Rep. E12/MF E01, Canada Mortgage and Housing Corp., Ottawa, Canada.

[25] Chung, H., Dodd, G., Emms, K., McGunnigie, K., Schmid, G. (2006), *Maximising impact sound reistance of timber framed floor ceiling systems – Volume 1*, Tech. Rep. PN04.2005, Australian Government – Forest and Wood Products Research and Development Corporation, Melbourne, Australia.

[26] Sipari, P. (2000), *Sound insulation of multi-storey houses – A summary of Finnish impact sound insulation results*, Building Acoustics 7(1), 15–30.

[27] Bolmsvik, Å., Linderholt, A., Jarnerö, K. (2012), *FE modeling of a lightweight structure with different junctions*, in: *Proceedings of Euronoise 2012*, Prague, Czech Republic.

[28] ISO (2013), *ISO 717-1: Acoustics – Rating of sound insulation in buildings and of building elements – Part 1: Airborne sound insulation*, International Organization for Standardization, Geneva, Switzerland.

[29] ISO (2013), *ISO 717-2: Acoustics – Rating of sound insulation in buildings and of building elements – Part 2: Impact sound insulation*, International Organization for Standardization, Geneva, Switzerland.

[30] ISO (2010), *ISO 10140-1: Acoustics – Laboratory measurement of sound insulation of building elements – Part 1: Application rules for specific products*, International Organization for Standardization, Geneva, Switzerland.

[31] ISO (2010), *ISO 10140-2: Acoustics – Laboratory measurement of sound insulation of building elements – Part 2: Measurement of airborne sound insulation*, International Organization for Standardization, Geneva, Switzerland.

[32] ISO (2010), *ISO 10140-3: Acoustics – Laboratory measurement of sound insulation of building elements – Part 3: Measurement of impact sound insulation*, International Organization for Standardization, Geneva, Switzerland.

[33] ISO (2010), *ISO 10140-4: Acoustics – Laboratory measurement of sound insulation of building elements – Part 4: Measurement procedures and requirements*, International Organization for Standardization, Geneva, Switzerland.

[34] ISO (2010), *ISO 10140-5: Acoustics – Laboratory measurement of sound insulation of building elements – Part 5: Requirements for test facilities and equipment*, International Organization for Standardization, Geneva, Switzerland.

[35] ISO (2014), *ISO 16283-1: Acoustics – Field measurement of sound insulation in buildings and of building elements – Part 1: Airborne sound insulation*, International Organization for Standardization, Geneva, Switzerland.

[36] ISO (2014), *ISO 16283-2: Acoustics – Field measurement of sound insulation in buildings and of building elements – Part 2: Impact sound insulation*, International Organization for Standardization, Geneva, Switzerland.

[37] ISO (2014), *ISO 16283-3: Acoustics – Field measurement of sound insulation in buildings and of building elements – Part 3: Facade sound insulation*, International Organization for Standardization, Geneva, Switzerland.

[38] Hagberg, K., Bard, D. (2010), *Sound insulation descriptors in Europe – Special rules complicate harmonization within lightweight industry*, Building Acoustics **16**(4), 277–290.

[39] Parmanen, J. (1998), *Comments and conclusions based on "Alternative reference curves for evaluation of the impact sound insulation between dwellings"*, Journal of Sound and Vibration **213**(4), 763–773.

[40] Mortenssen, F.R. (1999), *Subjective evaluation of noise from neighbours with focus on low frequencies*, Tech. Rep. No. 53, Department of Acoustic Technology, Technical University of Denmark, Lyngby, Denmark.

[41] *Silent Timber Build for the European Market – A WoodWisdom-Net project*, Website: `http://silent-timber-build.com`.

[42] SIS (2015), *SS 25267: Acoustics – Sound classification of spaces in buildings – Dwellings (in Swedish)*, Swedish Standards Institute, Stockholm, Sweden.

[43] SIS (2007), *SS 25268: Acoustics – Sound classification of spaces in buildings – Institutional premises, rooms for education, preschools and leisure-time centres, rooms for office work and hotels (in Swedish)*, Swedish Standards Institute, Stockholm, Sweden.

[44] CEN (2000), *EN 12354-1 (ISO 15712-1:2005): Building acoustics – Estimation of acoustic performance of buildings from the performance of elements – Part 1: Airborne sound insulation between rooms*, European Committee for Standardization, Brussels, Belgium.

[45] CEN (2000), *EN 12354-2 (ISO 15712-2:2005): Building acoustics – Estimation of acoustic performance of buildings from the performance of elements – Part 2: Impact sound between rooms*, European Committee for Standardization, Brussels, Belgium.

[46] CEN (2000), *EN 12354-3 (ISO 15712-3:2005): Building acoustics – Estimation of acoustic performance of buildings from the performance of elements – Part 3: Airborne sound insulation against outdoor noise*, European Committee for Standardization, Brussels, Belgium.

[47] CEN (2000), *EN 12354-4 (ISO 15712-4:2005): Building acoustics – Estimation of acoustic performance of buildings from the performance of elements – Part 4: Transmission of indoor sound to the outside*, European Committee for Standardization, Brussels, Belgium.

[48] CEN (2000), *EN 12354-5: Building acoustics – Estimation of acoustic performance of buildings from the performance of elements – Part 5: Noise from technical installations and equipment*, European Committee for Standardization, Brussels, Belgium.

[49] CEN (2000), *EN 12354-6: Building acoustics – Estimation of acoustic performance of buildings from the performance of elements – Part 6: Sound absorption in enclosed spaces*, European Committee for Standardization, Brussels, Belgium.

[50] Simmons, C. (2009), *Managing uncertainty in building acoustics – Comparisons of predictions using the EN 12354 standards to measurements*, Ph.D. thesis, Department of Human Work Sciences, Division of Sound and Vibration, Luleå University of Technology, Sweden.

[51] ISO (2006), *ISO 10848-1: Acoustics – Laboratory measurement of the flanking transmission of airborne and impact sound between adjoining rooms – Part 1: Frame document*, International Organization for Standardization, Geneva, Switzerland.

[52] ISO (2006), *ISO 10848-2: Acoustics – Laboratory measurement of the flanking transmission of airborne and impact sound between adjoining rooms – Part 2: Application to light elements when the junction has a small influence*, International Organization for Standardization, Geneva, Switzerland.

[53] ISO (2006), *ISO 10848-3: Acoustics – Laboratory measurement of the flanking transmission of airborne and impact sound between adjoining rooms – Part 3: Application to light elements when the junction has a substantial influence*, International Organization for Standardization, Geneva, Switzerland.

[54] ISO (2010), *ISO 10848-4: Acoustics – Laboratory measurement of the flanking transmission of airborne and impact sound between adjoining rooms – Part 4: Application to junctions with at least one heavy element*, International Organization for Standardization, Geneva, Switzerland.

[55] Schoenwald, S. (2008), *Flanking sound transmission through lightweight framed double leaf walls – Prediction using statistical energy analysis*, Ph.D. thesis, Department of Architecture, Building and Planning, Eindhoven University of Technology, Netherlands.

[56] Mahn, J. (2008), *Prediction of flanking noise transmission in lightweight building constructions – A theoretical and experimental evaluation of the application of EN 12354-1*, Ph.D. thesis, Department of Mechanical Engineering, University of Canterbury, Christchurch, New Zealand.

[57] Dickow, K.A., Kirkegaard, P.H., Andersen, L.V. (2012), *An evaluation of test and physical uncertainty of measuring vibration in wooden junctions*, in: *Proceedings of International Conference on Noise and Vibration Engineering (ISMA2012)*, Leuven, Belgium.

[58] Craik, R.J., Steel, J.A. (1989), *The effect of workmanship on sound transmission through buildings: Part 1 – Airborne sound*, Applied Acoustics **27**(1), 57–63.

[59] Craik, R.J., Evans, D.I. (1989), *The effect of workmanship on sound transmission through buildings: Part 2 – Structure-borne sound*, Applied Acoustics **27**(2), 137–145.

[60] Johansson, C. (2000), *Field measurements of 170 nominally identical timber floors: a statistical analysis*, in: *Proceedings of Internoise 2000*, Nice, France.

[61] Trevathan, J., Pearse, J. (2008), *The effect of workmanship on the transmission of airborne sound through light framed walls*, Applied Acoustics **69**(2), 127–131.

[62] Öqvist, R., Ljunggren, F., Ågren, A. (2011), *Variations in sound insulation in cross laminated timber housing construction*, in: *Proceedings of Forum Acusticum*, Aalborg, Denmark.

[63] Coguenanff, C. (2015), *Robust design of lightweight wood-based systems in linear vibroacoustics*, Ph.D. thesis, École Doctorale Sciences, Ingénierie et Environnement (Spécialité: Mécanique), Université Paris-Est, France.

[64] Griffin, M.J. (1996), *Handbook of human vibration*, Academic Press Limited, London, UK.

[65] Pavic, A., Reynolds, P. (2002), *Vibration serviceability of long-span concrete building floors. Part 1: Review of background information*, The Shock and Vibration Digest **34**(3), 191–211.

[66] ISO (2003), *ISO 2631-1: Vibration and shock – Evaluation of human exposure to whole-body vibration – Part 1: General requirements*, International Organization for Standardization, Geneva, Switzerland.

[67] ISO (2003), *ISO 2631-2: Vibration and shock – Evaluation of human exposure to whole-body vibration – Part 2: Vibration in buildings (1 Hz to 80 Hz)*, International Organization for Standardization, Geneva, Switzerland.

[68] SIS (2004), *SS 4604861: Vibration and shock – Measurement and guidelines for the evaluation of comfort in buildings (in Swedish)*, Swedish Standards Institute, Stockholm, Sweden.

[69] ISO (2007), *ISO 10137: Bases for design of structures – Serviceability of buildings and walkways against vibrations*, International Organization for Standardization, Geneva, Switzerland.

[70] CEN (2004), *EN 1995-1-1: Eurocode 5 – Design of timber structures – Common rules and rules for buildings*, European Committee for Standardization, Brussels, Belgium.

[71] Weckendorf, J. (2009), *Dynamic response of structural timber flooring systems*, Ph.D. thesis, The Centre for Timber Engineering, School of Engineering and the Built Environment, Napier University, Edinburgh, Scotland.

[72] Hagberg, K. (2005), *Evaluation of sound insulation in the field*, Tech. Rep. Licentiate dissertation, Report TVBA-3127, Department of Construction Sciences, Division of Engineering Acoustics, Lund University, Sweden.

[73] Ljunggren, F. (2006), *Floor vibration – Dynamic properties and subjective perception*, Ph.D. thesis, Department of Human Work Sciences, Division of Sound and Vibration, Luleå University of Technology, Sweden.

[74] Ohlsson, S. (1988), *Springiness and human-induced floor vibrations – A design guide*, Tech. Rep. D12:1988, Swedish Council for Building Research, Stockholm, Sweden.

[75] Ohlsson, S. (1982), *Floor vibrations and human discomfort*, Ph.D. thesis, Department of Structural Engineering, Chalmers University of Technology, Göteborg, Sweden.

[76] Smith, I., Chui, Y.H. (1988), *Design of light-weight wooden floors to avoid human discomfort*, Canadian Journal of Civil Engineering **15**, 254–262.

[77] Smith, I., Chui, Y.H. (1992), *Construction methods for minimizing vibration levels in floors with lumber joists*, Canadian Journal of Civil Engineering **19**, 833–841.

[78] Brigham, E.O. (1974), *The fast Fourier transform*, Prentice-Hall Inc., Englewood Cliffs, New Jersey, USA.

[79] Chopra, A.K. (2007), *Dynamics of structures*, Prentice Hall, New Jersey, USA.

[80] Craig, R.R., Kurdila, A.J. (2006), *Fundamentals of structural dynamics*, Hoboken, John Wiley & Sons, New Jersey, USA.

[81] Austrell, P.E., Dahlblom, O., Lindemann, J., Olsson, A., Olsson, K.G., Persson, K., Petersson, H., Ristinmaa, M., Sandberg, G., Wernberg, P.A. (2004), *CALFEM – A finite element toolbox version 3.4*, Studentlitteratur.

[82] Labonnote, N. (2012), *Damping in timber structures*, Ph.D. thesis, Department of Structural Engineering, Norwegian University of Science and Technology (NTNU), Trondheim, Norway.

[83] Srikantha-Phani, A., Woodhouse, J. (2007), *Viscous damping identification in linear vibration*, Journal of Sound and Vibration **303**(3–5), 475–500.

[84] Warnock, A. (1998), *Floor research at NRC Canada*, in: *Conference in building acoustics "Acoustic performance of medium-rise timber buildings"*, Dublin, Ireland.

[85] Warnock, A. (2000), *Low-frequency impact sound transmission through floor systems*, in: *Proceedings of Internoise 2000*, Nice, France.

[86] Shi, W., Johansson, C., Sundbäck, U. (1996), *Assessment of the sound insulation of a wood joist construction due to different types of impact sources*, Applied Acoustics **48**(3), 195–203.

[87] Techibana, H., Tanaka, H., Koyasu, M. (1992), *Heavy impact source for the measurement of impact sound insulation of floors*, in: *Proceedings of Internoise 1992*, Toronto, Canada.

[88] Shi, W., Johansson, C., Sundbäck, U. (1997), *An investigation of the characteristics of impact sound sources for impact sound insulation measurement*, Applied Acoustics **51**(1), 85–108.

[89] Forthergill, L.C., Carman, T. (1990), *A comparison of methods for rating the insulation of floors against impact sound*, Building Research and Practice. The Journal of CIB **18**(4), 245–249.

[90] Homb, A. (2005), *Low frequency sound and vibrations from impacts on timber floor constructions*, Ph.D. thesis, Department of Structural Engineering, Norwegian University of Science and Technology (NTNU), Trondheim, Norway.

[91] Cremer, L., Heckl, M., Petersson, B. (2005), *Structure-borne sound – Structural vibrations and sound radiation at audio frequencies*, Springer, Berlin, Germany.

[92] Vér, I.L. (1971), *Impact noise isolation of composite floors*, The Journal of the Acoustic Society of America **50**, 1043–1050.

[93] Scholl, W., Maysenhölder, W. (1999), *Impact sound insulation of timber floors: interaction between source, floor coverings and bearing floor*, Building Acoustics **6**, 43–61.

[94] Brunskog, J., Hammer, P. (2003), *The interaction between the ISO tapping machine and lightweight floors*, Acta Acustica united with Acustica **89**, 296–308.

[95] Rabold, A., Buchschmid, M., Düster, A., Müller, G., Rank, E. (2010), *Modelling the excitation force of a standard tapping machine on lightweight floor structures*, Building Acoustics **17**(3), 175–197.

[96] Coguenanff, C., Guigou-Carter, C., Jean, P. (2015), *Probabilistic model of the impact force spectrum for the standard ISO tapping machine*, in: *Proceedings of the 22nd International Congress of Sound and Vibration (ICSV)*, Florence, Italy.

[97] JIS (2000), *JIS A 1418-2: Measurement of floor impact sound insulation of buildings – Part 2: Method using standard heavy impact sources*, Japanese Standards Association, Tokio, Japan.

[98] JIS (2000), *JIS A 1418-1: Measurement of floor impact sound insulation of buildings – Part 1: Method using standard light impact source*, Japanese Standards Association, Tokio, Japan.

[99] Shi, W., Johansson, C., Sundbäck, U. (1997), *An investigation of the characteristics of impact sound sources for impact sound insulation measurement*, Applied Acoustics **51**(1), 85–108.

[100] Heylen, W., Lammens, S., Sas, P. (2007), *Modal analysis – Theory and testing*, Heverlee, Katholieke Universiteit Leuven, Belgium.

[101] Reynolds, P., Pavic, A. (2000), *Impulse hammer versus shaker excitation for the modal testing of building floors*, Experimental Techniques **24**(3), 39–44.

[102] Agilient Tecnologies (2000), *Application note – The fundamentals of modal testing*, Tech. Rep. 243-3, Agilient Tecnologies, USA.

[103] Brandt, A. (2011), *Noise and vibration analysis – Signal analysis and experimental procedures*, Wiley, Chichester, UK.

[104] Herlufsen, H. (2012), *Bruel & Kjaer application note – Modal analysis using multi-reference and multiple-input multiple-output techniques*, Tech. Rep. BO0505-12, Bruel & Kjaer, Denmark.

[105] Fischer, M. (2006), *Vibrations and structure-borne sound in civil engineering – Theory and applications: statistical energy analysis*, in: *Proceedings of the Joint Advanced Student School (JASS)*, Saint Petersburg, Russia.

[106] Atalla, N., Sgard, F. (2015), *Finite element and boundary methods in structural acoustics and vibration*, CRC press, Taylor & Francis, Boca Ratón, FL, USA.

[107] Antes, H. (2010), *A short course on boundary element methods*, Institut für Angewandte Mechanik, Technische Universität Braunschweig, Germany.

[108] Chen, G., Zhou, J. (2010), *Boundary element methods*, Academic Press (Computational Mathematics and Applications), London, UK.

[109] Ciskowski, R., Brebbia, C. (1991), *Boundary element methods in acoustics*, Springer, Amsterdam, Netherlands.

[110] Lyon, R.H. (1975), *Statistical energy analysis of dynamical systems*, Tech. rep., MIT Press, USA.

[111] Hopkins, C. (2007), *Sound Insulation*, Elsevier/Butterworth-Heinemann, Oxford, UK.

[112] Díaz Cereceda, C. (2013), *Efficient models for building acoustics: combining deterministic and statistical methods*, Ph.D. thesis, Applied Mathematics Department, Politechnical University of Cataluña, Barcelona, Spain.

[113] Lafont, T., Totaro, N., Le Bot, A. (2013), *Review of statistical energy analysis hypotheses in vibroacoustics*, Proceedings of the Royal Society of London A: Mathematical, Physical and Engineering Sciences **470**(2162), 1–20.

[114] Wu, T., Dandapani, A. (1994), *A boundary element solution for sound transmission through thin panels*, Journal of Sound and Vibration **171**(2), 145–157.

[115] Borello, G., Courjal, R., NGuyen, R. (2004), *Combining finite element and SEA approach in vibroacoustic analysis*, in: *Proceedings of 7th French Acoustic Congress*, Strasbourg, France.

[116] Borello, G., Gagliardini, L., Houillon, L., Petrinelli, L. (2005), *Virtual SEA-FEA-based modeling of mid-frequency structure-borne noise*, Sound and Vibration Magazine 22–28.

[117] Müller, G., Buchschmid, M. (2014), *Hybrid approaches for vibroacoustical problems based on the finite element method and statistical energy analysis*, Wave Motion **51**(4), 622–634.

[118] Ottosen, N., Petersson, H. (1992), *Introduction to the finite element method*, Prentice Hall, London, UK.

[119] Bathe, K.J. (1994), *Finite element procedures*, Prentice Hall, New York, USA.

[120] Sandberg, G., Ohayon, R. (2008), *Computational aspects of structural acoustics and vibration – Series: CISM International Centre for Mechanical Sciences, Number 505*, Springer-Verlag Wien, New York, USA.

[121] Flodén, O., Persson, K., Sandberg, G. (2014), *Reduction methods for the dynamic analysis of substructure models of lightweight building structures*, Computers & Structures **138**, 49–61.

[122] Flodén, O., Persson, K., Sandberg, G. (2014), *Coupling elements for substructure modelling of lightweight multi-storey buildings*, in: *Proceedings of the XXXII International Modal Analysis Conference (IMAC)*, Orlando, FL., USA.

[123] Park, K.C. (presented at Lund University on October 28th, 2013), *Analyses, model tests and design modifications for vibration/noise mitigation*, Lecture notes, Center for Aerospace Structures, Department of Aerospace Engineering Sciences, University of Colorado at Boulder, CO, USA.

[124] Allemang, R.J., Brown, D.L. (1982), *A correlation coefficient for modal vector analysis*, in: *Proceedings of the I International Modal Analysis Conference (IMAC)*, Orlando, FL., USA.

[125] Gané, A. (2012), *Análisis de componentes principales (in Spanish), [Principal component analysis]*, Lecture notes, Department of Statistics, University Carlos III Madrid, Spain.

[126] González Martín, P., Díaz de Pascual, A., Torres Lezama, E., Garnica Olmos, E. (1994), *Una aplicación del análisis de componentes principales en el área educativa (in Spanish), [An application of the principal component analysis in the educational area]*, Revista Economía **9**, 55–72.

[127] De Leeuw, J. (2003), *Principal component analysis of binary data: Applications to roll-call analysis*, Tech. Rep. n°364, UCLA Department of Statistics, Los Angeles, CA, USA.

[128] Chang, J.J., Carroll, J.D. (1969), *How to use MDPREF: a computer program for multidimensional analysis of preference data*, Tech. rep., Bell Telephone Laboratories, Murray Hill, NJ, USA.

[129] Carroll, J.D. (1972), *Individual differences and multidimensional scaling*, in: Shepard, R. N., Romney, A. K. and Nerlove S. B. (ed.), *Multidimensional scaling: theory and applications in the behavioral sciences*, 105–155, Seminar Press, New York and London.

[130] Eckart, C., Young, G. (1936), *The approximation of one matrix by another of lower rank*, Psychometrika **1**, 211–218.

[131] The New MDSX Project (1981), *The MDS(X) series of multidimensional scaling programs. User's manual. Report 51*, Inter-University / Research Council Series, Edinburgh, Scotland.

[132] Cattell, R.B. (1966), *The Scree test for the number of factors*, Multivariate Behavioral Research **1**, 245–276.

[133] Coxon, A.P.M. (1982), *The user's guide to multidimensional scaling*, Heinemann Educational Books, London, UK.

[134] Schroeder, M.R., Gottlob, D., Siebrasse, K.F. (1974), *Comparative study of European concert halls – Correlation of subjective preference with geometric and acoustic parameters*, Journal of the Acoustical Society of America **56**(4), 1195–1201.

[135] Gelman, A., Hill, J. (2007), *Data analysis using regression and multilevel/hierarchical models*, Cambridge University Press, New York, USA.

[136] Hox, J.J. (2010), *Multilevel analysis – Techniques and applications*, Hogrefe and Huber, New York, USA.

[137] Goldstein, H. (2011), *Multilevel statistical models*, Wiley, London, UK.

[138] Tabachnick, B.G., Fidell, L.S. (2011), *Using multivariate statistics*, Pearson A & B, Boston, USA.

[139] Buchschmid, M., Kohrmann, M., Winter, C., Müller, G., Völtl, R., Schanda, U. (2013), *Vibroacoustic characteristics of light-weighted slabs – Part 2: Measurement-based investigation of the sound radiation of suspended ceilings*, in: *Proceedings of AIA-DAGA 2013*, Merano, Italy.

[140] Buchschmid, M., Kohrmann, M., Müller, G., Schanda, U. (2015), *Vibroacoustic investigation of light-weight ceilings – Modeling aspects and design guidelines*, in: *Proceedings of Euronoise 2015*, Maastricht, Netherlands.

Part II

Appended publications

Paper A

Investigation of the vibration transmission through a lightweight junction with elastic layer using the finite element method

Juan Negreira Montero[a)]
Anders Sjöström[b)]
Delphine Bard[c)]
Department of Constuction Sciences – Division of Engineering Acoustics
Lund Tekniska Högskola, BOX 118, 22100 Lund, Sweden

When the Swedish construction code in 1994 allowed wooden multi-storey buildings, this type of lightweight structures became popular due to low cost and ease of construction[1]. A drawback in those buildings is disturbing vibrations and noise propagating in the construction, especially through the junctions - for example between floor and wall. These structures should not just meet the demands of structural integrity but also the dynamic requirements. Therefore, gaining knowledge about their dynamic behaviour is of crucial importance. To reduce noise and vibration through the junctions, rubber foam materials may be introduced between the walls and the floors and ceilings[1]. Hence, finite element simulations are useful as a prediction tool during the design phase. In this study, the properties of a junction when introducing a rubber foam material - Sylodyn® - in between were investigated by means of the finite element method using the commercial software Abaqus. The flanking transmission was specifically analysed.

1 INTRODUCTION

Lightweight structures made of timber material have a number of advantages; they may become cost effective in the future and they demand relatively short production time. However, one of the main drawbacks is related to the sound transmission, as it is becoming an increasing nuisance. The differences in weight, stiffness, density and repartition compared to traditional materials have repercussions on how the sound propagates throughout the structures. Due to this, problems with sound insulation at low frequencies through the junctions may arise. In order to avoid such problems, the weight of the construction could be increased, but this would go counter the main advantage of these constructions, i.e. being light. Another solution, which has been proved to be effective via measurements[1] but not yet accurately modelled using the finite element method (FEM), is to introduce a rubber foam material within the junction. The main

[a)] email: juan.negreira_montero@construction.lth.se
[b)] email: anders.sjostrom@construction.lth.se
[c)] email: delphine.bard@construction.lth.se

purpose is to reduce noise and vibration in the low frequency range (i.e. 20 Hz – 200 Hz). In this investigation, the influence of *Sylodyn* when placed in junctions between floor, walls and ceilings is studied. Several types of floors and ceilings as well as different placements and properties of the *Sylodyn* have been analysed.

1.1 Problem Description

In this investigation, a standard volume of a room was considered. Its inner dimensions are 3.6 m width and 6 m long, whilst the height is 3 m. In Figure 1 and 2, the drawings from *Lindbäcks Bygg's* project Brunnby Park in Upplands Väsby are shown. This lightweight structure using volume modules was chosen in order to carry out this flanking transmission investigation. The reason for this choice was its widespread use in Sweden and also because of a feasible future comparison between finite element simulations and in-situ measurements which have already been performed.

Two different placements of the *Sylodyn* were analysed as shown in Figure 3. One hereafter denoted as *case A*, where the *Sylodyn* is placed in between the top and the bottom part of the walls and the floor and ceiling on the side of the vertical partitions. The second, *case B*, where the *Sylodyn* is positioned underneath the floor and on top of the wall below. In this case, the upper wall is resting on the floor whereas the ceiling is fitted into the cavity left by the walls.

In both *case A* and *B*, the beams comprising the floor and the ceiling were considered to be placed along the shorter dimension, i.e. widthwise. Furthermore, for *case A,* the variation on the flanking transmission was also investigated when considering the beams along the lengthwise direction. A parameter study varying the material properties for the *Sylodyn* was also carried out. Finally, an analysis of the same junction without *Sylodyn* was performed.

2 FINITE ELEMENT MODEL

2.1 Introduction

Modelling a junction to represent all the phenomena involved and thus its real behaviour is a very complicated task[2]. The objective is to find a finite element model that is able to capture the phenomena that are occurring in reality. As previously mentioned, the main objective of this investigation is to study the effects of different placements of the *Sylodyn* on the flanking transmission. Hence, the relative differences between the modelled results are of greater importance than the absolute correlation between the model and the existent measurements. By doing so, one gains knowledge on the behaviour of the structure by investigating the parameters influencing the response and therefore enabling to eventually create a more refined model. With the latter model, one could try to correlate both experimental and simulation results.

As seen in Figures 1 and 2, the construction elements are composed by different materials, i.e. plasterboards, parquet, massive wood, etc. However, for this first investigation, wood was considered all over the whole model with exception of the *Sylodyn*. This simplification will not disrupt the relative differences between the different cases studied. Furthermore, only negligible vibrations are transmitted through the insulation existent in the partitions[3] and since modelling it would drastically increase the computational time, the insulation was excluded and taken into account by slightly increasing the damping of the other materials.

2.2 Materials

The structure will only be exposed to loads and displacements with low magnitude. Therefore, all non-linear behaviour was neglected and the materials may be modelled as linear elastic.

The elastomer introduced in the model to reduce the noise and vibration transmission was *Sylodyn NE*, a mixed cellular polyurethane dampening material developed by *Getzner Werkstoffe GmbH*. These viscoelastic construction elements are aligned in the path of propagation of the vibrations. Compared to existing dampening rubber, *Sylodyn* is more durable, more stable and is able to be made thinner in order to fit into small spaces[4]. *Sylodyn* can be used in many different ways, e.g., covering the whole surface, in stripes or in block shapes. In this study, it was modelled as squared blocks with dimensions 100 mm x 100 mm x 25 mm. The distance c/c (centre-to-centre) between two blocks in the junction was set to 400 mm.

In Figure 4, the load-deflection curve under compression loads for a block of *Sylodyn* is shown[4]. This curve, as all the material properties, is dependent on a parameter called shape factor; a geometric measure for the shape of an elastomeric bearing. It is defined as the ratio of the loaded area and the sum of the area of the perimeter surfaces. It has an influence in the deflection and the static load limit respectively. It can be observed that in the lower load ranges, there is a linear relationship between compression and deformation. After the linear load range, the curve moves on a degressive path, i.e. the material reacts to additional static and dynamic loads in a particularly soft manner, thus allowing for highly effective vibration isolation. For loads and deformation exceeding the degressive range, the deflection curve is progressive. The material becomes stiffer and therefore the vibration isolation is reduced. This material is not affected by overload as it recovers almost completely after load removal[4]. Furthermore, as all elastomers, *Sylodyn* reacts to dynamic loads more stiffly than to static loads.

Poisson's ratio can only be stated with adequate precision for materials that are loaded in the linear range. It was set to 0.44, whilst the loss factor considered was 0.20[4]. Due to this assumption (Hooke's law applies), the preload on the *Sylodyn* due to the walls resting on top of the blocks will not have an influence on the results. The material properties are listed in Table 1, where E [MPa] is the modulus of elasticity, ν [-] the Poisson's ratio, η [-] the loss factor, d [-] the damping ratio, ρ [kg/m^3] the mass density and G [MPa] the shear modulus.

The other material used in the model was wood. It is an anisotropic material, implying different material properties in different directions. It was modelled in *Abaqus* with the engineering constants shown in Table 1[5]. Direction 3 was considered to be along the fibre direction whilst direction 1 and 2 are perpendicular to the fibre direction. Damping prevents the structure from oscillating infinitely. It is always present in real structures and thus considered also here. It was modelled as Rayleigh damping[6] and the damping ratio was set to 3%.

2.3 Mesh

Initial calculations, i.e. convergence analyses, were carried out on single beams with different lengths and on plates with different dimensions in order to establish an appropriate mesh size that provides adequate results with low computational cost. Consequently, one ensures

that all the beams and plates assembled to create the entire model are correctly meshed and thus providing reliable results. Note the importance of this fact since we are dealing with a large model; the FE-model contains approximately 2 millions of degrees of freedom. A too fine mesh will most certainly cause an unacceptable long computation time. Only 8-nodes brick elements (C3D8R) were tried, because quadratic 20-node brick elements (C3D20R) have a tendency to create a model stiffer than reality[2]. Besides, they also cause long computation times and are therefore disregarded as element type for the complete structure.

When performing the convergence analyses, it was noticed that the biggest differences between the results of the reference mesh and the chosen FE solution are in the torsional modes; but the fact that the structure will mainly be excited by vertical loads makes the mode shapes with movement in vertical direction more important in this investigation. The vertical oscillations are also assumed to create most of the disturbing vibrations and noises that can occur in lightweight structures[2].

The most difficult challenge when creating a model of an assembled structure is to model the connections between the parts accurately. The connections determine most of the torsional rigidity and influence the behaviour of the whole structure[2]. In this study, the interactions between parts were modelled with tie constraints (full coupling). This creates stiff connections, as it happens to be the case in the real structure, where the elements are rigidly constructed using glue and screws.

The load considered was a 5 N harmonic concentrated force located at the middle of the room. A frequency sweep from 10 to 100 Hz in steps of 1 Hz was carried out. Fixed boundary conditions were applied at the free end of the walls. The different models for all studied cases can be seen in Figures 5-7. The blocks of *Sylodyn* are shown in grey colour, the floor in blue, the ceiling in red, the inner walls in yellow and the outer walls in green. Apartment separating walls (inner walls) were considered along the long edge of the room, whereas facade walls (outer walls) along the shorter sides. The height of each room was set to 1.5 m.

3 RESULTS

The following results show the performance of the junctions regarding the flanking transmission by means of plots “acceleration versus frequency”. Furthermore, the transmission from the source, located on the middle of the floor, to the ceiling underneath through the inner wall junction was investigated, i.e. the vertical transmission from the floor to the ceiling through the long side of the room. The frequency dependent acceleration was evaluated at 6 nodes along the floor, walls and ceiling, all placed 0.2 m from the junction. Likewise, the acceleration magnitudes were also evaluated on top and bottom of the *Sylodyn* blocks. An average acceleration for the 6 nodes was carried out and plotted for the different elements composing the junction. In Figure 3 the evaluation points are shown.

3.1 Case A with beams oriented widthwise

In Figure 5, one can observe that the *Sylodyn* blocks (grey) are placed between the partitions whereas the floor and the ceiling are fitted into the space created by the walls, see Figure 3. The beams are oriented widthwise.

As shown in Figure 8, the maximum acceleration magnitudes occur between 35 and 60 Hz. One can also identify that *Sylodyn* dissipates nearly all vibrations, i.e. dampens vibrations (see Figure 13), as the acceleration levels evaluated on the ceiling and the wall underneath are very low.

3.2 Case A with beams oriented lengthwise

This case is comparable with the previous case, although the beams in the floor and ceiling are now placed lengthwise, see Figure 6. The peak acceleration magnitudes existent on the floor are higher than in the previous case, probably due to the change of the orientation in the load bearing beams of the horizontal partitions. Likewise, the shape of the plots is also changed as seen in Figure 9. In this case, the acceleration peaks occur between 25 and 50 Hz as well as between 80 and 95 Hz approximately. However, the acceleration magnitudes on the ceiling and wall underneath are still very low, depicting the efficiency of the *Sylodyn* when dissipating the energy of the vibrations.

3.3 Case B with beams oriented widthwise

In Figure 7 the changed placement for the *Sylodyn* is shown. The walls on the upper floor now rest on the floor itself, being the *Sylodyn* in contact with the floor and the walls in the floor underneath. The ceiling is, as in the other cases, fitted into the cavity left by the vertical partitions. The shape of the plots resembles the ones in c*ase A* widthwise but with smaller acceleration magnitudes almost over all the frequency range as shown in Figure 10. This shows *a priori* a better performance of the junction regarding flanking transmission, although a more extensive study is needed to confirm this. As in the other cases, the *Sylodyn* performs very well when reducing the transmitted vibrations.

3.4 Parameter study

The modulus of the elasticity of the *Sylodyn* was varied in order to investigate its influence on the response of the structure. The *case A* with the beams of the floor and the ceiling along the widthwise direction was considered for this purpose. The initial value of the modulus of elasticity, i.e. 3 MPa was varied and set to 6 MPa and 9 MPa respectively. In Figure 11, the results are shown. It can be observed that the variation on the acceleration magnitude when increasing the value of the modulus of elasticity is not as large as it could be expected beforehand.

3.5 Junction without Sylodyn

The performance of the junction without *Sylodyn* was also investigated. Thus, all contacts were wood-wood connections. The performance of *case A* with beams placed widthwise was compared in both cases. The results are shown in Figure 12. It is apparent that the acceleration magnitudes evaluated at the bottom room without the *Sylodyn* are much higher, which indicates the advantages of using the *Sylodyn* as a vibration insulator in the junction.

4 CONCLUSIONS

An extensive investigation regarding the flanking transmission when introducing *Sylodyn* in a lightweight junction was carried out. It was shown that regardless of the orientation of the load bearing beams in the floor and ceiling or the placement of the *Sylodyn*, the reduction of acceleration magnitudes within the blocks of *Sylodyn* is very effective. In Figure 13 one is able to perceive how the vibrations, i.e. acceleration magnitudes, are reduced inside the block.

It was also portrayed by a parameter study that a variation in the modulus of elasticity of the *Sylodyn* does not greatly influence the vibration transmission through the junction. Likewise, it was seen that *case B* for the placement of the Sylodyn may perform better than *case A*, although a more extensive study is needed in order to confirm this fact.

In addition, the performance of a junction with *Sylodyn* was compared to the same junction without *Sylodyn*, i.e. wood-wood connections all over. It was observed that the vibrations transmitted are much higher in the latter than in the former case. Hence, the advantages of using *Sylodyn* for this type of junction were proved.

An extensive insight into the performance of the junction regarding flanking transmission has been gained. Ultimately, this will eventually allow the creation of more refined models in order to correlate both experimental and simulation results, which could be used as a prediction tool during the design phase of the structures. However, in these advanced models, more realistic boundary conditions, connections as well as the accurate material properties may be considered. All in all, it can be said that improvements in the models are needed for results to be accurate.

Note that the conclusions drawn in this investigation correspond to this specific type of junction, although many junctions found in real lightweight structures have similar features.

5 ACKNOWLEDGEMENTS

This research was funded by the Silent Spaces project, a part of the EU program Interreg IV.

6 REFERENCES

1. J. Forssén et al. "Acoustics in wooden buildings. State of the art 2008. Vinnova Project 2007-01653*". SP Technical Research Institute of Sweden Report 2008:16*. Stockholm (2008).

2. J. Negreira Montero, O. Flodén and D. Bard, "Reflection and transmission properties of a wall-floor building element: comparison between finite element model and experimental data", *Acoustics 2012 Hong Kong* (conference proceedings), Hong Kong (May 2012).

3. L. Holterman and A. Peterson. *Vibrations in a seven-storey wood building.* Master thesis. Division of Structural Mechanics, Lund University, Sweden (2008).

4. Getzner Werkstoffe GmbH (2004). *Data sheet of the Sylodyn NE.*

5. F. Morianon, S. Fortino and T. Toratti, “A method to model wood by using Abaqus finite element software. Part 1: Constitutive model and computational details”, *VTT Technical Research Center of Finland -Report 687-*, VTT Publications, Helsinki (2008).

6. A. K. Chopra, *Dynamics of structures*, 3rd Edition, Prentice Hall, New Jersey, USA (2007)

7. L. Cremer, M. Heckl, B. A. T. Petersson. *Structure borne-sound*. 3rd Edition. Springer-Verlag. Berlin (2005).

8. K.J. Bathe, *Finite Element Proceedures*, Prentice Hall, New York, United States (1996).

9. C. Hopkins, *Sound Insulation*, Elsevier, Oxford, UK (2007).

10. L. Galbrun, “Vibration transmission through plate/beam structures typical of lightweight buildings: Applicability and limitations of fundamental theories”, *Applied Acoustics*; 71:587-596 (2010).

Table 1 – Material Properties

Wood		*Sylodyn*	
E_1 [MPa]	900	E [MPa]	3 (varied)
E_2 [MPa]	500	ν [-]	0.44
E_3 [MPa]	12500	ρ [kg/m^3]	750
G_{12} [MPa]	40	η [-]	0.1
G_{13} [MPa]	700		
G_{23} [MPa]	700		
ν_{12} [-]	0.558		
ν_{13} [-]	0.038		
ν_{23}[-]	0.015		
ρ [kg/m^3]	550		
d [-]	0.03		

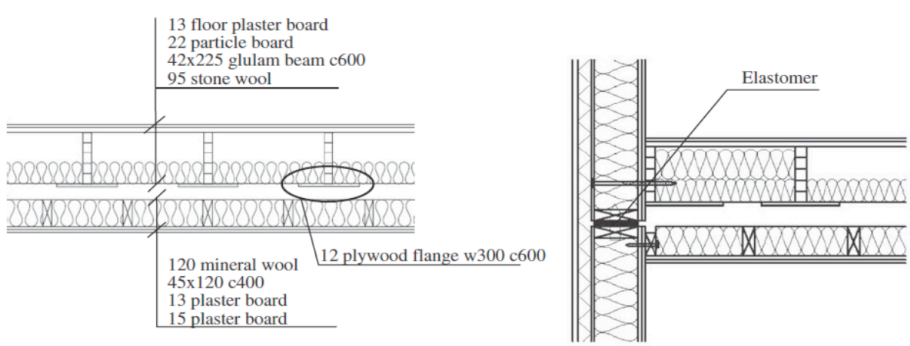

Fig. 1 - Floor/Ceiling drawings (left) and assemblage with the façade element, the so-called outer-wall (right).

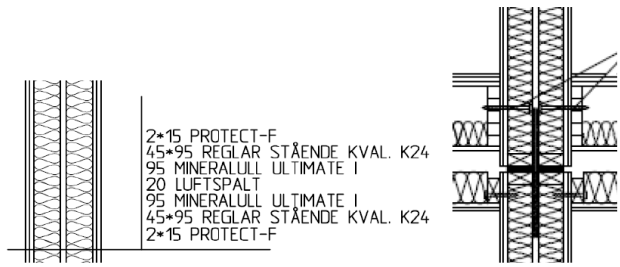

Fig. 2 - Drawings of the separating walls, i.e. inner walls (left) and the assemblage with the floor/ceiling (right).

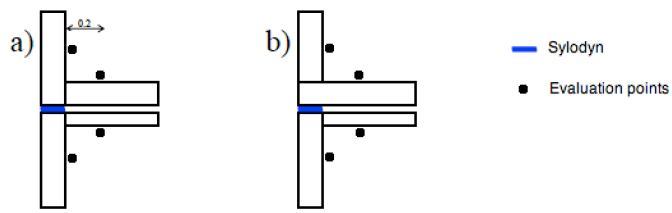

Fig. 3 - Different Sylodyn positions: (a) floor and ceiling installed between the walls and (b) floor installed upon walls. The evaluation points are dots in the figure (6 evaluation points along each line are considered).

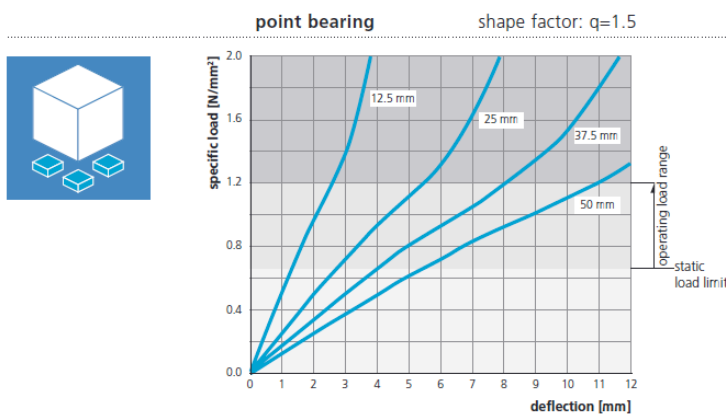

Fig. 4 - Quasy-static load-deflection curve for the Sylodyn under compression load[4].

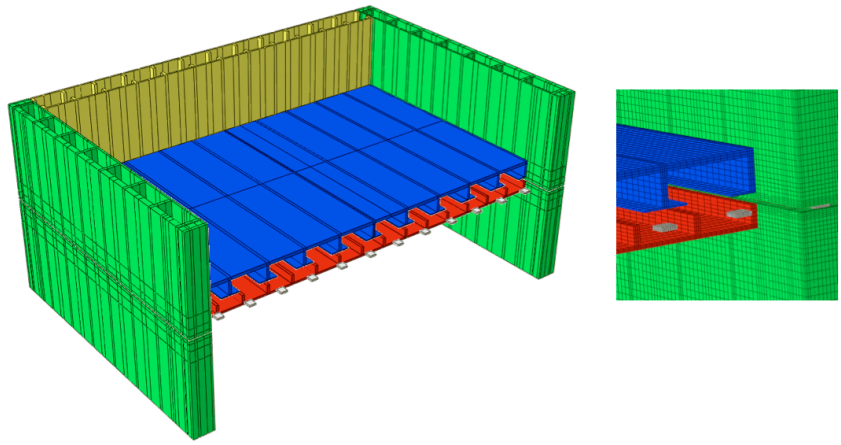

Fig. 5 - Case A with beams oriented widthwise.

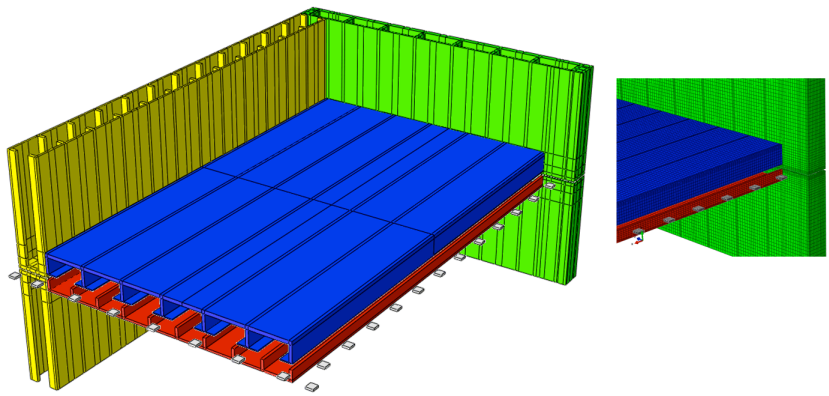

Fig. 6 - Case A with beams oriented lengthwise.

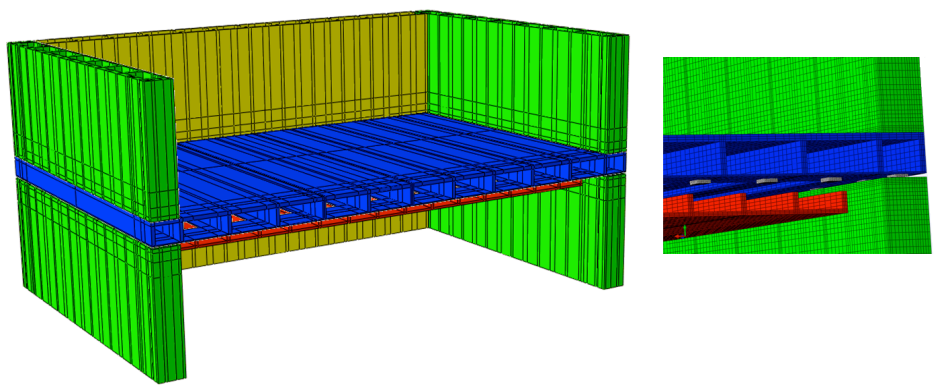

Fig. 7 - Case B with beams oriented widthwise.

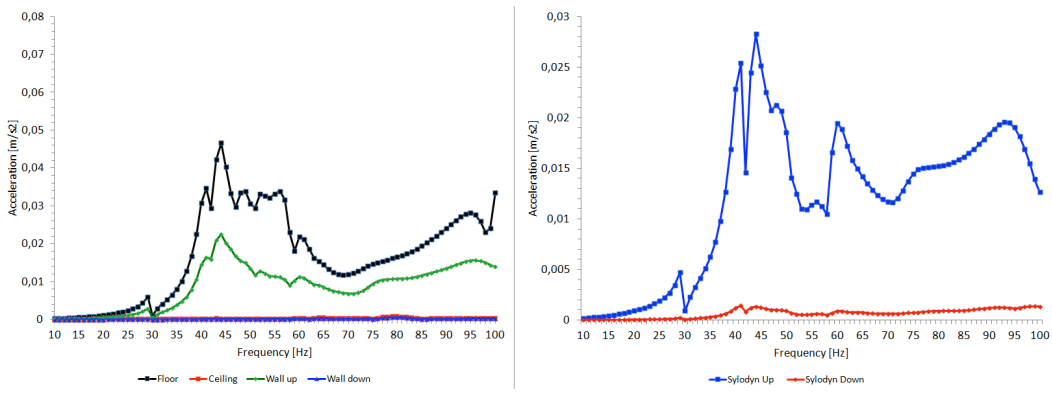

Fig. 8 - Case A widthwise. Acceleration magnitudes evaluated on the floor, ceiling, upper and bottom walls (left) and acceleration magnitudes evaluated on top and bottom of the Sylodyn (right).

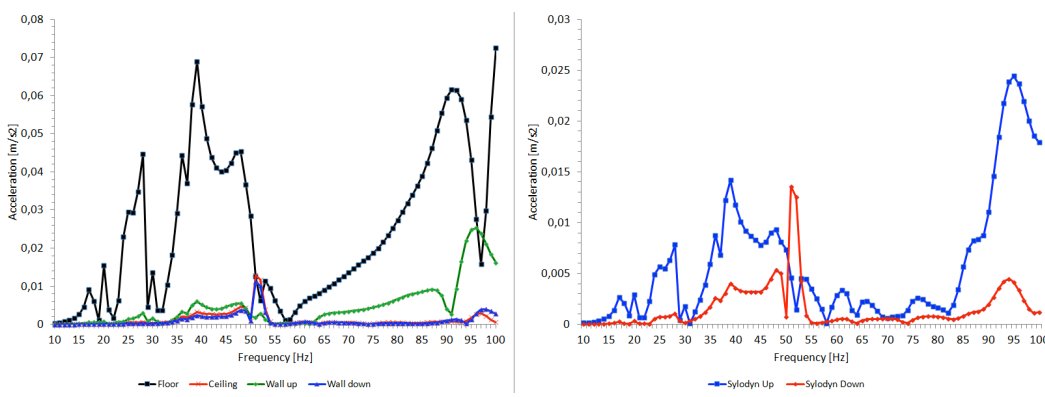

Fig. 9 - Case A lengthwise. Acceleration magnitudes evaluated on the floor, ceiling, upper and bottom walls (left) and acceleration magnitudes evaluated on top and bottom of the Sylodyn (right).

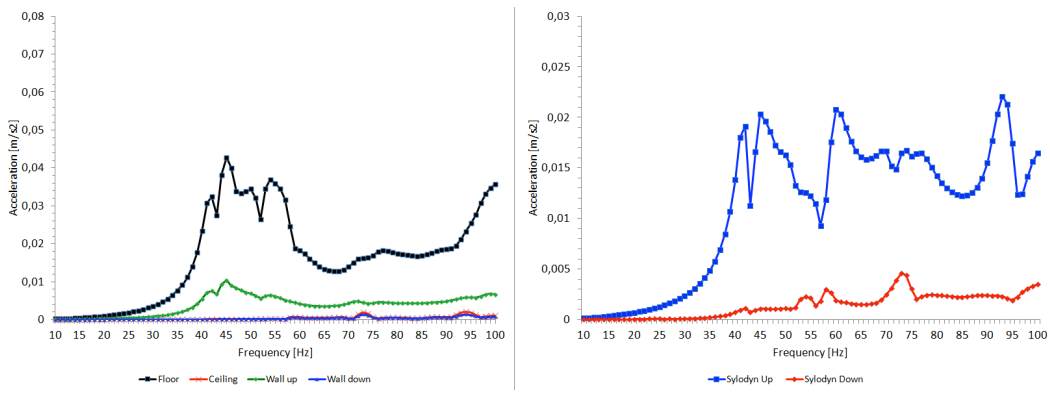

Fig. 10 - Case B widewise. Acceleration magnitudes evaluated on the floor, ceiling, upper and bottom walls (left) and acceleration magnitudes evaluated on top and bottom of the Sylodyn (right).

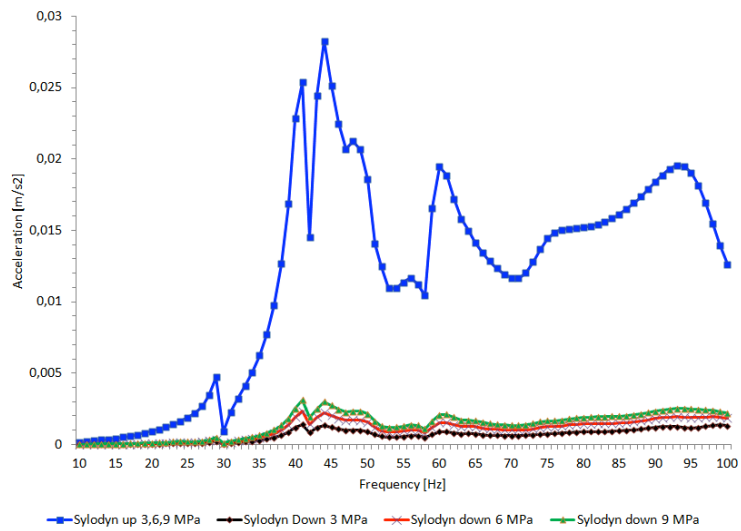

Fig. 11 - Parameter study. Comparison between the acceleration magnitudes evaluated on top and bottom of the Sylodyn blocks when varying their modulus of elasticity.

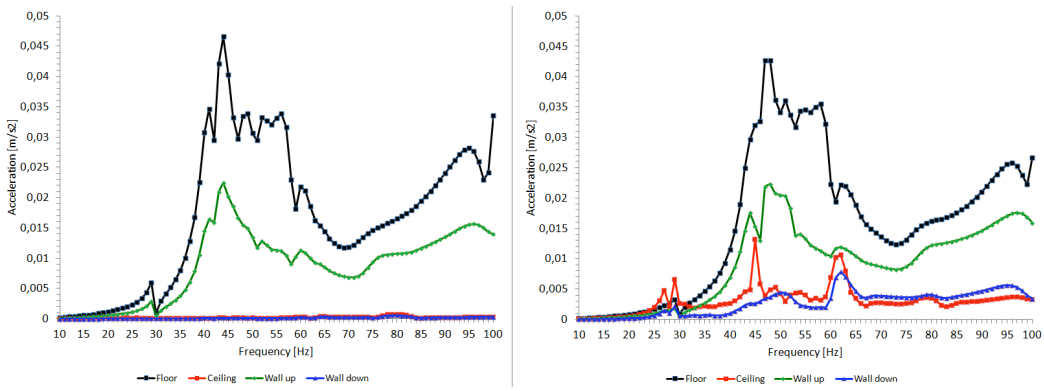

Fig. 12 - Comparison between the acceleration magnitudes for the junction using Sylodyn (left) and without Sylodyn (right). Case A widhwise was considered. The acceleration was evaluated on the floor, the ceiling and the both wall in the upper and lower floor.

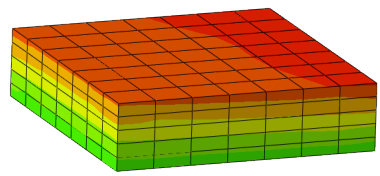

Fig. 13 -Example of reduction of the acceleration magnitudse in a block of Sylodyn for a given frequency (44 Hz) in case A widthwise. Red indicates high acceleration magnitudes whereas green shows low magnitudes.

Paper B

Engineering Structures 83 (2015) 7–16

Contents lists available at ScienceDirect

Engineering Structures

journal homepage: www.elsevier.com/locate/engstruct

The effect of modelling acoustic media in cavities of lightweight buildings on the transmission of structural vibrations

O. Flodén *, J. Negreira, K. Persson, G. Sandberg

Department of Construction Sciences, Lund University, P.O. Box 118, SE-22100 Lund, Sweden

ARTICLE INFO

Article history:
Received 20 February 2014
Revised 14 July 2014
Accepted 20 October 2014
Available online 21 November 2014

Keywords:
Structure–acoustic interaction
Porous materials
Vibration transmission
Lightweight buildings
Finite element method

ABSTRACT

Determining the dynamic behaviour of lightweight buildings by means of finite element analyses requires models representing the geometry involved in great detail, resulting in systems having many millions of degrees of freedom. It is, therefore, important to avoid unnecessarily detailed models by carefully considering what is essential to include in the models and the level of details required for describing the phenomena of interest accurately. In the study presented here, it was investigated whether or not air and insulation in cavities of multi-storey wood buildings affect the transmission of low-frequency structural vibrations. It was concluded, by means of numerical studies, that including air and insulation in cavities, modelled as acoustic media, affects the transmission from a floor to the underlying ceiling and surrounding walls.

1. Introduction

In 1994, a century-old ban on the construction of wooden buildings more than two storeys in height in Sweden was lifted, leading to the reintroduction of such structures. Compared to heavier structures, the lightweight buildings are more sensitive to vibrations, making it difficult to construct multi-storey wood buildings in such a way that noise and disturbing vibrations in the different storeys and rooms are avoided. Specifically problematic is the issue of low-frequency vibrations [1]. Wooden constructions involving long spans have low resonance frequencies that, in combination with low damping, are easily excited by loads with low-frequency content. The vibrations can be caused by, for example, footsteps, airborne sound, vibrating machines and external sources such as railway and road traffic. To design buildings of adequate performance regarding sound and vibrations, it is desirable to have tools for predicting the effects of structural modifications prior to construction. Testing prototypes and performing experiments are both time-consuming and expensive, the long-term aim therefore being to develop prediction tools that are valid for general load-cases by making use of finite element (FE) models.

Accurately assessing the dynamic behaviour of multi-storey lightweight buildings, even at lower frequencies, requires FE models representing the geometry in considerable detail, resulting in the models being very large. The number of degrees of freedom of such models easily exceeds the limits of computer capacity, at least for computations to be performed within reasonable time. It is, therefore, important to avoid unnecessarily detailed models by carefully considering what is essential to include in the models and the level of details required for describing the phenomena of interest accurately. The issue considered here is whether or not air and insulation in cavities of multi-storey wood buildings affect the transmission of structural vibrations.

The acoustic pressure field in a room can interact with the vibrations in the floor, ceiling and walls. For heavier structures, the acoustic pressure waves usually have a negligible effect on the structural vibrations. It is, therefore, possible to analyse the acoustic pressure field by applying the structural displacements, obtained from a precedent analysis of the structural domain, as boundary conditions. Moreover, the effect of the acoustic media in a structure, on the transmission of structural vibrations, depends on the flexibility of the structure, a more flexible structure tending to interact more with the acoustic media. It was concluded in [2] that the acoustic pressure field in the rooms is negligible also for lightweight buildings; studies on a 2D FE model of a two-storey wood building showing that the effect of including air in the rooms, on the displacements of the building, is small for frequencies below 250 Hz. The air was modelled to have a realistic acoustic damping, which is present in buildings due to objects and porous materials such as curtains and carpets.

In multi-storey wood buildings, there are acoustic media not only in the rooms, but also in the many cavities containing both air and insulation. The effect of modelling air in cavities of lightweight

* Corresponding author.
E-mail address: ola.floden@construction.lth.se (O. Flodén).

http://dx.doi.org/10.1016/j.engstruct.2014.10.037
0141-0296/

double-plate wall panels was investigated in [3,4]. In [3], the vibration transmission was investigated for a model including two double-plate wall panels connected in an L-shape, with and without air in the cavities. Both eigenvalue and steady-state analyses showed that the inclusion of air in the cavities of the structure has a large effect on its dynamic characteristics at high frequencies and a noticeable effect already at the first eigenfrequency. In [4], the response of a double-plate wall panel, with and without air in the cavities, exposed to diffuse field excitation was investigated. Simulations in terms of eigenvalue and steady-state analyses showed that the air has a negligible effect on the dynamic characteristics of the structure, contradicting the results in [3].

The studies presented here aim at determining whether or not air and insulation in cavities have to be considered when performing numerical analyses of the low-frequency vibration transmission in multi-storey lightweight buildings. The low-frequency range is defined here as frequencies below 200 Hz. As a first step, different porous material models for modelling of the insulation were compared, a frame of a double-plate wall panel being employed as a test model. Subsequently, numerical studies were carried out for a section of a multi-storey wood building constructed with timber volume elements (TVEs), such buildings being described in Section 1.1. The response of a floor, exposed to a harmonic point load, and the vibration transmission from the floor to the underlying ceiling and the surrounding walls were investigated, comparing FE models including air and insulation as acoustic media in cavities to models without acoustic media.

The models employed in the numerical studies are representative for a wide range of residential wood buildings of the type studied here, in terms of both dimensions and material properties. It is, therefore, believed that the conclusions presented in the paper are valid for such structures. Moreover, a wide range of frequencies are considered, resulting in the same phenomena being captured also for models having slightly different dimensions, as the shift in eigenfrequencies in such cases is small compared to the width of the frequency range.

1.1. Timber volume element buildings

The conceptual layout of a TVE building is illustrated in Fig. 1. A TVE is a prefabricated volume module consisting of wood framed floor-, roof- and wall-elements, each TVE typically constituting a small apartment, one room or part of a larger room. As much of the construction work as possible is performed indoors at a factory, including electrical installations, flooring, cabinets, wardrobes etc. The prefabricated modules are transported to the construction site where they are stacked to form a complete building. In between the TVEs, several elastomer blocks are introduced to reduce the flanking transmission of vibrations. Each elastomer block has an interface area of approximately 0.1×0.1 m^2 and is placed between the walls of two stacked modules. The only additional connection between modules is through a number of tie plates, ensuring the global stability of the building. Vibrations transmitted in TVE buildings are, therefore, mainly passing through the elastomer layers or through the air and the insulation in the cavities of the buildings. The FE models employed in the numerical studies presented here were constructed according to the drawings shown in Fig. 2.

2. Governing theory

2.1. Structure–acoustic analysis

Structure–acoustic systems can be analysed by deriving FE formulations for both the structural domain and the acoustic fluid domain. By imposing continuity conditions for displacements and pressures at domain-separating boundaries, the domains form a coupled FE equation system. Vibrations in lightweight buildings are usually of such amplitudes that any non-linear behaviour can be neglected and, therefore, linear behaviour is assumed here for both domains. In the following derivations, a subscript S denotes a quantity in the structural domain, whereas a subscript F indicates a quantity in the acoustic fluid domain.

2.1.1. Structural domain

The equations describing the structural domain follow the notation in [6]. For a detailed derivation of the FE formulation of a solid, see e.g. [6,7]. The differential equation of motion for the continuum formulation of a three-dimensional solid, occupying the domain Ω_S, is given by

$$\tilde{\nabla}^T \boldsymbol{\sigma}_S + \mathbf{b}_S = \rho_S \frac{\partial^2 \mathbf{u}_S}{\partial t^2}, \tag{1}$$

where $\boldsymbol{\sigma}_S$ is the matrix representation of the stress tensor, $\mathbf{b}_S$ is the body force vector, ρ_S is the mass density, $\mathbf{u}_S$ is the displacement vector, $\tilde{\nabla}$ is a differential operator matrix and t is the time [8]. A FE discretisation and use of Galerkin's method results in a FE formulation in the structural domain, given by

$$\mathbf{M}_S \ddot{\mathbf{a}}_S + \mathbf{K}_S \mathbf{a}_S = \mathbf{f}_{l,S} + \mathbf{f}_{b,S}, \tag{2}$$

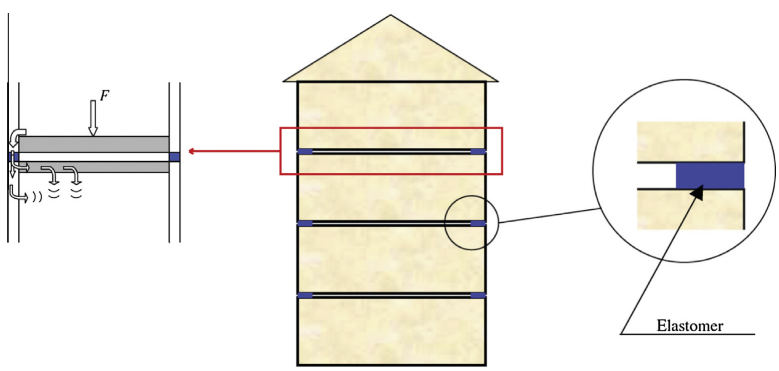

Fig. 1. Sketch of a TVE building [5]. The path of structural vibrations between storeys is illustrated in the figure to the left and an elastomer block is illustrated in the figure to the right.

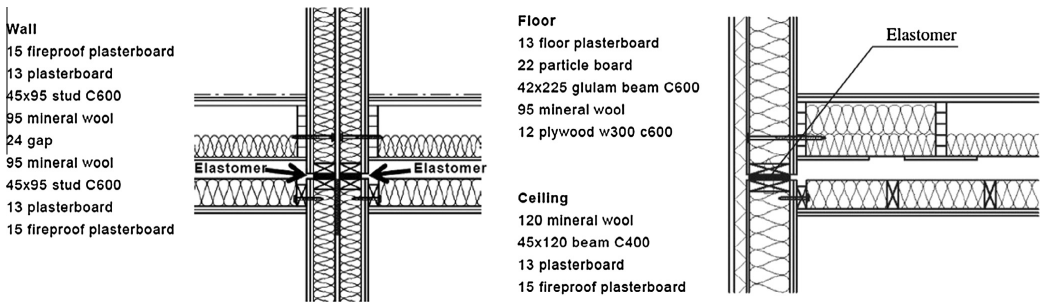

Fig. 2. Drawings of the TVE building system, showing sections of the floor and ceiling structures and the junctions with apartment separating wall (left) and façade wall (right).

$$\begin{aligned} \mathbf{M}_S &= \int_{\Omega_S} \mathbf{N}_S^T \rho_S \mathbf{N}_S \, \mathrm{d}V, \quad \mathbf{K}_S = \int_{\Omega_S} (\widetilde{\nabla}\mathbf{N}_S)^T \mathbf{D}_S \widetilde{\nabla}\mathbf{N}_S \, \mathrm{d}V, \\ \mathbf{f}_{l,S} &= \int_{\Omega_S} \mathbf{N}_S^T \mathbf{b}_S \, \mathrm{d}V, \qquad \mathbf{f}_{b,S} = \int_{\partial\Omega_S} \mathbf{N}_S^T \mathbf{t}_S \, \mathrm{d}S. \end{aligned} \tag{3}$$

where $\mathbf{M}_S$ is the mass matrix, $\mathbf{K}_S$ is the stiffness matrix, $\mathbf{a}_S$ is the nodal displacement vector, $\mathbf{f}_{l,S}$ is the body load vector, $\mathbf{f}_{b,S}$ is the boundary load vector, $\mathbf{N}_S$ contains the FE interpolation functions, $\mathbf{D}_S$ is the constitutive stress-strain matrix and $\mathbf{t}_S$ is the surface traction vector. Normally, a term $\mathbf{C}_S\dot{\mathbf{a}}_S$, where $\mathbf{C}_S$ is the damping matrix, is added to the left-hand side of Eq. (2) to account for viscous forces present in the structure.

2.1.2. Acoustic fluid domain

In addition to the assumption of small displacements, the governing equations of the acoustic fluid are derived supposing the fluid to be irrotational. The motion of an acoustic fluid can be described using different primary variables, such as the fluid displacement or a fluid displacement potential. In the FE formulation presented here, the acoustic pressure is used as primary variable. A detailed description of the FE formulation of an acoustic fluid, and the structure-acoustic coupling, can be found in [9], for example. The motion of the fluid in the acoustic fluid domain Ω_F is governed by the equation of motion and the continuity equation

$$\rho_0 \frac{\partial^2 \mathbf{u}_F}{\partial t^2} + R\frac{\partial \mathbf{u}_F}{\partial t} + \nabla p_F = 0, \tag{4}$$

$$\frac{\partial p_F}{\partial t} + \rho_0 c_0^2 \nabla \cdot \frac{\partial \mathbf{u}_F}{\partial t} = 0, \tag{5}$$

where p_F is the acoustic pressure, ρ_0 is the static density, R is the flow resistivity, c_0 is the speed of sound and ∇ is the gradient operator. By differentiating Eq. (5) with respect to time and inserting Eq. (4), the wave equation in the acoustic fluid domain is obtained as

$$\frac{1}{c_0^2}\frac{\partial^2 p_F}{\partial t^2} + \frac{R}{\rho_0 c_0^2}\frac{\partial p_F}{\partial t} - \nabla^2 p_F = 0. \tag{6}$$

An FE discretisation and use of Galerkin's method results in an FE formulation in the acoustic fluid domain, given by

$$\mathbf{M}_F \ddot{\mathbf{p}}_F + \mathbf{C}_F \dot{\mathbf{p}}_F + \mathbf{K}_F \mathbf{p}_F = \mathbf{f}_{b,F}, \tag{7}$$

$$\begin{aligned} \mathbf{M}_F &= \tfrac{1}{c_0^2}\int_{\Omega_F} \mathbf{N}_F^T \mathbf{N}_F \, \mathrm{d}V, \qquad \mathbf{C}_F = \tfrac{R}{\rho_0 c_0^2}\int_{\Omega_F} \mathbf{N}_F^T \mathbf{N}_F \, \mathrm{d}V, \\ \mathbf{K}_F &= \int_{\Omega_F} (\nabla \mathbf{N}_F)^T \nabla \mathbf{N}_F \, \mathrm{d}V, \quad \mathbf{f}_{b,F} = \int_{\partial\Omega_F} \mathbf{N}_F^T \mathbf{n}_F^T \nabla p_F \, \mathrm{d}S, \end{aligned} \tag{8}$$

where $\mathbf{p}_F$ is the nodal pressure vector, $\mathbf{f}_{b,F}$ is the boundary load vector and $\mathbf{n}_F^T$ is the boundary normal vector, pointing outwards from the acoustic fluid domain.

2.1.3. Coupling of domains

At interfaces connecting a structural domain to an acoustic fluid domain, denoted $\partial\Omega_{SF}$, there will naturally be a continuity in terms of both displacements and pressures. By imposing conditions of continuity as boundary conditions at the interfaces, the two equation systems describing the separate domains are coupled into a single system, including the interaction of the domains. The continuity in displacements and pressures at $\partial\Omega_{SF}$ can be expressed as

$$\mathbf{u}_S \mathbf{n}_F = \mathbf{u}_F \mathbf{n}_F, \tag{9}$$

$$\boldsymbol{\sigma}_S|_{n_F} = -p_F, \tag{10}$$

where $\boldsymbol{\sigma}_S|_{n_F}$ is the stress normal to $\partial\Omega_{SF}$. By introducing the spatial coupling matrix

$$\mathbf{H}_{SF} = \int_{\partial\Omega_{SF}} \mathbf{N}_S^T \mathbf{n}_F \mathbf{N}_F \, \mathrm{d}S, \tag{11}$$

the boundary load vectors at $\partial\Omega_{SF}$ can be rewritten as

$$\mathbf{f}_{b,S} = \mathbf{H}_{SF}\mathbf{p}_F, \tag{12}$$

$$\mathbf{f}_{b,F} = -\rho_0 \mathbf{H}_{SF}^T \ddot{\mathbf{a}}_S - R\mathbf{H}_{SF}^T \dot{\mathbf{a}}_S. \tag{13}$$

Using Eqs. (12) and (13) in combination with Eqs. (2) and (7) results in the structure-acoustic system of equations

$$\begin{bmatrix} \mathbf{M}_S & \mathbf{0} \\ \rho_0 \mathbf{H}_{SF}^T & \mathbf{M}_F \end{bmatrix} \begin{bmatrix} \ddot{\mathbf{a}}_S \\ \ddot{\mathbf{p}}_F \end{bmatrix} + \begin{bmatrix} \mathbf{C}_S & \mathbf{0} \\ R\mathbf{H}_{SF}^T & \mathbf{C}_F \end{bmatrix} \begin{bmatrix} \dot{\mathbf{a}}_S \\ \dot{\mathbf{p}}_F \end{bmatrix} + \begin{bmatrix} \mathbf{K}_S & -\mathbf{H}_{SF} \\ \mathbf{0} & \mathbf{K}_F \end{bmatrix} \begin{bmatrix} \mathbf{a}_S \\ \mathbf{p}_F \end{bmatrix} = \begin{bmatrix} \mathbf{f}_{l,S} \\ \mathbf{0} \end{bmatrix} + \begin{bmatrix} \mathbf{f}_{b,S} \\ \mathbf{f}_{b,F} \end{bmatrix}, \tag{14}$$

where $\mathbf{f}_{b,S}$ and $\mathbf{f}_{b,F}$ contain contributions from the parts of the domain boundaries $\partial\Omega_S$ and $\partial\Omega_F$, respectively, that are separated from the interface boundary $\partial\Omega_{SF}$.

2.2. Porous material models

The use of different types of mineral wool in facades and interior walls of lightweight buildings is common in order to improve both thermal and acoustic insulation. The interaction between air and fibres of the wool affects the propagation of pressure waves in the air, the porous structure forcing the waves to travel a longer distance and a dampening effect occurring due to friction at the surface of the fibres. Moreover, the pressure waves in the air interact with any potential motion of the fibres. Different approaches for modelling porous materials have been proposed in the literature, some being based on empirical studies, suggesting prediction formulae of acoustic properties based on parameter fitting to experimental data. Others are analytical and based on certain assumptions regarding the geometry and behaviour of the structural frame and the interaction with the air.

This section presents three porous material models, two of them empirical and one analytical, as well as brief literature reviews concerning other models within the two categories. The three models presented here consider the porous materials as equivalent acoustic fluids. They can, therefore, be analysed with the numerical methods employed for acoustic fluids and are integrated in a structure-acoustic model in a straightforward manner by modifying the, possibly complex, coefficients in Eq. (5).

In Eqs. (4) and (5), two material parameters describing an acoustic fluid were introduced, namely the speed of sound c_0 and the static density ρ_0. A common, alternative, way of describing an acoustic fluid is by its static density together with the bulk modulus K_0, related to the speed of sound according to

$$K_0 = \rho_0 c_0^2. \tag{15}$$

Another pair of material parameters that are frequently employed to describe an acoustic fluid are the characteristic impedance Z_0 and the wavenumber k_0. The two latter alternatives of material parameters are related according to

$$Z_0 = \sqrt{\rho_0 K_0}, \tag{16}$$

$$k_0 = \omega\sqrt{\frac{\rho_0}{K_0}}, \tag{17}$$

where ω is the angular frequency.

2.2.1. Empirical models

2.2.1.1. Delany–Bazley. Empirical models relating the real and imaginary parts of the complex characteristic impedance Z and the complex wavenumber k to the quotient (f/R), where f is frequency, were developed in [10]. Measurements of the characteristic impedance, the wavenumber and the flow resistivity were carried out for a range of mineral wools and the following power law relations were obtained by fitting the coefficients to experimental data:

$$Z = Z_0\left(1 + \alpha_1(f/R)^{-\beta_1} - i\,\alpha_2(f/R)^{-\beta_2}\right), \tag{18}$$

$$k = k_0\left(1 + \alpha_3(f/R)^{-\beta_3} - i\,\alpha_4(f/R)^{-\beta_4}\right), \tag{19}$$

where the coefficients are given in Table 1. Data in the range $0.01 \leqslant f/R \leqslant 1.0$ ($\mathrm{N^{-1}\,m^4\,s^{-2}}$) were used and it is advised not to extrapolate the power law relations outside this range.

2.2.1.2. Miki. The real part of the surface impedance when calculated according to the Delany–Bazley formulae sometimes becomes negative at low frequencies. To avoid this unphysical phenomenon, new power law relations were developed in [11], making use of the experimental data utilised in [10] and imposing constraints for the real part of the characteristic impedance to be positive, resulting in empirical formulae of the form in Eqs. (18) and (19) with the coefficients given in Table 2.

These empirical formulae are physically realisable at lower frequencies compared to the formulae by Delany and Bazley. Unphysical properties will, however, occur also in this case, the real part of the density becoming negative at low frequencies. As the power law relations were fitted to the experimental data used in [10], no conclusions can be made regarding the validity of the model outside the range $0.01 \leqslant f/R \leqslant 1.0$ ($\mathrm{N^{-1}\,m^4\,s^{-2}}$).

Table 1
Coefficients for the Delany–Bazley model.

α_1	α_2	α_3	α_4	β_1	β_2	β_3	β_4
0.0511	0.0768	0.0858	0.175	0.750	0.730	0.700	0.590

Table 2
Coefficients for the Miki model.

α_1	α_2	α_3	α_4	β_1	β_2	β_3	β_4
0.0699	0.107	0.109	0.160	0.632	0.632	0.618	0.618

2.2.1.3. Other empirical models. In addition to the formulae by Delany & Bazley and Miki, a number of empirical relations for Z and k have been suggested in the literature. The same procedure as in [10] was applied to measurement data for foam materials in [12]. In [13], measurements were performed for a wide range of glass and rock wools, concluding that prediction formulae involving logarithmic terms resulted in better correlation to the measurement data in comparison with power law relations developed in the same manner as in [10]. In [14,15], porous material models combining the empirical formulae by Delany and Bazley with analytical microstructure models, assuming parallel fibres, were presented, resulting in physically meaningful predictions also at lower frequencies.

2.2.2. Analytical models

Already in 1868, a theory for sound propagation in cylindrical tubes, including both viscous and thermal effects, was presented in [16], a simplified model later being presented in [17]. Porous materials generally have complex geometries, making it practically impossible to analyse the exact microstructure. This is why most porous material models are phenomenological, an approach being valid in case the wave lengths are much larger than the characteristic dimensions of the microstructure. Several analytical models for porous materials, involving different assumptions regarding the geometry and behaviour of the structural frame as well as the interaction between the frame and the acoustic fluid, have been proposed.

2.2.2.1. Equivalent acoustic fluid model – rigid structural frame. Phenomenological equivalent acoustic fluid models assuming the structural frame to be rigid have been presented in [17,18]. These models involve two properties of the structural frame, namely the porosity ϕ and the structure factor K_S, also known as the tortuosity. ϕ is the ratio of fluid volume to total volume, while K_S is defined as $\rho_e = K_S\rho_0$, relating the density of the acoustic fluid in the pores to an effective density ρ_e of the equivalent acoustic fluid. With a rigid structural frame, the equation of motion and the continuity equation in Eqs. (4) and (5), respectively, become

$$K_S\rho_0\frac{\partial^2 u_F}{\partial t^2} + R\frac{\partial u_F}{\partial t} + \nabla p_F = 0, \tag{20}$$

$$\phi\frac{\partial p_F}{\partial t} + \rho_0 c_0^2 \nabla\cdot\frac{\partial u_F}{\partial t} = 0. \tag{21}$$

By differentiating Eq. (21) with respect to time and inserting Eq. (20), the wave equation for the equivalent acoustic fluid is obtained as

$$\frac{K_S\phi}{c_0^2}\frac{\partial^2 p_F}{\partial t^2} + \frac{R\phi}{\rho_0 c_0^2}\frac{\partial p_F}{\partial t} - \nabla^2 p_F = 0, \tag{22}$$

which is similar to the wave equation for an acoustic fluid given in Eq. (6), the coefficients being modified by the properties of the structural frame. In Eq. (6), R accounts for the dissipation of energy in an acoustic fluid domain in a smeared approach while it is a property of the structural frame in Eq. (22).

2.2.2.2. Other analytical models. Most of the porous material models available in the literature assume the structural frame to be rigid, a thorough review of such models developed before and after 1980 being found in [19,20], respectively. A model assuming the structural frame to be limp is presented in [21]. In [22], a model assuming a rigid frame and one assuming a limp frame were compared to measurements, studying the high and low frequency limits of the resulting effective densities. Biot's theory [23] includes the flexibility of the structural frame at the cost of introducing displacement degrees of freedom, the porous material no longer being modelled as an equivalent acoustic fluid. The theory combines an elastic continuum formulation for the structural frame with the theory for sound propagation in a rigid structural frame by considering a coupling of the stress-strain relationships and the inertial and viscous forces.

3. Numerical studies

In the numerical studies presented here, the effect of modelling the air and the insulation in cavities of TVE buildings on the vibration transmission was investigated. First, a comparative study was carried out for the three porous material models introduced in Section 2.2, a section of a wooden double-plate wall panel being employed as test model. Furthermore, the vibrations induced by a load acting on a floor structure in a TVE-based building were analysed, comparing models including acoustic media in different ways. All models were created in the commercial FE software *Abaqus* [24].

Point loads were used as excitations in all the models, as the transmission of low-frequency vibrations in residential buildings mainly originate from structural excitations and not the acoustic pressure fields in the rooms, these being more dominant at higher frequencies. Structural loads, for example footsteps or rotating machines, are often distributed over small surfaces compared to the wavelengths of the structural vibrations, a point load therefore providing a good approximation.

In the models including air as an acoustic medium, it is assumed to be non-absorbing, i.e. the flow resistivity is zero ($R = 0$ in Eq. (4)). Hence, the energy dissipation in the acoustic media only takes place in the insulation.

The result plots presented below show the root mean square (RMS) values of the acceleration amplitudes, as a function of frequency, for a certain set of FE nodes. The RMS values are presented in decibel (dB) with 1 $\mu m\,s^{-2}$ as reference value.

3.1. Comparative study – porous material models

The empirical models by Delany & Bazley and Miki as well as the equivalent acoustic fluid model with rigid structural frame were compared for a FE model of a section in a wooden double-plate wall panel, shown in Fig. 3. The three methods were compared in order to study if the selection of method affects the vibration transmission over cavities of lightweight buildings. The methods are fairly simple, but the objective here is not to create an accurate and validated model of the acoustic media, but rather to investigate whether it has to be considered in the models. If so, the models of the buildings, including acoustic media in the cavities, will have to be validated to measurement data, possibly resulting in the need for a more sophisticated porous material model.

The wall panel consisted of a $2500 \times 650 \times 120\,mm^3$ wood frame covered with gypsum plates on both sides, creating a low-stiffness model with a cavity between the plates. The cavity was modelled in five different ways: (1) with no acoustic media, (2) filled with air and (3–5) filled with insulation, employing the three different porous material models. The coefficients in Eqs. (18) and (19) for the Delany & Bazley and Miki models are slightly modified in the implementation of the models in Abaqus, employed in the numerical calculations presented here. The coefficients used in Abaqus are shown in Table 3.

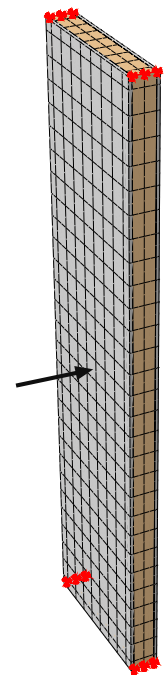

Fig. 3. FE model of a section in a wood-framed wall panel, employed for comparing different porous material models. The arrow illustrates the applied load.

Measured values for the porous material properties of glass- and mineral wools can be found in, for example, [13,25–28]. The measured values fall within the ranges $0.95 \leqslant \theta \leqslant 0.99, 1.01 \leqslant \alpha \leqslant 1.08$ and $6000 \leqslant R \leqslant 90,000$. The properties used in the comparative study are presented in Table 4. A relatively low value for the flow resistivity is selected in order for the empirical models to be physically valid in a major part of the frequency range of interest. Consequently, the energy dissipation in the insulation is relatively low compared to most glass- and mineral wools. For the selected flow resistivity, the models by Delany & Bazley and Miki are feasible for analysis above 70 Hz and 40 Hz respectively. Below those frequencies, unphysical values of the complex bulk modulus and complex density for the Delany & Bazley and Miki models, respectively, are obtained.

Steady-state analyses were performed up to 200 Hz, locking the displacements at the four corners of the panel. The wall panel was excited by a harmonic unit point load in the middle of one of the gypsum plates, the source plate, and the accelerations were evaluated at the opposite side of the other plate, the receiver plate. The acceleration amplitudes were evaluated in terms of an RMS value of the magnitude in all nodes of the receiver plate's outer surface, given by

$$a_{\mathrm{RMS}}(f) = \sqrt{\frac{1}{n}\sum_{i=1}^{n} a_i^2(f)}, \tag{23}$$

where a_i is the magnitude of the complex acceleration in node i and n is the number of nodes in the outer surface of the receiver plate.

Table 3
Coefficients used in Abaqus for the Delany & Bazley and Miki models.

	α_1	α_2	α_3	α_4	β_1	β_2	β_3	β_4
Delany–Bazley	0.0571	0.0870	0.0978	0.189	0.754	0.732	0.700	0.595
Miki	0.0786	0.121	0.123	0.179	0.632	0.632	0.618	0.618

Table 4
The porous material properties employed in the comparative study.

R (Nm^{-4} s)	ϕ (−)	α (−)
6000	0.96	1.1

An RMS value was calculated for each excitation frequency in the steady-state analysis.

In Fig. 4, the acceleration amplitudes for the different models of the wall cavity, in the frequency range 20–200 Hz, are shown. For frequencies below the first resonance frequency, located at 30 Hz, the acoustic media has a negligible effect on the acceleration amplitudes, whereas for frequencies in the range 30–90 Hz, there is a small effect of including air in the cavity. Including a porous material, however, lowers the acceleration amplitudes due to its viscous effects. Above 90 Hz, it is evident that a large part of the energy is transmitted through the acoustic media, since its inclusion increases the acceleration amplitudes significantly. Generally, using the porous material models results in lower acceleration amplitudes compared to the model with only air in the cavity. In their valid frequency ranges, the different methods for modelling the porous material yield very similar results. It is, hence, sufficient to include only one of the three models in the subsequent analyses and the model with rigid structural frame was selected due to the unphysical behaviour of the empirical models at lower frequencies.

3.2. Acoustic media in cavities of TVE buildings

A section of a TVE-based building was analysed in order to investigate the effect of modelling air and insulation, as acoustic media, in the cavities on the vibrations caused by a harmonic point load acting on a floor structure. Specifically, the response of the floor, as well as the transmission to the underlying ceiling and surrounding walls, was investigated for a model containing two stacked TVEs, a quarter of the model being shown in Fig. 5. Each TVE was 9000 x 3900 x 3400 mm^3 large (the long side walls being apartment separating and the short side walls being facades) and modelled according to the drawings in Fig. 2. Moreover, the walls of the neighbouring TVEs were included at the apartment separating walls, meaning that the cavities in those walls were included in the model as well. No structural connection to the walls of the neighbouring TVEs was, however, included.

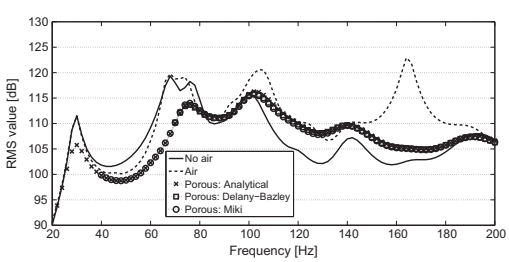

Fig. 4. RMS values of the acceleration amplitudes at the receiver plate of the wall panel model employed for comparing different porous material models.

The materials of the structural components are listed in Fig. 2; the particle board, plaster board and plywood being modelled as isotropic materials with properties according to Table 5, whereas the wood beams were modelled as orthotropic materials with properties according to Table 6. A type of elastomer often used in TVE buildings is Sylodyn, a mixed cellular polyurethane dampening material developed by Getzner Werkstoffe GmbH. The blocks modelled in this study were 100 × 95 × 25 mm^3 large, of type Sylodyn NE, and placed along the walls between the two stacked TVEs with a centre-to-centre distance from one another of 600 mm. Frequency-dependent viscoelastic material properties for the elastomers were determined in [29] by performing laboratory testing and FE simulations to match experimental data. The porous material properties used for modelling the insulation were selected according to Table 7. The analytical porous material model assuming a rigid structural frame was employed for the insulation. In contrast to the comparative study in Section 3.1, a higher flow resistivity was used here, namely 40,000 Nm^{-4} s. The selected value falls within the mid-range of values for glass- and mineral wools found in the literature ($6000 \leqslant R \leqslant 90,000$). Hence, the damping in the porous material is higher compared to the FE model employed in the comparative study presented in Section 3.1. As the objective here is not to study a specific porous material, but rather to investigate whether this type of materials need to be considered in the models, it is sufficient to employ parameters that are realistic compared to the measured values found in the literature.

The structural parts were meshed with 20-node solid hexahedral elements, employing quadratic interpolation and reduced integration. For the elastomer blocks, elements with a hybrid formulation were used in order to avoid locking. The air and the insulation, in turn, were meshed with 20-node acoustic hexahedral elements, employing quadratic interpolation. The mesh sizes both for the structural and the acoustic parts were decided based on the wavelengths expected to occur at the highest frequency of interest, namely 200 Hz.

Due to the complexity when assessing damping in building structures, a global damping ratio of 6% was assigned to all materials, as opposed to considering damping for each material and in the different junctions. The damping ratio was determined in [30], with the use of experimental data obtained from measurements in a TVE building [31], by fitting an exponential function to the transient response of a floor structure. The damping ratio was used to establish a damping matrix by means of the Rayleigh method, see e.g. [32]. The C_S-matrix in Eq. (14) was, hence, constructed as a linear combination of the mass- and stiffness matrices, selecting the proportionality constants to be 17.37 and $9.77 \cdot 10^{-5}$, respectively. Since the damping ratio was calculated from measurements on a real building, involving insulation in the cavities, the damping in the structure may be overestimated as the insulation is modelled explicitly. The possible overestimation is, however, believed to have a negligible effect on the conclusions of the studies presented here.

In the analyses, the surfaces of the two TVEs, where elastomer blocks would be placed if further storeys were included, were modelled as clamped. Moreover, the walls of the neighbouring

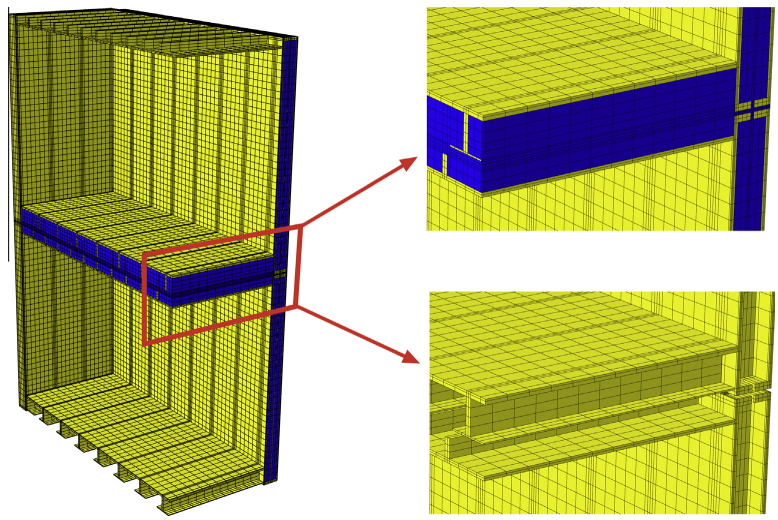

Fig. 5. A quarter of the model of two TVEs. The acoustic media are shown in blue. The junction between floor, ceiling and apartment separating walls is shown to the right, with and without acoustic media in the cavities.

Table 5
Material parameters used for the isotropic materials.

Material	E (MPa)	ν (−)	ρ (kg m^{-3})
Particle board	3000	0.3	767
Plaster board	2000	0.2	692.3
Plywood	12,400	0.3	710

Table 6
Material parameters used for the wood beams.

E_1 (MPa)	E_2	E_3	G_{12} (MPa)	G_{13}	G_{23}	ν_{12} (−)	ν_{13}	ν_{23}	ρ (kg m^{-3})
8500	350	350	700	700	50	0.2	0.2	0.3	432

Table 7
Porous material properties used in the numerical studies.

R (N/m^{-4} s)	ϕ (−)	α (−)
40,000	0.96	1.1

modules were clamped at the vertical edges. A vertical unit point load, acting on the middle of the floor in the upper TVE, was applied, and steady-state analyses were performed for frequencies up to 200 Hz in steps of 5 Hz.

3.2.1. Vibrations in the floor and the underlying ceiling

First, the vibrations in the floor of the upper TVE and the underlying ceiling were investigated for different ways of modelling air and insulation in the cavity between the floor and the ceiling. A model without acoustic media was compared to models with air alone and air together with insulation in the cavity, the insulation being placed according to the drawings in Fig. 2. All analyses were performed applying two different boundary conditions, $p = 0$ and $\nabla p = 0$, at the interfaces of the acoustic media bordering to surrounding cavities, in order to investigate their effect on the vibrations transmitted over the cavity. These interfaces are illustrated in Fig. 6, where the full TVEs are shown. At all boundaries of the acoustic media in contact with structural components, structure-acoustic coupling was considered.

The acceleration amplitudes obtained in the analyses of the different models were extracted from half of the nodes (due to the symmetry) at the floor surface and the ceiling surface, respectively, and RMS values of the complex acceleration magnitudes were calculated according to Eq. (23).

In Fig. 7, the RMS values of the acceleration amplitudes at the floor are shown. Including air alone in the cavity has a small effect on the levels of vibration in the floor, the RMS values being changed by just over 1% in average. An exception is found at 30 Hz, where the inclusion of air lowers the vibration amplitudes. Considering both air and insulation in the cavity leads to a dampening effect, lowering the levels of vibration by approximately 15% while the frequency response function is similar in shape to that obtained when including no acoustic media in the cavity. Moreover, it can be observed that the choice of boundary conditions for the acoustic media has a negligible effect on the acceleration amplitudes at the floor.

In Fig. 8, the RMS values of the acceleration amplitudes at the ceiling are shown. It can be observed that including air alone results in higher acceleration amplitudes, especially at lower frequencies. For low frequencies, the modelling of both air and insulation results in acceleration amplitudes in-between the case with air alone and the case with no acoustic media in the floor-ceiling cavity. At higher frequencies, the acceleration amplitudes obtained for the case with air and insulation are similar to those obtained for the case without acoustic media, deviating with less than a factor of 2. At some frequencies, the dampening effect of the insulation results in reduced vibration amplitudes when including both air and insulation, as compared to having no acoustic media. When air alone is considered, the levels of vibration are affected by the choice of boundary conditions for the acoustic medium, the effect, however, being relatively small when both air and insulation are included in the model.

3.2.2. Vibrations in the surrounding walls

Next, the vibrations in the walls of the lower TVE were investigated for different ways of modelling the air and insulation in the

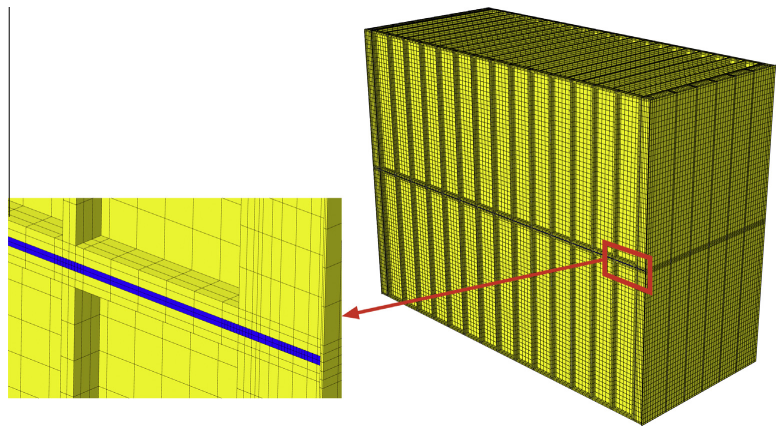

Fig. 6. The model of the two TVEs. The acoustic media in contact with the surrounding cavities, where different boundary conditions were applied, are shown to the left. The acoustic media are shown in blue.

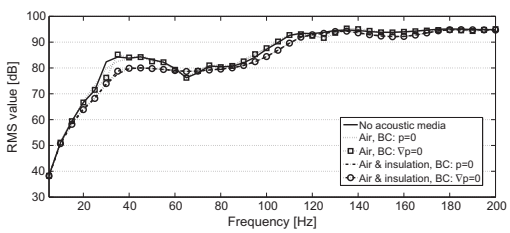

Fig. 7. RMS values of the acceleration amplitudes at the floor for the different models of the acoustic media in the floor-ceiling cavity.

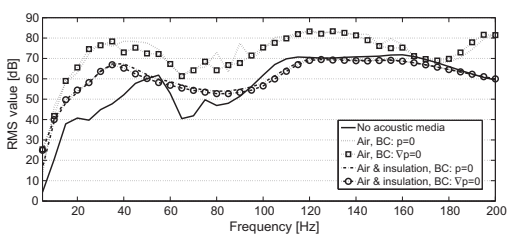

Fig. 8. RMS values of the acceleration amplitudes at the ceiling for the different models of the acoustic media in the floor-ceiling cavity.

cavity between the floor and the ceiling as well as the cavities in the apartment separating walls. Models including acoustic media either in the floor-ceiling cavity alone or in both the floor-ceiling cavity and the wall cavities were compared to a model without acoustic media. In the models including acoustic media, it was included as air alone or air together with insulation. The insulation in the walls was placed according to the drawings in Fig. 2, i.e. between the beams of each wall, having a small air gap between the walls of two neighbouring TVEs. Moreover, models having the floor-ceiling cavity and the wall cavities separated were created by introducing a separating wall in the junction between the cavities, the junction being shown in Fig. 5. These models were compared to the models with connected cavities in order to investigate if the acoustic pressure waves travelling between the cavities affect the vibration amplitudes in the walls.

At the boundaries to the acoustic media in surrounding cavities, only $\nabla p = 0$ was applied as it was observed in the evaluation of the ceiling vibrations that the boundary conditions have a small effect on the vibration transmission. The acceleration amplitudes obtained in the analyses of the different models were extracted in all nodes at the surface of an apartment separating wall of the lower TVE. RMS values of the complex acceleration magnitudes were calculated according to Eq. (23).

In Fig. 9, the RMS values of the acceleration amplitudes at the wall of the lower TVE are shown for the models where air alone was used as acoustic medium in the cavities. In Fig. 10, the RMS values are shown for the models where both air and insulation were included as acoustic media. The frequency range is divided into two parts, including frequencies in the ranges 0–100 Hz and 100–200 Hz, respectively. Observe that different scales are employed for the y-axes in the two frequency ranges.

It can be observed in Fig. 9 that including acoustic medium in terms of air alone in the cavities has a large effect on the vibration transmission from the floor to the walls of the TVE below. The system becomes more resonant when air is included and the acceleration amplitudes at the wall panel are generally higher, except at some frequencies between resonance peaks, where the amplitudes are reduced compared to the model with no acoustic media. At most frequencies, the acceleration amplitudes are higher when the floor-ceiling cavity is connected to the wall cavities compared to having the cavities separated. At low and high frequencies (below 15 Hz and above 155 Hz), the model with air in all cavities, having the cavities separated, results in acceleration amplitudes similar to the model with air only in the floor-ceiling cavity. Hence, if the cavities are separated, the inclusion of air in the wall panels has a negligible effect at those frequencies.

In Fig. 10, it can be observed that considering both air and insulation as acoustic media in the cavities results in smoother spectrums compared to including air alone. For most frequencies, with the exception being frequencies below 40 Hz, the acceleration amplitudes are decreased when including air and insulation in the cavities compared to having no acoustic media. A resonance frequency is observed at 20 Hz for the model with acoustic media only in the floor-ceiling cavity which is not present for any of the other models. Hence, a resonance occurs due to the inclusion of

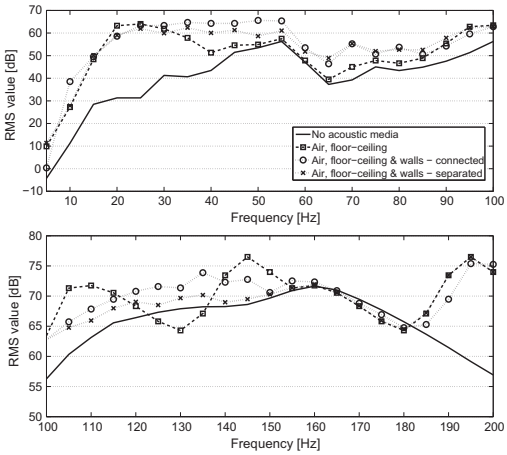

Fig. 9. RMS values of the acceleration amplitudes at the apartment separating wall of the lower TVE for the different models including air alone as acoustic medium. Note that the two plots employ different scales at the *y*-axis.

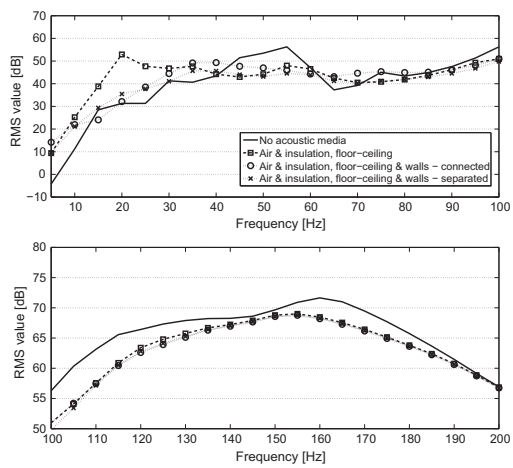

Fig. 10. RMS values of the acceleration amplitudes at the apartment separating wall of the lower TVE for the different models including both air and insulation as acoustic media. Note that the two plots employ different scales at the *y*-axis.

air and insulation in the floor-ceiling cavity which is cancelled when considering the acoustic media also in the wall cavities. In general, the acceleration amplitudes when considering both air and insulation, as compared to including air alone in the cavities, are closer to the case with no acoustic media. Above 60 Hz, the inclusion of air and insulation as acoustic media results in acceleration amplitudes deviating with a factor of less than 2 compared to having no acoustic media. Above 100 Hz, all three models with air and insulation in the cavities result in very similar acceleration amplitudes. This shows that at higher frequencies, the effect of including acoustic media in the wall cavities, on the vibration transmission to the wall panels, is small in case both air and insulation are considered.

4. Conclusions

The main conclusion from the numerical studies is that acoustic media in the cavities of wooden buildings affect the vibration transmission. It was observed that the vibrations transmitted from a load acting on a floor structure affected the acceleration amplitudes in both the underlying ceiling, structurally separated from the floor, and the walls of the storey below. The effect is especially distinct when air alone is considered as acoustic medium. Generally, including air alone results in a more resonant system with higher acceleration amplitudes while including both air and insulation introduces a dampening effect, especially at higher frequencies. The dampening effect of the insulation results in decreased acceleration amplitudes at higher frequencies as compared to including no acoustic media. In reality, the cavities normally contain insulation, the modelling of air alone, thus, leading to an overestimation of the transmitted vibrations.

The level of vibrations in the floor was only marginally affected by the inclusion of air alone as acoustic medium in the floor-ceiling cavity. When considering both air and insulation as acoustic media, the shape of the frequency response function did not change to any appreciable extent, while a dampening effect was observed in the floor vibrations.

In the analyses of the vibrations in the floor and in the ceiling, it was concluded that the choice of boundary conditions for the acoustic media bordering to surrounding cavities has a small effect in terms of vibration transmission from the floor to the ceiling below. This implies that the acoustic media in surrounding cavities has a weak effect on the vibrations transmitted locally over the floor-ceiling cavity.

In the analyses of the vibrations in the walls of the lower TVE, it was observed that including air and insulation in the wall cavities had no effect on the transmission to the wall panels above 100 Hz. If the vibrations transmitted from the floor to surrounding walls are studied for frequencies over 100 Hz, it is, hence, sufficient to include the air and insulation only in the floor-ceiling cavity. This result indicates that the effect of including acoustic media in cavities is decreasing with the distance from the load. It should be investigated further how far from the load the acoustic media has to be considered.

The porous material models investigated in this paper are only a few of many available in the literature. Specifically, no models assuming limp or elastic structural frame have been evaluated here. As it was concluded that acoustic media in cavities of multi-storey wood buildings have to be considered when performing low-frequency vibration analyses, the material model for the insulation should be validated.

Acknowledgement

The financial support for this work provided by the Silent Spaces project, a part of the EU program Interreg IV A, is gratefully acknowledged.

References

[1] Forssén J, Kropp W, Brunskog J, Ljunggren S, Bard D, Sandberg G, Ljunggren F, et al. Acoustics in wooden buildings – state of the art 2008. Vinnova project 2007-01653, report 2008:16, SP Trätek, Stockholm; 2008.
[2] Andersen L, Kirkegaard PH, Dickow KA, Kiel N, Persson K. Influence of wall surface and air modelling in finite-element analysis of sound transmission between rooms in lightweight buildings. In: Proceedings of the internoise 2012/ASME NCAD meeting, New York.
[3] Domadiya PG, Dickow KA, Andersen L, Sorokin SV. Mitigation of flanking noise in double-plate panel structures by periodic stiffening – finite element analysis in the low-frequency range. In: Proceedings of COMPDYN 2011, Corfu, Greece.
[4] Dickow KA, Gandalal PD, Andersen L, Kirkegaard PH. Transmission of sound through double-plate panel structures – a numerical study of coupling

parameters in lightweight panel structures. In: Proceedings of COMPDYN 2011, Corfu, Greece.
[5] Ljunggren F, Ågren A. Potential solutions to improved sound performance of volume based lightweight multi-storey timber buildings. Appl Acoust 2011;72:231–40.
[6] Ottosen N, Petersson H. Introduction to the finite element method. Harlow (United Kingdom): Pearson Education Ltd.; 1992.
[7] Bathe KJ. Finite element procedures. New York: Prentice Hall; 1996.
[8] Holzapfel GA. Nonlinear solid mechanics: a continuum approach for engineering. Chichester (United Kingdom): John Wiley & Sons Ltd.; 2000.
[9] Sandberg G. Finite element modelling of fluid-structure interaction. Ph.D. thesis. Division of Structural Mechanics, Lund University, Sweden; 1986.
[10] Delany ME, Bazley EN. Acoustical properties of fibrous absorbent materials. Appl Acoust 1970;3(2):105–16.
[11] Miki Y. Acoustical properties of porous materials-modifications of Delany–Bazley models. J Acoust Soc Jpn 1990;11(1):19–24.
[12] Dunn IP, Davern WA. Calculation of acoustic impedance of multi-layer absorbers. Appl Acoust 1986;19(5):321–34.
[13] Komatsu T. Improvement of the Delany–Bazley and Miki models for fibrous sound-absorbing materials. Acoust Sci Technol 2008;29(2):121–9.
[14] Mechel FP. Ausweitung der absorberformel von delany and bazley zu tiefen frequenzen. Acustica 1976;35(3):210–3.
[15] Kirby R, Cummings A. Prediction of the bulk acoustic properties of fibrous materials at low frequencies. Appl Acoust 1999;56(2):101–25.
[16] Kirchhoff G. On the influence of heat conduction in a gas on sound propagation. Annu Phys Chem 1868;134:177–93.
[17] Zwikker C, Kosten CW. Sound absorbing materials. Amsterdam: Elsevier; 1949.
[18] Morse PM, Ingard KU. Theoretical acoustics. New Jersey: Princeton University Press; 1968.
[19] Attenborough K. Acoustical characteristics of porous materials. Phys Rep 1982;82(3):179–227.
[20] Allard JF, Atalla N. Propagation of sound in porous media – modelling sound absorbing materials. 2nd ed. Chichester (United Kingdom): John Wiley & Sons Ltd.; 2009.
[21] Göransson P. Acoustic finite element formulation of a flexible porous material – a correction for inertial effects. J Sound Vib 1995;185(4):559–80.
[22] Panneton R. Comments on the limp frame equivalent fluid model for porous media. J Acoust Soc Am 2007;122(6):217–22.
[23] Biot MA. Theory of propagation of elastic waves in a fluid-saturated porous solid. I. Low-frequency range. J Acoust Soc Am 1956;28(2):168–78.
[24] Dassault Systèmes. Abaqus 6.12 documentation; 2012.
[25] Schiavi A, Guglielmone C, Miglietta P. Effect and importance of static-load on airflow resistivity determination and its consequences on dynamic stiffness. Appl Acoust 2011;72(9):705–10.
[26] Olny X, Panneton R. Acoustical determination of the parameters governing thermal dissipation in porous media. J Acoust Soc Am 2008;123(2):814–24.
[27] Sagartzazu X, Hervella-Nieto L, Pagalday JM. Review in sound absorbing materials. Arch Comput Methods Eng 2008;15(3):311–42.
[28] Kino N, Takayasu U. Experimental determination of the micro-and macrostructural parameters influencing the acoustical performance of fibrous media. Appl Acoust 2007;68(11):1439–58.
[29] Negreira J. Vibrations in lightweight buildings – perception and prediction. Licentiate dissertation. Division of Engineering Acoustics, Lund University, Sweden; 2013.
[30] Negreira J, Bard D. Finite element modelling of a timber volume element based building with elastic layer insulators. SP Technical Research Institute of Sweden, report 2013: 27.
[31] AkuLite. Mätrapport 10052. Brunnby Park, Upplands Väsby, Sweden; 2012.
[32] Chopra AK. Dynamics of structures. New Jersey: Prentice Hall; 2007.

Paper C

Characterisation of an Elastomer for Noise and Vibration Insulation in Lightweight Timber Buildings

by

Juan Negreira, Per-Erik Austrell, Ola Flodén and Delphine Bard

Reprinted from

JOURNAL OF
BUILDING ACOUSTICS

Volume 21 · Number 4 · 2014

MULTI-SCIENCE PUBLISHING CO. LTD.
26 Eldon Way, Hockley, Essex SS5 4AD, United Kingdom

BUILDING ACOUSTICS · Volume 21 · Number 4 · 2014 Pages 251–276

Characterisation of an Elastomer for Noise and Vibration Insulation in Lightweight Timber Buildings

Juan Negreira, Per-Erik Austrell, Ola Flodén and Delphine Bard
[1]*Lund University, Department of Construction Sciences, P.O. Box 118, 221 00 Lund, Sweden.*
juan.negreira@construction.lth.se, per_erik.austrell@construction.lth.se, ola.floden@construction.lth.se, delphine.bard@construction.lth.se

(Received 16 January 2014 and accepted 28 October 2014)

ABSTRACT
Regulations regarding impact and airborne sound insulation for lightweight timber constructions have become increasingly stringent due in particular to complaints by inhabitants. Accordingly, some building techniques frequently use elastomers at junctions so as to reduce low frequency noise. Development of accurate predictive tools (involving exact material properties) by using numerical methods such as the finite element (FE) method is needed in tackling flanking transmission problems during the design phase of buildings. The present research concerns the characterisation of an elastomer, presenting an accurate method for extracting its material properties from the manufacturer's data sheet (properties there being often linked to such structural effects as shape factors and boundary conditions of samples and tests). The properties were extracted by comparing results obtained by analytical calculations, FE simulations, and mechanical testing, separating geometry and material dependence and ultimately serving as input to commercial FE software for setting up the aforementioned prediction tools.

Keywords: Lightweight, elastomer, finite element method, vibrations, measurements.

1. INTRODUCTION

Although lightweight timber structures have many advantages, a high level of acoustic quality in them tends to be difficult to achieve. Even if such buildings fulfill all current regulations with respect to impact sound quality, complains amid inhabitants often arise due to structure-borne sound in the low frequency range, i.e. up to approximately 200 Hz. The relatively poor sound insulation at the junctions within this frequency span makes flanking transmission a problem that needs to be tackled if the comfort of the occupants in this respect is to be improved. To this end, elastomers are occasionally introduced at the junctions between floors and walls due to their sound- and vibration-insulating effects, their use being especially common in wooden buildings [1].

There have been, however, no reliable methods thus far for predicting the vibratory and acoustic performance of lightweight buildings, product development being carried

out up to now on simply an empirical basis, i.e. through utilising observations and the experience of engineers [2]. Both time and costs could be reduced by addressing issues of flanking transmission during the design phase, for example by use of finite element (FE) simulations as predictive tools. Accurate and handy methods for the characterisation of elastomers are therefore needed so as to be able to obtain the exact material properties involved to use as inputs in simulations.

In the present study, the characterisation of an elastomer was carried out. More specifically, frequency-dependent Young's, bulk, and shear complex moduli are sought to use as input to commercial FE software. The aforementioned properties of Sylodyn, a resilient material of this sort, were investigated by comparing results stemming from analytical calculations, FE analysis through use of the commercial software Abaqus, and mechanical testing of the material in a uni-axial testing machine. Static and dynamic material models were established in terms of both linear elastic and viscoelastic models. In calibrating the models, data from the manufacturer and from the uni-axial tests were used in the fitting of the material models available in Abaqus. The load case that was investigated was a large static load to which a small vibration was added. The static load comes from the dead weight of the building elements, the vibration being the noise transmitted through the junctions. Both linear and non-linear elastic models are available for taking the dead load into account. The model employed depends upon the value of the static load involved. In connection with this, one should note that the working zone for the material should always be kept within the linear range in order to maximise the insulating properties. The dynamic part of the loading is dealt with by use of viscoelastic models. This approach is rational as it enables the geometric and the material properties to be separated.

A general method for extracting the material properties of an elastomer from the manufacturer's data sheet for use as input to FE simulations is presented here.

2. LITERATURE REVIEW

Traditionally, in single-family timber houses, the different elements converging at the junctions are connected by use of screws or nails, sometimes in combination with glue. After the construction of multi-storey wooden buildings was authorised in Sweden in 1994, more stringent sound-reduction requirements than earlier concerning impact noise were set, various new construction techniques to meet these requirements having been developed since [1].

An early measure taken regarding flanking transmission insulation of impact noise between floors was performed by installing additional wall plates at varying distances along the walls of the sending room or the walls of the receiving room [3]. Hanging the ceilings on resilient channels was also shown to improve the vibratory performance of timber constructions. Decoupled radiation-isolated walls is another solution that is often taken [3]. The use of roller bearings to prevent shearing and avoid moment transmission was tested more than a decade ago, this also being found to result in a decrease in the impact sound transmission [4]. Construction modifications such as adding extra mass and damping to the floor through insertion of an extra board layer, use of elastic glue between boards, and utilisation of a floating floor, have also been shown to be able to

reduce vibrations created by impacts and travelling throughout the structure [2]. In [5], different types of vibration reduction measures are discussed, namely tuned mass dampers (which provide an effective way of cancelling the vibrations caused by a single mode of vibration), semi-active absorbers (which can adjust the damping force rapidly) and active control systems (which drive the systems through feedback loops).

A more recent method of reducing noise and vibrations is to place various construction elements (e.g. floor, walls, and whole rooms) on top of a resilient layer – in the form of blocks, strips or a layer covering the entire surface. Albeit this technique is used in lightweight constructions of many types, it is in volume based wooden buildings in which its use has been widespread. For a volume system, the idea is to construct prefabricated modules containing floors, walls and ceilings together with electrical, heating, water sanitation and ventilation installations [2]. Those box-like modules are then transported to the construction site and stacked on top of each other with an elastomer layer being placed in between. A distinct advantage of this type of building system as regards vibrations and acoustic performance is that, for any two volumes placed above the other, the upper volume contains the upper part of the floor to it, being the ceiling comprised in the lower volume. In between every two volumes, elastomers like the one dealt with in this investigation are usually inserted. Those elastomers are placed along the flanks, and together with some tie plates and metal studs (to ensure positioning and horizontal stability), provide the only mechanical contact between two adjacent Timber Volume Elements (TVEs). The flanking transmission can be markedly reduced if the elastomer layer is designed properly. In Section 5.2, FE simulations stacking modules of this type will be carried out as example of a predictive tool using elastomer layers.

The solution of including elastomers in the construction obviously modifies the dynamics of the floor. One of the findings reported in [6] was that the first eigenfrequency sank when elastomers were employed and rose with increased elastomer stiffness. Measurements performed in [3] revealed that floors resting on top of elastomer layers will have higher modal damping and eigenfrequencies shifted to lower values. It was also stated, however, that the relative importance of this statement regarding these phenomena on the vibration and impact sound pressure on site is not clearly known thus far. In [5], an experimental investigation about the use of viscoelastic material in the junctions of a steel floor-ceiling structure is presented. It was found to be an effective method for reducing the vibrations caused by modes where the floor and the ceiling move out of phase.

In [7], comparisons between measurements and FE simulations of a given junction were carried out. The measurements showed that the insertion of elastomers is beneficial if one simply considers the vertical vibrations in the story below. When looking at the horizontal direction, i.e. a direction that can contribute strongly to the sound emission from the walls in the apartment below, use of elastomers show a positive effect in the region up to 30 Hz and above 70 Hz. Within the region 30-70 Hz, however, the resilient strips actually increase the velocity levels, probably due to the shear resonances that occur in particular at low frequencies. This finding was highly consistent with the results of FE simulations, which showed that the levels of

acceleration in the horizontal direction increased for frequencies between 40 and 70 Hz.

In [8], a full-scale mockup of a floor placed on top of three walls, with the floor either screwed directly to the walls or resting on top of elastomer strips, was measured in a laboratory environment. It was found that above approximately 70 Hz, the mean acceleration vibration level for the elastomer configuration was significantly lower than for the screwed configuration. Below 70 Hz, however, the mean vibration level for the elastomer configuration was higher overall than it was for the screwed junction. The authors pointed out that the elastomer layers could heighten footstep impact noise in the low frequency range, despite the acoustic performance being improved at higher frequencies. The conclusions drawn there regarding the higher frequencies concur with those reported in [2], in which two volumes were stacked, with and without an elastomer layer in between. It was found that the use of elastomers leads to an improved sound insulation for frequencies of 80 Hz to 500 Hz, reducing the impact sound levels 1 dB.

In both the studies presented in [2] and [9], static loads were found to affect the insulation performance, the extent to which this occurred depending upon the storey within a building that was involved. In [2], the two-volume laboratory setup was modified by raising the uppermost one, with use of an overhead crane, to a level at which ideally, the two volumes would have mechanical contact with one another simply by means of the elastomer, at the same time as the upper volume would not transmit any static load to the lower volume. The tests conducted showed the impact sound pressure level to be reduced by 2 dB as compared with the situation in which static load was transmitted from the upper volume to the one beneath it. This confirmed what had previously been shown in [9], in which 31 nominally identical lightweight timber constructions were analysed, in each of which elastomer strips were placed between the load bearing walls and the prefabricated floors. It was found that the sound reduction was better higher up in the building. Thus, it can be concluded that when two structures are brought together, their mechanical coupling increases, compressing the elastomer and thus worsening the sound insulation.

Elastomers have a behaviour that can be described as being both elastic and viscous (i.e. viscoelastic), dependent upon the frequency [10]. In modelling elastomers at junctions of lightweight buildings, by means of FE software, they are often dimensioned as representing a vertical single-degree-of-freedom point loaded mass-spring-dashpot system (cf. [7, 11]) so as to simplify the numerical calculations. In practice, however, they also act as shearing insulators in the horizontal plane and they are not being strictly point-loaded [3]. In addition, according to [11], there is a need of modelling the rotational stiffness and damping of an elastomer in a manner that matches the results of experiments and FE simulations (i.e. development of a 6-degree-of-freedom spring-dashpot system).

If a general conclusion can be drawn from the literature, it is that when using resilient strips between different parts of lightweight buildings, it is of crucial importance to select the most adequate properties for the material and to prepare it accordingly if the degree of insulation aimed at is to be achieved. For instance, a static load higher than the recommended one compresses the elastomer to a level at which its

insulating properties are greatly reduced, which is believed to sometimes be the case for some buildings nowadays.

All in all, it can be concluded that there is still a lack of sufficient knowledge regarding the vibrational performance of elastomers in lightweight buildings. In order to gain a better understanding of their performance, use of accurate FE prediction tools having reliable material properties as input are needed. Determining how such properties can be achieved is thus the aim in the investigation reported on here.

3. GOVERNING THEORY: LINEAR VISCOELASTICITY

Viscous materials resist straining linearly over time when a load is applied. Elastic materials, in turn, when stretched, return to their original state once the stress ceases. Viscoelastic materials possess both viscous and elastic properties to varying degrees when they undergo deformations. Their material properties depend on time or, in the frequency domain, on frequency. Specifically, if the material is subjected to deformations or stresses small enough that its rheological properties do not depend upon the value of the deformation stress, the material is said to behave in a linear viscoelastic way, this being the simplest response of a viscoelastic material. The latter is the case for the elastomers under study here, as vibrations in dwellings due to its occupants or to machinery are normally of small amplitude.

Buildings are subjected both to transient loads (people walking, objects striking the floor, and the like) and harmonic ones (rotatory machinery, for example). However, for reasons of computational costs, FE models of such constructions are often subjected to steady-state dynamic loading. If a specific transient load needs to be modelled, the process in such case would be to first fit a Maxwell model in the frequency domain, the parameters obtained there being then used directly in the time domain. Both approaches (i.e. frequency and time domain) are closely related by the Fourier transform, as explained for example in [12].

The response of linear viscoelastic materials to a stationary sinusoidal stress history is thus of interest in the application under study here, for which such materials present a certain lag in strain. Also, the effective stiffness of such materials depends upon the rate of application of the load. Thus, by performing some mathematical manipulations such as shown in [12], for example, the stress σ^* corresponding to a harmonic strain ϵ^* can be expressed through a simple multiplication by a complex function, the so-called complex Young modulus $E^*(\omega)$, as

$$\sigma^* = E^*(\omega)\epsilon^*. \tag{1}$$

Equation (1) can be also expressed as

$$\sigma^* = \sigma_0 e^{i(\omega t+\delta)} = |E^*|e^{i\arg(E^*)}\epsilon_0 e^{i\omega t} = |E^*|\epsilon_0 e^{i(\omega t+\arg(E^*))}, \tag{2}$$

$\in_0$ being the amplitude of the strain, i the complex number, t the time, ω the angular frequency and $\delta = \arg(E^*)$ the phase lag. Comparing equations (1) and (2), leads to an interpretation of the complex modulus in terms of measurable quantities as

$$|E^*| = E^{dyn} = \frac{\sigma_0}{\epsilon_0} \quad \text{and} \quad \arg(E^*) = \delta, \tag{3}$$

meaning that the absolute value $|E^*(\omega)|$ is the amplitude ratio of the stress to the strain (this being termed the *dynamic modulus*, E^{dyn}), and the phase angle arg (E^*) being the phase shift between the stress and the strain. The complex modulus can thus be expressed in polar form as

$$E^* = \frac{\sigma^*}{\epsilon^*} = \frac{\sigma_0 e^{i(\omega t+\delta)}}{\epsilon_0 e^{i\omega t}} = \frac{\sigma_0}{\epsilon_0} e^{i\delta}, \tag{4}$$

and in rectangular form using Euler's formula as

$$E^* = E^{dyn}\cos\delta + iE^{dyn}\sin\delta = E_s + iE_l, \tag{5}$$

where the real part of it, E_s, is called *storage modulus* (representing the in-phase response, i.e. the elastic response) whereas the imaginary part E_l is termed *loss modulus* (representing the out-of-phase response, i.e. the energy dissipation that occurs).

An alternative form to this rectangular formulation is

$$E^* = E_s(1 + i\tan\delta), \tag{6}$$

the term tan δ being called the loss factor. The relation between the polar and the rectangular form of the complex modulus can be simplified for small values of δ, as in the particular case under study here. These approximations are

$$\sin\delta \approx \tan\delta \approx \delta \quad \text{and} \quad \cos\delta \approx 1. \tag{7}$$

In addition, dynamic measurements of linear viscoelastic materials under harmonic loading show curves of dynamic modulus and damping which basically look like those shown in Figure 1, in which E^0 is the instantaneous Young's modulus for very fast loading and E^∞ is the long-term modulus for a very slow loading rate or none at all. Both the instantaneous and the long-term modulus are connected to other constants, namely the shear G and the bulk K modulus, by relationships of linear elasticity; see equations (11) and (12).

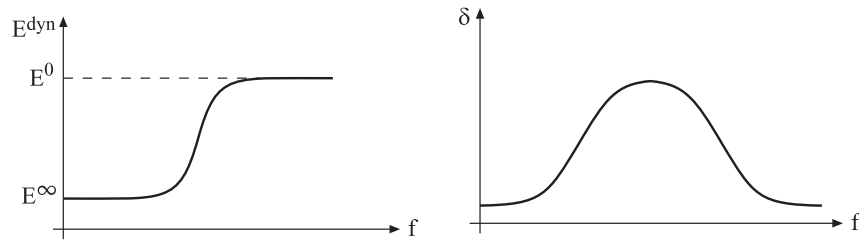

(a) Dynamic modulus. (b) Damping – by the phase angle.

Figure 1: Dynamic measurements of linear viscoelastic materials

The shear modulus G^*, which describes the material's response to shear strain, is defined as the ratio of the shear stress to the shear strain. It is given, in complex rectangular form, as

$$G^* = G_s + iG_l, \tag{8}$$

where G_s and G_l are the storage and the loss shear moduli respectively. Similarly, the bulk modulus K^* describes the material's response to uniform pressure, and is defined as the ratio of the infinitesimal pressure increase to the resulting relative decrease in the volume, given in rectangular form as

$$K^* = K_s + iK_l, \tag{9}$$

where K_s and K_l are the storage and the loss bulk moduli respectively.

4. EXTRACTION OF MATERIAL PROPERTIES

In the present study, Sylodyn was investigated, its being a closed-cell polyurethane material manufactured by Getzner Werkstoffe. Its material parameters were determined from the manufacturer's data sheet, together with static measurements and FE simulations. Since buildings of the sort for which the predictive tools are sought are often subjected to serviceability vibrations of small amplitude, a linear viscoelastic model was chosen, due to the small size of the deformations. An advantage of this choice is that it yields a linear dynamic system for a structure containing elastomers at the junctions. Also, through use of material parameters, elements of any size and shape can be included in the structural model employed in the dynamic analysis carried out (different construction types use different elastomer configurations).

4.1 Static parameters

Isotropic linear elasticity serves as the basis for the linear viscoelastic model and thus two parameters define the static behaviour. Looking at different commercial FE software (Abaqus [13] was the one specifically employed here), material behaviour can be defined in terms of a shear and a bulk modulus. This is a natural choice for a rubber-like material, since the behaviour that occurs in shear is usually fairly linear, even in the case of rather large strains. Also, the bulk behaviour can be characterised rather accurately in terms of a constant.

4.1.1 Measurements

Preliminary static compression tests on Sylodyn samples were performed in an uni-axial testing machine. To eliminate structural effects and obtain homogeneous state of stress, the test specimen was situated between lubricated plates. The results of the testing, giving a static Young's modulus $E^{\infty} = \Delta\sigma / \Delta\in = 3.2$ MPa, are shown in Figure 2. This, together with the data contained in the manufacturer's data sheet, will be the only measurement data used for extracting all material parameters used as input to the FE software.

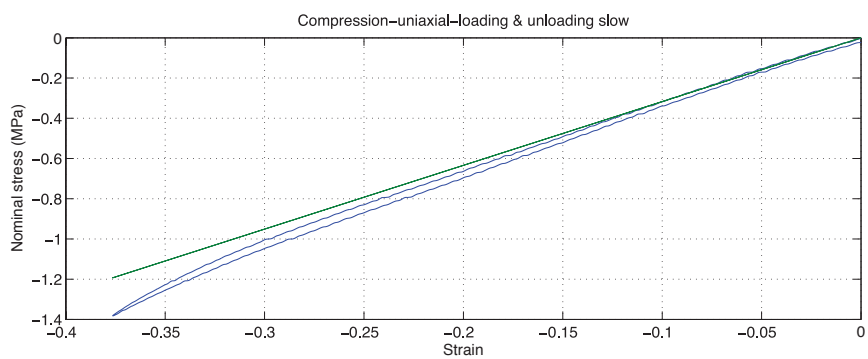

Figure 2: Compression-tests results. Loading and unloading curves –slow– (blue) and tangential straight line to find the initial static moduli (green).

4.1.2 FE calibration

In the data sheet of the Sylodyn NE [14], a compression modulus is defined and is determined experimentally for different configurations (blocks, strip and surface) and shape factors of the elastomer (cf. Figure 4). What a shape factor represents is defined in equation (10) and in Figure 3. Although this compression modulus is related to the Young's modulus of the material, it is not a material parameter. It depends upon the shape factor and the boundary conditions of the test piece employed. Such is often the case when manufacturers provide data concerning materials they produce, hindering the use of the properties in connection with an arbitrary size or shape.

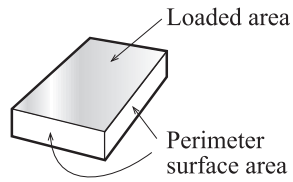

Figure 3: Shape factor definition.

$$q = \frac{\text{loaded area (on one side)}}{\text{perimeter surface area}} \tag{10}$$

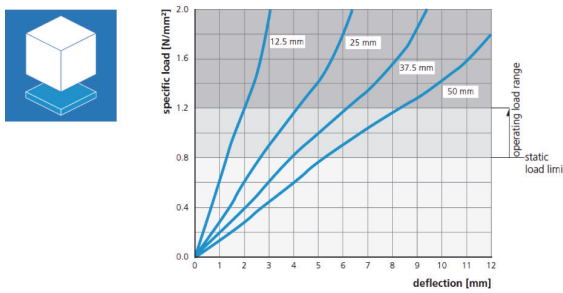

(a) Full surface bearing, $q = 6$.

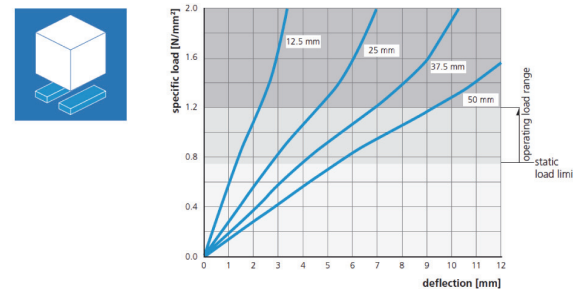

(b) Strip bearing, $q = 3$.

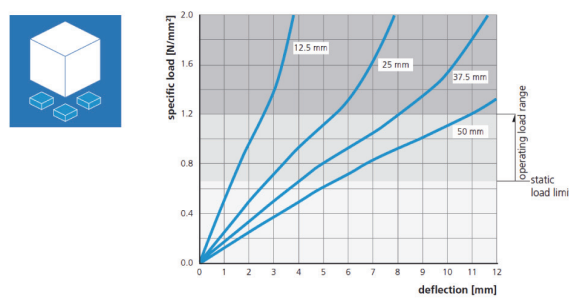

(c) Point bearing, $q = 1.5$.

Figure 4: Quasi-static load deflection curve measured at a velocity of deformation of 1% of the thickness per second; testing between flat steel-plates (i.e. with friction); recording of the 3rd loading; testing at room temperature [14].

FE simulations made in endeavoring to calibrate the model by mimicking the tests performed in [14], as shown in the plots displayed in Figure 4, were carried out in order to separate material and structural dependent properties. In so doing, the following steps were performed:

1. A block of Sylodyn having the shape factor q = 1.5, calculated according to equation (10), and the thickness t = 12.5 mm, was modelled, employing the same boundary conditions as those used for the tests shown in Figure 4a. The blocks were meshed with hybrid elements (denoted as C3D8RH in Abaqus), which are generally used for nearly incompressible materials so as to avoid numerical issues. A linear elastic material model (being the basis for the linear viscoelastic model which will be eventually used) was employed. A Poisson's ratio of ν^{∞} = 0.44 was assumed initially, this being a reasonable value for a slightly compressible material, which is the case of the elastomer dealt with in here. Also, a density measured simply as $\rho = m \,/\, V$ = 750 kg/m^3 was assigned to the block. The Young's modulus E^{∞} was then varied following an iterative process until the simulated curve and the corresponding plot given in the data sheet matched; see Figure 5. The result obtained for q = 1.5 and the thickness 12.5 mm, E^{∞} = 3.25 MPa, was then also tried for the other thicknesses considered in Figure 4 [14], i.e. 25, 37.5 and 50 mm, yielding rather close matches throughout. Note that the E^{∞} obtained (3.25 MPa) is very similar to the one obtained by means of measurements (3.2 MPa).
2. A block with a shape factor of q = 6 and t = 12.5 mm (Figure 4c) was created, its being assigned a Young's modulus of E^{∞} = 3.25 MPa (obtained in the previous step). This time, the Poisson's ratio was varied in an iterative manner, a rather close match being obtained for ν^{∞} = 0.42; cf. Figure 6. Again, using this value, each of the thicknesses were tried for q = 6, a rather close match being achieved.
3. Once this calibration was carried out, the properties obtained, namely E^{∞} = 3.25 MPa and ν^{∞} = 0.42, were ascribed to the material. The rest of the curves of the data sheet with q = 3, i.e. Figure 4b, (for thicknesses of 12.5, 25, 37.5 and 50 mm), were reproduced, portraying the static parameters derived to provide a close match for this one case as well. This therefore indicates that the properties obtained and to be used thereafter, are reliable. Plots relating the calibrated FE models to measurements from [14] are shown in Figure 7.

The Young's modulus and the Poisson's ratio need then to be converted to shear and bulk modulus by use of equations (11) and (12) respectively, assuming an isotropic material.

$$G^{\infty} = \frac{E^{\infty}}{2(1+\nu^{\infty})}, \tag{11}$$

$$K^{\infty} = \frac{E^{\infty}}{3(1-2\nu^{\infty})}. \tag{12}$$

The FE simulations and the static measurements in the uni-axial testing machine were shown to be consistent. The value of the Poisson's ratio also appears reasonable in view of the material being nearly incompressible. Inserting the values through the calibration into equations (11) and (12) results in $G^{\infty} = 1.14$ MPa and $K^{\infty} = 6.8$ MPa, these being the basis for the viscoelastic parameters considered next.

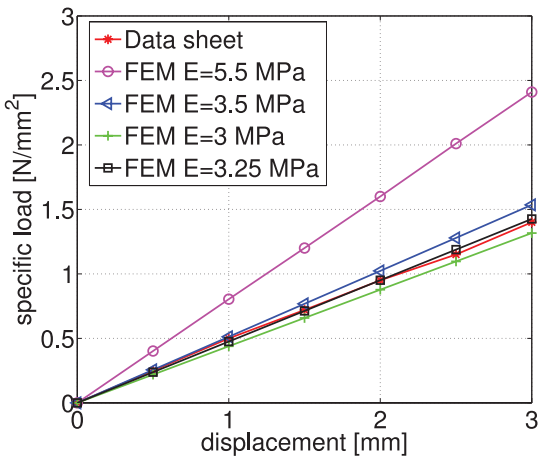

Figure 5: Iterative calibration for varying E, $q = 1.5$, $t = 12.5$ mm, $\nu = 0.44$, $\rho = 750$ kg/m^3.

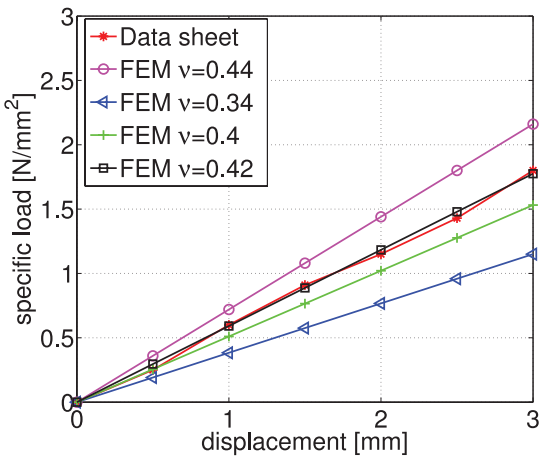

Figure 6: Iterative calibration for varying ν, $q = 6$, $t = 12.5$ mm, $E = 3.25$ MPa, $\rho = 750$ kg/m^3.

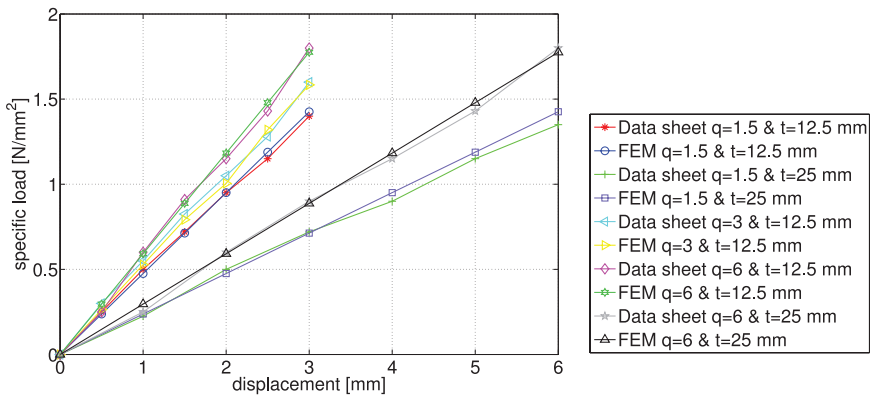

Figure 7: Comparison between the FE results and the data sheet tests (Figure 4, [14]) for different shape factors and thicknesses of the test samples. For simplicity's sake and for clarity of the plot, not all cases under study are shown.

4.2 Dynamic parameters

It is desirable to analyse lightweight structures containing elastomers in steady-state dynamic analyses. In terms of linear dynamic analyses, this means solving for displacement amplitudes and phase lag in linear systems of equations containing complex numbers. Accordingly, the material parameters are given in the form of complex numbers depending on the frequency. The extraction of the values for the dynamic shear and bulk moduli is taken up hereafter.

4.2.1 Methodology – justification of the scaling method

Hypothesis: The entire scaling process relies on the hypothesis, or underlying assumption, that a frequency dependent proportionality factor $\alpha(f)$ can be defined as follows for the conversion to material parameters suitable for use as input in the FE simulations:

$$\alpha(f) = \underbrace{\frac{E^{dyn}(f)}{E^{\infty}} = \frac{G^{dyn}(f)}{G^{\infty}} = \frac{K^{dyn}(f)}{K^{\infty}}}_{Homogeneous\ (I)} = \underbrace{\frac{E_c^{dyn}(f)}{E_c^{\infty}}}_{Inhomogeneous\ (II)}, \tag{13}$$

E being the Young's modulus of the material, G the shear modulus, and K the bulk modulus. Note that the subscript c denotes structural dependent properties, the superscript ∞ indicates static properties and the term dyn is used to denote the modulus of the complex dynamic magnitude in question (E^*, G^* or K^*). The phase lag of these dynamic magnitudes will be dealt with later. The relationship is derived in the following manner:

Proof of term (I) in equation (13): Consider a three dimensional case and steadystate loading. The method presented here relies on the hypothesis of neglecting the frequency dependence of the Poisson's ratio. This means that ν^* is assumed to be real and constant, i.e. $\nu^* = \nu^\infty$. Then, for all frequencies, it holds:

$$|G^*| = G^{dyn}(f) = \frac{E^{dyn}(f)}{2(1+\nu^\infty)}, \tag{14}$$

$$K^*| = K^{dyn}(f) = \frac{E^{dyn}(f)}{3(1-2\nu^\infty)}. \tag{15}$$

Comparing, for the shear modulus, with the static case (i.e. relating equations (11) and (14)) and keeping in mind the hypothesis of $\nu^* = \nu^\infty$, it yields

$$\frac{G^{dyn}(f)}{G^\infty} = \frac{\frac{E^{dyn}(f)}{2(1+\nu^\infty)}}{\frac{E^\infty}{2(1+\nu^\infty)}} = \frac{E^{dyn}(f)}{E^\infty}, \tag{16}$$

and in the same way, comparing equations (12) and (15),

$$\frac{K^{dyn}(f)}{K^\infty} = \frac{\frac{E^{dyn}(f)}{3(1-2\nu^\infty)}}{\frac{E^\infty}{3(1-2\nu^\infty)}} = \frac{E^{dyn}(f)}{E^\infty}. \tag{17}$$

Both equations (16) and (17) prove the equality of term (I) in equation (13), i.e.

$$\alpha(f) = \frac{E^{dyn}(f)}{E^\infty} = \frac{G^{dyn}(f)}{G^\infty} = \frac{K^{dyn}(f)}{K^\infty}, \tag{18}$$

which defines $\alpha(f)$ as being ratios of different dynamic to static constants, without any structural dependence being involved. The latter formula involves that the dynamic stiffness in the various loading cases varies in the same manner with frequency.

Hence, the dynamic proportionality factor $\alpha(f)$ to transform static to dynamic non-structural dependent properties can be defined and discussed in accordance with

$$E^{dyn} = \alpha(f)E^\infty \begin{cases} \alpha(f) = 1 \text{ for } f = 0 \text{ Hz} \\ \alpha(f) = E^0/E^\infty \text{ for } f = \infty \text{ Hz} \end{cases} \tag{19}$$

where the latter definition given in equation (19) can be proved by comparing it with Figure 1(a).

Proof of term (II) in equation (13): To be obtained next is $\alpha(f)$ defined as the ratio of the structural dependent dynamic to static properties. By inhomogeneous loading is meant that the boundary conditions result in a change in stiffness as compared to the homogeneous case. In compression, for example, the situation is that described in Figure 8.

The behaviour of the tests shown there is governed by the following equations:

$$\begin{aligned} \frac{P}{A} &= E_c^{\infty}\frac{u_c}{H} && \text{for Figures 8(a) and 8(c),} \\ \frac{P}{A} &= E^{\infty}\frac{u}{H} && \text{for Figures 8(b) and 8(d).} \end{aligned} \tag{20}$$

where u is the vertical displacement of the sample test when it is compressed, H is the original height of it, A is the cross section of it, P the compressive force and E_c^{∞} and E^{∞} are the Young's modulus (the structural and the non-structural dependent one, respectively).

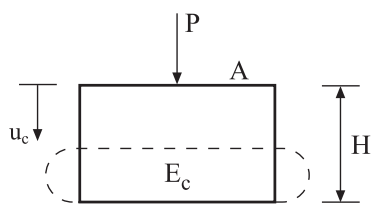

(a) Inhomogeneous loading case.

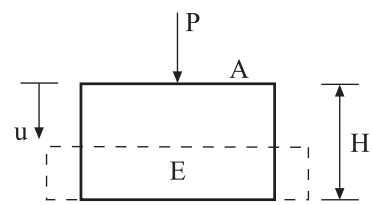

(b) Homogeneous loading case.

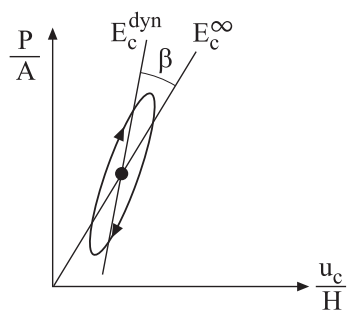

(c) Inhomogeneous loading case response plot.

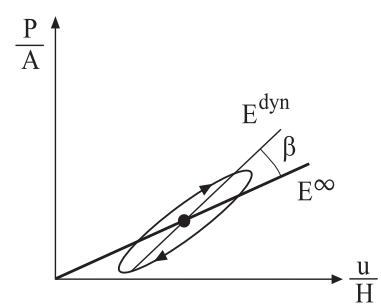

(d) Homogeneous loading case response plot.

Figure 8: Compression test between non lubricated plates (a), allowing the material to bulge and thus creating structural effects, together with its response (c); and compression test between lubricated plates (b), showing ideal behaviour eliminating any structural effect, together with its stress-strain response (d). Note the higher value (higher slope of the curves) of the Young's moduli in the inhomogeneous case due to structural effects.

It can thus be stated, in comparing the two equations given in (20), that a proportionality factor k_c exists in accordance with

$$E_c^{\infty} = k_c E^{\infty}, \tag{21}$$

the boundary conditions affecting the instantaneous modulus in the same way, i.e.

$$E_c^{0} = k_c E^{0}, \tag{22}$$

and thus

$$E_c^{dyn}(f) = \underbrace{k_c E^{\infty}}_{E_c^{\infty}} \alpha(f), \tag{23}$$

and finally

$$\alpha(f) = \frac{E_c^{dyn}}{E_c^{\infty}}. \tag{24}$$

Equation (24) justifies, together with equation (18), the assumption given in equation (13).

4.2.2 Application – obtaining the material properties

Through use of the underlying assumption discussed in the previous section, the material properties were extracted from the data contained in the data sheet. The Sylodyn NE data sheet [14], yields a dynamic compression modulus (E_c^{dyn}) and a loss angle (tan δ) for a case mixing in a structural dependence as discussed; see Figure 9. The parameters E_c^{dyn} (f) and $\delta(f)$, with f being given in Hertz and the subindex c denoting the structural dependent properties, can be looked upon as the absolute value and the phase angle of a frequency dependent complex quantity $|E_c^*|$, where

$$E_c^{dyn} = |E_c^*| \quad \text{and} \quad \delta = \arg E_c^*. \tag{25}$$

Looking at Figure 9(a), one finds that E_c^{dyn} is weakly dependent upon the frequency, its having a value of around 6 MPa. The dynamic modulus is always larger than the static one [12], and in this case it is even higher, due to structural effects (compare the slopes in Figures 8(c)-8(d)). Thus, in order to find $|G^*|$ and $|K^*|$, these being the dynamic complex shear and the bulk moduli, respectively, the values need to be properly scaled, so as to eliminate structural effects, as explained in section 4.2.1.

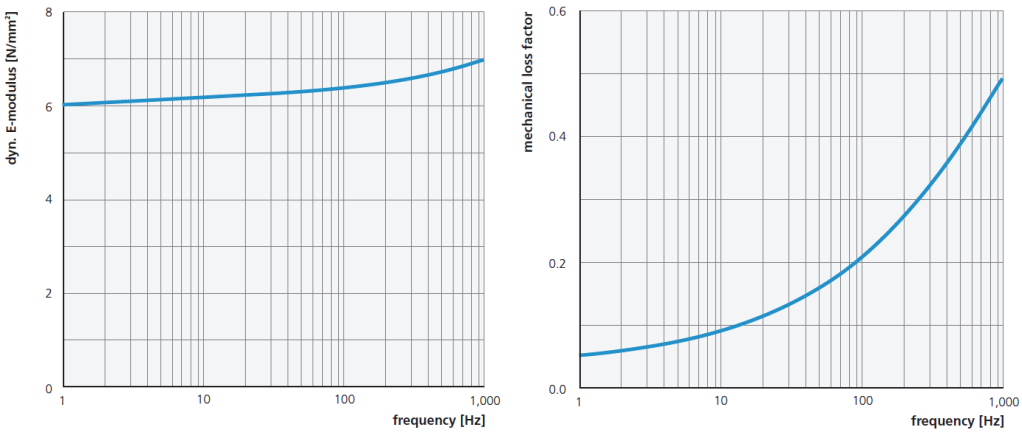

(a) Dynamic Young's modulus. (b) Loss factor.

Figure 9: DMA-tests; mastercurve with a reference temperature of 21°C; tests within the linear area of the load deflection curve, at low specific loads [14].

In [15], it was shown (based on the linearity of the complex quantities) that the losses represented by δ are no more than weakly dependent upon the boundary conditions, and that they can thus be taken as corresponding to the phase angle of the complex material parameters, i.e. they can be directly taken from the data sheet (i.e. Figure 9(b) in this case). Finding material parameters for the input to the FE simulations is thus a matter of carrying out a proper scaling of the dynamic stiffness given in the data sheet.

The scaling of the shear modulus G, is done by working out equation (13) in the following manner:

$$G^{dyn}(f) = \alpha(f) \cdot G^{\infty} = \frac{E_c^{dyn}(f)}{E_c^{\infty}} \cdot G^{\infty}, \tag{26}$$

where $E_c^{dyn}(f)$ can be taken directly from Figure 9(a) for each frequency of interest, and E_c^{∞} can be taken from Figure 10. In the latter Figure, it can also be seen that E_c^{∞} has a value for the lowest shape factor (q = 1.5) which is fairly constant (one of approximately 6 MPa) if the preload is less than about 0.6 MPa, which should be the operating range for the material. Therefore, the value of E_c^{∞} should be taken from the curve termed as *static* and below the value of 0.6 MPa in the horizontal axis. The static shear modulus G^{∞} present in equation (26) was determined earlier by use of equation (11).

Note that both Figures 9(a) and 10 have redundant data, i.e. they are equivalent in some respects. Thus, if the material is operating in the recommended range up to

0.6 MPa (above that value, E_c^{∞} varies due to non-linear effects which are outside of the scope of this investigation), the curves termed as *10 Hz* and *30 Hz* in Figure 10 are equivalent to the values given in Figure 9(a) if one looks in the horizontal axis at the values for the frequencies of 10 Hz and 30 Hz, as these yield the same value for $E_c^{dyn}(f)$. Since no value for 0 Hz is given in Figure 9(a) (it contains data down to 1 Hz), the value for E_c^{∞} has to be obtained from the curve *static* in Figure 10 instead.

Accordingly, the material parameters can be obtained directly from the static parameters by scaling them in terms of a frequency-structural dependent parameter $\alpha(f)$, as determined for each frequency directly from the data sheet [14].

The loss angle δ, as already mentioned, is not affected by the boundary conditions or by structural effects [15]. This has not just been shown experimentally, it in fact is inherent in the assumption of proportionality. This means that the phase angle for $G^*(f)$ can be taken directly also from the data sheet (cf. Figure 9(b)), with use of the simplification given in equation (7), i.e. arg $G^*(f) = \delta(f)$.

The parameters determined thus far ($G^{dyn}(f)$ and $\delta(f)$) give the complex shear modulus in polar form. Abaqus requires G^* and K^* in a rectangular form, i.e. $G^* = G_s + iG_l$, with G_s and G_l being the storage and loss moduli, respectively. The conversion can be done by applying the simple trigonometric principles of

$$\begin{aligned} G_s &= G^{dyn} \cos\delta, \\ G_l &= G^{dyn} \sin\delta. \end{aligned} \tag{27}$$

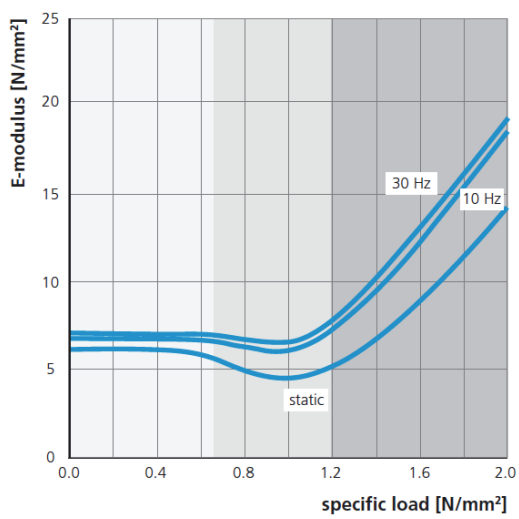

Figure 10: Static modulus of elasticity as a tangent modulus taken from the load deflection curve; dynamic modulus of elasticity due to sinusoidal excitation with a velocity level of 100 dBv re. $5{\cdot}10^{-8}$ m/s; test according to DIN 53513, $q = 1.5$ [14].

For the complex bulk modulus, the same procedure applies, where

$$K^{dyn}(f) = \alpha(f) \cdot K^{\infty} = \frac{E_c^{dyn}(f)}{E_c^{\infty}} \cdot K^{\infty}, \tag{28}$$

$\alpha(f)$ having the same values and thus being obtained in the same way as for the case of the dynamic shear modulus, and K^{∞} being calculated on the basis of equation (12). Again, the phase angle for $K^*(f)$ is taken directly from the data sheet (cf. Figure 9(b)) making use of the simplifications given in equation (7), i.e. $\arg K^*(f) = \delta(f)$.

The bulk modulus is hence given, in rectangular form, as

$$\begin{aligned} K_s &= K^{dyn} \cos\delta, \\ K_l &= K^{dyn} \sin\delta. \end{aligned} \tag{29}$$

Results obtained in employing this scaling procedure for use in Abaqus are presented in section 5.1.

5. VERIFICATION

In this section, the method developed here is tested for purposes of verification.

5.1 Material properties

The material properties of the elastomer in question that were obtained in employing this method are presented in Tables 1 and 2.

Table 1: Linear viscoelastic properties (of the dynamic shear modulus). For simplicity's sake, only certain frequencies amongst all that were determined are presented. The values for other frequencies can be obtained either through the linear interpolation between the values presented in the table or through obtaining $\alpha(f)$ from Figures 9(a) and 10.

	Data Sheet			Scale factor	MTS&FEM	Scaling Eq.(26)	Simulation input	
f [Hz]	E_c^{dyn} [MPa]	E_c^{∞} [MPa]	$\delta \approx \tan\delta$	$\alpha(f)$	G^{∞} [MPa]	G^{dyn} [MPa]	G_s [MPa]	G_l [MPa]
1	6.0000	6	0.0500	1.0000	1.14	1.1400	1.13857530	0.05697625
5	6.1000	6	0.0700	1.0167	1.14	1.1590	1.15616161	0.08106376
10	6.2000	6	0.0900	1.0333	1.14	1.1780	1.17323232	0.10587693
15	6.2125	6	0.1000	1.0354	1.14	1.1804	1.18031598	0.11803550
20	6.2250	6	0.1100	1.0375	1.14	1.1828	1.17424441	0.12994457
25	6.2300	6	0.1200	1.0383	1.14	1.1837	1.17654583	0.14158961
30	6.2500	6	0.1300	1.0417	1.14	1.1875	1.17747975	0.15394054

Table 2: Linear viscoelastic properties (of the dynamic bulk modulus). For simplicity's sake, only certain frequencies amongst all that were determined are presented. The values for other frequencies can be obtained either through the linear interpolation between the values presented in the table or through obtaining $\alpha(f)$ from Figures 9(a) and 10.

	Data Sheet			Scale factor	MTS&FEM	Scaling Eq.(28)	Simulation input	
f [Hz]	E_c^{dyn} [MPa]	E_c^{∞} [MPa]	$\delta \approx \tan\delta$	$\alpha(f)$	K^{∞} [MPa]	K^{dyn} [MPa]	K_s [MPa]	K_l [MPa]
1	6.0000	6	0.0500	1.0000	6.8	6.8000	6.79150177	0.33985835
5	6.1000	6	0.0700	1.0167	6.8	6.9133	6.89640258	0.48353822
10	6.2000	6	0.0900	1.0333	6.8	7.0267	6.99822787	0.63154661
15	6.2125	6	0.1000	1.0354	6.8	7.0408	7.04048129	0.70407160
20	6.2250	6	0.1100	1.0375	6.8	7.0550	7.04264930	0.77510799
25	6.2300	6	0.1200	1.0383	6.8	7.0607	7.01799269	0.84456962
30	6.2500	6	0.1300	1.0417	6.8	7.0833	7.02356341	0.91824184

Note that the dynamic behaviour of any linear viscoelastic material is defined by a pair of parameters, say (E^*, ν^*) or (G*, K*). The latter pair of parameters is used here, the reason being that Abaqus requires those parameters. A manipulation of G_s, G_l, K_s and K_l must be carried out before introducing the values, since in Abaqus they are given in terms of the real and imaginary parts of the Fourier transform of the non-dimensional shear and bulk relaxation functions $g(t)$ and $k(t)$, respectively (cf. [13] for more information). These are defined as follows:

$$\begin{aligned} \omega\Re(g^*) &= \frac{G_l}{G_\infty}, \qquad & \omega\Im(g^*) &= 1 - \frac{G_s}{G_\infty}, \\ \omega\Re(k^*) &= \frac{K_l}{K_\infty}, \qquad & \omega\Im(k^*) &= 1 - \frac{K_s}{K_\infty}. \end{aligned} \tag{30}$$

Note also again that a real and constant Poisson's ratio has been assumed, its being the main hypothesis for the methodology presented in here. In section 5.1.1, it will be proven if this assumption is correct for this type of problem.

5.1.1 Dynamic finite element calibration

The material properties presented in Tables 1 and 2 set the scene for viscoelastic linear dynamic calculations to be performed in Abaqus. The test specimen employed to perform the measurements shown in Figure 9(a) was a block of Sylodyn with $q = 3$ and dimensions $300\times300\times25$ mm^3. Thus, such a shape was modelled in Abaqus, the properties shown in section 5.1 being ascribed to it, as well as the same boundary conditions as those involved in the tests. A frequency sweep was carried out and the dynamic modulus was obtained as $|E^*| = \sigma_{nom}/\epsilon = (R/A) \,/\, (u/H)$; R being the reaction force on the surface of the block, and A, u and H being defined in Figure 8. As one can see, there is a fairly close agreement between the data as taken from Figure 9(a) and the simulated results; see Figure 11. On top of that, and as a matter of verification,

another block with shape factor $q = 3$ and dimensions $225 \times 112.5 \times 12.5$ mm^3 was modelled and simulated, a very good match being obtained for this one case as well (cf. Figure 11). Note that the small mismatches between simulated results and the data given in [14] can be in part due to the fact that data was read manually from the data sheet.

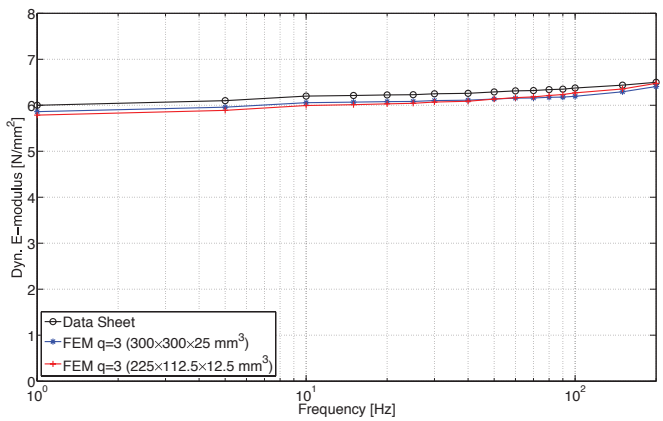

Figure 11: Verification of the dynamic properties obtained.

The results presented in Figure 11 confirm that the material properties obtained through the methodology developed in this manuscript are correct. They have also portrayed that the assumption of ν^* being real and constant works properly for this type of elastomers. This finding will eventually allow the modelling of elastomer blocks of any size and shape, which can be integrated in FE predictive tools of buildings, such as the one taken up in the next section.

5.2 Study case: Timber Volume Element based building

Although lightweight timber frame buildings can be put up completely on site, the tendency leans towards them being erected by assembling prefabricated elements at the building site. Specifically, the box-assembly construction method (described in section 2) is in steady increase in the industrial production of volume building, due mostly to the standardisation of the building technique it involves. An accurate FE predictive tool for this type of building is ultimately sought, the first simulations being presented in this section. It is believed that having accurate material properties for the elastomers is the first step to achieve a good accuracy of the predictive tools, therefore the existence of the investigation presented in here. A real module in the factory is shown in Figure 12, whereas a scheme of a complete building can be seen in Figure 13.

Figure 12: TVE manufacturing.

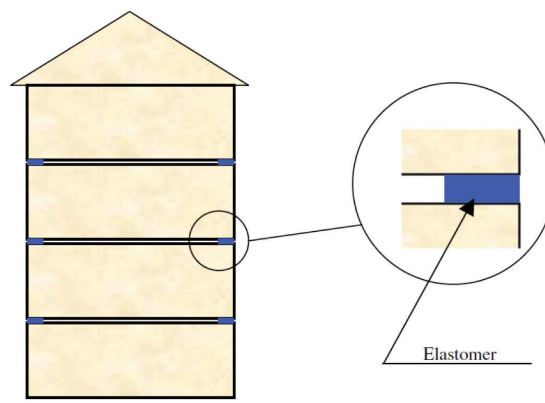

Figure 13: TVE based building [2].

In order to verify the methodology for a simple structure by comparing the results for some simple but unknown structural situations, two TVEs (with inner dimensions $3.6\times8.6\times3$ m^3) were stacked (cf. Figure 14) and FE simulations were carried out using Abaqus [13]. Specifically, a comparison between two cases, one where elastomers are introduced between the modules and other one with no elastomers (i.e. wood-to-wood connections) was performed (cf. Figure 15). The drawings of one such building, specifically those pertaining to Lindbäcks Bygg's project Brunnby Park in Upplands Väsby (Sweden), together with a list of materials employed in its construction, are shown in Figure 16. The material properties used for all parts in the modelling were either provided by the manufacturers or assessed via measurements, except the ones for the elastomer, which were extracted with the methodology presented in here (i.e. those shown in Tables 1 and 2).

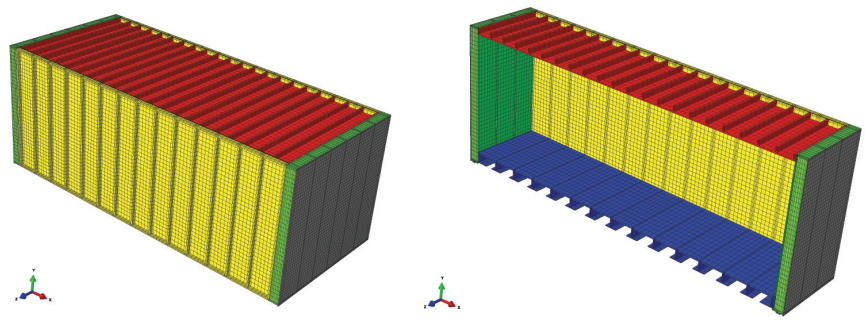

Figure 14: Model of one TVE. The floor is shown in blue, the ceiling in red, the apartment separating walls shown in yellow and the facade walls in green. Weather boards on the outside of the facade vertically embracing TVEs when stacked are shown in grey. In the model used for the comparison, two of such modules were stacked on top of each other.

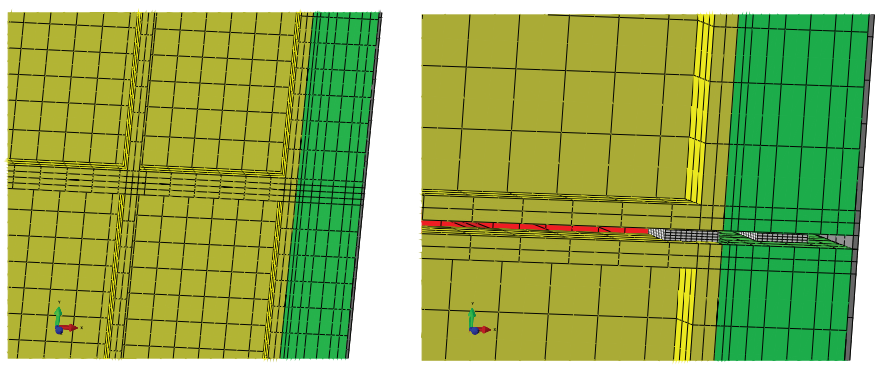

Figure 15: Detail of the FE models without (left) and with Sylodyn (right) in between. Again, the apartment separating walls are shown in yellow, the facade walls in green, whereas the elastomer blocks are depicted in white.

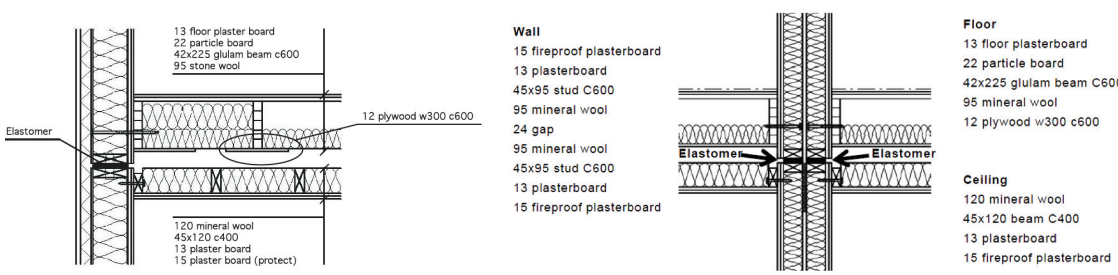

(a) Facade walls. (b) Apartment separating walls.

Figure 16: Drawings of a TVE-based building.

The elastomers used at the junctions were modelled with dimensions 100×95×25 mm^3, their being meshed with hybrid linear elements denoted in Abaqus as C3D8RH in order to avoid numerical issues. The distance c/c (centre-to-centre) between two blocks was set to 600 mm as in reality. The computational mesh for the rest of the parts involved was obtained using hexahedral solid 3-D stress finite elements (C3D20R) with 20 nodes and quadratic interpolation. The element size was decided based on the wavelengths expected to occur in the model. Full coupling between all individuals parts within the TVE was considered. This is believed to be the real case in constructed buildings, as discussed with the manufacturers. The results described correspond to an unit harmonic concentrated force placed at the middle of the floor in the top volume, a frequency sweep from 1 to 200 Hz being carried out. The RMS acceleration magnitudes were extracted at five nodes along the floor, ceiling and wall of the volume below, 20 cm from the junction, an average then being carried out according to

$$a_{\text{mean}}(f)\ [\text{m/s}^2] = \sqrt{\frac{1}{\text{mp}} \cdot \sum_{\text{n=1}}^{\text{mp}} a_i(f)}, \tag{31}$$

where mp is the number of evaluation points and $a_i(f)$ the frequency dependent simulated acceleration. Note that the nodes where accelerations were evaluated were exactly the same in both cases under study.

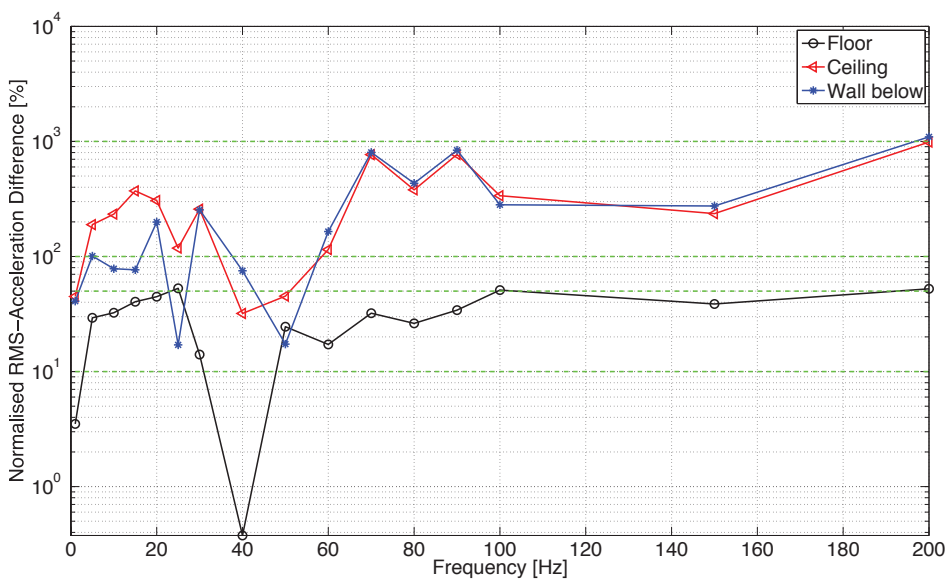

Figure 17: Normalised acceleration difference between the case with elastomer and the one without.

The normalised acceleration difference (i.e. NAD) was computed, for every frequency and each structural part (i.e. floor, ceiling and wall) according to

$$\mathrm{NAD}(f) = \left| \frac{a_{\mathrm{mean}}(f)_{\mathrm{NoElastomer}} - a_{\mathrm{mean}}(f)_{\mathrm{Elastomer}}}{a_{\mathrm{mean}}(f)_{\mathrm{NoElastomer}}} \right| \cdot 100. \tag{32}$$

The results between the two cases are depicted in Figure 17.

Also, in order to have an idea between the difference between both cases, an average over all the frequency range was calculated as

$$\overline{\mathrm{NAD}} = \frac{1}{\mathrm{NFreq}} \sum_{\mathrm{i}=1}^{\mathrm{NFreq}} \mathrm{NAD}(f), \tag{33}$$

NFreq being the number of frequencies analysed. The results are: $\overline{\mathrm{NAD}}_{\mathrm{floor}}$ = 30.8 %, $\overline{\mathrm{NAD}}_{\mathrm{ceiling}}$ = 324.6 % and $\overline{\mathrm{NAD}}_{\mathrm{wall}}$ = 297.0 %.

The latter results show the efficiency of introducing an elastic strip between volumes. The vibration levels at the floor (i.e. top volume) remain almost unchanged, whereas in the lower volume (i.e. wall and ceiling), the difference becomes much larger (up to 324.6 %). This portrays the importance of having accurate properties for the elastomer layers when setting up FE prediction tools, since wrong simulation results could yield to miss-predictions when erecting or predicting the behaviour of such buildings.

6. CONCLUSIONS

Low frequency prediction tools for assessing vibratory performance of lightweight buildings are needed due to complaints in this respect often arising on the part of the inhabitants. Since the current standards leave low frequencies out of the scope, acoustic comfort may not be met, even when buildings fulfill all of the regulations currently in force. Assessing the dynamic behaviour of a building accurately requires of FE models representing the geometry involved in great detail, as any geometric variations may have an effect. Likewise, reliable input of the material properties in question are needed, since even small changes can have a marked effect on the results obtained.

In wooden buildings, elastomers are often introduced at the junctions in order to reduce noise and vibration transmission. In setting up the FE prediction tools referred to here, it is of particular interest to have knowledge of the material properties involved, so as to be able to model elastomers of any size and shape. The properties of rubber-like materials and elastomers are often given on data sheets by the manufacturers, these often being bonded to structural effects such as shape factors or boundary conditions, possibly limiting and hindering their use for a general arbitrary case. In the present study, a method for determining the material properties of elastomers (specifically those

of Young's, bulk and shear complex moduli) based on laboratory testing, material modelling, and FE simulations was developed. Ultimately, the method can be expected to permit the material properties to be obtained simply on the basis of the manufacturer's data sheet and knowledge of the static modulus of elasticity of the material. This can facilitate the introduction of accurate frequency-dependent material properties into FE commercial software in a handy way.

ACKNOWLEDGEMENTS
This research was funded by the Silent Spaces project a part of the EU program Interreg IV. The authors very much appreciate the financial support provided.

REFERENCES

[1] Forssén, J., Kropp, W., Brunskog, J., Ljunggren, S., Bard, D., Sandberg, G., Ljunggren, F., Ågren, A., Hallström, O., Dybro, H., Larsson, K., Tillberg, K., Sjökvist, L-G., Östman, B., Hagberg, K., Bolmsvik, Å., Olsson, A., Ekstrand, C-G., Johansson, M., Acoustics in wooden buildings, State of the art 2008, Vinnova project 2007-01653, Report 2008:16, SP Trätek (Technical Research Institute of Sweden), Stockholm, 2008.

[2] Ljunggren, F. and Ågren, A., Potential solutions to improved sound performance of volume based lightweight multistory timber buildings, Applied Acoustics 72 (2011) 231–240.

[3] Ågren, A., Ljunggren,F. and Bolmsvik, Å., Flanking transmission in light weight timber houses with elastic flanking isolators, Proceedings of Internoise, New York, USA, 2012.

[4] Ljunggren, S., Measurement of the performance of noise controlling devices in buildings of massive wood, Working Report 2001:42001, Department of Civil and Architectural Engineering, Division of Building Technology, KTH, Stockholm, Sweden, 2001.

[5] Ljunggren, F. and Ågren, A., Development of a new damper to reduce resonant vibrations in lightweight steel joist floors, Applied Acoustics 63 (2002) 1267–1280.

[6] Jarnerö, K., Bolmsvik, Å., Brandt, A. and Olsson, A., Effects of flexible supports on vibration performance of floors, Proceedings of Euronoise 2012, Prague, Czech Republic, 2012.

[7] Bolmsvik, Å., Linderholt, Å. and Jarnerö, K., FE modeling of a lightweight structure with different junctions, Proceedings of Euronoise, Prague, Czech Republic, 2012.

[8] Bolmsvik, Å. and Brandt, A., Damping assessment of light wooden assembly with and without damping material, Engineering Structures 49 (2013) 434–447.

[9] Ökvist, R., Ljunggren, F. and Ågren A., Variations in sound insulation in nominal identical prefabricated lightweight timber constructions, Journal of building acoustics, 17(2) 2009, 91–103.

[10] Bolmsvik, Å., Structural-acoustic vibrations in wooden assemblies – Experimental modal analysis and finite element modelling, PhD thesis, Linnaeus University, Sweden, 2012.

[11] Bolmsvik, Å., Linderholt, A., Brandt, A. and Ekevid, T., FE Modelling of Light Weight Wooden Assemblies – Parameter study and comparison between analyses and experiments. Engineering Structures 73 (2014) 125–142.

[12] Austrell, P-E., Modeling of elasticity and damping for filled elastomers, PhD thesis, Division of Structural Mechanics, Lund University, Sweden, 1997.

[13] Dassault Systèmes, Abaqus theory manual, Version 6.11, 2012.

[14] Getzner Werkstoffe GmbH (2004), Data sheet of the Sylodyn NE.

[15] Olsson, A. K. and Austrell, P-E., Finite element analysis of a rubber bushing considering rate and amplitude dependence effects. Proceedings of 3rd European Conference on Constitutive Models for Rubber (ECCMR), London, UK, 2003.

[16] Ljunggren F., Using elastic layers to improve sound insulation in volume based multistory lightweight buildings, Proceedings of Internoise, Ottawa, Canada, 2009.

[17] Ågren A., Acoustic highlights in Nordic light weight building tradition – focus on ongoing development in Sweden, Proceedings of BNAM, Bergen, Norway, 2010.

[18] Meyers, M. and Chawla, K., Mechanical Behavior of Materials, Cambridge University Press, New York, USA, 2009.

[19] Cremer, L., Heckl, M. and Petersson, B. A. T., Structure-borne sound, Springer, Berlin, Germany, 2004.

[20] Hassan O. A. B., Building acoustics and vibrations – Theory and practice, World Scientific, Singapore, 2009.

[21] Ökvist, R., Ljunggren, F., and Ågren A., Variation in sound insulation in multistory lightweight timber constructions, Proceedings of Internoise, Ottawa, Canada, 2009.

[22] Bolmsvik, Å. and Ekevid T., Flanking transmission in a timber-framed building – A comparison of structural vibrations in measurements and FE analyses, Submitted to The International Journal of Acoustics and Vibration , January 2013.

[23] Bolmsvik, Å. and Ekevid T., FE modeling of wooden building assemblies, Proceedings of Internoise 2010, Lisbon, Portugal, 2010.

[24] Ljunggren F., Long-term effects of elastic glue in lightweight timber constructions, Proceedings of Forum Acusticum. Aalborg, Denmark, 2011.

[25] Chopra A. K., Dynamics of structures, Prentice Hall, New Jersey, USA, 2007.

[26] Ottosen, N. and Petersson, H., Introduction to the finite element method, Prentice Hall, England, 1992.

[27] Bathe, K. J., Finite Element Procedures, Prentice Hall, New York, USA, 1996.

[28] Hopkins, C., Sound Insulation, Elsevier, Oxford, UK, 2007.

Paper D

Applied Acoustics 105 (2016) 1–12

Contents lists available at ScienceDirect

Applied Acoustics

journal homepage: www.elsevier.com/locate/apacoust

Low frequency vibroacoustic investigation of wooden T-junctions

J. Negreira *, A. Sjöström, D. Bard

Lund University, Department of Construction Sciences, Division of Engineering Acoustics, P.O. Box 118, SE-221 00 Lund, Sweden

ARTICLE INFO

Article history:
Received 19 June 2015
Received in revised form 26 October 2015
Accepted 23 November 2015

Keywords:
Finite element method
T-junctions
Prediction tools
Low frequency vibration
Wooden structures
Measurements

ABSTRACT

In this paper, an experimental investigation on the influence of glue on the low frequency vibroacoustic performance (up to 200 Hz) of wooden T-junctions is presented along with a discussion of modelling issues related to the junctions. The mock-ups studied represent cut-outs of full size timber floor assemblies typically used in Sweden. Their dynamic performance was first studied experimentally by means of modal analysis. Moreover, finite element (FE) simulations of the T-junctions were carried out to establish reliable prediction tools, using the measurement data as calibration input. Modelling issues were addressed to investigate the influence of different features that must be taken into account when simulating the connections as part of larger structures. Guidelines for modelling these type of connections, when developing low frequency FE predictive tools, are presented here.

1. Introduction

Lightweight wood-framed constructions have steadily increased their market share in Sweden during the last two decades. Their vibration and acoustic performance was initially approved by applying the exact same regulations as for concrete buildings, despite their different behaviour; without thoroughly investigating whether the existent standardised sound insulation evaluation methods were appropriate. In spite of wooden buildings complying with the regulations currently in force, complaints often arise amid residents mainly due to consideration of low frequency noise (below 100 Hz) which is left out of the scope of the norms. Consequently, the frequency range of analysis was enlarged down to 50 Hz in the year 1999, the requirements in Sweden thus currently demanding measurements and evaluations in the extended frequency range 50–3150 Hz.

The investigations reported in [1] highlighted the importance of including low frequencies when evaluating sound insulation in lightweight buildings. Statistical analyses between measured objective parameters (accelerations, deflections, etc.) and subjective ratings by people living in the apartments that were measured, were performed. Regarding impact sound, the statistical term R^2 describing the correlation of measurements and resident's ratings of annoyance was improved from 32% to 74% when including frequencies down to 20 Hz, and even further improved up to 85% if a new proposed spectrum adaptation term was utilised. The latter stresses the need of encompassing low frequencies in the current evaluation procedures of impact sound insulation [2].

The fact that modern product improvement in timber buildings is carried out based on analyses of existing measurements and engineers' experience, calls for the development of prediction tools that could accurately predict impact sound transmission. To that end, finite element (FE) simulations have huge potential when addressing low frequency vibroacoustic issues. The challenge here is to accurately model the structural components involved, such as floors and walls. Matters such as material properties, junction details or interaction between constituent parts may play an important role in the response of the structure. Hence, gaining understanding about the behaviour of connections by performing simulations, and validating these to experiments is required to enable reliable prediction tools.

1.1. Aim and objective

The aim of the investigation presented here is to acquire knowledge on the behaviour and the modelling of two particular types of connections typically used in Swedish wood floors, cf. Fig. 1, for frequencies up to 200 Hz. Moreover, the extent to which glue modifies the vibroacoustic properties of the junctions is ascertained by means of experimental modal analysis (EMA). Measurement data are used to calibrate FE models of the junctions and to investigate issues that need to be accounted for when developing prediction tools. To achieve the latter aims, four mock-ups representing cut-outs of two types of junctions found in real floors were built (for each of the two types, one specimen glued and one without).

* Corresponding author. Tel.: +46 462224884; fax: +46 462227619.
E-mail address: juan.negreira@construction.lth.se (J. Negreira).

http://dx.doi.org/10.1016/j.apacoust.2015.11.016
0003-682X/

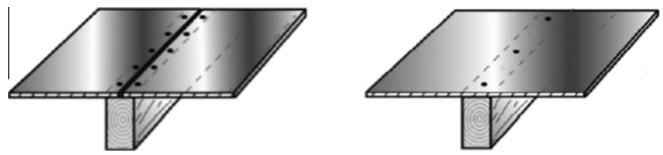

Fig. 1. Dual-plate junction (left) and single-plate junction (right).

Note that this work does not concern matters related to uncertainties in material properties which could influence the behaviour of nominally identical structures from one another. Also, statistical analyses involving workmanship are not taken account for in this work as just two specimens of each junction type (one using glue and one without) are studied. This is a step to be addressed eventually, its being initially tackled in e.g. [3].

To achieve the ultimate aim of determining the extent to which adhesives affect the low frequency performance of the T-junctions in question, as well as to draw guidelines to accurately model them when setting up FE prediction tools, the procedure adopted was the following:

1. For the case of a T-junction comprised by a single plate and starting with the simplest case (i.e. no screws being modelled, full interaction being considered between plate and beam), the eigenmodes from the FE simulations were matched with those obtained from measurements by tweaking the material parameters for the wooden beam and the particle board. The material parameters for which the match was achieved were maintained constant for all subsequent analyses (the mockups are later described in Section 3.1). Note that the main aim here is not to investigate the most accurate way to model the materials, but rather to study to what extent details in the junctions affect their behaviour by analysing relative differences between various cases.
2. With the material properties kept constant throughout, details which could potentially influence the performance of the junction (such as screws, thickness of the glue layer, and properties of the adhesive) were varied for each type of T-junction, extensive parametric studies being carried out and conclusions concerning the modelling details being drawn.

The work performed regarding FE modelling of timber structures has increased considerably in the last years (see Section 2). Nonetheless, not much work has been performed regarding the conjoint use of glue and screws in this type of junctions, hence this investigation aiming at lessening that knowledge gap.

2. Literature review

The process of conducting measurements of test buildings is costly and tedious. Prediction models, despite their high usefulness for designing new buildings and preventing severe and costly changes in the aftermath of construction, are still very much lacking. By using the FE method in developing numerical prediction tools, time and costs can be saved by tackling vibroacoustical issues during the design phase. However, before an adequate substitution of experimental investigations by numerical simulations takes place, modelling knowledge must be increased. Hereafter, a brief summary of most relevant work done thus far on the modelling of lightweight structures and its junctions using the FE method, is presented.

Coupling in joints between plates and beams occurs theoretically either on a surface, along a line or at individual points depending on the distance between the screws or nails with regard to the bending wavelength. In [4], vibration transmission between the two leaves of a wall for a wide variety of structures was modelled using two different theories (line- and point-based connections). The applicability and limitations of those fundamental theories regarding vibration transmission through lightweight plate-beam structures was checked in [5], the conclusions there being that more complex models than the ones employed should be used in order to be able to predict transmission through the variety of structures found in lightweight buildings. The match between measurements and calculations in [4,5] are, however, based on statistical energy analysis and therefore very low frequencies are out of the scope.

In [6], vibrational tests were carried out on a full-scale wooden construction consisting of a floor supported on beams so as to investigate the effect of having different types of junctions (one where the floor was resting on top of elastomers embedded in laths and one where the floor was screwed directly onto the beams). The correlation between test and analytical results was strongly dependent on the material properties for the wood. The connections between the floor and the walls in the FE model were assumed to be fully coupled for the wood-wood and modelled with spring-dashpot systems when elastomers were involved. It was concluded that more sophisticated models are needed to fully simulate the dynamic behaviour of the structure under study there.

The main objective of the investigation presented in [7] was to investigate the effect that elastomers have on the vibration properties of wooden constructions. A full scale structure comprised by three walls and one ceiling was built and its performance compared with measurements for the case where elastomers were introduced in the junctions and for the one without them. Elastomers showed to change the behaviour of the structure significantly, the vibration transmission from the floor to the walls below being markedly reduced for frequencies above 70 Hz. Below that threshold, however, not much reduction was achieved, even vibration amplification occurring at certain frequencies. The structure studied in [7] was simulated in [8]. The aim was to make correlation and calibration between tests and analyses of the full scale wooden structure to ultimately enhance modelling of sound distribution. Spring-dashpots systems were used to model the elastomers in the junctions, not accounting for frequency dependency. In line with the conclusions drawn in [6], it was also concluded here that there is a large influence on the simulation results depending on the selection of material properties. On top of that, the need of modelling the rotational stiffness and damping of an elastomer in a manner so that the results of experiments and FE simulations match (i.e. development of a 6-degree-of-freedom spring-dashpot system) was highlighted. An investigation aiming at fulfilling the need for accurately modelling elastomers was presented in [9], where a method for determining the frequency dependent material properties of elastomers (specifically those of Young's, bulk and shear complex moduli) based on laboratory testing, material modelling, and FE simulations, was developed. Ultimately, the method permits the material properties to be obtained simply on the basis of the manufacturer's data sheet and knowledge of the static modulus of elasticity of the material

so as to facilitate the introduction of material properties into FE models.

A concept introduced in [10] was that of load-slip modulus, its accounting for the semi-rigid attachments between various structural components, albeit torsion of joists and lateral bending were not accounted for there. In [11], a finite element model for predicting static and dynamic characteristics of wood-based floor structures with lateral reinforcements was set-up and compared to experimental results. Use was made of both slip-modulus and nail withdrawal modulus (i.e. an axial load–displacement modulus of fastener-to-wood connections, considering nails and screws) to create connector elements for modelling the fasteners, a reliable model being achieved. The slip-moduli values were taken from literature, whereas the withdrawal moduli were measured by the authors. Along the same lines, the aim of [12] was to replace a wood connector consisting on a folded sheet plate with nails and/or screws by an equivalent element in terms of a transfer function. The identification of the equivalent parameters was done by combining numerical analyses and experimental studies. A method for determining the stiffness matrix of the wood connector from the frequency responses of the global assembly was developed.

The work presented in [13] deals with the dynamic response and vibrational characteristics of timber flooring systems, identifying improved structural design as well as vibration prediction so as to address serviceability issues. Correlation for different floors are presented, several modelling techniques being investigated there. Among other conclusions, the fact of combining springs at supports and in connections, tuning the withdrawal stiffness to match the fundamental mode, was proved to yield an error of 1% in average for the first mode, and about 5–10% for modes two through five. The correlation to experimentally obtained modes was done by visual comparison.

Numerical modelling, model updating and parametric studies were performed in [14] with the goal of developing guidelines for predicting the acoustical and dynamical behaviour of wooden ceiling constructions and to design reduction measures regarding vibrations. To calibrate the model, parameters (namely the orthotropic properties of wood, FE type and size, contact parameters for adjusting the coupling and support conditions as well as the geometrical parameters) were calibrated using experimental data, following a developed algorithm, until a good match was achieved. Making use of the calibrated model, simulations with multiple sets of geometrical parameter combinations were run to predict the sound radiation.

Airborne sound transmission through a single-stud double-plate panel under diffuse field excitation was investigated in [15] utilising the FE method, with different coupling configurations between plates and the frame structure (e.g. structural contact completely tied, tying only some nodes on the centre lines of the structure, using a narrow strip of tied elements connect the frame to the plates and evenly spaced discrete elements tied). The investigations were performed as parametric studies focusing on the parameters' effect on the eigenfrequencies. The results indicate that in order to accurately model sound transmission through double-plate panels, the choice of coupling is an important factor.

3. Measurements

3.1. Experimental structures

The type of junctions investigated here are illustrated in Fig. 1. Four mock-ups were built. Firstly, a single $1200 \times 600 \times 22\ mm^3$ chipboard plate fixed onto a spruce beam of dimensions $45 \times 220 \times 600\ mm^3$, was built. The second junction was made of two squared chipboard plates with flat edges and dimensions $600 \times 600 \times 22\ mm^3$, each one of them fixed onto one beam with the same dimensions as in the first specimen. For both mock-ups, the plates were fixed to the beams solely by means of equidistant screws. Moreover, two structures were built a second time, but this time applying glue on the contact surfaces, i.e. in a horizontal layer around the screws and in a vertical layer between the two plates (when two plates were involved). The distance between the screws connecting the chipboard plates to the bearing beam, following the recommendations of manufacturers, was set to 250 mm in the case of a single plate and 125 mm in the case of two plates. The outmost screws were placed with a distance of 50 mm from the ends of the beams.

The mock-ups were built using materials of the same quality and from the same producer, thus ensuring that material properties do not vary unreasonably throughout the different pieces employed. The latter was checked on several plates and beams employed in the construction of the mock-ups, whose properties were assessed by laboratory measurements. EMA was performed in each of the specimens separately, providing similar results in terms of eigenfrequencies. The adhesive that was utilised was ordinary commercial PVAc glue commonly used in real constructions. In Fig. 2, the dual-plate set-up with flat edges and no glue applied can be seen.

3.2. Measurement procedure

In order to measure the vibrations as accurately as possible, the set-ups were suspended from the ceiling by using soft rubber springs. The resonance frequency of those springs was calculated beforehand, assuring that it was sufficiently low and specifically lower than the lowest eigenfrequency of the mock-ups so that no effect from them was caught in the measurements. The structure was excited with a hammer, nine different excitation points being considered with an average of 4 hammer blows at each excitation spot. Dual-axis microelectromechanical systems (MEMS) accelerometers, types iMEMS ADXL203 and ADXL202E, were used. A total of 28 sensors were screwed to the plate in the single-plate cases forming an equidistant 7×4 grid, whereas 32 were used in the dual-plate set-ups, since one row was considered at each side of the junction between the plates (i.e. a 4×4 grid pattern was laid on each plate). Special attention must be paid to the fixation of the transducers, the cabling and their mass, since those factors could alter the recorded accelerations. Details concerning mounting of accelerometers are found in [16]. When an accelerometer is fixed onto a surface, a mass is effectively added to it and can reduce the vibration level at the measurement point. It is important to ensure that the accelerometers are capable of accurately quantify the actual vibration level. According to [17], for a thin homogeneous isotropic plate this mass requirement can be calculated using the infinite plate impedance according to

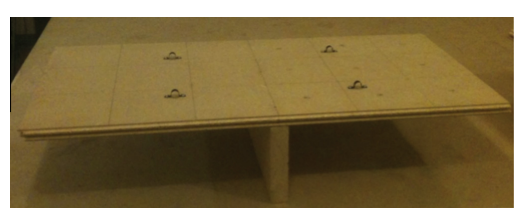

Fig. 2. Dual-plate set-up having flat edges at the junction and no glue applied. The four loops located on the top of the plate were used to hang the structure from the ceiling on rubber springs.

$$m_{\mathrm{acc}} \ll \frac{0.37\rho c_L h^2}{f}, \tag{1}$$

where ρ is the density of the plate, c_L the phase velocity of quasi-longitudinal waves in the plate, h the thickness of the plate and f the actual frequency.

A force transducer was placed on the tip of the instrumental hammer in order to get the force applied. All the accelerometers and the transducer were connected to a computer with a 32-channel acquisition system. The software used for the acquisition was Spectrum SBench 6.1. The raw data were saved as Matlab files for later analysis using a code developed by the author. Note that a frequency resolution of 1 Hz was chosen to analyse the raw data from the measurements, the latter choice being based on the observation of the frequency response functions (FFTs) before plotting the modes of vibration. This resolution proved to be enough when further calibrating against simulation results. The experimental set-up can be seen in Fig. 3.

Accelerometers and calibration: a typical MEMS accelerometer is composed of a movable proof mass with plates, i.e. a capacitor that is attached through a mechanical suspension system to a reference frame. The way MEMS accelerometers measure the acceleration is by sensing changes in capacitance when the geometry of the capacitor inside them is changing (either the area of the electrodes, the distance between them or the permittivity of the material separating them). All the MEMS accelerometers were calibrated before the measurements using the back-to-back method so as to accurately determine their sensitivity at the various frequencies of interest (up to 200 Hz here). The method involves coupling the accelerometer to be calibrated to a double-ended standard accelerometer and driving the coupled pair with a shaker, carrying out a frequency sweep; see Fig. 4. Since they are tightly coupled together, they will both experience the same motion, thus the calibration being done by comparing both responses and taking into account that the ratio between their sensitivities is known. For more information, see [18].

4. Finite element simulations

4.1. Finite element models

The T-junctions described in Section 3.1 were modelled in Abaqus [19]. The plate, the beam and the screws (manifested as square pins with a $5 \times 5\ \mathrm{mm}^2$ cross-section going through the plate and into the beam) were meshed with 8-node solid hexahedral elements using linear interpolation. For the glue, 20-node solid hexahedral elements, employing quadratic interpolation and hybrid formulation in order to avoid locking, were utilised.

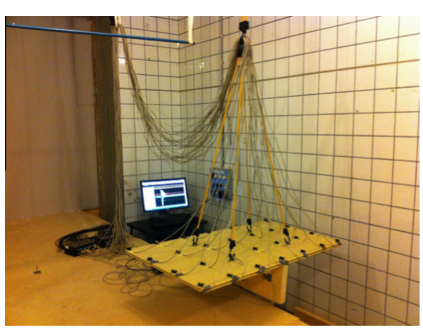

Fig. 3. Measurement set-up (single-plate mock-up shown).

In general, a difficult challenge when creating models of assembled structures is to create proper constrains at the connections between parts. These connections have strong influence on the stiffness of the structure and thus its dynamic behaviour. In here, the way those connections can be modelled so they represent the real behaviour described by measurements is sought. The FE models of the four mock-ups are shown in Fig. 5.

The problems dealt with here, as discussed in Section 1, are related with serviceability matters, meaning that the structures are exposed to relatively small loads and displacements. Consequently, all non-linear behaviour is neglected, allowing the materials to be modelled as linear elastic. The FE models were used to perform a modal analysis for the four different mock-ups, determining the eigenfrequencies and the corresponding eigenmodes for the various cases. The Lanczos solver implemented in Abaqus was applied for the structural analyses and the modes below 210 Hz were requested (to ensure finding the corresponding measured ones below 200 Hz).

4.2. Model validation

Modal assurance criterion: To compare measured and simulated eigenmodes (or also two different FE models) denoted as cases Φ_i^{a} and Φ_i^{b} respectively, the modal assurance criterion (MAC) was used [20]. The MAC-value for the ith eigenmode is defined as

$$\mathrm{MAC} = \frac{\left|(\Phi_i^{\mathrm{a}})^{\mathrm{T}}(\Phi_i^{\mathrm{b}})^{\mathrm{T}}\right|^2}{\left|(\Phi_i^{\mathrm{a}})^{\mathrm{T}}(\Phi_i^{\mathrm{a}})\right|\left|(\Phi_i^{\mathrm{b}})^{\mathrm{T}}(\Phi_i^{\mathrm{b}})\right|}. \tag{2}$$

Eq. (2) is the normalised scalar product of the eigenmodes from the measurements and the simulations (or from two FE models). The MAC-value is in the range 0–1, where 1 represents total correlation and 0 means no correlation at all.

Normalised relative frequency difference: Discrepancies in eigenfrequencies between simulations and measurements and also between different models when performing the parametric studies, were checked using the normalised relative frequency difference (NRFD), its being defined as

$$\mathrm{NRFD}_i[\%] = \frac{\left|f_{\mathrm{ij}} - f_{\mathrm{ref}_i}\right|}{f_{\mathrm{ref}_i}} \cdot 100, \tag{3}$$

where f_{ij} is the eigenfrequency of the analogous mode $i = 1, 2, \ldots 9$ and for the studied case j (e.g. measurements or any simulated case) and f_{ref_i} is the eigenfrequency for the same mode number i in the reference case considered.

Note that the MAC plots complete those of NRFD's, since the former give the degree of correlation in terms of mode shapes and the latter the differences in the eigenfrequencies. One type of plot alone would not be enough, since for example, two modes could be shifted in the measurements and simulations whilst still having a low NRFD value. All in all, to validate a predictive tool, one should look at both indicators.

5. Results

In order to compare the behaviour of all set-ups and in particular to investigate the influence of using glue for a given junction type, experimental modal analysis was performed. Moreover, correlations between measurements and simulations, and parametric studies modifying different features in the FE models, were carried out.

Fig. 4. Details of the fixation of the MEMS to the reference accelerometer and the shaker.

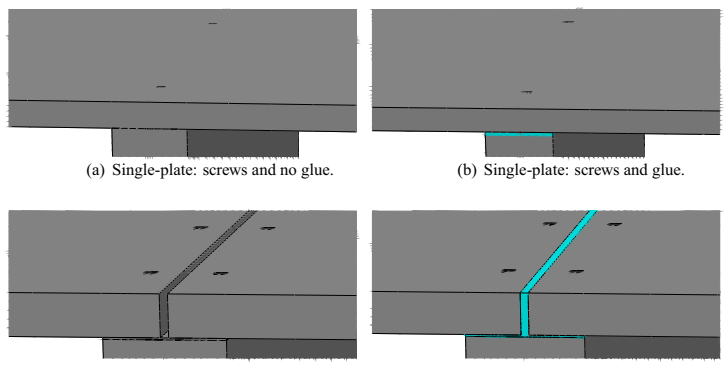

Fig. 5. Junction details of the FE models employed. The beam and the chipboard plate are shown in grey, respectively, whereas the screws are displayed in colour black. The glue, when present, is shown in light blue. (For interpretation of the references to colour in this figure legend, the reader is referred to the web version of this article.)

5.1. Single-plate junctions

In Table 1, the eigenfrequencies for the single-plate T-junctions from experiments as well as for simulations, are shown. Details and discussions are described and given below.

5.1.1. Measurements

In Table 1, it can be observed that the glue has a negligible influence on the eigenfrequencies, as the glued and non-glued case result in similar values. Nevertheless, it can be noted that the glue slightly stiffens the junction around approximately 1% in terms of eigenfrequencies. The stiffening effect is particularly larger in the 5th mode (bending) since the eigenfrequency in the glued case increases substantially as compared with the unglued case. The movement of the plate on top of the beam is constrained by the glue layer, as opposed to the unglued case, where some motion of the plate is allowed on top of the beam with exception of the places where the screws are present.

Table 1
Measured eigenfrequencies for the single-plate T-junctions. Note the different amount of significant figures in the results, as the resolution of the measurements was 1 Hz.

Mode	Glue		No glue	
	Meas. (Hz)	FEM (Hz)	Meas. (Hz)	FEM (Hz)
1	36	36.2	36	35.9
2	52	52.6	50	48.6
3	–	87.9	–	–
4	87	89.8	89	89.3
5	136	142.9	111	109.4
6	177	178.7	179	178.1
7	180	185.4	178	179.9
8	189	189.4	190	187.8
9	200	203.7	198	199.1

5.1.2. Simulations

5.1.2.1. No glue. First, a model comprising just a beam and a plate was created (i.e. no screws included). The connections were made by fully tying squared surfaces of 5×5 mm^2 between the plate and the beam at the positions where the screws would be placed otherwise (i.e. 250 mm between screws, being the outmost ones placed 50 mm from the ends of the beams). The beam and chipboard properties were varied within realistic values found in the literature (e.g. [6,8]) until a good match for the measured and simulated case was achieved, see Table 1. The material properties are those shown in Table 2. Note that a layered structure was assumed for the chipboard due to the layered appearance of the plates utilised, following [21–23], where two outer stiffer layers of 4.5 mm and a core of 13 mm were considered. Hereafter, these material properties will be kept constant for all other cases.

Secondly, a model including the actual steel screws was created, the screws (placed 250 mm from each other, being the outmost ones 50 mm from the ends of the beams) being modelled as squared pins of cross-Section 5×5 mm^2 going through the plate and into the beam (cf. Fig. 5(a)) and assigning them the steel properties shown in Table 2. The results, in terms of eigenfrequencies, showed no appreciable differences as compared to the first model. In Fig. 6, the eigenmodes up to 200 Hz are depicted for the screwed unglued single-plate case. In the left column, the measured ones are presented, whereas the simulated ones are shown in the right column. For the sake of simplicity and brevity, just the eigenmodes for this case are displayed graphically.

Table 2
Material properties employed in the models. The elastic and shear moduli, E and G respectively, are given in [Pa], whereas the densities ρ have units of [kg/m^3]. ν [–] denotes the Poisson's ratio.

Spruce	$E_1 = 8.5 \cdot 10^9$	$E_2 = E_3 = 3.5 \cdot 10^8$	$G_{12} = G_{13} = 7 \cdot 10^8$	$G_{23} = 5 \cdot 10^7$	$\nu_{12} = \nu_{13} = 0.2$	$\nu_{13} = 0.3$	$\rho = 432$
Chipboard	$E_{core} = 3 \cdot 10^9$	$E_{outer} = 6.5 \cdot 10^9$	–	–	$\nu = 0.3$	–	$\rho = 767$
Screws	$E = 2.1 \cdot 10^{11}$	–	–	–	$\nu = 0.3$	–	$\rho = 7800$
Glue	$E_{ref} = 0.5 \cdot 10^9$	–	–	–	$\nu_{ref} = 0.3$	–	$\rho = 1100$

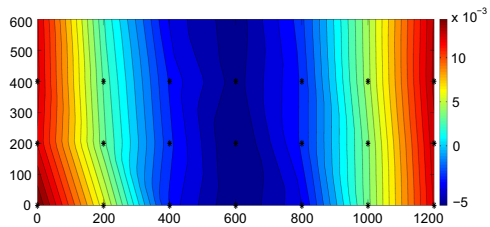

(a) 1st measured mode: 36 Hz

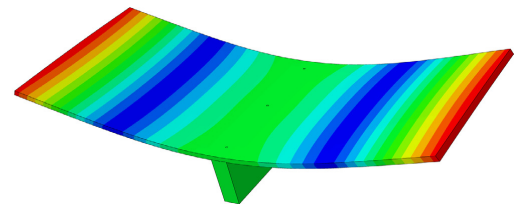

(b) 1st simulated mode: 35.9 Hz

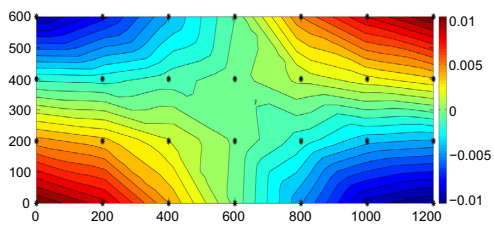

(c) 2nd measured mode: 50 Hz

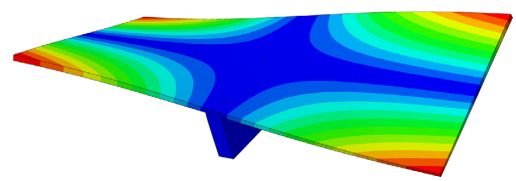

(d) 2nd simulated mode: 48.6 Hz

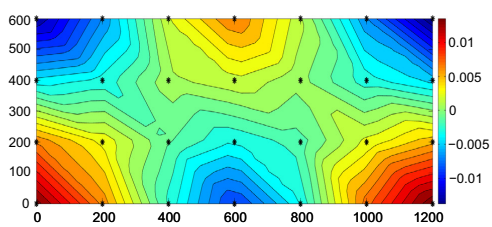

(e) 4th measured mode: 89 Hz

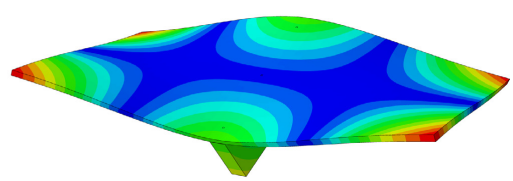

(f) 4th simulated mode: 89.3 Hz

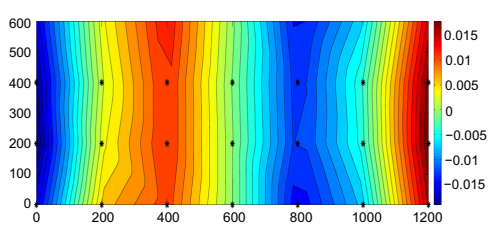

(g) 5th measured mode: 111 Hz

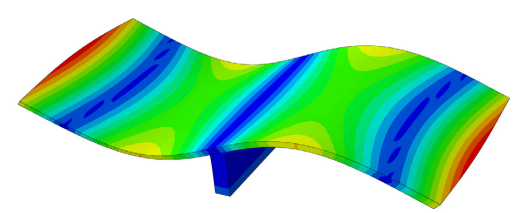

(h) 5th simulated mode: 109.4 Hz

Fig. 6. Measured (left column) and simulated (right column) vibration modes for the single-plate unglued case. The black crosses on the measured cases mark the placement of the accelerometers.

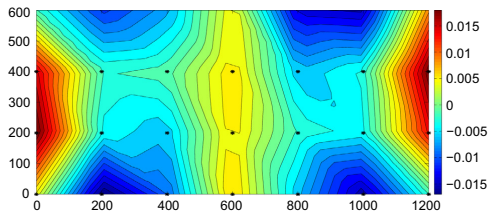

(i) 6^{th} measured mode: 179 Hz

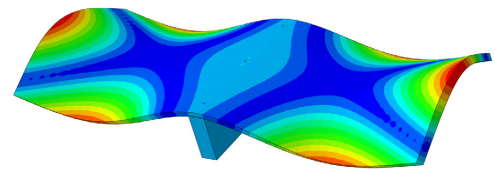

(j) 6^{th} simulated mode: 178.1 Hz

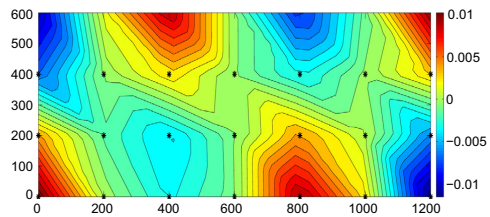

(k) 7^{th} measured mode: 178 Hz

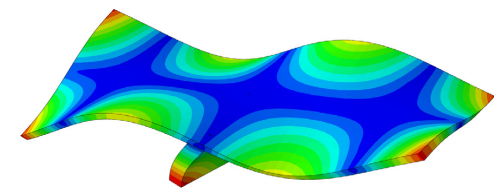

(l) 7^{th} simulated mode: 179.9 Hz

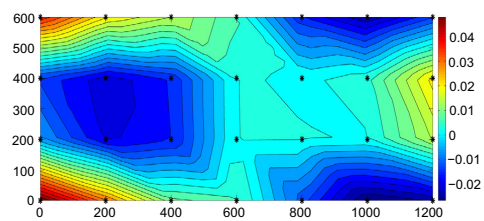

(m) 8^{th} measured mode: 190 Hz

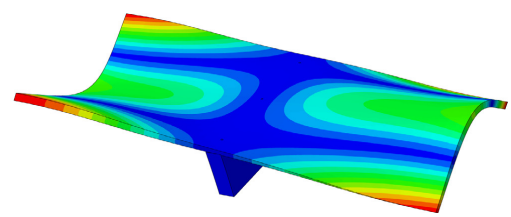

(n) 8^{th} simulated mode: 187.8 Hz

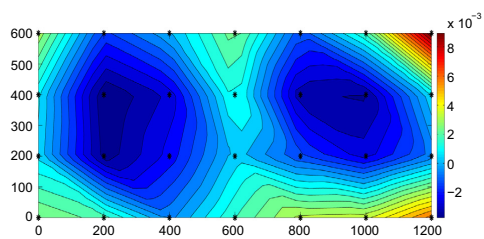

(o) 9^{th} measured mode: 198 Hz

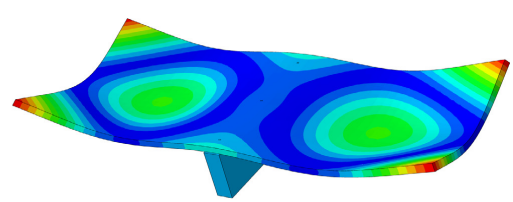

(p) 9^{th} simulated mode: 199.1 Hz

Fig. 6 (*continued*)

5.1.2.2. With glue. A model with a single plate and glue between the plate and the beam (cf. Fig. 5(b)) was assembled, the properties shown in Table 2 being assigned to the different materials. No screws were present here in the model that was considered as the reference one. The plate and the beam were fully fixed to the glue layer. Initially, the properties of the glue were varied, the properties for the chipboard and the wooden beam being maintained from the previous case. A good match between measurements and simulations was achieved, as shown in Table 1, for the glue properties used in Table 2 (those falling close to the ones provided by the manufacturer and also within realistic values for similar adhesives found in literature e.g. [24]). The degree of correlation between the measured and the simulated eigenmodes and eigenfrequencies was addressed with use of MAC- and NRFD-values respectively. In Fig. 8, the MAC-values comparing the simulated reference cases of the glued and the unglued single-plate junctions to measurements are shown. It is depicted that a good correlation between simulated and measured mode shapes is obtained for both cases. This, together with the NRFD shown in Fig. 7, where the errors between the measured and simulated case fall below 4.8%, proves the reliability of the predictive tool developed.

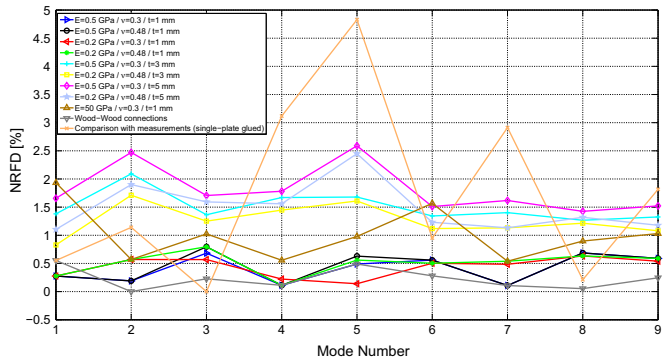

Fig. 7. NRFDs (with respect to the reference model) for the different simulated cases involved in the parametric study for the single-plate glued situation. Different parameters for the glued are investigated. A comparison between the simulated reference model and the corresponding measured case is also depicted.

A parametric study was then carried out for this single-plate glued case. As the material properties for the chipboard and the spruce beam were calibrated to match the measurements for the non-glued case, parameters related to the glue were modified here to check their influence in the dynamic behaviour of the junction. Its Young's modulus, its Poisson's ratio as well as the thickness of the horizontal layer involved (cf. Fig. 5(b)) were varied. The reference model which against all the modifications are compared with, is one comprised by a single plate on top of a beam, a thickness of the horizontal glue layer of 1 mm, no screws modelled and full tie interaction between the glue and the surfaces of the beam and the plate. In Table 3, the results of the parametric study are presented, those being summarised and presented graphically in Fig. 7 in terms of NRFDs. For the sake of brevity, not other MAC-plots than those shown in Fig. 8 are presented, although they were created and analysed for all the cases involved in the parametric studies to validate the FE models against measurements.

5.1.2.3. Discussion. From the measurements performed, it can be seen that the glue does not influence the mode shapes or the eigenfrequencies to a great extent in the case of a single-plate junction, just a slight stiffening effect of around 1% in terms of eigenfrequencies occurring. At the 5th mode (bending), however, the stiffening effect is particularly larger because the movement of the plate on top of the beam is constrained by the glue layer, as compared to the unglued case, where some motion of the plate is allowed on top of the beam except at those places where the screws are present. The latter will dictate differences when modelling the glued and unglued case, as different features will need to be taken into account when modelling the two connections.

Based on the parametric studies carried out, in Fig. 7 it can be observed that the parameters of the glue that were varied (Young's modulus, Poisson's ratio and thickness of the layer) do not affect results appreciably as the connections between different parts are considered fully fixed. The latter is evident if one compares the right column of Table 3 (where no glue layer is modelled) with any other. The fact of modelling the screws proved to have a negligible effect on the eigenmodes and eigenfrequencies of the structure, meaning that the punctual increase of stiffness brought into the junction by the steel screws is negligible in comparison to the stiffness of the connection between beam, plate and glue along the adhesive layer. Moreover, even though small differences can be observed in the eigenfrequencies, the NRFDs fall below 2.6% amid the modelled cases. Comparing the model used as reference to measurements, the NRFD peaks up at 4.8%. This means that for the problems considered here, assuming small amplitudes of vibrations, these types of junctions could be simplified by neither mod-

Table 3
Parametric study in terms of simulated eigenfrequencies for the single-plate case using glue. Glue parameters varied, namely its Young's modulus (E_{glue}), its Poisson's ratio (ν_g) and the thickness of the glue layer (t_{glue}). Also, the fact of modelling the screws in the connection and a comparison with a fully fixed wood-wood connection (i.e. neither glue nor screws involved) is presented.

Mode (Hz)	Reference										Wood-wood
	No screws	Screws									
	t_{glue} = 1 mm	t_{glue} = 1 mm					t_{glue} = 3 mm			t_{glue} = 5 mm	
	E_{glue} = 0.5 GPa	E_{glue} = 0.5 GPa		E_{glue} = 0.2 GPa		E_{glue} = 50 GPa	E_{glue} = 0.5 GPa	E_{glue} = 0.2 GPa	E_{glue} = 0.5 GPa	E_{glue} = 0.2 GPa	
	ν_g = 0.3	ν_g = 0.3	ν_g = 0.48	ν_g = 0.3	ν_g = 0.48	ν_g = 0.3	ν_g = 0.3	ν_g = 0.48	ν_g = 0.3	ν_g = 0.48	
1	36.2	36.3	36.3	36.3	36.3	36.9	36.7	36.5	36.8	36.6	36.0
2	52.6	52.5	52.5	52.3	52.3	52.9	53.7	53.5	53.9	53.6	52.6
3	87.9	88.5	88.6	88.4	88.6	88.8	89.1	89.0	89.4	89.3	87.7
4	89.8	89.7	89.7	89.6	89.7	90.3	91.3	91.1	91.4	91.2	89.7
5	142.9	143.6	143.8	143.1	143.7	144.3	145.3	145.2	146.6	146.4	142.2
6	178.7	179.7	179.7	179.6	179.6	181.5	181.1	180.7	181.4	180.9	178.2
7	185.4	185.2	185.2	184.5	184.4	186.4	188.0	187.5	188.4	187.5	185.2
8	189.4	190.7	190.7	190.6	190.6	191.4	191.8	191.7	192.1	191.9	189.3
9	203.7	204.9	204.9	204.8	204.9	205.8	206.4	205.9	206.8	206.1	203.2

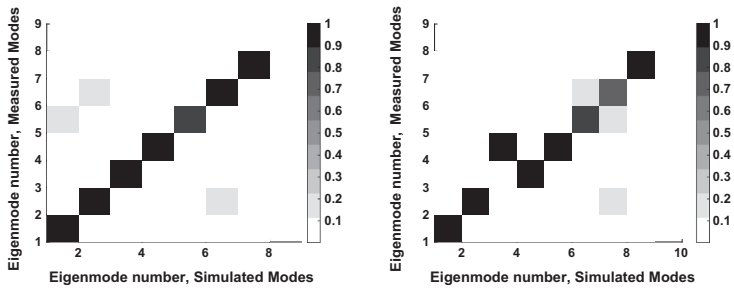

(a) Single-plate non-glued (b) Single-plate glued

Fig. 8. MAC-values for the single-plate case.

elling the screws nor the glue in detail, and instead using full interaction between the contact surfaces.

That is, for the glued case, the glue layer and the screws can be neglected as long as full interaction is considered along the interface between the beam and the plate. For the unglued case, small surfaces coincident with the screw's cross-section should be tied to the corresponding surfaces of the plates (no actual screws being needed). The errors obtained when considering such type of connection in the models were not larger than 2.6%. These errors would most likely be reduced further when the junctions are part of a larger structure due to restricted motion of the plate as compared to the cut-out T-junctions (i.e. different boundary conditions involved around the plates).

5.2. Dual-plate junction

In Table 4, the eigenfrequencies for the dual-plate T-junctions from experiments as well as for simulations, are shown. Details and discussions are described and given below.

5.2.1. Measurements

In Table 4, it can be observed that the fact of having glue between the two plates influences the dynamic performance of the junction. The non-glued case is, as expected, less stiff and the eigenfrequencies are, consequently, lower than for the glued case. This is distinct especially in the far low frequency range, which is, as stated in [1], the source of many complaints by residents in lightweight timber framed buildings. Thus, this is an issue that needs to be taken into account when developing FE prediction tools. Furthermore, it can be observed in Table 4 that the response of the glued case is practically identical to the single-plate glued case, the glue pulling the plates together and letting them behave as a single entity.

Table 4
Measured eigenfrequencies for the dual-plate T-junctions. Note the different amount of significant figures in the results, as the resolution of the measurements was 1 Hz.

Mode	Glue		No glue	
	Meas. (Hz)	FEM (Hz)	Meas. (Hz)	FEM (Hz)
1	36	36.1	17	13.2
2	52	52.3	48	49.3
3	85	88.6	50	51.5
4	91	89.4	75	76.8
5	147	144.0	120	117.8
6	176	178.9	134	134.9
7	179	184.9	177	177.9
8	187	190.6	185	188.1
9	195	204.1	188	189.4

5.2.2. Simulations

5.2.2.1. No glue. A model comprising a beam and two plates screwed on top of it was created as a reference one. The connections were made by tying the screws to all surfaces they are in contact with. No constraints were used between the plates or between the plates and the beam. With the properties listed in Table 2 being assigned to the different materials, the eigenfrequencies presented in Table 4 were obtained. Note that the first eigenfrequency differs 30% compared to the measurement results, which will later be improved (with the compromise of worsening other eigenfrequencies) by tweaking the steel properties. A reference model with no screws was also initially investigated, following the same procedure as for the single-plate case. In doing so, however, the plate is much softened and the eigenmodes differ appreciably from the measured ones (as it will be shown in the parametric study). Hence, screws were involved in the reference model for this case.

Parametric studies varying both the thickness of the air gap between the plates and the Young's modulus of the steel were performed. In Table 5, the results are presented, those being summarised graphically in Fig. 9 in terms of NRFDs calculated according to Eq. (3).

5.2.2.2. With glue. The reference FE model for the glued case, which was matched to measurements, involved two plates meeting on top of a beam and a 1 mm glue layer both on the horizontal surface between the beam and the plates as well as in the vertical layer between the two plates (cf. Fig. 5(d)). The initial properties assigned to the reference model are displayed in Table 2. The screws were not modelled in detail; instead all the parts were fully fixed to each other at all contact surfaces. The measured and simulated eigenfrequencies were well matched as it can be seen in Table 4.

The material properties for the chipboard and the spruce beam were assumed to be the same as for all other cases and parameters related to the glue were varied again here to check their influence on the dynamic behaviour of the junction. Its Young's modulus, its Poisson's ratio as well as the thickness of the vertical glue layer involved (cf. Fig. 5) were varied in a parametric study. As stated in Section 4.1, the plate and the beam were meshed using linear 8-node solid hexahedral elements with linear interpolation and reduced integration. In here, however, also 20-node solid hexahedral elements were tried, this case being denoted in the fourth column of Table 6 as "Q-NR". In addition, a calculation investigating the performance of a line connection between the glue and the wood as opposed to surface connections was included (denoted as "L-C" in Table 6). In Table 6, the results are presented, those being summarised graphically in Fig. 10 in terms of NRFDs calculated according to Eq. (3).

Table 5
Parametric study in terms of simulated eigenfrequencies for the unglued dual-plate case. The Young's modulus of the steel for the screws (E_{screws}) and the thickness of the gap between the two plates (t_{gap}) is varied. Also, a case where no screws are modelled is shown.

Mode (Hz)	Reference Screws	Screws			No screws
	t_{gap} = 1 mm E_{screws} = 2.1 GPa	t_{gap} = 3 mm E_{screws} = 2.1 GPa	t_{gap} = 0.25 mm E_{screws} = 2.1 GPa	t_{gap} = 1 mm E_{screws} = 5.1 GPa	t_{gap} = 1 mm
1	13.2	13.2	13.2	16.7	2.4
2	49.3	49.2	49.3	49.6	9.9
3	51.5	51.5	51.5	61.9	47.6
4	76.8	76.8	76.8	77.6	74.1
5	117.2	117.2	117.2	120.3	110.9
6	134.8	134.9	134.8	137.8	128.6
7	177.9	177.8	177.9	178.4	169.5
8	188.1	188.1	188.1	188.4	184.7
9	189.4	189.4	189.4	189.9	187.0

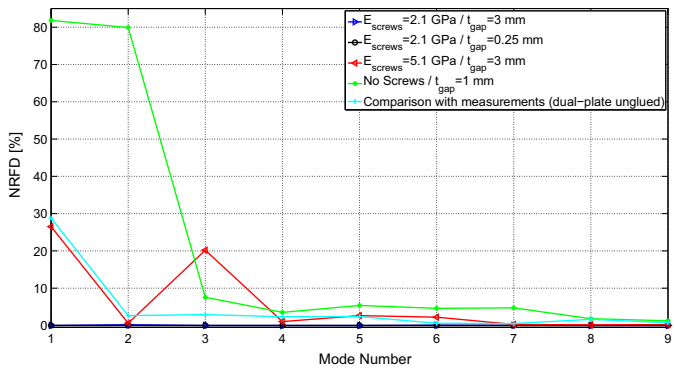

Fig. 9. NRFDs (with respect to the reference model) for the different simulated cases involved in the parametric study for the dual-plate unglued situation. Different parameters for the air gap between plates and the steel varied. A comparison between the simulated reference model and the corresponding measured case is also depicted.

Table 6
Parametric study evaluating the simulated eigenfrequencies for the double plate case using glue. Glue parameters varied, namely the Young's modulus (E_{glue}), the Poisson's ratio (ν_g) and the thickness of the vertical glue layer (t_{glue}). The horizontal glue layer between the beam and the plates is 1 mm in all cases. Also, the fact of varying the element type in the plate and beam from linear 8-node solid hexahedral elements to quadratic 20-node solid hexahedral elements (denoted as "Q-N" in the table), and the investigation of a line connection instead of surface connections (shown as as "L-C" in the table) are presented.

Mode (Hz)	Reference No screws	Screws					
	t_{glue} = 1 mm	t_{glue} = 1 mm					t_{glue} = 3 mm
	E_{glue} = 0.5 GPa	E_{glue} = 0.5 GPa			E_{glue} = 50 GPa	E_{glue} = 0.2 GPa	E_{glue} = 0.5 GPa
	ν_g = 0.3	ν_g = 0.3	ν_g = 0.3 (Q-NR)	ν_g = 0.3 (L-C)	ν_g = 0.3	ν_g = 0.48	ν_g = 0.3
1	36.1	36.0	36.6	27.8	37.0	36.1	35.5
2	52.3	52.6	52.9	49.4	52.9	52.2	52.4
3	88.6	89.5	90.7	62.4	89.0	89.3	89.2
4	89.4	89.2	90.1	83.5	90.3	89.3	88.8
5	144.0	147.4	148.6	116.8	145.0	146.9	146.9
6	178.9	178.8	181.6	156.1	181.5	179.1	177.4
7	184.9	185.1	187.0	180.2	186.4	184.0	184.6
8	190.6	190.9	193.6	188.1	191.1	190.7	190.8
9	204.1	204.6	207.2	192.7	207.1	204.3	202.7

5.2.2.3. Discussion. There is a substantial difference between the glued and unglued case. As a matter of fact, and considering the results in Table 4, both for the measurements and simulations, the dual-plate glued case exhibits strong resemblance with the single-plate cases, as the glue connects both plates together tightly, making them behave as one single entity. This latter comparison is displayed in Fig. 10. As well as for the single-plate case, the parametric studies carried out for the unglued case (varying the steel properties and the thickness of the gap between plates) and for the glued case (modifying the properties of the glue layer and type of elements) resulted in NFRDs lower than 5%. This means that the dual-plate glued case can be modelled as a single plate continuous over the bearing beam, considering full interaction between parts and no screws being included. For the unglued case, however, it is important that both plates are modelled and assembled using pins as screws, which will account for a realistic stiffness in the

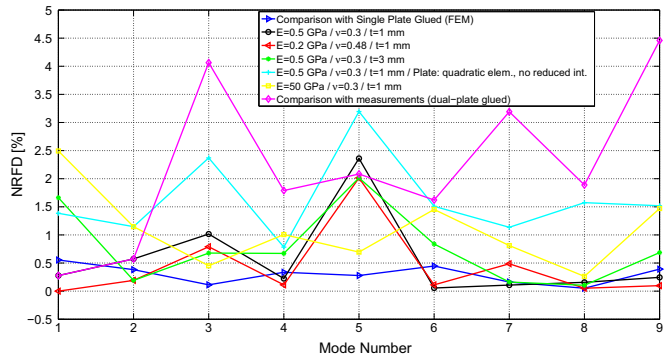

Fig. 10. NRFDs (with respect to the reference model) for the different simulated cases involved in the parametric study for the dual-plate glued situation. Different parameters for the glue, a different type of elements and connections, and a comparison with a single-plate glued case are shown. A comparison between the simulated reference model and the corresponding measured case is also depicted. Note that the case were line connections were investigated is not shown in the table so that the other analysed scenarios can be better distinguished due to the *y*-axis scale.

connection (see Fig. 9 where it is depicted that the two first modes are not well captured due to the junction being too soft if no screws are considered).

In addition, the influence of using another type of elements when meshing was proved to have a weak influence on the dynamic behaviour of the T-junction for the dual-plate case, its NFRDs exhibiting peaks of 3.2%. In contrast to the latter, a line connection between the structural parts instead of a surface connection does not realistically mimic the measurements performed, especially in those modes where there is much movement on top of the beam and therefore the surface is not constrained enough from being set into movement (i.e. the connection is softened, NRFDs amounting up to 30%). Surface connections should be used instead, those resembling also better the way glue is applied in practical situations.

6. Concluding remarks

In the paper, the influence of glue on the low frequency vibroacoustic performance of two types of wooden T-junctions, representing cut-outs of actual full size floor assemblies, was investigated via measurements. Furthermore, FE prediction tools, using the measurements as calibration input, were created so as to study modelling issues related to the connections. The conclusions drawn are:

It was observed that in the single-plate case, the glue had a negligible influence, except for a stiffening effect occurring at the 5th mode (bending). The slight differences observed in the other modes may be due to anisotropy of the spruce beam and its different properties among the different mock-ups.

Regarding the modelling, it can be concluded for the single-plate case that:

- The non-glued case can be modelled by tying the plate and the beam on discrete surfaces coincident with the cross-section of the screws. Modelling the actual screws had a negligible effect in the dynamic response of the junction.
- For the glued case, it was proven that the glue had an insignificant effect on the results. Modelling the actual screws as square pins going through the plate and into the beam did not improve the model either. Hence, this type of junction can be simplified by fully connecting the chipboard plate to the bearing wooden beam.

In the dual-plate, it was noticed via measurements that the glue plays an important role since it stiffens the junction by tying the plates together. As a matter of fact, the glued dual-plate case behaves similar to the single-plate glued case. The non-glued case is much softer and its eigenfrequencies therefore lower, especially below 150 Hz. Regarding the modelling, the following conclusions were drawn for the dual-plate case:

- It is important for the non-glued case that both plates are modelled and assembled using pins as screws, which will account for a realistic stiffness in the connection. By just tying discrete surfaces of the beam to the corresponding ones of the chipboard, as in the single-plate case, it results in a too soft connection.
- The glued case can be modelled as a single plate continuous over the bearing beam with a full connection between them, neither screws nor glue having to be modelled in detail.

The latter conclusions should be verified for junctions embedded in models of larger structures. It can be expected that the differences observed between different types of T-junctions would decrease in larger structures due to restricted deformations of the junctions compared to the free-free T-junctions, which would stiffen the structure. In the cases where it was concluded that screws had to be modelled in detail, techniques to simplify the fact of modelling the actual pins, like the introduction of a withdrawal modulus accounting for a smeared stiffness, could be adopted.

All in all, a deeper understanding about the vibroacoustical behaviour of these types of wood connections was gained, its enabling accurate and simplified FE models to be created when developing numerical prediction tools. These conclusions will ease the modelling and reduce the size of the models whilst still predicting the vibroacoustics behaviour accurately.

Acknowledgement

The research reported on here was funded by the Silent Timber Build project (WoodWisdom-Net). The authors very much appreciate the financial support provided.

References

[1] Ljunggren F, Simmons C, Hagberg K. Correlation between sound insulation and occupants' perception – proposal of alternative single number rating of impact sound. Appl Acoust 2014;85():57–68.

[2] International Organization for Standardization ISO 717-2. Acoustics – rating of sound insulation in buildings and of building elements – Part 2: impact sound insulation; 2013.

[3] Dickow KA, Kirkegaard PH, Andersen LV. An evaluation of test and physical uncertainty of measuring vibration in wooden junctions. In: Proceedings of ISMA 2012, Leuven, Belgium; 2012.

[4] Craik RJM, Smith RS. Sound transmission through lightweight parallel plates – Part II: structure borne sound. Appl Acoust 2000;61(2):247–69.

[5] Galbrun L. Vibration transmission through plate/beam structures typical of lightweight buildings: applicability and limitations of fundamental theories. Appl Acoust 2010;71:587–96.

[6] Bolmsvik Å, Linderholt A, Jarnerö K. FE modeling of a lightweight structure with different junctions. In: Proceedings of Euronoise 2012, Prague, Czech Republic; 2012.

[7] Bolmsvik Å, Brandt A. Damping assessment of light wooden assembly with and without damping material. Eng Struct 2013;49:434–47.

[8] Bolmsvik Å, Linderholt A, Brandt A, Ekevid T. FE modelling of light weight wooden assemblies – parameter study and comparison between analyses and experiments. Eng Struct 2014;73:125–42.

[9] Negreira J, Austrell P-E, Flodén O, Bard D. Characterisation of an elastomer for noise and vibration insulation in lightweight timber buildings. Build Acoust 2014;21(4):251–76.

[10] Thompson EG, Goodman JR, Vanderbilt MD. Finite element analysis of layered wood systems. J Struct Div 1975;101(12):2659–72.

[11] Jiang L, Hu L, Chui Y-H. Finite-element model for wood-based floors with lateral reinforcements. J Struct Eng 2004;130:1097–107.

[12] Tribaleau A, Tahani N, Brouard B, Génevaux J-M, Dazel O. Geometric simplification of a wooden building connector in dynamic finite element model. In: Proceedings of the acoustics 2012 Nantes conference, Nantes, France; 2012.

[13] Weckendorf J. Dynamic response of structural timber flooring systems. PhD thesis. Scotland (UK): The Centre for Timber Engineering, School of Engineering and the Built Environment, Edinburgh Napier University; 2009.

[14] Kohrmann M, Buchschmid M, Greim A, Müller G, Schanda U. Vibroacoustic characteristics of light-weighted slabs – Part 1: aspects of numerical modeling, model updating and parametric studies using the Buckingham π-theorem. In: Proceedings of 40th Italian (AIA) annual conference on acoustics and the 39th German annual conference on acoustics (DAGA), Merano, Italy; 2013.

[15] Dickow KA, Domadiya PG, Andersen L, Kirkegaard PH. Parameter study of coupling properties in finite element models of single-stud double-plate panels. In: Proceedings of internoise 2011, Osaka, Japan; 2011.

[16] International Organization for Standardization ISO 5348. Mechanical vibration and shock – mechanical mounting of accelerometers; 1998.

[17] Hopkins C. Sound insulation. 1st ed. Elsevier; 2007.

[18] International Organization for Standardization ISO 16063-21. Methods for the calibration of vibration and shock transducers – Part 21: vibration calibration by comparison to a reference transducer; 2003.

[19] Dassault Systèmes. Abaqus documentation. Version 6.12; 2012.

[20] Allemang RJ, Phillips AW. Techniques for evaluation of modal vector contamination. In: Proceedings of 32nd international modal analysis conference (IMAC XXXII), Orlando, FL; 2014.

[21] Nemli G, Demirel S. Relationship between the density profile and the technological properties of the particleboard composite. J Compos Mater 2007;41(15):1793–802.

[22] Wong E-D, Zhang M, Wang Q, Kawai S. Formation of the density profile and its effects on the properties of particleboard. Wood Sci Technol 1999;33:327–40.

[23] Wilczynski A, Kociszewski M. Determination of elastic constants of particleboard layers by compressing glued layer specimens. Wood Res 2011;56(1):77–92.

[24] Adams RD, Comyn J, Wake WC. Structural adhesive joints in engineering. 2nd ed. London: Chapman & Hall; 1997.

Paper E

ICA 2016 BUENOS AIRES
Buenos Aires – 5 to 9 September 2016
Acoustics for the 21st Century…
PROCEEDINGS of the 22nd International Congress on Acoustics

AA: Paper 132

Modelling of the tapping machine for finite element prediction tools – Preliminary parametric studies

Juan Negreira[(a)], Delphine Bard[(b)].

[(a)] Lund University, Sweden, juan.negreira@construction.lth.se
[(b)] Lund University, Sweden, delphine.bard@construction.lth.se

Abstract

Dissatisfaction of dwellers apropos acoustic comfort is a common problem often encountered in wooden multi-storey buildings. Such problems could be lessened by addressing vibroacoustic issues during the design phase of buildings if proper prediction tools were available for the engineer. Nevertheless, product development nowadays is still carried out in the aftermath of the construction based on engineers' experience and measurements performed on already existent buildings. The substitution of measurements by easy-to-use numerical predictive models, however, must take place only after those have proven to possess enough accuracy for the predictions carried out. The procedures to evaluate impact sound insulation performance, as described in the ISO 717-2, involve the use of a standardised excitation source: the tapping machine. Even though considerable research concerning the modelling of wooden floor structures (e.g. connections and material properties) has been carried out within recent years, few investigations have been conducted in a way aiming at characterising and modelling the excitation source, its hindering the development of models which could foresee and mimic results stemming from standardised measurements. The study reported on the paper aims at suggesting improvements of low frequency tools for purposes of prognosis by gaining insight about the modelling of the tapping machine. General simplified guidelines for its introduction into finite element commercial software were drawn. Ultimately, a prediction tool combining the knowledge stemming from the investigations performed will enable the determination of the standardised single number ratings obtained from measurements.

Keywords: finite element method; prediction tools; tapping machine; low frequency impact sound.

Paper F

Journal of Sound and Vibration 340 (2015) 383–408

Contents lists available at ScienceDirect

Journal of Sound and Vibration

journal homepage: www.elsevier.com/locate/jsvi

Psycho-vibratory evaluation of timber floors – Towards the determination of design indicators of vibration acceptability and vibration annoyance

J. Negreira [a,*], A. Trollé [a], K. Jarnerö [b], L.-G. Sjökvist [b], D. Bard [a]

[a] Lund University, Department of Construction Sciences, Division of Engineering Acoustics, P.O. Box 118, SE-221 00 Lund, Sweden
[b] SP Technical Research Institute of Sweden, Vidéum Science Park, SE-351 96 Växjö, Sweden

ARTICLE INFO

Article history:
Received 4 February 2014
Received in revised form
23 November 2014
Accepted 1 December 2014
Handling Editor: J. Macdonald
Available online 22 December 2014

ABSTRACT

In timber housing constructions, vibrations can be a nuisance for inhabitants. Notably, the vibrational response of wooden floor systems is an issue in need of being dealt with more adequately in the designing of such buildings. Studies addressing human response to vibrations are needed in order to be able to better estimate what level of vibrations in dwellings can be seen as acceptable. In the present study, measurements on five different wooden floors were performed in a laboratory environment at two locations in Sweden (*SP* in Växjö and *LU* in Lund). Acceleration measurements were carried out while a person either was walking on a particular floor or was seated in a chair placed there as the test leader was walking on the floor. These participants filled out a questionnaire regarding their perception and experiencing of the vibrations in question. Independently of the subjective tests, several static and dynamic characteristics of the floors were determined through measurements. The ultimate aim was to develop indicators of human response to floor vibrations, specifically those regarding vibration acceptability and vibration annoyance, their being drawn based on relationships between the questionnaire responses obtained and the parameter values determined on the basis of the measurements carried out. To that end, use was made of multilevel regression. Although the sample of floors tested was small, certain clear trends could be noted. The first eigenfrequency (calculated in accordance with Eurocode 5) and Hu and Chui's criterion (calculated from measured quantities) proved to be the best indicators of vibration annoyance, and the Maximum Transient Vibration Value (computed on the basis of the accelerations experienced by the test subjects) to be the best indicator of vibration acceptability.

1. Introduction

Timber floors have traditionally been designed with respect to their static load-carrying capacity and static stiffness when uniformly distributed loads are involved [1]. However, this criterion has proved to not be sufficient in regard to vibration serviceability for timber constructions, complaints by inhabitants there being frequent, even when present-day building code regulations are met [2].

* Corresponding author. Tel.: +46 462224884; fax: +46 462227619.
E-mail address: juan.negreira@construction.lth.se (J. Negreira).

http://dx.doi.org/10.1016/j.jsv.2014.12.001
0022-460X/

In 1994, Swedish building regulations authorised the construction of wooden multi-storey buildings. This led to an increasing demand for open planning in both residential and office buildings, involving use of long-span floor structures. Both strength and stiffness are high in relation to the weight for wood compared to other materials, making it possible to build very long spans, especially with use of glue-laminated (glulam) timber. However, slender floor constructions with long spans have low resonance frequencies that, in combination with low damping, are easily excited by human activities such as walking, running and jumping. Since humans are very sensitive to the vibrations thus produced, such floors are often regarded as annoying. Thus, obtaining adequate indicators of human response to vibrations in slender or lightweight structures dynamically excited by human activities is of considerable importance.

In the present work, in efforts to assess how floor vibrations are perceived under various conditions, psycho-vibratory tests on five different wooden prefabricated floors were carried out in a laboratory environment at two different locations in Sweden (Lund University – referred to here as *LU* – and the SP Technical Research Institute of Sweden – referred to as *SP*). The present study aims to find relationships between perceived vibrational discomfort and certain objective engineering parameters. More specifically, suitable indicators of vibration acceptability and vibration annoyance are suggested here, based on an analysis of outcomes (i.e. subjects' questionnaire responses and values of objective parameters). To do so, use was made of multilevel regression. Multilevel regression, not yet in wide use, was proved to be a suitable statistical method for modelling repeated measures data in which inter-individual differences in rating are substantial, just like in the present work.

2. Literature review

Extensive research in the area of human perception of whole-body vibration, and human response to such vibration has been carried out. Due to the complexity, sensitivity, subjectivity and variability of the human body, there are no clearly stated limits for acceptable vibration levels that are used in the design of buildings nowadays but simply certain guidelines that have been developed. For more information in this respect, see for example [3,4].

In the following, a literature review is presented. In relation to the current work, it focuses on two main topics: (i) human perception of structural vibrations and (ii) serviceability criteria to minimise annoying vibrations in floor systems, applicable to timber constructions nowadays.

2.1. Human perception of structural vibrations

Pioneering work in the field of human perception of vibration is that of Reiher and Meister [5], in which human sensitivity to vibrations was investigated. Ten test persons were exposed to vertical and to horizontal steady-state vibrations while standing or lying on a platform, the frequencies ranging from 5 to 100 Hz and the amplitudes from 0.01 mm to 10 mm. Subjects' reactions were classified and were labelled in categories extending from "barely perceptible" to "intolerable". The perception threshold was reached at a constant value of the product of amplitude (displacement) and frequency, and thus at a constant vibration velocity. A vibration perception scale was proposed on the basis of these findings. The scale was eventually modified in [6] to make it applicable as well to vibrations due to walking impact, being observed that for transient vibrations the main factor affecting human beings was that of damping, variations in amplitude and in frequency having little effect. It was suggested that if the amplitude scale is increased by a factor of ten the original Reiher–Meister scale can be seen as applicable to floor systems having less than 5 per cent critical damping.

In [7], transient vibrations from a single-frequency component were investigated. Forty persons standing on a floor were exposed to vertical vibrations created by a shaker of varying frequency, peak amplitude and damping. The vibrations involved were then rated on a 1–5 scale extending from "imperceptible" to "severe". Statistical analyses were carried out for identifying relationships between the response rate and various parameters, both for damped and undamped vibrations. These investigations showed the product of the frequency and the displacement to be constant and the transient vibrations of a given frequency and peak displacement to become progressively less perceptible as the damping was increased.

A vibration criterion for the degree of acceleration and damping appropriate for quiet human occupancies such as residential buildings and offices was developed in [8]. As the damping increases, the steady-state response produced by walking becomes a series of transient responses, resulting in a less significant response. A human perception scale for the degree of damping required was presented as a function of the product of initial displacement and the frequency in [9].

In [1], springiness and vibrations in timber floors and steel floors were investigated in a laboratory environment with use of subjective rating tests, 15 persons taking part. A rating of different timber test floors in comparison with a reference floor was also carried out. The tests on laboratory timber floors showed that both a reduction in the length of the span and the existence of a ceiling have a positive effect in terms of subjective judgements of the degree of vibration, but that the use of glue to fix the deck to the joists has little effect in this respect. It was also pointed out that the spacing between adjacent natural frequencies should be at least 5 Hz in order to prevent annoyance.

Field tests were carried out and vibration ratings were collected in [10]. Human perception was found to not be correlated with either peak acceleration, filtered peak acceleration, Root-Mean-Square (RMS) acceleration, the fundamental frequency or the product of the fundamental frequency and peak acceleration. In [11], it was reported that in terms of the subjective assessments made, none of the structural modifications investigated, except for a reduction in joist depth and an insert of rubber pads, resulted in any improvement in dynamic serviceability.

There are several standards concerning human perception of structural vibrations that are or have been employed, the two most prominent ones being the following.

The International Standard ISO 2631-1:1997 [4] provides guidelines on how to perform vibration measurements, what to report, and how to evaluate the results obtained, these guidelines being used to standardise reporting and to simplify comparisons. Although this standard is provided with three annexes containing suggestions, as well as current information on the possible effects of vibrations on health, comfort and perception, and motion sickness, it does not present any vibration exposure limits for whole-body vibrations.

The International Standard ISO 2631-2:1989 [12] was applicable to the evaluation of vibrations in buildings with respect to matters of comfort and annoyance of occupants. Tentative vibration serviceability limits were given in the form of base curves for the vibration magnitudes that cause approximately the same degree of annoyance. But this earlier version has been cancelled and been replaced with a newer edition, i.e. Standard ISO 2631-2:2003 [13]. In this edition, the base curves have been withdrawn; limit values are no longer stated. Instead, methods of measurement and evaluation concerned with whole-body vibrations in buildings have been suggested in order to encourage a uniform approach to the collection of data. A frequency weighting W_m (coincident with W_k as defined in [4]) is recommended for use, irrespective of the measurement posture of an occupant.

In [14], it was concluded that the frequency weighting of the Standard ISO 2631-2 [13] and the overall weighted amplitude obtained succeed well in describing the degree of annoyance felt regarding a single sinusoidal vibration, but that they are less accurate in regard to a vibratory signal involving a limited number of discrete frequencies. To overcome these difficulties, a prediction model was developed in which both the overall weighted amplitude and the fundamental frequency are taken account of [14].

2.2. Serviceability criteria to minimise annoying vibrations in floor systems

2.2.1. ISO 10137:2007

Standard ISO 10137:2007 [15] gives recommendations on the evaluation of vibration serviceability of buildings, and walkways within buildings or connecting them or outside of buildings. Recommendations on vibration are given in terms of Vibration Dose Values (VDV), which are based upon a root-mean-quad (RMQ) evaluation. Although VDV is seemingly a more reliable parameter in terms of correlation with human experiencing of vibrations [3], it does not have any physical meaning (its unit is $\mathrm{m\,s^{-1.75}}$). Its main advantage is that it considers the intermittency of the walking activity, and allows the response factor thresholds to be exceeded occasionally, which are dependent on the environment and on the time of day.

2.2.2. Criteria limiting point-load deflections

The earliest attempts to provide some degree of control over vibration problems in timber floors involved limiting the static deflection of joists under uniformly distributed load conditions so as to ensure the floor stiffness being sufficient [16]. For instance, the traditional $L/360$ deflection limit (L being the span of the floor) was in broad use for a considerable period of time. A numerical investigation performed in [17] led to an improved stiffness-based criterion for floor vibration serviceability, limiting the midspan deflection of the floor system to 1 mm for a point load of 1 kN, independently of the span. In [18], another stiffness-based criterion, incorporated into the National Building Code of Canada, was employed, requiring that the static deflection produced by a 1 kN load at midspan be limited to $8.0/L^{1.3}$, and also that it should not be greater than 2 mm for spans ranging from 3 to 6 m in length.

If the same traditional design criteria for deflection are employed, vibration serviceability is not guaranteed [19], thus paving the way for the development of criteria involving dynamic parameters.

2.2.3. Criteria limiting the frequency-weighted RMS acceleration

The guideline [20] was developed for steel–concrete floors. The RMS acceleration response for low-frequency floors (defined here as those with a fundamental frequency between 3 and 10 Hz) is calculated assuming a resonant response to one of the harmonics of the walking excitation, whereas the RMS acceleration response for the high-frequency floors (those whose fundamental frequency is greater than 10 Hz) is calculated, in turn, assuming that the floor has a transient response. Formulae for both cases are given as combinations of several parameters in [20]. Once $a_{w,\mathrm{RMS}}$ is obtained, the response factor is calculated, showing how many times the calculated RMS accelerations are greater than the threshold of feeling vibrations ($0.005\ \mathrm{m/s^2}$ according to the standard [4]). This value should not exceed the values of some multiplying factors given in the guideline for different usages. Should the response factor exceed the recommended multiplying factors, a method based on VDV, which takes account of the intermittency of the dynamic forces, should be checked instead.

Serviceability for in situ post-tensioned concrete long-span office floors under human-induced excitations is addressed in the technical report [21]. A method for calculating the dynamic response of such floors for various structural configurations is likewise presented in Appendix G. The formula for the response factor given in the guideline is based on the calculation of the total RMS acceleration of the floor due to a walking force alone (modelled with its harmonics up to the 13th following [1]). By including the harmonics, one ensures to completely excite the first resonant frequency of the floor. The floor response is calculated using a mode superposition technique, reducing the problem to the analysis of individual modes, i.e. a single-degree-of-freedom (SDOF) system for each harmonic. By summing all individual SDOF systems' responses in terms of sinusoidal peak acceleration responses (the dynamic characteristics of the floor, i.e.

eigenfrequencies and mode shapes being calculated according to the simplified rectangular plate method), the response factor is obtained with empirical formulae presented in the guideline. According to [22], however, the methods presented in [21] require a significant number of simplifications whose consequences are sometimes unreliable. The fact that the methods proposed in [21] oversimplify a very complex engineering problem should strengthen the development of more reliable design guidelines for such types of floors, the suggestion being that Appendix G should be withdrawn.

2.2.4. Criteria limiting point-load deflection, velocity due to a unit impulse, and RMS velocity

Criteria taking account of several modes of vibration as well as of modal damping, and limiting point-load deflection, velocity due to a unit impulse and RMS velocity, can be found in [1,23]. The development of these criteria was based on measurements of floors and subjective evaluation of their vibration performance, mainly in single-family houses. Three types of limits are to be noted: (i) the floor system needs to have a flexibility of no more than 1.5 mm/kN in the case of a concentrated load located at midspan; (ii) for floors with a fundamental frequency greater than one of 8 Hz, the values of the velocity due to a unit impulse ($h'_{\max}$) and of a damping coefficient ($\sigma_0 = f_1\zeta$ [Hz]) need to fall within a given region of the graph $h'_{\max} = f(\sigma_0)$ in order to ensure that the performance achieved will be acceptable [23]; and (iii) the RMS velocity for steady-state vibration needs to be less than tabulated values as given for similar floor systems that show acceptable vibration performance. Yet, values of this sort have never been available. Rather, the first two criteria, namely (i) and (ii), have provided the basis for the vibration serviceability criteria in Eurocode 5 [24].

2.2.5. Criteria limiting the fundamental frequency and the frequency-weighted RMS acceleration

The design criterion developed in [25] requires that the fundamental frequency of a floor be greater than 8 Hz, and that the frequency-weighted RMS acceleration obtained during the first second of vibration be less than 0.45 m/s^2 when loaded by a specific impulse. The first part of the criterion is determined by the stiffness and the mass of the floor system, whereas the second part is a function of its damping. Theoretically, therefore, it is necessary that the designer estimates the damping at the time that designing is carried out. Since doing this is virtually impossible, however, due to the damping of the timber floors varying considerably depending upon the construction type selected, and the techniques and workmanship employed, methods requiring that damping calculations be performed may not be practical for design engineers to utilise.

2.2.6. Criteria limiting the fundamental frequency

The investigation performed in [19] suggests that if the fundamental frequency of a floor is maintained above 15 Hz in the case of unoccupied floors, and above 14 Hz in the case of occupied floors, the furniture or whatever and the persons involved being included, acceptable levels of vibration will be obtained.

The work presented in [14] is in opposition to the latter reference, as it shows that human perception of vibration is strongly affected by the composition of the vibration signal in terms of the number of frequency components involved and their mutual amplitude relationships. Thus, in line with [14], it can be argued that the multiple natural frequencies inherent in a floor need to be taken account of in determining the design rules to be followed. This is in agreement with the criteria for design rules proposed in [1,26] (in which it is suggested that up to the 8th harmonic should be taken account of), contradicting many presently used floor design criteria that often rely on the fundamental frequency alone.

2.2.7. Criteria limiting the fundamental frequency and point-load deflection

In [27], rules for the design of floors with "high-" and with "low-" requirements and those with "no-" requirements, resulting in the fundamental frequency being maintained at above a level of 8 and of 6 Hz for "high-" and for "low-" requirement floors, respectively, were proposed. A stiffness criterion is also specified there, such that the deflection due to a static load of 2 kN, w, is to be less than the limit value w_{limit}, the size of which depends upon the requirements that apply to the floor in question.

Suggested criteria and limiting values for the classifying of floors into five different classes (A–E) are proposed in [28]. It was found there that the point-load deflection and the fundamental frequency are two of the best indicators of vibration performance in the case of lightweight floors.

2.2.8. Criteria limiting a combination of parameters

In [29], a new design method consisting of a vibration-controlled criterion and a calculation method for determining the criterion parameters were developed. The design criterion states that if the ratio (fundamental frequency)/(1 kN deflection)$^{0.44}$ of an unoccupied floor is larger than 18.7, the floor is most likely satisfactory for the occupants.

In [30], a guideline based on [31], the ratio of the peak acceleration achieved by walking to the force of gravity, expressed as a function of the fundamental frequency, the floor effective weight and the damping ratio, is used as a design guideline, its value depending upon the use of the building.

The guideline [32] concerns floors in office or residential buildings normally excited by people walking, which could affect the comfort of other building users. It gives guidance for (i) specification of tolerable vibration by the introduction of acceptance classes and (ii) prediction of floor response due to human-induced vibration with respect to the intended use of the building. Comfort requirements are specified in terms of one-step RMS values (OS-RMS), which correspond to the vibrations caused by one relevant step onto the floor. Since different factors (such as weight and speed of walking, shoes, and flooring) have an influence on the dynamic effect of people walking on a floor, the 90 per cent OS-RMS value (denoted

OS-RMS$_{90}$) is recommended as assessment value instead. This value is defined as the 90 per cent percentile of all the OS-RMS values obtained for a set of loads representing all possible combinations of persons' weights and walking speeds. After determining the basic dynamic floor characteristics as a first step, the OS-RMS$_{90}$ value is obtained with help of those OS-RMS values and a set of graphs relating the latter with modal mass, damping ratio and fundamental frequency. This value is then compared to recommended values for different floor usages.

2.2.9. Eurocode 5

The methods presented in [1,23] served as the basis for the vibrational serviceability criteria developed in Eurocode 5 [24]. Specifically, the design of timber structures is dealt with in EC5-1-1 and in the serviceability limit state design guidelines regarding floor-vibration performance. The design criteria are applicable to residential wood-based joist-type floors with a fundamental frequency greater than 8 Hz, in which the human sensitivity is related to the effects of the vibration amplitude and velocity caused by the dynamic footfall forces involved [33]. Three points must thus be checked on

- The fundamental frequency of the floor, f_1, should be at least 8 Hz in order for the floor to be regarded as a high-frequency one (otherwise a special investigation of it is needed), the requirement thus being that

$$f_1 \geq 8 \text{ Hz} \tag{1}$$

- Low-frequency effect (coming from step actions and dealt with a static criterion): the maximum instantaneous vertical deflection, w, due to a single force should be less than a deflection of a varying size a [24]:

$$\frac{w}{F} \leq a \ (\text{mm/kN}) \tag{2}$$

  where F is a vertical concentrated static force applied at the point of the floor that results in a maximum vertical deflection.
- High-frequency effect (consequence of heel impact actions that occur and handled by a dynamic criterion): the maximum initial value of the vertical floor vibration velocity, v, produced by an impulse of 1 N s, applied at the point on the floor giving the maximum response – where components above 40 Hz can be disregarded – should verify the inequality:

$$v \leq b^{(f_1 \zeta - 1)} \ (\text{m/N s}^2) \tag{3}$$

  where the dimension b is defined in [24] and ζ is the modal damping ratio (a value of 1 per cent is recommended in [24] unless some other value has been found to be more appropriate).

For more detailed information regarding Eurocode 5 calculations, see Section 4.1.3.

2.2.10. Design tools

Various numerical methods, the finite element method, for example, are often used as design tools nowadays for checking on the serviceability of floors of different types, in line with the development of commercial software solutions. Often highly versatile, they can enable floors to be very much improved and various criteria described above to be verified during the design phase. Examples of the use of such tools are to be found in [34–36].

3. Experiment: methods

3.1. The floors tested

In the present investigation, five separate floors, differing one from another but each of a type used frequently in residential buildings (the suppliers of each playing an active role in the Swedish construction market), were tested in a laboratory environment. Due to differences between them in the structural conceptions they embodied (box-floor-type, surface-floor-type), they can differ in design, in their dimensions and in various construction features. For each floor, Table 1 shows its labelling, manufacturer and design features. During the tests, each floor was simply supported on two sides by glulam beams having dimensions 90×180 mm^2. The glulam beams, in turn, were supported by studs at a centre-to-centre distance from one another of 600 mm. These studs were stabilised by use of plywood slabs, and they were bolted to the concrete floor of the laboratory. In attaching the floor elements to the supporting beams, the floor suppliers' instructions were followed.

3.2. Data collection

3.2.1. Non-subject-dependent measurements

Prior to the subjective psycho-vibratory testing, objective measurements for each of the five floors were performed in order to determine various static and dynamic parameters, e.g. subfloor and topfloor deflections, eigenfrequencies and

Table 1
Floor design, all sizes in (mm). For a description of the various engineered wood products involved, see e.g. [37].

Feature	Label				
	A	*B*	*C*	*D*	*E*
Manufacturer	Moelven Töreboda	Martinssons Byggsystem	Lindbäcks Bygg	Masonite Beams	Masonite Lättelement
Length	6800	8500	3700	7966	8100
Width	4800	4800	2400	4804	4848
No. elements	2 (2 × 2400)	4 (4 × 1200)	1	2 (2 × 2402)	2 (2 × 2424)
Flooring	–	–	13 mm gypsum boards	–	13 mm gypsum boards
Sheating	33 mm Kerto[a] Q511	73 mm CLT	22 mm chipboards	43 mm plyboard	43 mm plyboard
Beams	Web: Kerto S80	Web: Glulam C40	Web: Glulam	Web: Masonite beam	Masonite beam
	51 × 360 s587	42 × 220 s400	42 × 225 s600	HB 350 C24 s480	H300 C24 s585
	Flange: Kerto	Flange: Glulam	Flange: Plywood	Flange: 45 × 98	Flange: 45 × 45
	S16 45 × 300	C40 42 × 180	12 × 300		
Strutting	2 rows of beams			2 rows of Masonite beams	2 rows of Masonite beams
	Kerto S75 52 × 360 L_1=2392 L_2=4362	–	–	H350 K24 L_1=3079 L_2=6079	H300 K24 L_1=3079 L_2=6079
Junction (between floor elements)	WT-T screw 6.5 × 130 s300 every second from left and right element respectively	Plywood strip 12 × 160 P30 screwed with WFR 4 × 50 s125	–	Glued with	Overlapping plyboard screwed with 5 × 90 s300
				SikaBond-540 Chipped nails 34 × 45 s300	
Ceiling	–	–	–	2 × 13 mm gypsum board	13 mm gypsum board

[a] Commercial type of Laminated Veneer Lumber (LVL).

modal damping ratios. These parameters were used to classify the floors in terms of various criteria taken up in the literature review, use being made here both of methods proposed in Eurocode 5 [24], and of methods employed by Hu and Chui [29] and by Dolan et al. [19], as taken up in Section 4.1.3. The parameters assessed on the basis of these objective measurements were also used in the statistical analysis to determine which parameters were correlated most closely with vibration acceptability and with vibration annoyance (see Section 3.3.2).

Eigenfrequencies and damping ratios: Dynamic tests were carried out in order to measure the eigenfrequencies and damping ratios of the floors. Excitation was performed by use of a shaker driven by a pseudo-random signal, the strength of it being measured by a force transducer attached to the floor by a wood screw and to the shaker by a threaded rod. The vertical floor accelerations were measured by accelerometers located at ten separate points placed within one quadrant of the floor area.

For frequencies of up to 40 Hz, the eigenfrequencies, damping ratios ζ_i (per cent) and modal density, n_{40}, were extracted from the measured frequency response functions (FRFs) using the Matlab toolbox *VibraTools Suite* [38]: a poly-reference time domain method [39] was used for determining the poles and the modal participation factors, a least-squares frequency-domain method then being employed to fit estimates made to the measured data. Also, the impulse velocity response was calculated from the driving point mobility.

Subfloor deflection: To classify the floors in terms described by Hu and Chui [29] and in Eurocode 5 [24], the midspan deflection produced by a static point load of 1 kN was measured using the software *TracerDAQPro*. The measurement procedure was based on that proposed in [40].

The displacement gauge was fastened to a reference system consisting of a magnetic stand that was attached to a metal weight hung from an overhead crane. The loading was performed by a person weighing approximately 80 kg who stood with his feet straddling the measurement point, facing in the direction of the load-bearing beams. The deflection was

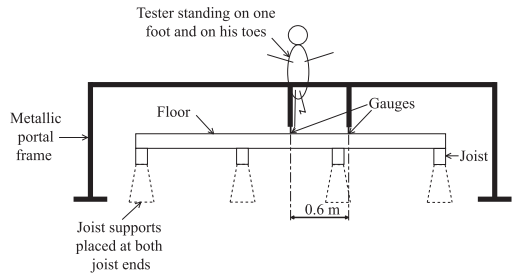

Fig. 1. Side view of the topfloor deflection measurement setup.

averaged from five measurements performed in the same way for each floor in order to ensure a good repeatability. The deflection produced by a 1 kN point load, $d_{1,m}$, was then obtained by extrapolation.

Topfloor deflection: The topfloor deflection, i.e. the deflection on the sheating of the floor, was measured using the same software. For each wooden floor, two displacement gauges were placed on its upper surface, the first one located at the midpoint of the floor and the second one placed 0.6 m from it (see Fig. 1). The gauges were fixed to a reference system consisting of a metallic portal frame (moved from one floor to another) that remained motionless during recordings.

The measurement procedure was based on that proposed in [28]. The midpoint was loaded by the tester's weight of approximately 80 kg. The displacement time histories were recorded by both gauges while the tester was standing on his toes of one foot in the middle of the floor (see Fig. 1). Three trials were carried out for each floor, in order to ensure a good repeatability. The maximum displacement recorded by the one gauge was subtracted from that recorded by the other, the resulting difference being extrapolated as proposed in [28] so as to obtain the topfloor deflection, $d_{2,m}$, produced by a 1 kN point load.

3.2.2. Subject-dependent measurements

Subject-dependent measurements were carried out both at *LU* and at *SP*. Sixty persons differing in age and gender (31 at *LU* and 29 at *SP*) participated in the tests. They performed the following tasks on each floor, the tasks at both locations being the same, the five floors being presented to each subject in random order:

- *Seated subtest*: the subject was first seated in a chair placed at the observation point (located 0.6 m from the midline of the floor, see Fig. 2), she or he gazing in the direction of the walking line. The experimenter walked along the walking line at a step velocity of about 2 Hz, back and forth between the two limits indicated by the solid horizontal lines in Fig. 2, his passing the observation point three times. Three accelerometers were used during the test, the first one placed on the floor between the feet of the subject, the second one placed under the chair seat, and the third one placed on the backrest of the chair (marked by crosses in Fig. 2). Although the acceleration would normally be measured on the upper surface of the seat [4], in this case it was placed beneath the seat so as to not create discomfort for the test person. A situation similar to this was investigated in [14], being shown there that the transmissibility, i.e. the gain between the one way of measuring and the other (under the seat versus on top of it), both types of measurements being performed by a seated person, was approximately 1.0, showing that this alternative also works properly.
- *Walking subtest*: after the seated subtest was completed, the chair was removed and the subject was asked to walk in a rather free manner along the walking line, between the two limits marked by the solid horizontal lines in Fig. 2. No other specific instruction was given to the subject concerning her or his way of walking. Five accelerometers were placed along the walking line to measure the floor vibrations (their locations being marked by crosses in Fig. 2).

After completion of each subtest for a given floor, the subjects were asked, as to describe, through filling in a questionnaire, their experience of the given floor in terms of various subjective attributes. The questionnaires used at *LU* and *SP* were not identical, the questionnaires for use in the two organisations having been developed separately, yet questions concerning certain matters of central interest – primarily matters of whether one is annoyed by vibrations and whether or not one considers the vibrations to be acceptable – were either exactly the same or rather similar in both cases, which led to a merging of the questionnaire answers of this character in reporting the results here. The reason behind this merging of results and the methods involved are presented in Section 3.3.1.

For the walking subtest at *LU*, the subjects were asked about vibration annoyance, vibration acceptability and springiness. For the seated subtest, the subjects were asked about noise annoyance, vibration annoyance and vibration acceptability. In particular, the vibration annoyance question was “Imagine that you live in a newly built multi-storey building equipped with this floor, you are seated on a chair and another person is walking by: what number from 0 to 10 best shows how much you are bothered, disturbed or annoyed by the floor vibrations?”. The response scale was an eleven-point numerical one, the numbers ranging from 0 to 10. Two labels, “not at all” and “extremely”, were attached to the respective ends of the scale, at 0 and 10. The vibration acceptability question was “Imagine that you live in a newly built

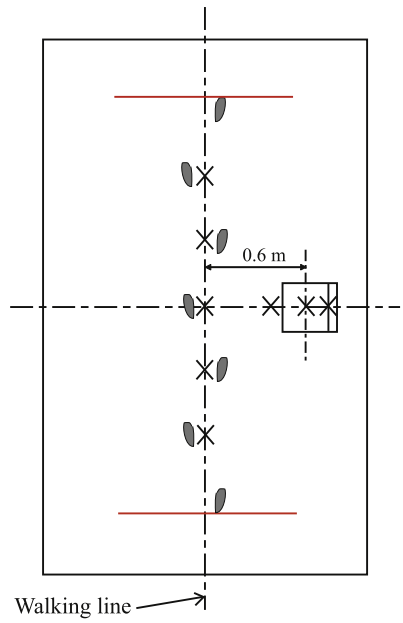

Fig. 2. Top view of the acceleration measurement setup. X: accelerometers. The ends of the walking line are marked by solid horizontal lines.

multi-storey building equipped with this floor, you are seated on a chair and another person is walking by: do you find the floor vibrations acceptable?". The two response alternatives were "Yes, acceptable" and "No, not acceptable". The questions and answers were available both in English and in Swedish.

For the walking subtest at *SP* the subjects were asked about springiness, vibration annoyance and vibration acceptability. They were also asked to describe in their own words their experiencing. For the seated subtest, the subjects were asked about noise annoyance, vibration annoyance and vibration acceptability. In particular, the vibration annoyance question was: "How do you experience the vibrations when I walk on the floor?". The response scale was a six-point verbal one, having the following alternatives: "not at all disturbing", "barely disturbing", "a little disturbing", "disturbing", "very disturbing", "extremely disturbing". The vibration acceptability question was: "Considering a newly built residential building: do you experience the vibrations that occur as?". The response scale was again a six-point verbal one, having the following alternatives: "definitely not acceptable", "not acceptable", "barely acceptable", "acceptable", "fully acceptable", and "definitely acceptable". The questions and answers were in Swedish, and are translated here to English. The subjects were also asked to describe in their own words their experiencing. Finally, the subjects were asked to rank the floors on a scale from the one they would prefer most to have at home to the one they would prefer least.

For each subtest and floor, the time histories of acceleration measured by the apropos accelerometers were recorded simultaneously during testing. The objective parameters extracted for each subject are presented below.

Overall frequency-weighted RMS accelerations: For each accelerometer, the frequency-weighted RMS acceleration, a_w, was computed (in the frequency range [1, 80] Hz) in accordance with Standard ISO 2631-1:1997 [4]. An overall frequency-weighted RMS acceleration was determined finally on the basis of the root-sum-of-squares of the frequency-weighted RMS accelerations as computed for the different accelerometers (see Standard ISO 2631-1:1997 [4], Section 8.2.3).

Overall frequency-weighted RMS velocities: In addition, for each accelerometer, velocity time histories were determined by integration on the basis of the acceleration time histories. The frequency-weighted RMS velocity, v_w, was computed (in the frequency range [1, 80] Hz) in accordance with Standard DIN 45669-1[41]. In the end, an overall frequency-weighted RMS velocity was determined from the root-sum-of-squares of the frequency-weighted RMS velocities computed for the different accelerometers.

Note that the frequency-weighted RMS values are highly dependent upon the time window for analysis. Accordingly, this time window needs be chosen carefully and be stated in connection with the results. In the present case, frequency-weighted RMS values were computed using a time window corresponding to only one of the three "walking lines" (a "walking line" is defined as one completed stroll along the floor in the one direction or the other). Thus, the periods of time in which the subject just stood on the floor, not creating any noticeable vibrations, or moved by simply turning around, were not taken into account in the computations. Had such periods of time been taken into account, the frequency-weighted RMS values could well have been markedly reduced.

Maximum transient vibration value: For each accelerometer, the Maximum Transient Vibration Value (MTVV) was computed in accordance with Standard ISO 2631-1:1997 [4]. A Matlab code was created here in order to calculate MTVV. With use of that code, the entire duration of the recording was swept over, a one-second window being employed. Each of the computed frequency-weighted accelerations was saved. The output produced, i.e. MTVV, is the "worst" (i.e. the maximum) of these accelerations. In the end, an overall MTVV was determined on the basis of the root-sum-of-squares of the MTVVs computed for the different accelerometers.

3.3. Joined analysis of subjective data and objective parameter values

3.3.1. Merging the subjective data

Of the rather many questions posed to the subjects either at the *SP* location or at the *LU* location, only two of them were considered to be equivalent in the sense that the subjects' answers to them at the two locations could be combined. These two questions, both posed for the seated subtest, concerned vibration annoyance and vibration acceptability, respectively (see Section 3.2.2). Since the two studies differed in the response scale used regarding both vibration annoyance and vibration acceptability, the issue arose of how to merge the subjective data coming from the two locations, at *SP* and *LU*.

For the vibration annoyance question, the responses from both data sources could be translated into scores ranging from 0 to 100. This translation procedure is based on the assumption that the different response categories available divide up the range extending from 0 to 100 into equally spaced intervals [42]. The general rule followed here for assigning a particular score on the 0–100 scale is that described by Passchier–Vermeer and Zeichart [43]:

$$\text{score}(0-100) = 100(i-\tfrac{1}{2})/m \tag{4}$$

where m is the number of categories ($m=6$ in the *SP* study, and $m=11$ in the *LU* study) and $i=1,\ldots, m$ is the rank number of a given category, starting with the lowest response category. After this translation, the scores ranging from 0 to 100 from both studies could be merged.

Regarding the vibration acceptability question, in the *SP* study the responses were translated into dichotomic responses in accordance with the following rules: the responses "definitely not acceptable" and "not acceptable" were transformed into the response "no, not acceptable", and the responses "barely acceptable", "acceptable", "fully acceptable" and "definitely acceptable" were transformed into the response "yes, acceptable". After this transformation, the dichotomic responses from both studies could be merged.

3.3.2. Statistical data analysis

The data analysis aimed at assessing relationships between the two subjective attributes (vibration annoyance and vibration acceptability) and the objective parameters involved, and at eventually finding a satisfactory indicator for each subjective attribute, that is, an objective parameter that best explains the subjective data. To this end, use was made of multilevel regression.

The large amount of non-subject-dependent objective parameters available made it impossible to determine by means of multilevel regression analysis the relationships between each and every one of these objective parameters, on one hand, and the subjective attributes, on the other. Thus, a preliminary analysis based on Principal Component Analysis (PCA) was carried out first, in order to select beforehand a small number of objective parameters that could best explain the subjective data.

Preliminary selection of relevant non-subject-dependent objective parameters: The merged vibration annoyance scores ranging from 0 to 100 were analysed using linear PCA, or more specifically the MDPREF model [44]. This model provides a multidimensional space in which the floors are represented by points and the subjects by unit vectors passing through the origin. These entities are located in such a way that the projections of the points on the vectors are in maximal agreement with the subjects' scores. A vector endpoint represents the point of maximum vibration annoyance of the subject in question. In order to identify the vibratory features of the floors able to affect vibration annoyance, the non-subject-dependent objective parameters were fitted into the space as non-normalised vectors, using a PREFMAP procedure [45]. An objective parameter vector then points in a direction such that the projections of the points on the vector are in maximum agreement with the values of the objective parameter. The length of the vector, which is equivalent to the linear correlation coefficient between the projections and the values of the objective parameter, indicates the quality of representation of the objective parameter in the space [46]. The non-subject-dependent objective parameters that were fitted are presented in Table 2. The values of most parameters, for each floor, are shown in Section 4.1.

The merged vibration acceptability responses were analysed using logistic PCA, a tool especially well suited for analysing binary data. More specifically, the model proposed by De Leeuw [47] was employed. Similarly, this model provides a multidimensional space consisting of a configuration of floor points and of subject vectors passing through the origin. For convenience sake, the subject vectors were normalised *a posteriori*. A vector endpoint represents the point of maximum acceptability for the subject in question. In order to identify the vibratory features of the floors that could affect vibration acceptability, the objective parameters were also fitted into the space as non-normalised vectors by use of a PREFMAP procedure. Again, all objective parameters shown in Table 2 were fitted.

Determination of an indicator of vibration annoyance and vibration acceptability: In efforts to find adequate indicators of vibration annoyance and of vibration acceptability, a regression analysis involving the vibration annoyance and acceptability

Table 2
List of non-subject-dependent objective parameters.

Symbol	Objective parameter
$d_{1,m}$	Measured subfloor deflection
$d_{1,c,\mathrm{EC5}}$	Calculated subfloor deflection, according to Eurocode 5
$d_{1,c,\mathrm{HC}}$	Calculated subfloor deflection, according to Hu and Chui
$d_{2,m}$	Measured topfloor deflection
$n_{40,m}$	Measured number of modes below 40 Hz
$n_{40,c,\mathrm{EC5}}$	Calculated number of modes below 40 Hz, according to Eurocode 5
$n_{40,c,\mathrm{FEM}}$	Calculated number of modes below 40 Hz, obtained by use of Finite Element (FE) simulations
$f_{1,c,\mathrm{EC5}}$	Calculated first eigenfrequency, according to Eurocode 5
$f_{1,c,\mathrm{FEM}}$	Calculated first eigenfrequency, obtained by use of FE simulations
$f_{1,c,\mathrm{HC}}$	Calculated first eigenfrequency, according to Hu and Chui
$f_{1,c,\mathrm{D}}$	Calculated first eigenfrequency, according to Dolan et al.
$f_{1,m,v}$	Measured first eigenfrequency in the *SP* study
v_m	Measured impulse velocity response
$v_{c,\mathrm{EC5}}$	Calculated impulse velocity response, according to Eurocode 5
ζ_1	Measured damping ratio for the first eigenmode
ζ_2	Measured damping ratio for the second eigenmode
m	Mass
$(\mathrm{EI})_l$	Longitudinal stiffness of the load-bearing beams
$(\mathrm{EI})_b$	Transverse stiffness of the load-bearing beams
$r_{\mathrm{HC},c}$	Hu and Chui's criterion, as calculated from the calculated quantities $f_{1,c,\mathrm{HC}}$ and $d_{1,c,\mathrm{HC}}$
$r_{\mathrm{HC},m}$	Hu and Chui's criterion, as calculated from the measured quantities $f_{1,c,v}$ and $d_{1,m}$

responses, on one hand, and the values of relevant appearing objective parameters, on the other, was carried out. More specifically, for analysing the repeated measures data[1] that were collected, use was made of multilevel regression models, within a Bayesian framework. This regression method has been used for meta-analysis of in situ noise annoyance studies earlier (see e.g. [42]); it has been sparsely used for modelling subjective data collected under laboratory conditions [48,49]. Multilevel regression has advantages over classical regression for the modelling of repeated measures data: (i) multilevel regression formulation complies strictly with the hierarchical structure of repeated measures data that consists of occasions (floors in our case) nested within individuals (test participants in our case); it thus takes account of the fact that the observations collected for an individual are not independent, and (ii) multilevel regression is a statistical method suitable for modelling subjective judgements which generally show inter-individual differences, just like in the present work (as will be shown in Section 4.2.1); these inter-individual differences can be taken into account through the multilevel formulation that involves both individual and occasion levels. For an introduction to multilevel regression models, the reader is referred to the textbooks [50,51].

Here, a two-level random-intercept-only model was first fitted to the subjective responses. This model provides a baseline for comparisons with models that include occasion-level predictors, for this reason being referred to henceforth as a "null" model.

Then, for each subjective attribute, objective parameters were inserted successively into two-level models as occasion-level predictors. For each objective parameter, two models, the one with a fixed regression slope and the other with a random regression slope, were tested. For each objective parameter, these two models were compared with the corresponding null model in order to check to what extent it could account for the subjective responses.

Finally, for each subjective attribute, the models of interest, each including an objective parameter thought to be able to account to some extent for the subjective responses, were compared with one another. These comparisons aimed at determining which indicator was best, this being the one provided by the model making it possible to best explain the subjective responses.

Model specification: A two-level random-intercept-only model (one that included no explanatory variable at the occasion level) was first fitted to the data in question. For the vibration annoyance data, this null model ($M0$) can be written as follows:

$$\begin{aligned} Y_{fi} &= (\beta_{00} + u_{0i}) + e_{fi} \\ u_{0i} &\sim N(0, \sigma^2_{u_0}) \quad \text{for } i = 1, \ldots, I \\ e_{fi} &\sim N(0, \sigma^2_e) \quad \text{for } i = 1, \ldots, I \text{ and } f = 1, \ldots, F \end{aligned} \tag{5}$$

[1] In the field of experimental psychology, repeated measures data stem from the application of a repeated measures design. This kind of design uses the same individuals (test participants in our case) with every condition (floor in our case) of the research.

where Y_{fi} is the vibration annoyance score obtained for floor f and participant i, F is the number of floors, I is the number of participants, β_{00} is the fixed intercept, the terms u_{0i} are (random) residual error terms (for the intercept) at the individual level, and e_{fi} are (random) residual error terms at the occasion level. The residual errors u_{0i} are assumed to have a mean of zero, and a variance $\sigma^2_{u_0}$ to be estimated. The residual errors e_{fi} are assumed to have a mean of zero, and a variance σ^2_e to be estimated.

For the vibration acceptability data (binary data), this null model ($M0$) can be written as follows:

$$\begin{aligned} \text{logit}(p_{fi}) &= \beta_{00} + u_{0i} \\ u_{0i} &\sim N(0, \sigma^2_{u_0}) \quad \text{for } i = 1, \ldots, I \end{aligned} \tag{6}$$

where p_{fi} is the probability that the binary response Y_{fi} obtained for floor f and participant i is equal to 1 (here 1="acceptable") and $\text{logit}(p_{fi}) = \log(p_{fi}/(1-p_{fi}))$.

Two-level models with a fixed regression slope were then tested. For the vibration annoyance data, these models can be written as follows:

$$\begin{aligned} Y_{fi} &= (\beta_{00} + u_{0i}) + \beta_{10} X_{fi} + e_{fi} \\ u_{0i} &\sim N(0, \sigma^2_{u_0}) \quad \text{for } i = 1, \ldots, I \\ e_{fi} &\sim N(0, \sigma^2_e) \quad \text{for } i = 1, \ldots, I \text{ and } f = 1, \ldots, F \end{aligned} \tag{7}$$

where β_{10} is the fixed slope, X_{fi} is the value of the occasion-level predictor (i.e. the objective parameter which is being tested) for floor f and participant i.

For the vibration acceptability data, these models can be written as follows:

$$\begin{aligned} \text{logit}(p_{fi}) &= (\beta_{00} + u_{0i}) + \beta_{10} X_{fi} \\ u_{0i} &\sim N(0, \sigma^2_{u_0}) \quad \text{for } i = 1, \ldots, I \end{aligned} \tag{8}$$

Finally, two-level models with a random regression slope were tested. For the vibration annoyance data, these models can be written as follows:

$$\begin{aligned} Y_{fi} &= (\beta_{00} + u_{0i}) + (\beta_{10} + u_{1i}) X_{fi} + e_{fi} \\ \begin{bmatrix} u_{0i} \\ u_{1i} \end{bmatrix} &\sim N\left(\mathbf{0}, \begin{bmatrix} \sigma^2_{u_0} & \sigma_{u_{01}} \\ \sigma_{u_{01}} & \sigma^2_{u_1} \end{bmatrix} \right) \quad \text{for } i = 1, \ldots, I \\ e_{fi} &\sim N(0, \sigma^2_e) \quad \text{for } i = 1, \ldots, I \text{ and } f = 1, \ldots, F \end{aligned} \tag{9}$$

where the terms u_{1i} are (random) residual error terms (for the slope) at the individual level. The residual errors u_{1i} are assumed to have a mean of zero, and a variance $\sigma^2_{u_1}$, which is to be estimated. The term $\sigma_{u_{01}}$ is the covariance between the residual error terms u_{0i} and u_{1i}.

For the vibration acceptability data, these models can be written as follows:

$$\begin{aligned} \text{logit}(p_{fi}) &= (\beta_{00} + u_{0i}) + (\beta_{10} + u_{1i}) X_{fi} \\ \begin{bmatrix} u_{0i} \\ u_{1i} \end{bmatrix} &\sim N\left(\mathbf{0}, \begin{bmatrix} \sigma^2_{u_0} & \sigma_{u_{01}} \\ \sigma_{u_{01}} & \sigma^2_{u_1} \end{bmatrix} \right) \quad \text{for } i = 1, \ldots, I \end{aligned} \tag{10}$$

Computation: Gamma distributions were used as non-informative prior distributions for the variance and the covariance parameters. The posterior distributions of the model parameters were computed using Markov Chain Monte Carlo simulations involving up to 40,000 iterations. These computations were performed using the Software MLwiN[Á] [52]. For each model parameter, a median value (i.e. a point estimate) and a 95 per cent credibility interval were determined from its posterior distribution.

Model comparison: The models were compared in terms of the following criteria:

- DIC – Deviance Information Criterion: This criterion provides a measure of out-of-sample predictive error [50]. This measure takes the degree of complexity of the model into account. The DIC values are not bounded; the lower DIC is, the better the predictive power of the model is assumed to be. In comparing two models, differences in DIC of more than 10 may definitely rule out the model having the higher DIC value, differences of between 5 and 10 being regarded as substantial [53]. For differences in DIC of less than 5, it can be misleading to simply report the model having the lower DIC value [53].
- R^2_1 – The proportion of variance explained at the measurement occasion level. It is computed for the vibration annoyance data. This criterion, which provides a measure of the goodness-of-fit of the model to the data, is defined as follows [50]:

$$R^2_1 = 1 - \frac{E(V(e_{fi}))}{V(Y_{fi})} \tag{11}$$

where V represents the finite-sample variance operator, the expectation $E()$ averages over the uncertainty in the fitted model (using the posterior simulations). The quantity R^2_1 varies between 0 and 1; the closer R^2_1 is to 1, the better the goodness-of-fit of the model to the data is.

- $\hat{\Delta}$ – The proportion of risk explained at the measurement occasion level. It is computed for the vibration acceptability data. This criterion provides a measure of the goodness-of-fit of the logistic model to the data. It is defined as follows [50,54]:

$$\hat{\Delta} = 1 - \frac{E\left(\frac{\sum_{i=1}^{I}\sum_{f=1}^{F}\hat{p}_{fi}(1-\hat{p}_{fi})}{I \times F}\right)}{p(1-p)} \tag{12}$$

where $\hat{p}_{fi}$ are the estimated probabilities that $Y_{fi} = 1$ (i.e. "acceptable"), the expectation $E()$ averages over the uncertainty in the fitted model (using the posterior simulations), p is the sample marginal probability that $Y_{fi} = 1$ (that is, p is given by the proportion of 1's occurring in the $I \times F$ binary responses). The quantity $\hat{\Delta}$ varies between 0 and 1; the closer $\hat{\Delta}$ is to 1, the better the goodness-of-fit of the logistic model to the data is.

Thus, for vibration annoyance, the model comparisons are based on two criteria: DIC and R_1^2. For vibration acceptability, the model comparisons are likewise based on two criteria, here DIC and $\hat{\Delta}$. A given model will only be considered to clearly outperform another model if it performs better in terms of both criteria.

4. Results and discussion

4.1. Analysis of objective data

4.1.1. Non-subject-dependent objective parameters

Eigenfrequencies and damping ratios: The eigenfrequencies and modal damping ratios up to 40 Hz were extracted (as described in Section 3.2.1), fairly close agreement of the *LU* and the *SP* results and good reproducibility of the measurements being obtained. It was thus concluded that the floors were mounted in a similar way at both locations, allowing the data to be used interchangeably, measurements at both locations thus theoretically providing basically the same results. The results obtained at *SP* are presented in Table 3.

Not surprisingly, floor *C*, with the shortest span, has the highest fundamental frequency, whereas floors *B*, *D* and *E*, with the longest spans, have the lowest fundamental frequencies. Also, floor *C* has the lowest value for n_{40}, whereas floors *B* and *D* have the highest values for n_{40}. In examining the modal damping ratios for the three first eigenmodes, one can note that floor *C* has the strongest damping properties, whereas floor *B* has the weakest damping properties.

Floor deflections: The subfloor deflection, $d_{1,m}$, and the topfloor deflection, $d_{2,m}$, were measured as described in Section 3.2.1. The results are shown in Table 4.

The deflection $d_{1,m}$ appears to covary with $d_{2,m}$, e.g. floor *A* (the rigidity of which is among the highest) has the lowest subfloor and topfloor deflections, whereas floor *B* has both the highest subfloor and topfloor deflections.

4.1.2. Subject-dependent objective parameters

The 2.5 per cent, 50 per cent and 97.5 per cent percentiles for a_w, v_w and MTVV for the seated subtest, for all floors and subjects, are given in Table 5. The parameter a_w appears to strongly covary with v_w and MTVV. Floors *A* and *C* have the lowest median values of a_w, v_w and MTVV, whereas floors *B*, *D* and *E* have the highest median values of a_w, v_w and MTVV. The dispersion of the a_w, v_w and MTVV values for each floor is large. This high degree of dispersion may have come about through the large differences in weight between the test participants (extending from 50.7 to 140 kg). Indeed, subjects differing appreciably in weight have been found to differ in the levels of acceleration and velocity of vibration they experience [3]. This dispersion may also be due to differences between subjects in their manner of walking.

Table 3
Measured eigenfrequencies in (Hz), modal damping ratios ζ_i in (%) and number of modes below 40 Hz (i.e. n_{40}). Within a cell, the eigenfrequency is displayed in the left lower part, whereas the modal damping ratio is shown in the right upper part.

Floor	Mode number											n_{40}
	1	2	3	4	5	6	7	8	9	10	11	
A	1.6 / 16.3	1.5 / 17.7	1.5 / 18.3	8.0 / 30.0	5.0 / 36.0	-	-	-	-	-	-	5
B	0.7 / 9.9	1.1 / 10.5	0.9 / 11.1	1.2 / 17.3	1.1 / 24.2	1.4 / 27.8	1.6 / 29.5	1.0 / 33.7	1.2 / 36.6	2.1 / 38.9	1.3 / 39.6	11
C	2.3 / 24.3	2.6 / 26.1	5.0 / 36	-	-	-	-	-	-	-	-	3
D	1.8 / 8.8	2.1 / 9.9	2.2 / 14.0	2.0 / 22.7	2.0 / 24	1.5 / 28.3	1.6 / 31.7	2.0 / 37	-	-	-	8
E	1.1 / 8.2	1.8 / 12.0	3.5 / 20.2	2.6 / 25.9	3.2 / 28.4	4.0 / 34.1	-	-	-	-	-	6

Table 4
Measured subfloor deflection $d_{1,m}$ and topfloor deflection $d_{2,m}$, produced by a 1 kN load.

Floor	*A*	*B*	*C*	*D*	*E*
$d_{1,m}$ (mm/kN)	0.260	0.660	0.560	0.530	0.440
$d_{2,m}$ (mm/kN)	0.101	0.529	0.335	0.320	0.230

Table 5
Percentiles of frequency-weighted parameters for each floor, in the seated subtest.

Parameter	Percentile	Floor				
		A	*B*	*C*	*D*	*E*
a_w (m/s^2)	0.025	0.001	0.003	0.001	0.003	0.003
	0.50	0.012	0.054	0.021	0.055	0.063
	0.975	0.026	0.144	0.041	0.116	0.116
v_w (m/s)	0.025	0.00004	0.00010	0.00005	0.00009	0.00010
	0.50	0.00030	0.00140	0.00060	0.00140	0.00160
	0.975	0.00070	0.00341	0.00110	0.00320	0.00331
MTVV (m/s^2)	0.025	0.004	0.011	0.003	0.012	0.009
	0.50	0.034	0.150	0.058	0.151	0.163
	0.975	0.054	0.291	0.091	0.242	0.292

4.1.3. Classification of the floors

Floor classification according to Eurocode 5: The degree to which the design guidelines given in Eurocode 5 [24] (see Section 2.2.9) were met was also investigated, for the calculated data, in line with instructions given in [33]. The calculations were carried out under the assumption that the floor was unloaded, i.e. that only the weight of the floor and other permanent actions need to be taken into account. For the individual materials of the floor structures, the mean values for the modulus of elasticity involved were employed, these being provided by the material suppliers. In calculating the flexural rigidity in the span direction, $(EI)_l$, composite action between the floor sheating and the floor joists was assumed to occur on each floor. In calculating the corresponding flexural rigidity in the cross-joist direction $(EI)_b$, however, only the contribution from the floor sheating was taken into account. The fact of not considering the positive effect of strutting between joists when calculating $(EI)_b$ means that the rigidity of the floors *A*, *D* and *E* is underestimated somewhat, since two rows of strutting are present in each of them. On the basis of the results of laboratory tests, the rotational rigidity $(EI)_T$ was assumed to be equal to $(EI)_l/500$ in the finite element (FE) analysis and hand calculations.

For a rectangular floor having overall dimensions of $L \times B$, simply supported along two or all four edges and having timber beams with span of L, the fundamental frequency f_1 can be calculated in an approximate manner with Eq. (4.46) given in [33].

For floors having a fundamental frequency of more than 8 Hz (this is the case for all of the floors under study here), the requirements to be satisfied are the following:

- *Low-frequency effects*: the requirement given in Eq. (2) needs to be met. The deflection produced by a point load of 1 kN, w, given in (mm), as calculated using Eq. (4.49) in [33], must not exceed the limit, a, given for each country in the National Annex. In the Swedish National Annex, the deflection limit a is equal to 1.5 mm, no consideration being taken of the floor span.
  In calculating the deflection produced by a point load, w, account is taken of only a single joist. The effect of load sharing between joists is taken account of by use of a reduction factor k_{dist} (see Eq. (4.50) in [33]).
- *High-frequency effects*: when an impulse force of 1 (N s) is applied to the centre of the floor in a manner simulating heel impact, the unit impulse velocity response v needs to comply with Eq. (3), the value of v being given by Eq. (4.54) in [33], and the value of b being set to 100 in the Swedish National Annex.

For purposes of verification, the eigenfrequencies up to 40 Hz were also calculated for each floor using the Matlab FE toolbox *Calfem* [55]. For the sake of brevity, these calculations are not presented here.

A summary of the calculations and requirements, as stated in [24] for the five floors studied, is presented in Table 6. All of the requirements are fulfilled for each floor.

It should be pointed out that there is still concern regarding the accuracy both of the proposed damping ratios ζ_i and of the procedures for calculating n_{40}. This also raises serious doubts regarding the accuracy of the simplified procedures used for calculating the impulse velocity response v. Specifically, it is stated in [36] that the current EC5-1-1 design criteria do not

Table 6
Calculations in terms of Eurocode 5 [24].

Floor	f_1 (Hz)	Low frequency effects			High frequency effects					Requirements		
		k_{dist}	w (mm)	a (mm)	n_{40}	v (mm/N s^2)	v_{limit} (mm/N s^2)	b	ζ(%)	$f_1 > 8$ Hz	$w/F \le a$	$v \le b^{(f_1\zeta-1)}$
A	23.5	0.396	0.167	1.5	7	8.54	29.18	100	1	✓	✓	✓
B	12.0	0.300	0.501	1.5	3	3.18	17.36	100	1	✓	✓	✓
C	23.5	0.300	0.498	1.5	4	19.19	29.57	100	1	✓	✓	✓
D	11.5	0.488	0.730	1.5	5	6.39	16.97	100	1	✓	✓	✓
E	11.0	0.300	0.593	1.5	5	6.12	16.58	100	1	✓	✓	✓

Table 7
Classification of the floors according to Hu and Chui [29] and Dolan et al. [19]. The subindex *m* denotes measured values whereas *c* indicates calculated values; *HC* stands for Hu and Chui and *D* for Dolan.

Floor	Hu and Chui [29]								Dolan et al. [19]			Acceptability rate (%)
	$f_{1,m}$ (Hz)	$d_{1,m}$ (mm)	$f_{1,c,HC}$ (Hz)	$d_{1,c,HC}$ (mm)	$r_{HC,m}$	$r_{HC,c}$	$r_{HC,m} > 18.7$	$r_{HC,c} > 18.7$	$f_{1,c,D}$ (Hz)	$f_{1,m} > 15$ Hz	$f_{1,c,D} > 15$ Hz	
A	16.3	0.26	23.3	0.29	29.5	40.1	✓	✓	15.9	✓	✓	56.7
B	9.9	0.66	12.6	0.28	11.9	22.3	×	✓	6.1	×	×	30.0
C	24.3	0.56	23.7	0.89	31.4	24.7	✓	✓	21.9	✓	✓	58.3
D	8.8	0.53	11.6	0.61	11.6	14.5	×	×	2.9	×	×	35.0
E	8.2	0.44	11.1	0.62	11.8	13.7	×	×	2.2	×	×	25.0

adequately address issues concerning the dynamic response of timber flooring systems and their associated vibrational problems. Reconsideration of the design criteria is thus called for.

Floor classification according to Hu and Chui: The criterion for floor vibration acceptability proposed in [29] states, regarding unoccupied floors, that if the ratio of the fundamental frequency, f_1, to the deflection due to a 1 kN point load, d_1, expressed as $r_{HC} = [f_1/d_1^{0.44}]$, is larger than 18.7, the floors are most likely satisfactory for occupants. In such a case, the criterion has been evaluated both with use of the measured first eigenfrequency and deflection as well as with use of the first eigenfrequency and deflection, as assessed on the basis of calculations.

The formulae used in the design method employed are based on the ribbed-plate theory. The floor stiffness parameters should then be calculated taking account of the semi-rigid connections between the joist and the sheating, of the torsional rigidity of the joists and of the sheating stiffness in both the span and the across-joist directions. In addition, performance-enhancement-related construction details such as between-joist bridging, strong-back and strapping, are accounted for in the formulae presented in [29]. The deflection $d_{1,c,HC}$, in (mm), due to a static point load P of 1 kN at the centre of the floor was calculated using Eq. (1) given in [29]. The fundamental frequency $f_{1,c,HC}$, in (Hz), of a floor system was, in turn, calculated here using Eq. (2) given in [29]. Table 7 presents the results for the classification of the floors. In that table, the acceptability rate is the percentage of the participants who considered the vibrations as acceptable. A value of 50 per cent of acceptability can be considered as the threshold for a floor being acceptable [28].

Albeit the criterion computed from the calculated data fails to correctly describe the vibration acceptability for floor *B*, the criterion does accurately portray the vibration acceptability for the measured data. The mismatch for floor *B* may be due to the fact that it has a high cross-joist rigidity, due to the thick cross-laminated timber (CLT) plate and the fact that the model proposed in [29] assumes lower cross-joist rigidity.

The supporting method used for the floors in the laboratory during the tests is obviously not resembling the one taking place in a real building. The latter can be one of the reasons for which the acceptability rates shown in Table 7 are lower than those who could be beforehand expected, since those floors are supposedly good enough to be installed in real constructions. This does not disrupt, nevertheless, the results presented in this investigation, as the answers given by the participants are in accordance with the measured objective dynamic properties of the floors (i.e. both were obtained with the floor structures supported in the same fashion). Another reason for the acceptability rates being low could be the fact that the laboratory environment does not exactly mimic the environment of a conventional apartment, the participants feeling probably less comfortable during testing.

Floor classification according to Dolan et al.: The design criterion presented in [19] states that if the stiffness of the floors is sufficient to maintain the fundamental frequency of the floor system at a level above 15 Hz for unoccupied floors, and above 14 Hz for occupied floors (i.e. including furniture and/or persons), an acceptable level of vibration will be obtained. The fundamental frequency, f_1, of the joists and the girders alone can be estimated using Eq. (1) given in [19]. If the floor system includes joists and girders, the fundamental frequency can be estimated using the Dunkerly equation [19].

This criterion is simple to use and restricts only the stiffness of a floor system relative to its weight. Damping is not included since it cannot be effectively estimated or controlled by the designer, and if the level of damping is high, this

improves the vibration performance of the system. The criterion involved also ignores any composite action between the joists and the sheating which if present would improve performance and be effective at the low displacement amplitudes associated with vibrations. Both of these concerns have been investigated experimentally and been discussed in [19]. The results for each of the five floors can be seen in Table 7.

The criterion based on both the measured and the calculated fundamental frequencies appears to predict the subjects' acceptability. Despite this, it is our belief that the failure of the formulae involved to take account of composite actions between parts when the bending stiffness is calculated can lead to results being too conservative in predictions made on the basis of these calculations.

4.1.4. Discussion

For each floor, the degree to which the requirements proposed by Eurocode 5 [24] met was checked. Each floor met the requirements as stated in EC5-1-1. This is not very surprising, however, since Eurocode 5 regulates the structural design of construction work carried out in the European Union and the five floors studied were ones of a type used in real buildings. Also, the requirements stated in EC5-1-1 were drawn up on the basis of measurements and subjective ratings made in lightweight timber houses, which happens to be our working scenario.

In addition, in considering the value of 50 per cent of acceptability (i.e. half of the participants considering the floor vibrations to be acceptable) as the threshold for a floor being "acceptable", it was found that the Hu and Chui [29] criterion works well for the measured data here, since it matches the acceptability results for all of the floors under study. A match with the calculated data, however, fails for floor *B*, since the degree of acceptability for subjects cannot be predicted there. This is probably due to the assumption in the analytical formulae proposed that the connections between joists and sheating be semi-rigid, whereas floor *B* has rigid connections and a high level of across-joist rigidity due to the thick CLT layer on the surface of it.

The applicability of Dolan et al.'s criterion [19] was examined. It was observed that these guidelines could be applied and that they worked properly with the use of the measured data for each of the five floors included in the study. Nonetheless, although the criteria worked properly as well for the calculated data, the fact that the composite action that occurs is not accounted of in the formulae proposed for use there means that the calculations underestimate the fundamental frequency, which could lead to the results obtained being unrealistically conservative.

4.2. Joined analysis of subjective data and objective parameter values

The results reported in Sections 4.2.2 and 4.2.3 are obtained from the analysis of the merged data by use of the methods presented in Section 3.3.2. Beforehand, the raw subjective data are examined in Section 4.2.1.

4.2.1. Inspection of the raw subjective data

Fig. 3 shows the individual vibration annoyance scores (between 0 and 100) and box plots, for the five floors. One can observe that all the interquartile ranges have an important size, which shows that the differences in vibration annoyance score between the subjects are large for all the floors. Thus, carrying out a classical regression analysis between the mean annoyance scores computed for the five floors, on one hand, and the values of relevant objective parameters measured or calculated for the five floors, on the other hand, is not recommended. In fact, the mean annoyance scores are meaningless here, since for each floor, the dispersion of the individual annoyance scores around the mean annoyance score is large, implying that the mean score is not representative of the individual scores, and thus individual scores must be considered by themselves instead. This clearly legitimises the use of multilevel regression for drawing up relationships between vibration annoyance and relevant objective parameters (see Section 3.3.2).

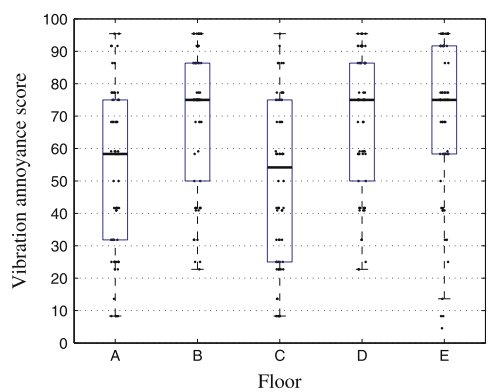

Fig. 3. Individual vibration annoyance scores (between 0 and 100) and box plots, for the five floors. ·: individual scores; ▬: median; ——: first and third quartiles; and -: extreme values.

Fig. 4 shows the distribution of the binary vibration acceptability responses (i.e. "No, not acceptable" and "Yes, acceptable"), for the five floors. One can observe that, for each floor, "No, not acceptable" and "Yes, acceptable" responses are both present, which clearly reveals substantial inter-individual differences in vibration acceptability judgement for all the floors. Once again, this supports the use of multilevel regression for drawing up relationships between vibration acceptability and relevant objective parameters (see Section 3.3.2).

4.2.2. Preliminary selection of relevant non-subject-dependent objective parameters

Vibration annoyance data: The vibration annoyance data could be represented in a 2-D MDPREF space. The two first dimensions were found to account for 73 per cent of the total variance. The optimal dimensionality was selected by use of the Scree test method [56], applied to the plot of the eigenvalues against the number of dimensions. The space is shown in Fig. 5. For greater readability, only the endpoints of the subject vectors are reported there. The labels that begin with "V" designate subjects from the *SP* study, and those beginning with "L" subjects from the *LU* study (for the sake of clarity, not all labels are shown).

Most of the endpoints of the subject vectors lie within the left-hand part of the space. This shows there a relatively close consensus among the subjects in terms of their responses. The average subject vector (marked in Fig. 5 by a black circle),

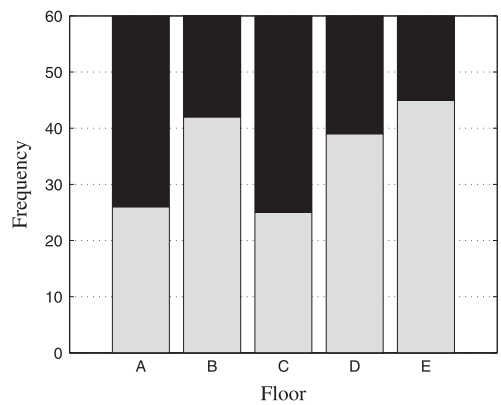

Fig. 4. Distribution of the binary vibration acceptability responses (i.e. "No, not acceptable" and "Yes, acceptable"), for the five floors. In grey: "No, not acceptable" responses; in black: "Yes, acceptable" responses.

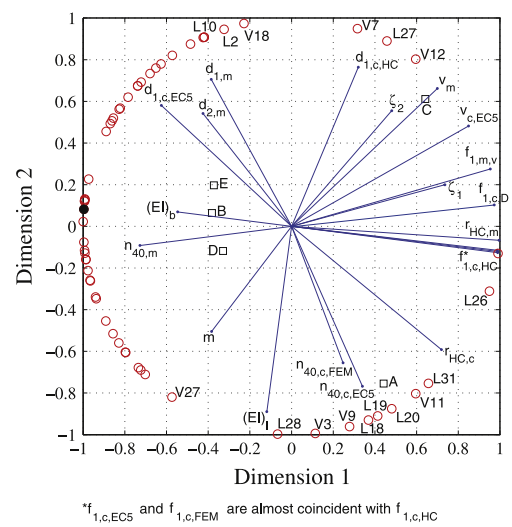

Fig. 5. Vibration annoyance data – 2-D MDPREF space. □: floors; ○: endpoints of the subject vectors; ●: endpoint of the average subject vector; and —: objective parameter vectors.

which appears in the left-hand part of the space, nearly coincides with the first dimension, indicating that consensus is basically found regarding this dimension of the space (its accounting for 50 per cent of the total variance). Nevertheless, some endpoints are to be found elsewhere, notably in the upper and lower right-hand parts of the space. One can also note that the subject vectors in both studies are well mixed, there thus appearing to be no study effect on the vibration annoyance responses.

The $\mathbf{f}_{1,c,EC5}$, $\mathbf{f}_{1,c,FEM}$ and $\mathbf{f}_{1,c,HC}$ vectors, which appear in the right-hand part of the space, are very close in position to the average subject vector. Their length (close to the unit) shows there a very high quality of representation ($r=0.997$, $p=0.001$, $r=0.997$, $p=0.001$, and $r=0.994$, $p=0.003$, respectively). Also, the $\mathbf{f}_{1,m,v}$ and $\mathbf{f}_{1,c,D}$ vectors, which appear in the right-hand part of the space, are likewise close in position to the average subject vector, although to a lesser extent. Their length reveals a very high quality of representation ($r=0.993$, $p=0.004$ and $r=0.981$, $p=0.015$, respectively). All in all, the first eigenfrequency is able, on the average, to explain the subjects' responses rather well. The higher the first eigenfrequency is, the lower on the average the level of vibration annoyance is. In addition, the $\mathbf{r}_{HC,m}$ vector, which appears in the right-hand part of the space, is close in position to the average subject vector. Its length indicates a very high quality of representation ($r=0.998$, $p=0.001$). These various observations show that Hu and Chui's criterion (calculated from measured quantities) can explain the subjects' responses on the average rather well. The higher this criterion is, the lower on the average the level of vibration annoyance is. The ζ_1 vector, finally, which appears in the right-hand part of the space, is close to the average subject vector, yet its somewhat shorter length indicates a lower quality of representation ($r=0.763$, $p=0.323$), this objective parameter thus being correlated to a lesser degree with the average response.

Vibration acceptability data: The vibration acceptability data were represented in a 2-D space. The space is shown in Fig. 6; for greater readability, only the endpoints of the subject vectors are reported there. Again, the labels beginning with "V" designate subjects from the *SP* study, and those beginning with "L" subjects from the *LU* study.

Most of the endpoints of the subject vectors lie within the upper right-hand, lower right-hand and left-hand parts of the space. This dispersion shows the subjects' vibration acceptability responses to be less consensual than their vibration annoyance responses are. The average subject vector (marked by a black circle in Fig. 6) appears in the lower right-hand part of the space. One can note too that the subject vectors in both studies are quite well mixed, no study effect on the vibration acceptability responses being evident, therefore.

The ζ_1 vector, which appears in the lower right-hand part of the space, is very close in position to the average subject vector. Its length shows a moderate quality of representation ($r=0.890$, $p=0.146$). These observations show that the damping ratio for the first eigenmode appears to be able to explain the subjects' responses on the average here rather well. The higher the value of ζ_1 is, the greater on the average vibration acceptability is assumed to be. The $\mathbf{f}_{1,m,v}$, $\mathbf{f}_{1,c,EC5}$, $\mathbf{f}_{1,c,FEM}$, $\mathbf{f}_{1,c,HC}$ and $\mathbf{f}_{1,c,D}$ vectors, which appear in the lower left-hand part of the space, are less close in position to the average subject vector. Their length indicates them to have a high quality of representation ($r=0.952$, $p=0.053$, $r=0.986$, $p=0.01$, $r=0.986$, $p=0.01$, $r=0.982$, $p=0.014$, and $r=0.965$, $p=0.034$, respectively). These observations show that the first eigenfrequency can on the average explain the subjects' responses rather well. The higher the first eigenfrequency is, the greater on the average the vibration acceptability is assumed to be. In addition, the $\mathbf{r}_{HC,m}$ vector, which appears in the lower left-hand part of the space, is as close in position to the average subject vector. Its length shows a very high quality of

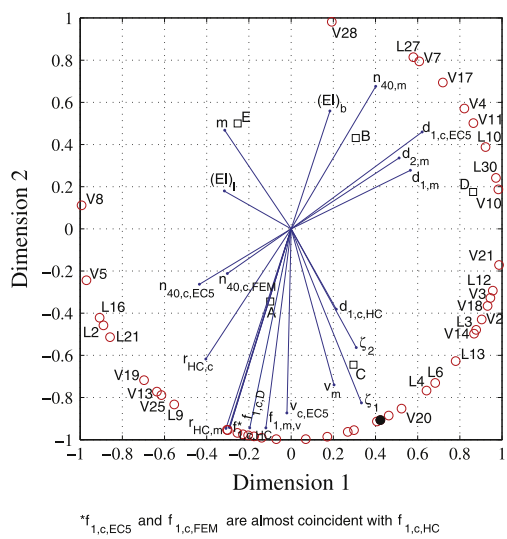

*$f_{1,c,EC5}$ and $f_{1,c,FEM}$ are almost coincident with $f_{1,c,HC}$

Fig. 6. Vibration acceptability data – 2-D logistic PCA space. □: floors; ○: endpoints of the subject vectors; ●: endpoint of the average subject vector; and —: objective parameter vectors.

representation ($r=0.998$, $p=0.001$). This indicates that Hu and Chui's criterion (calculated from measured quantities) can explain the subjects' responses on the average rather well. The higher this criterion is, the greater on the average the vibration acceptability is assumed to be.

Discussion: The PCA results showed there to be several non-subject-dependent objective parameters that can explain the subjective data rather well.

Regarding vibration annoyance, the linear PCA results showed $f_{1,c,EC5}$, $f_{1,c,FEM}$, $f_{1,c,HC}$ and $r_{HC,m}$ to be the most relevant parameters for explaining, on the average, the subjects' responses. Regarding the first eigenfrequency, it appears as though any one of the three parameters $f_{1,c,EC5}$, $f_{1,c,FEM}$ and $f_{1,c,HC}$ could be selected, since each of them seems equally relevant, although $f_{1,c,EC5}$ was finally selected due its widespread use and the ease of the calculations it involves. Although ζ_1 appeared to be correlated with the average response to a lesser extent, this design parameter seemed to possibly also be relevant in accounting for the subjects' responses, thus being selected as well, and $r_{HC,m}$ finally being selected too.

Regarding vibration acceptability, the logistic PCA results showed $f_{1,m,v}$, $f_{1,c,EC5}$, $f_{1,c,FEM}$, $f_{1,c,HC}$, $f_{1,c,D}$, ζ_1 and $r_{HC,m}$ to be the parameters most relevant in accounting for the subjects' responses, on the average. As far as the first eigenfrequency is concerned, any one of the five parameters that were tested could have been selected, since these appeared to be about equally relevant, yet $f_{1,c,EC5}$ was selected finally, in order to be consistent with the choice made regarding vibration annoyance, $r_{HC,m}$, and ζ_1 being selected as well.

4.2.3. Determination of indicators of vibration annoyance and vibration acceptability

All the objective parameters tested are presented in Table 8.

Vibration annoyance data: Figs. 7 and 8 show the differences in DIC and in R^2_1, respectively, between the null model *M*0 (taken as a reference model) and the models involving occasion-level predictors.

Models involving non-subject-dependent parameters: Including $f_{1,c,EC5}$ or $r_{HC,m}$ in a model as an occasion-level predictor with a fixed slope enables the model's goodness-of-fit and out-of-sample predictive power to be improved (in both cases, $\Delta R^2_1 = 2.5$ per cent and $\Delta DIC \ll -10$ as compared with the null model *M*0). Employing a fixed-slope model involving $f_{1,c,EC5}$ or $r_{HC,m}$ is thus found to outperform the null model. Making the slope random then enables the model's goodness-of-fit and out-of-sample predictive power to be improved ($\Delta R^2_1 = 6.3$ per cent and $\Delta R^2_1 = 6.6$ per cent, respectively for $f_{1,c,EC5}$ and

Table 8
Objective parameters tested for vibration annoyance and vibration acceptability.

Type of objective parameters	Objective parameter
Non subject-dependent parameters	Calculated first eigenfrequency, obtained in accordance with Eurocode 5 ($f_{1,c,EC5}$) Hu and Chui's criterion ($r_{HC,m}$) Damping ratio for the first eigenmode (ζ_1)
Subject-dependent parameters	Frequency-weighted RMS acceleration (a_w) Frequency-weighted RMS velocity (v_w) Maximum Transient Vibration Value (MTVV)

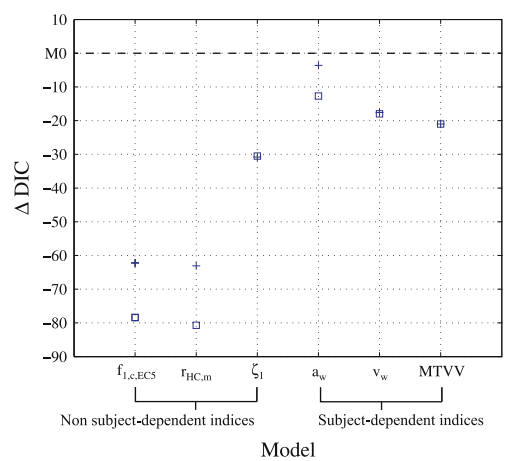

Fig. 7. Vibration annoyance – differences in DIC (ΔDIC) between null model *M*0, and the models involving occasion-level predictors. +: fixed-slope model; and □: random-slope model.

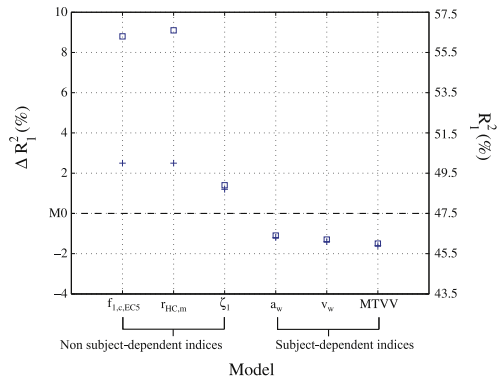

Fig. 8. Vibration annoyance – differences in R_1^2 (ΔR_1^2) between null model *M*0, and the models involving occasion-level predictors. +: fixed-slope model; and □: random-slope model.

$r_{HC,m}$, and $\Delta DIC < -10$ in both cases, as compared with the fixed-slope model). In regard to both criteria, therefore, the random-slope model involving $f_{1,c,EC5}$ or $r_{HC,m}$ is the one to select. It should also be emphasised that, for both parameters, 98 per cent of the random slopes (the median values of these) are negative. Thus, for nearly all of the subjects, vibration annoyance is negatively correlated with $f_{1,c,EC5}$ and $r_{HC,m}$, so that the lower $f_{1,c,EC5}$ and $r_{HC,m}$ are, the greater the vibration annoyance is. Thus, there is rather close consensus among the subjects in terms of the effect of $f_{1,c,EC5}$ or $r_{HC,m}$ on vibration annoyance. Accordingly, the model just described appears to definitely be the one to select. Moreover, one can note that a random-slope model involving $r_{HC,m}$ appears to perform as well as a random-slope model involving $f_{1,c,EC5}$ does ($\Delta R_1^2 = 0.3$ per cent and $\Delta DIC > -5$). It appears, therefore, that $r_{HC,m}$ and $f_{1,c,EC5}$ are about equally good indicators of vibration annoyance.

Inserting ζ_1 into the model as an occasion-level predictor with a fixed slope tends to improve the model's goodness-of-fit ($\Delta R_1^2 = 2.5$ per cent in comparison with the null model *M*0) and makes it possible to improve its out-of-sample predictive power ($\Delta DIC \ll -10$ as compared with the null model *M*0). Making the slope random does not serve to further improve the goodness-of-fit or the out-of-sample predictive power of the model, however ($\Delta R_1^2 = 0.2$ per cent and $\Delta DIC > 0$ in comparison with the fixed-slope model). Thus, a random-slope model containing ζ_1 does not outperform a fixed-slope model containing ζ_1. All in all, in making use of the fixed-slope model, ζ_1 appears to be an adequate indicator of vibration annoyance.

Finally, one can note that the random-slope models involving $f_{1,c,EC5}$ or $r_{HC,m}$ clearly outperform the fixed-slope model involving ζ_1, in terms both of goodness-of-fit and of out-of-sample predictive power (at least $\Delta R_1^2 = 7.6$ per cent and $\Delta DIC \ll -10$). Thus, $f_{1,c,EC5}$ and $r_{HC,m}$ appear to be better than ζ_1 as indicators of vibration annoyance.

Models involving subject-dependent parameters: Including a_w in a model as an occasion-level predictor with a fixed slope does not serve to improve the model's goodness-of-fit or its out-of-sample predictive power ($\Delta R_1^2 = -1.2$ per cent and $\Delta DIC > -5$ as compared with the null model *M*0). A fixed-slope model involving a_w thus does not outperform the null model. Including a_w in the model as an occasion-level predictor with a random slope enables the model's out-of-sample predictive power to be improved ($\Delta DIC < -10$ in comparison with the null model *M*0), but it does not serve to improve its goodness-of-fit ($\Delta R_1^2 = -1.1$ per cent in comparison with the null model *M*0). Thus, a random-slope model does not clearly outperform the null model. Therefore, the models involving a_w do not clearly outperform the null model, a_w thus not being an indicator of vibration annoyance.

Including v_w or MTVV in a model as an occasion-level predictor with a fixed slope enables the model's out-of-sample predictive power to be improved (in both cases $\Delta DIC < -10$, as compared with the null model *M*0), but it does not serve to improve its goodness-of-fit ($\Delta R_1^2 = -1.4$ per cent and $\Delta R_1^2 = -1.6$ per cent, respectively for v_w and MTVV, in comparison with the null model *M*0). Thus, the fixed-slope model involving v_w or MTVV appears to not clearly outperform the null model. Also, although including v_w or MTVV in a model as an occasion-level predictor with a random slope enables the model's out-of-sample predictive power to be improved (in both cases $\Delta DIC < -10$, as compared with the null model *M*0), it does not serve to improve its goodness-of-fit ($\Delta R_1^2 = -1.3$ per cent and $\Delta R_1^2 = -1.5$ per cent, respectively for v_w and MTVV, in comparison with the null model *M*0). Therefore, a random-slope model involving v_w or MTVV does not clearly outperform the null model. The models involving v_w or MTVV appear to not clearly outperform the null model, v_w and MTVV thus not being indicators of vibration annoyance.

Synthesis: Of the non-subject-dependent parameters that were tested, $f_{1,c,EC5}$ and $r_{HC,m}$ were found to be the best indicators of vibration annoyance. The multilevel models based on these parameters are shown in Table 9. None of the subject-dependent parameters that were tested appeared to be a good indicator of vibration annoyance.

Vibration acceptability data: Figs. 9 and 10 show the differences in DIC and in $\hat{\Delta}$, respectively, between the null model *M*0 (taken as a reference model) and the models involving occasion-level predictors.

Table 9
Vibration annoyance – random-slope models involving $f_{1,c,EC5}$ and $r_{HC,m}$ as occasion-level explanatory variables. 95% CI: 95% Bayesian credibility interval; β_{00}: fixed intercept; β_{10}: fixed slope; σ_e^2: variance of the residual errors at the occasion level; $\sigma_{u_0}^2$: variance of the residual errors u_0 (for the intercept) at the individual level; $\sigma_{u_1}^2$: variance of the residual errors u_1 (for the slope) at the individual level; DIC: Deviance Information Criterion; R_1^2: proportion of variance explained at the occasion level. The covariance between residual errors u_0 and u_1 at the individual level is not shown.

Objective parameter	$f_{1,c,EC5}$	$r_{HC,m}$
	Coefficient (95% CI)	Coefficient (95% CI)
Fixed part		
β_{00}	83.27 (75.19; 91.33)	78.06 (71.12; 84.90)
β_{10}	−1.35 (−1.77; −0.940)	−0.872 (−1.14; −0.603)
Random part		
σ_e^2	270.4 (220.6; 333.8)	267.8 (218.3; 330.3)
$\sigma_{u_0}^2$	517.7 (249.5; 964.0)	415.9 (219.8; 742.8)
$\sigma_{u_1}^2$	0.945 (0.333; 2.09)	0.400 (0.144; 0.870)
DIC	2562.8	2560.5
R_1^2	0.563	0.566

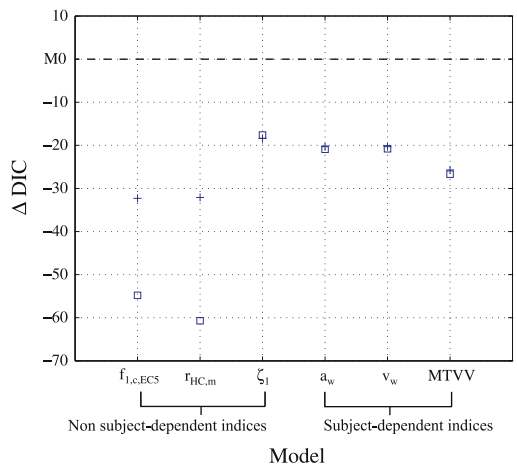

Fig. 9. Vibration acceptability – differences in DIC (ΔDIC) between null model *M*0, and the models involving occasion-level predictors. +: fixed-slope model; and □: random-slope model.

Models involving non-subject-dependent parameters: Including $f_{1,c,EC5}$ or $r_{HC,m}$ in a model as an occasion-level predictor with a fixed slope enables the model's goodness-of-fit and out-of-sample predictive power to be improved ($\Delta\hat{\Delta} = 10.5$ per cent and $\Delta\hat{\Delta} = 10.4$ per cent, respectively for $f_{1,c,EC5}$ and $r_{HC,m}$, in both cases $\Delta DIC \ll -10$, as compared with the null model *M*0). Thus, the fixed-slope model involving $f_{1,c,EC5}$ or $r_{HC,m}$ outperforms the null model. Making the slope random enables the model's goodness-of-fit and out-of-sample predictive power to be further improved ($\Delta\hat{\Delta} = 21.2$ per cent and $\Delta\hat{\Delta} = 23$ per cent, respectively for $f_{1,c,EC5}$ and $r_{HC,m}$, in both cases $\Delta DIC \ll -10$, as compared with the corresponding fixed-slope model). Although in terms of these two criteria the random-slope models involving $f_{1,c,EC5}$ or $r_{HC,m}$ should be selected, there is a serious problem connected with use of these models, namely that 75 per cent and 69 per cent of the random slopes (the median values of these) are positive, respectively for $f_{1,c,EC5}$ and $r_{HC,m}$, and 25 per cent and 31 per cent negative, respectively for $f_{1,c,EC5}$ and $r_{HC,m}$. Thus, for some subjects, vibration acceptability is positively correlated with $f_{1,c,EC5}$ or $r_{HC,m}$, whereas for others vibration acceptability is negatively correlated with them. The subjects thus differ regarding the effect that $f_{1,c,EC5}$ and $r_{HC,m}$ have on vibration acceptability. These models should thus not be selected here. All in all, $f_{1,c,EC5}$ and $r_{HC,m}$ are not found to be suitable as indicators of vibration acceptability.

Including ζ_1 in the model as an occasion-level predictor with a fixed slope enables the model's goodness-of-fit and out-of-sample predictive power to be improved ($\Delta\hat{\Delta} = 6.4$ per cent and $\Delta DIC \ll -10$ as compared with the null model *M*0). A fixed-slope model involving ζ_1 thus outperforms the null model. Making the slope random enables the goodness-of-fit to be improved slightly ($\Delta\hat{\Delta} = 3.4$ per cent as compared with the fixed-slope model) but does not help the out-of-sample

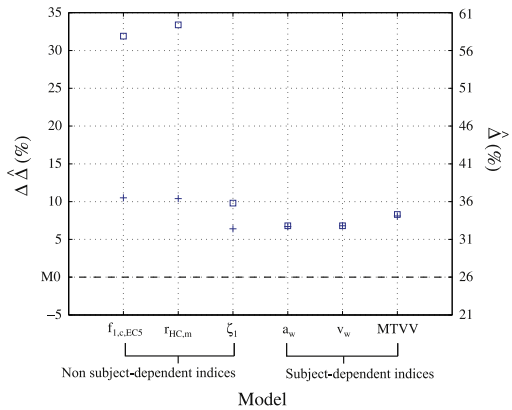

Fig. 10. Vibration acceptability – differences in $\hat{\Delta}$ ($\Delta\hat{\Delta}$) between null model *M*0, and the models involving occasion-level predictors. +: fixed-slope model; and □: random-slope model.

predictive power to be improved further ($\Delta\text{DIC} > 0$ as compared with the fixed-slope model). Thus, a random-slope model involving ζ_1 does not clearly outperform the fixed-slope model involving ζ_1. All in all, in making use of the fixed-slope model, ζ_1 may be suitable as an indicator of vibration acceptability.

Models involving subject-dependent parameters: Including a_w, v_w or MTVV in a model as an occasion-level predictor with a fixed slope enables the model's goodness-of-fit and out-of-sample predictive power to be improved ($\Delta\hat{\Delta} = 6.7$ per cent, $\Delta\hat{\Delta} = 6.8$ per cent and $\Delta\hat{\Delta} = 8.3$ per cent, respectively for a_w, v_w and MTVV, in all cases $\Delta\text{DIC} \ll -10$, as compared with the null model *M*0). Thus, a fixed-slope model involving a_w, v_w or MTVV clearly outperforms the null model. Making the slope random does not serve to further improve the model's goodness-of-fit or out-of-sample predictive power ($\Delta\hat{\Delta} = 0.1$ per cent, $\Delta\hat{\Delta} = 0$ per cent and $\Delta\hat{\Delta} = 0.2$ per cent, respectively for a_w, v_w and MTVV, in all cases $\Delta\text{DIC} > -5$, as compared with the corresponding fixed-slope model). The random-slope model thus does not outperform the fixed-slope model. In making use of the fixed-slope model, a_w, v_w and MTVV appear able to serve as indicators of vibration acceptability.

Finally, one can note that (i) the goodness-of-fit of the fixed-slope model involving MTVV is slightly better than that of the fixed-slope models involving a_w or v_w ($\Delta\hat{\Delta} \geq 1.3$ per cent), and (ii) its out-of-sample predictive power tends to be better as well ($-10 < \Delta\text{DIC} < -5$). Thus, MTVV appears to be a better indicator of vibration acceptability than a_w or v_w are.

Synthesis: Of the various non-subject-dependent parameters that were tested, it was ζ_1 that turned out to be the best indicator of vibration acceptability. Of the subject-dependent parameters that were tested, it was MTVV that appeared to be the best indicator of vibration acceptability. MTVV appears to also be a better indicator of vibration acceptability than ζ_1 is: (i) the goodness-of-fit of the fixed-slope model involving MTVV is slightly better than that of the fixed-slope model involving ζ_1 ($\Delta\hat{\Delta} = 1.7$ per cent), and (ii) its out-of-sample predictive power tends to be better as well ($-10 < \Delta\text{DIC} < -5$). The multilevel model based on MTVV is shown in Table 10.

4.2.4. Discussion

Different potential indicators of vibration annoyance and of vibration acceptability were investigated. It was found that $f_{1,c,EC5}$ and $r_{HC,m}$, i.e. two non-subject-dependent objective parameters, were the best indicators for vibration annoyance, and that MTVV, i.e. a subject-dependent objective parameter, was the best indicator for vibration acceptability.

Note that the damping ratio for the first eigenmode also turned out to be an important parameter in connection with both vibration acceptability and vibration annoyance. As Onysko [57] has indicated, studies carried out in the 1960s by Wiss, Lenzen and Hurz suggested damping to also be important. Indeed, increased exposure time is thought to lead to an increase in vibration annoyance. Sufficient damping reduces the duration of exposure to the effects of each step taken by a person walking on a floor, so that walking is perceived then to a lesser degree as involving a continuous vibrational disturbance. Note that, concerning vibration annoyance, including $f_{1,c,EC5}$ and ζ_1 in the same model (with a random slope and a fixed one, respectively) does not enable the goodness-of-fit and out-of-sample predictive power to be improved ($\Delta R_1^2 = -0.2$ per cent and $\Delta\text{DIC} > 0$ as compared with the random-slope model involving $f_{1,c,EC5}$). Regarding vibration acceptability, including MTVV and ζ_1 in the same model (with fixed slopes) enables the goodness-of-fit and out-of-sample predictive power to be slightly improved ($\Delta\hat{\Delta} = 2.3$ per cent and $\Delta\text{DIC} = -5$ as compared with the fixed-slope model involving MTVV). This improvement thus being small, it may be finally preferable to use the simpler model, i.e. the fixed-slope model only involving MTVV. Also, one should emphasise that the present study was conducted under controlled laboratory conditions. The dynamic properties of a floor will change when installed into a real building, as it interacts with the surrounding structure. The effects on mass, stiffness and damping depend on the characteristics of the supporting structure, on the design of the joint between the floor and the supporting walls and on the addition of fixtures, fittings and furnishing on the floor. In a combined laboratory and field study on vibration performance of a floor such as the one referred to "*B*" here [58],

Table 10
Vibration acceptability – fixed-slope model involving MTVV as an occasion-level explanatory variable. 95% CI: 95% Bayesian credibility interval; β_{00}: fixed intercept; β_{10}: fixed slope for MTVV; $\sigma^2_{u_0}$: variance of the residual errors u_0 (for the intercept) at the individual level; DIC: Deviance Information Criterion; $\hat{\Delta}$: proportion of risk explained at the occasion level.

	Coefficient (95% CI)
Fixed part	
β_{00}	0.307 (−0.296; 0.965)
β_{10}	−10.93 (−16.85; −6.11)
Random part	
$\sigma^2_{u_0}$	2.60 (1.10; 5.70)
DIC	329.9
$\hat{\Delta}$	0.341

it was shown that the effect of real build-in conditions is larger on the damping ratios than on the natural frequencies. In the present study, the damping ratios were derived from laboratory tests, which would, of course, differ when installed in a real building, depending on the construction system. Regression analysis between measured data and inhabitants' experience of vibrations from field floors could lead to different outcomes and prove that the damping ratio for the first eigenmode is definitely another important indicator of vibration acceptability and/or vibration annoyance due to floor vibrations, as have been previously shown by Lenzen [6]. However, the fact that damping is a property difficult to predict and measure with accuracy into a structure makes it a parameter that is not often used as a design indicator. In the present study, these facts have been considered and determining other indicators, easier to predict and use by engineers, has thus been given priority.

Furthermore, in the present study, neither vibration acceptability nor vibration annoyance was found to be directly correlated with floor deflection. This result contradicts both traditions and current regulations. Notably, Onysko [57] reported that already in 1840 Thomas Tredgold recommended making use of deflection limits. Toratti and Talja [28] also suggested that floor deflection is related to vibrational discomfort. In the present study, certain dynamic parameters, specifically $f_{1,c,EC5}$, $r_{HC,m}$ and MTVV, were shown to be more closely correlated with vibration discomfort than floor deflection was. This result seems not illogical at all, since floor deflection is a measure of floor stiffness alone, whereas the dynamic behavior of a floor also depends upon the mass inertia of the floor.

As regards vibration acceptability, MTVV may not be practical to use in connection with design guidelines for manufacturers regarding the vibration serviceability of timber floors, since it implies that already at the design phase one needs to deal directly with walking excitation and measurement of the accelerations experienced by subjects. In fact, for random-slope models involving $f_{1,c,EC5}$ or $r_{HC,m}$, the goodness-of-fit and the out-of-sample predictive power turned out to be highest in connection with vibration acceptability. It was also observed, however, that the effect of these parameters on vibration acceptability varied considerably from subject to subject, which thus precluded their being good indicators of vibration acceptability. This corroborates the results of logistic PCA showing subjects' vibration acceptability responses to be less consistent from one subject to another than the subjects' vibration annoyance responses are. Large inter-individual differences in acceptability ratings have also been observed by Aasvang and Engdahl [59], who studied subjective responses to aircraft noise in terms of noise annoyance and noise acceptability. Finding indicators of vibration annoyance to not represent adequate indicators of vibration acceptability, and *vice versa*, is not illogical, in view of the fact that the two subjective attributes involved are not perfectly (negatively) correlated. Indeed, a multilevel regression analysis of vibration annoyance (taken as the dependent variable) and vibration acceptability was carried out here. The proportion of variance explained at the occasion level, i.e. R^2_1, was found to be equal to 0.759, which is not particularly high.

Fig. 11 shows, for the two vibration annoyance models (involving $f_{1,c,EC5}$ and $r_{HC,m}$, respectively), the individual regression lines[2] for one subject (e.g. subject no. 8), together with their 95 per cent credibility interval. Fig. 12 shows, for the vibration acceptability model (involving MTVV), the individual regression line[3] for one subject (e.g. subject no. 7), together with its 95 per cent credibility interval.

It can be seen that, even though $f_{1,c,EC5}$ and $r_{HC,m}$ on one hand, and MTVV on the other, turned out to be the best indicators of vibration annoyance and vibration acceptability, respectively, the uncertainty regarding the individual regression lines remains substantial. In accordance with this, the goodness-of-fit of the three models was found to be only moderate ($R^2_1 = 0.563$ and $R^2_1 = 0.566$, and $\hat{\Delta} = 0.341$, see Tables 9 and 10). Nevertheless, certain trends can be noted.

For one thing, the first eigenfrequency may be an important objective parameter in link with vibration annoyance. The lower it is, the higher the individual annoyance scores tend to be. Fig. 13 shows the overall regression line[4] ($\beta_{00}+\beta_{10}f_{1,c,EC5}$)

[2] For the vibration annoyance models, the individual regression lines were computed as follows: $(\beta_{00}+u_{0i})+(\beta_{10}+u_{1i})f_{1,c,EC5_i}$ and $(\beta_{00}+u_{0i})+(\beta_{10}+u_{1i})r_{HC,m_i}$.

[3] For the vibration acceptability model, the individual regression lines were computed as follows: $(\beta_{00}+u_{0i})+\beta_{10}$ MTVV$_{fi}$.

[4] The overall regression line provides the predicted values for an "average" subject.

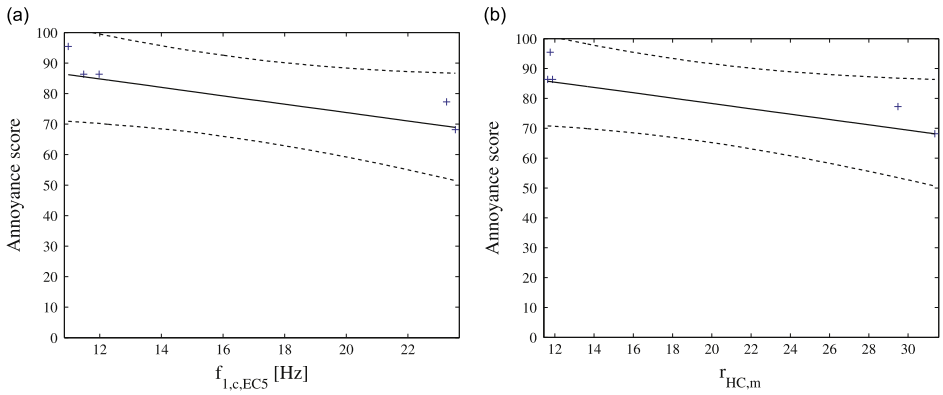

Fig. 11. Vibration annoyance models – individual regression lines for one subject (e.g. subject no. 8). —: median value; - -: lower and upper limits of the 95 per cent credibility interval; +: actual scores. (a) Model involving $f_{1,c,EC5}$; and (b) model involving $r_{HC,m}$.

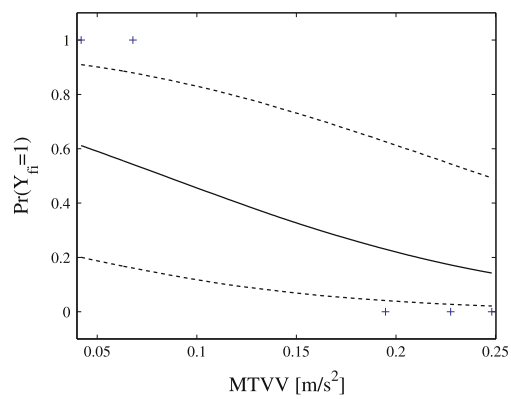

Fig. 12. Vibration acceptability model involving MTVV – individual regression line for one subject (e.g. subject no. 7). —: median value; - -: lower and upper limits of the 95 per cent credibility interval; and +: actual binary responses.

and its 95 per cent credibility interval, for the vibration annoyance model involving $f_{1,c,EC5}$. It can be noted that, on the average, the floor vibrations are not experienced as annoying (with scores < 58.3[5]) for an $f_{1,c,EC5}$ value (median value) greater than 18.5 Hz. Taking account of the uncertainty regarding the overall regression line, this threshold value may lie somewhere between 15 and 22 Hz. This interval includes the threshold value advanced by Dolan et al. [19], that of 15 Hz, for preventing wooden floor vibrations from being annoying.

Secondly, Hu and Chui's criterion may be an important objective parameter for vibration annoyance as well. The lower this criterion is, the higher the individual annoyance scores tend to be. Fig. 14 shows the overall regression line ($\beta_{00}+\beta_{10}r_{HC,m}$), together with its 95 per cent credibility interval, for the vibration annoyance model involving $r_{HC,m}$. One can observe that, on the average, for an $r_{HC,m}$ value (median value) of greater than 23, the floor vibrations are not experienced as annoying (with scores < 58.3). Taking account of the uncertainty regarding the overall regression line, this threshold value may lie somewhere between 18 and 29. This interval includes the threshold value advanced by Hu and Chui [29], i.e. 18.7, above which floors can be most likely regarded by occupants as satisfactory.

Thirdly, MTVV turned out to be the best indicator of vibration acceptability. The lower MTVV is, the more vibrations are judged to be acceptable. Fig. 15 shows the overall regression line ($\beta_{00}+\beta_{10}$ MTVV), together with its 95 per cent credibility interval, for the vibration acceptability model. One can observe that, on the average, the floor vibrations are judged to be acceptable ($\Pr(Y_{fi}) > 0.5$ [28]) for an MTVV value (median value) of 0.03 m/s^2 or less. Taking account of the uncertainty regarding the overall regression line, this threshold value can be extended to 0.08 m/s^2. No study claiming MTVV to be an adequate indicator of vibration acceptability has been reported in the literature. Toratti and Talja [28], notably, used the RMS velocity, v_{RMS}, to draw up a vibrational classification of high-frequency floors ($f_1 > 10$ Hz).

[5] This score corresponds to the category "disturbing" of the six-point verbal scale used in *SP* study.

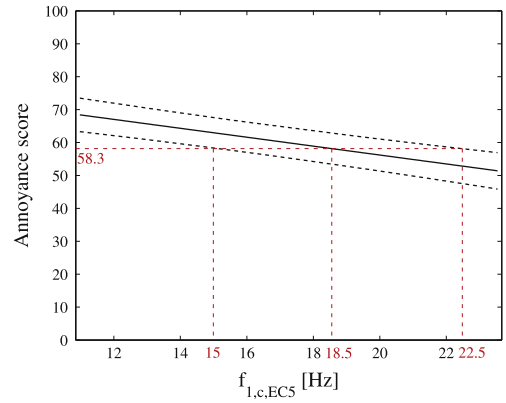

Fig. 13. Vibration annoyance model involving $f_{1,c,EC5}$ – overall regression line. —: median value; and - -: lower and upper limits of the 95 per cent credibility interval.

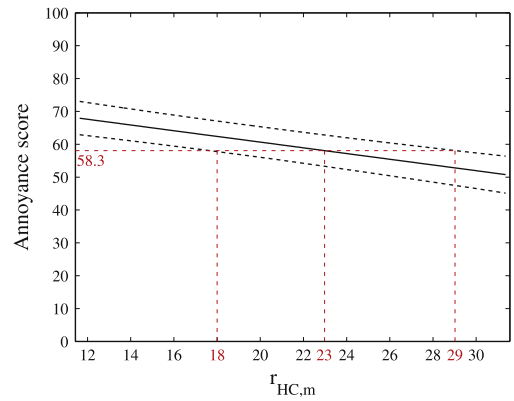

Fig. 14. Vibration annoyance model involving $r_{HC,m}$ – overall regression line. —: median value; and - -: lower and upper limits of the 95 per cent credibility interval.

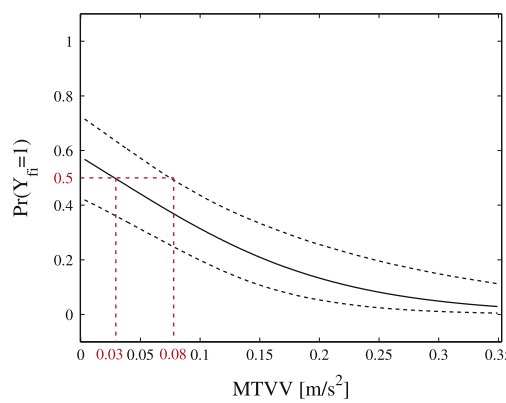

Fig. 15. Vibration acceptability model involving MTVV – overall regression line. —: median value; and - -: lower and upper limits of the 95 per cent credibility interval.

5. Conclusions

Psycho-vibratory tests were performed on 5 different timber floors in a laboratory environment at two different locations, merging the data stemming from both studies (that conducted at *SP* and that conducted at *LU*) for purposes of enhancing the statistical reliability of the results. All of the objective data gathered were post-processed and were used for classification of the floors in accordance with different criteria.

The criteria employed, described in [24,29,19], were found to describe fairly well the performance of the floors in terms of vibration acceptability (see Tables 6 and 7), especially in the case of measured data, certain discrepancies being found when calculated data were employed. Accordingly, results based on use of calculated data need to be interpreted with care.

Nevertheless, despite the timber floors basically complying with the criteria currently employed, subjective vibratory studies of modern timber framework buildings still frequently yield results showing the inhabitants involved to often be annoyed by vibrations [60]. This may be due in part to the design criteria employed being based originally on measurements and subjective ratings carried out in single-family houses. Thus, reconsideration of the questions of interest here and the development of new design criteria are needed.

Furthermore, the answers the subjects provided were confronted with the values of both measured and calculated objective parameters in efforts to determine the best design indicators of vibration acceptability and vibration annoyance, respectively. This involved use of multilevel regression. The paper can thus also be seen as exemplifying the fact that multilevel regression, not widely used as yet, can be a valuable tool for modelling repeated measures data that involves substantial inter-individual differences in rating. Two objective parameters were found to be the best indicators of vibration annoyance: Hu and Chui's criterion (calculated from measured quantities), $r_{HC,m}$, and the first eigenfrequency calculated according to Eurocode 5, $f_{1,c,EC5}$. The Maximum Transient Vibration Value, MTVV, determined on the basis of the accelerations experienced by the subjects, proved to be the best indicator of vibration acceptability. These findings, obtained in what can be considered a pilot study in the sense of its involving only a small sample of wooden floors (5 different ones), though there was a sufficiently large number of subjects to provide clear statistical support for the conclusions drawn concerning these floors, should be followed up by a more comprehensive study, involving a broader sample of wooden floors.

Policy and ethics

All procedures reported on this manuscript were undertaken, since they involved humans, in compliance with The Code of Ethics of the World Medical Association (Declaration of Helsinki), Lund University also approving their performance. Likewise, all tests were carried out with all participants' consent, the privacy rights of human subjects being always assured.

Acknowledgements

This research reported on here was funded by the Silent Spaces project, a part of the EU program Interreg IV and by the Vinnova and Formas project AkuLite. The authors thank Mr. Anders Sjöström and Mr. Thord Lundgren for their invaluable help during the psycho-vibratory tests, the reviewers for their helpful comments on the earlier version of this paper and all the participants who took part in the tests.

References

[1] S. Ohlsson, Floor Vibrations and Human Discomfort, PhD Thesis, Chalmers University, Göteborg, Sweden, 1982.
[2] J. Forssén, W. Kropp, J. Brunskog, S. Ljunggren, D. Bard, G. Sandberg, F. Ljunggren, A. Ågren, O. Hallström, H. Dybro, K. Larsson, K. Tillberg, L.-G. Sjökvist, B. Östman, K. Hagberg, Å. Bolmsvik, A. Olsson, C-G. Ekstrand, M. Johansson, Acoustics in Wooden Buildings, State of the Art 2008, Vinnova Project 2007-01653, Report 2008:16, SP Trätek (Technical Research Institute of Sweden), Stockholm, 2008.
[3] M.J. Griffin, *Handbook of Human Vibration*, Academic Press Limited, London, UK, 1996.
[4] International Organization for Standardization ISO 2631-1, Vibration and shock – evaluation of human exposure to whole-body vibration – Part 1: general requirements, 1997.
[5] H. Reiher, F. J. Meister, The Effect of Vibration on People, Published in German in 1931, English Translation in Report No. F-TS-616-R.E. Headquarters, Air Material Command, Wright Field, OH, USA, 1949.
[6] K.H. Lenzen, Vibration of steel joist-concrete slab floors, *AISC Engineering Journal* 3 (1966) 133–136.
[7] J.F. Wiss, R.A. Parmelee, Human perception of transient vibrations, *Journal of the Structural Division ASCE* 100 (4) (1974) 773–787.
[8] D.E. Allen, J.H. Rainer, Vibration criteria for long-span floors, *Canadian Journal of Civil Engineering* 3 (1976) 165–173.
[9] T.M. Murray, Acceptability criterion for occupant-induced floor vibrations, *Engineering Journal AISC*: *2nd Quarter* (1981) 62–70.
[10] S.R. Alvis, An Experimental and Analytical Investigation of Floor Vibrations, MSc Thesis, Virginia Polytechnic Institute and State University, USA, 2001.
[11] E.S. Bernard, Dynamic serviceability in lightweight engineered timber floors, *ASCE Journal of Structural Engineering* 134 (2) (2008) 258–268.
[12] International Organization for Standardization ISO 2631-2, Evaluation of human exposure to whole-body vibration – Part 2: continuous and shock-induced vibration in buildings (1 Hz to 80 Hz), 1989.
[13] International Organization for Standardization ISO 2631-2, Vibration and shock – evaluation of human exposure to whole-body vibration – Part 2: vibration in buildings (1 Hz to 80 Hz), 2003.
[14] F. Ljunggren, Floor Vibration – Dynamic Properties and Subjective Perception, PhD Thesis, Luleå University of Technology, Sweden, 2006.
[15] International Organization for Standardization ISO 10137, Bases for design of structure – serviceability of buildings and walkways against vibrations, 2007.
[16] L.J. Hu, Y.H. Chui, Vibration serviceability of timber floors in residential construction, *Progress in Structural Engineering and Materials* 3 (2001) 228–237.

[17] R.O. Foschi, A. Gupta, Reliability of floors under impact vibration, *Canadian Journal of Civil Engineering* 14 (1987) 683–689.
[18] D.M. Onysko, *Performance and Acceptability of Wood Floors – Forintek Studies*, National Research Council of Canada, Publication 28822, Forintek Canada Corp., Ottawa, 1988.
[19] J.D. Dolan, T.M. Murray, J.R. Johnsson, D. Runte, B.C. Shue, Preventing annoying wood floor vibrations, *Journal of Structural Engineering* 125 (1) (1999) 19–24.
[20] A.L. Smith, S.J. Hicks, P.J. Devine, *Design of Floors for Vibrations—A New Approach*. The Steel Construction Institute (SCI). Publication P354, 2009.
[21] UK Concrete Society, Technical Report 43—Post-Tensioned Concrete Floor Design Handbook, 1994.
[22] A. Pavic, P. Reynolds, P. Waldron, K.J. Bennett, Critical review of guidelines for checking vibration serviceability of post-tensioned concrete floors, *Cement & Concrete Composites* 23 (2001) 21–31.
[23] S. Ohlsson, *Springiness and Human-induced Floor Vibrations—A Design Guide*, Swedish Council for Building Research, Stockholm, 1988.
[24] European Committee for Standardization EN 1995-1-1, Eurocode 5 – design of timber structures – common rules and rules for buildings, 2004.
[25] I. Smith, Y.H. Chui, Design of light-weight wooden floors to avoid human discomfort, *Canadian Journal of Civil Engineering* 15 (1988) 254–262.
[26] B.R. Ellis, On the response of long-span floors to walking loads generated by individuals and crowds, *The Structural Engineer* 78 (10) (2000) 17–25.
[27] P. Hamm, A. Richter, S. Winter, Floor vibrations—new results, *Proceedings of the 11th World Conference on Timber Engineering*, Riva del Garda, Italy, 2010.
[28] T. Toratti, A. Talja, Classification of human induced floor vibrations, *Building Acoustics* 13 (3) (2006) 211–221.
[29] L.J. Hu, Y.H. Chui, Development of a design method to control vibrations induced by normal walking action in wood-based floors, *Proceedings of the 8th World Conference on Timber Engineering*, Lahti, Finland, 2004.
[30] T. Murray, D. Allen, E. Ungar, *Floor Vibration Due to Human Activities*, US AISC Design Guide 11, American Institute of Steel Construction, 1997.
[31] D.E. Allen, T.M. Murray, Design criteria for vibrations due to walking, *Engineering Journal AISC* 30 (4) (1993) 117–129.
[32] M. Feldmann, C. Heinemeyer, E. Caetano, A. Cunha, F. Galant, A. Goldack, O. Hechler, S. Hicks, A. Keil, M. Lukic, R. Obiala, M. Schlaich, A. Smith, P. Waarts, RFCS-Project: Human Induced Vibration of Steel Structures—HIVOSS: Design Guideline and Background Report, 2008.
[33] J. Porteus, A. Kermani, *Structural Timber Design to Eurocode 5*, Blackwell Science Ltd, Oxford, UK, 2007.
[34] A.A. Al-Foqaha'a, W.F. Cofer, K.J. Fridley, Vibration design criterion for wood floors exposed to normal human activities, *Journal of Structural Engineering* 125 (1999) 1401–1406.
[35] I. Glisovic, B. Stevanovic, Vibrational behaviour of timber floors, *Proceedings of the 11th World Conference on Timber Engineering*, Riva del Garda, Italy, 2010.
[36] J. Weckendorf, Dynamic Response of Structural Timber Flooring Systems, PhD Thesis, Edinburgh Napier University, UK, 2009.
[37] S. Thelandersson, H.J. Larsen, *Timber Engineering*, Wiley, Chichester, UK, 2003.
[38] Axiom EduTech AB, VibraTools Suite [computer program], Ljusterö, Sweden, 2007.
[39] W. Heylen, S. Lammens, P. Sas, *Modal Analysis—Theory and Testing*, Katholieke Universiteit Leuven, Belgium, 1995.
[40] L.J. Hu, Protocols for field testing of wood-based floor systems, Appendix V in Report of Serviceability design criteria for commercial and multi-family floors, Report No. 3 for Canadian Forest Service, FPInnovations, Quebec, 1998.
[41] Deutsches Institut für Normung DIN 45669-1, Measurement of vibration immission – Part 1: vibration meters – requirements and tests, 2010.
[42] H.M.E. Miedema, H. Vos, Noise annoyance from stationary sources: *relationships with exposure metric day-evening-night level (DENL) and their confidence intervals*, *Journal of the Acoustical Society of America* 116 (1) (2004) 334–343.
[43] W. Passchier-Vermeer, K. Zeichart, Vibrations in the Living Environment: Relationships between Vibration Annoyance and Vibration Metrics. Report no. 98.030, TNO-PG, Leiden, The Netherlands, 1998.
[44] J.J. Chang, J.D. Carroll, How to use MDPREF: A Computer Program for Multidimensional Analysis of Preference Data, Technical Report, Bell Telephone Laboratories, Murray Hill, NJ, USA, 1969.
[45] J.J. Chang, J.D. Carroll, How to Use PREFMAP and PREFMAP-2: Programs Which Relate Preference Data to Multidimensional Scaling Solutions, Technical Report, Bell Telephone Laboratories, Murray Hill, NJ, USA, 1972.
[46] M.R. Schroeder, D. Gottlob, K.F. Siebrasse, Comparative study of European concert halls: *correlation of subjective preference with geometric and acoustic parameters*, *Journal of the Acoustical Society of America* 56 (4) (1974) 1195–1201.
[47] J. De Leeuw, Principal Component Analysis of Binary Data: Applications to Roll-Call Analysis, Technical Report no. 364, UCLA Department of Statistics, Los Angeles, CA, USA, 2003. Available on ⟨http://escholarship.org/uc/item/7n7320n0#page-1⟩, viewed on 2013.02.18.
[48] Z. Schärer Kalkandjiev, S. Weinzierl, The Influence of room acoustics on solo music performance: *an empirical case study*, *Acta Acustica United with Acustica* 99 (3) (2013) 433–441.
[49] A. Trollé, C. Marquis-Favre, A. Klein, Short-term annoyance due to tramway noise: *determination of an acoustical indicator of annoyance via multilevel regression analysis*, *Acta Acustica United with Acustica* 100 (1) (2014) 34–45.
[50] A. Gelman, J. Hill, *Data Analysis using Regression and Multilevel/Hierarchical Models*, Cambridge University Press, New York, NY, 2007.
[51] J.J. Hox, *Multilevel Analysis—Techniques and Applications*, second edition, Routledge, New York, NY, 2010.
[52] W.J. Browne, *MCMC Estimation in MLwiN V2.1, Centre for Multilevel Modelling*, University of Bristol, Bristol, England, 2009.
[53] The BUGS Project, DIC: Deviance Information Criterion [online]. Available on ⟨http://www.mrc-bsu.cam.ac.uk/software/bugs/the-bugs-project-dic/⟩, viewed on 2014.07.15.
[54] A. DeMaris, Explained variance in logistic regression—a Monte Carlo study of proposed measures, *Sociological Methods & Research* 31 (1) (2002) 27–74.
[55] P-E. Austrell, O. Dahlblom, J. Lindemann, A. Olsson, K.-G. Olsson, K. Persson, H. Petersson, M. Ristinmaa, G. Sandberg, P-A. Wernberg, *CALFEM—A Finite Element Toolbox*. Version 3.4, Division of Structural Mechanics, Lund University, Sweden, 2004.
[56] R.B. Cattell, The Scree test for the number of factors, *Multivariate Behavioral Research* 1 (1966) 245–276.
[57] D. M. Onysko, Performance of Wood-Joist Floor Systems: A Literature Review, Information Report No. OP-X-24, Forest Products Laboratory, Canadian Forestry Service, Ottawa, Canada, 1970.
[58] K. Jarnerö, A. Brandt, A. Olsson, in situ testing of timber floor vibration properties, *Proceedings of the 11th World Conference on Timber Engineering*, Riva del Garda, Italy, 2010.
[59] G.M. Aasvang, B. Engdahl, Subjective responses to aircraft noise in an outdoor recreational setting: a combined field and laboratory study, *Journal of Sound and Vibration* 276 (2004) 981–996.
[60] K. Jarnerö, D. Bard, C. Simmons, Vibration Performance of Apartments Buildings with Wooden Framework—Residents' Survey and Field Measurements, AkuLite Report 6, SP Report 2013:17, ISBN: 978-91-87461-02-6, 2013.

Paper G

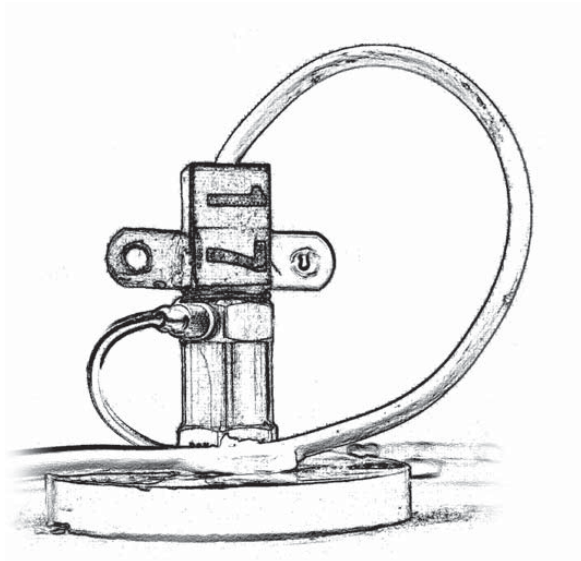

CONSTRUCTION AND IN-HOUSE CALIBRATION OF MEMS-BASED VIBRATION TRANSDUCERS

R. DARULA, A. SJÖSTRÖM, J. NEGREIRA and D. BARD

Engineering Acoustics

Measurement Report

DEPARTMENT OF CONSTRUCTION SCIENCES
DIVISION OF ENGINEERING ACOUSTICS

ISRN LUTVDG/TVBA--16/3131--SE (1-77) | ISSN 0281-8477

CONSTRUCTION AND IN-HOUSE CALIBRATION OF MEMS-BASED VIBRATION TRANSDUCERS

R. DARULA, A. SJÖSTRÖM, J. NEGREIRA and D. BARD

Online version available at: http://bit.ly/1WghuDr

Printed by Media-Tryck LU, Lund, Sweden, February 2016 *(Pl)*.

For information, address:
Div. of Engineering Acoustics, LTH, Lund University, Box 118, SE-221 00 Lund, Sweden.
Homepage: http://www.akustik.lth.se

Acknowledgements

The research reported on here was funded by the Silent Spaces project, a part of the EU program Interreg IV-A. The authors highly appreciate the financial support provided.

The authors would like to thank all people who helped to clarify the concepts of calibration or signal processing as such. Especially and firstly, we would like to thank Dr.Tom Sørensen from Bruel&Kjaer for his help, support and advices in tuning the methodology and for his help with the B&K PULSE system.

Special thanks as well to Jan Balle Larsen, GRUNDFOS, and Dr. George Juraj Stein for fruitful discussions on calibration procedures for piezo and MEMS devices as well as on signal processing in itself.

Last but not least, a word of thanks to all our project colleagues from the Department of Construction Sciences (Lund) and the Departments of Mechanical and Manufacturing Enginneering and Civil Engineering (Aalborg). It has been a pleasure to collaborate with all of you during the course of the Silent Spaces project.

Thanks to all!

The authors

Table of Contents

Nomenclature

Acronyms

AAU Aalborg University.

B&K Bruel & Kjaer (company).

CCLD Constant Current Linear Drive.

CPB Constant Power Bandwidth.

DAQ Data Acquisition.

DMME Department of Mechanical and Manufacturing Engineering (at AAU).

FE Finite Element.

FFT Fast Fourier Transform.

FRF Freqeuency Response Function.

GUI Graphical User Interface.

LCC Leadless Chip Carrier.

LU Lund University.

MEMS Micro Electro Mechanical System.

MTS Material Testing Machine.

PCB Printed Circuit Board.

RMS Root Mean Square.

SSR Steady State Response.

1 Preface

The report presented here summarises the process of development of Micro Electro Mechanical Systems (MEMS) capacitive accelerometers, from mounting to calibration, to be employed for low frequency vibration testing. This project was carried out within the frame of the Silent Spaces project, a part of the EU program Interreg-IVA, and more specifically in conjunction between the project partners Lund University (LU) in Sweden and Aalborg University (AAU) in Denmark.

1.1 Motivation

Wooden multi-storey buildings have steadily increased their market share in Sweden since 1994, the year in which their construction was reintroduced after a century-old-ban (due to numerous urban fires during the 1800s) was lifted. Ever since, product development has been carried out based on engineers' experience and measurements performed in already existing buildings. Despite of the many advantages that the use of wood as construction material involves, namely sustainability, reduction of the material transportation costs, smaller size of the foundations needed due to wood's light weight, wood being abundant particularly in Sweden, etc. (Negreira, 2013), complaints among residents often arise due to low frequency noise and vibrations, even when those buildings fulfil the standards currently in force (ISO, 2013a,b). It is believed that the main reason for peoples' discontent in their apartments is low frequency sound and vibrations below 50 Hz. Analyses below 50 Hz are seldom performed as those frequencies are left outside the scope in the current standards (Ljunggren et al., 2014) and evaluations methods do not yet exist. It is desired, therefore, to develop low frequency numerical prediction tools so as to be able to foresee the vibroacoustic performance of such structures during their design phase, the latter entailing savings in terms of money and time for the industry, as one would avoid the construction of mock-ups and test buildings. Nevertheless, the variability of a natural material such as wood, the complexity of the junctions between structural parts involved and external factors such as workmanship, makes it difficult to accurately predict the behaviour of wood. Hence, a significant part of the research in the field currently aims at gaining knowledge of such types of structures, its enabling the development of numerical prediction tools (most often by means of finite element (FE) models). The calibration of the aforementioned vibroacoustic prediction tools is carried out using measurement data as calibration input for the models. In line with the latter, having numerous transducers facilitates the acquisition of data as well as improves the richness of it and hence the quality of the predictions.

1.2 Objective and method

A hindrance in having such an extensive measurement equipment with many transducers is the price of the apparatus involved. Thus, the idea of this project was to develop accelerometers from scratch, by buying MEMS capacitive sensors (i.e. the inner-chip), mount the components and perform the calibration ourselves.

1.2.1 Outline

In the report, a theoretical background about accelerometers as well calibration methods found in the literature is given first. Subsequently, the mounting of the accelerometers is described step by step (i.e. soldering of the inner-chip, casing and cabling). Finally, the calibration procedure is presented. Special attention is paid to the description of all the tests performed in order to keep track of all that was tested

and which approach leads to a more precise calibration. After discussion with Dr. Tom Sørensen from Bruel & Kjaer (Sørensen, T., 2011), the back-to-back calibration procedure using an electrodynamic shaker as a source of vibration controlled via feedback loop in order to ensure a constant excitation level, was chosen.

1.2.2 Research limitations

The calibration described in this report is not an accredited one, but rather an unofficial in-house calibration, without any calibration certificate provided. However, the methods employed involve the usage and comparison with a calibrated reference accelerometer, the precision obtained hence being more than sufficient for academic purposes as the ones dealt with in our research.

1.3 Ultimate aim

The ultimate aim of this report is to increase the accuracy and reliability of the measurements carried out using these MEMS capacitive accelerometers and eventually thus have calibration input of better quality for the low frequency vibroacoustic prediction tools that are to be developed.

The authors

2 Introduction

In this chapter, the aim is to provide a background to the topic dealt with in the report. More specifically, concepts about accelerometers, namely different types, their parameters, fixation methods and calibration procedures will be presented.

2.1 Sensors and transducers

According to (Bishop, 2002), a sensor can be defined as "a device, that when exposed to a physical phenomenon (temperature, displacement, force, etc.) produces a proportional output signal (electrical, mechanical, magnetic, etc.)", i.e. a device that responds to a change in a measurand[1]. In contrast, a transducer is "a device that converts one form of energy to another". In other words, a sensor detects a change in a physical quantity that varies due to some type of excitation, whereas a transducer is also capable (apart from the detection) of communicating the measurand, i.e. it has a signal conditioning involved as well. All in all, every transducer is also in itself (or has inside it) a sensor, but the opposite is not always true (cf. Fig. 2.1).

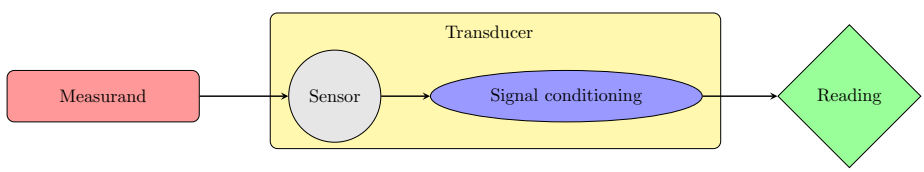

Fig. 2.1: Schematic drawing of a sensor and a transducer.

As stated in (Bishop, 2002), the sensors can be classified as passive or self-powered if the the power is provided by a sensed physical phenomenon (e.g. thermometer); or active, when external power is necessary for operation. Depending on the output signal, they can also be classified as analog, when the output signal is continuous; or digital when it is discretised. Likewise, according to (ISO, 1998), transducers can be classified as non-contact transducers, if they are located in a close vicinity of the structure to be measured (e.g. eddy-current, optical proximity); or contact, if mechanical contact between the transducer and the structure exists (e.g. piezoelectric, piezoresistive).

2.2 Accelerometers

The report presented here focuses in a special category of transducers: accelerometers, being defined as transducers which produce an output signal proportional to the acceleration sensed (Randall, 2011). More specifically, the report summarises the process of development of MEMS capacitive accelerometers, from mounting to calibration, to be employed for low frequency vibration testing.

2.2.1 Types of accelerometers

There are many types of accelerometers, the most common ones being the following (Negreira, 2013; Bishop, 2002):

[1] The physical phenomenon that is to be measured.

- **Capacitive:** a typical capacitive sensor (the MEMS accelerometers studied here are of this type) is composed of a movable proof mass provided with a plate (representing a capacitor) that is attached to a reference frame by a mechanical suspension system, as shown in Fig. 2.2a. The deflection of the suspended mass with respect to the suspension frame attached to the vibrating structure, causes a change of capacitance between the outer plates and the plates attached to the mass and thus in the output voltage, which is proportional to the sensed acceleration. In other words, the variation in the output signal is produced by sensing changes in capacitance when the geometry of the capacitor inside the sensor is changing due to the acceleration sensed (due either to the change of area of the electrodes, the distance between them or the permittivity of the material separating them).
- **Piezoelectric:** a piezoelectric accelerometer uses the piezoelectric effect of quartz or ceramic crystals to provide an electrical output which is proportional to the sensed acceleration. The piezoelectric effect produces a charge which is emitted by the crystal when it is subjected to a compressive force. A force applied to a quartz crystal lattice structure alters the alignment of the positive and the negative ions, which results in an accumulation of these charged ions on the opposing surfaces. These charged ions accumulate on an electrode that is ultimately conditioned by transistor microelectronics and designed to measure the acceleration. The piezoelectric crystal is normally bonded to a mass such that when the accelerometer is subjected to a force, the mass in question compresses the crystal, which produces an electric signal proportional to the acceleration; see Fig. 2.2b, (Negreira, 2013). Piezoelectric accelerometers can be used over a wide range of frequencies, showing an excellent linearity over a broad dynamic range. The measurements they provide are attainable with excellent accuracy for a large variety of environmental conditions. They require no power supply, are extremely durable since they contain no movable parts, are extremely compact and have a high sensitivity-to-mass ratio (Bruel&Kjaer, 1978). Their price is one of their main disadvantages, as they are much more expensive than MEMS accelerometers.

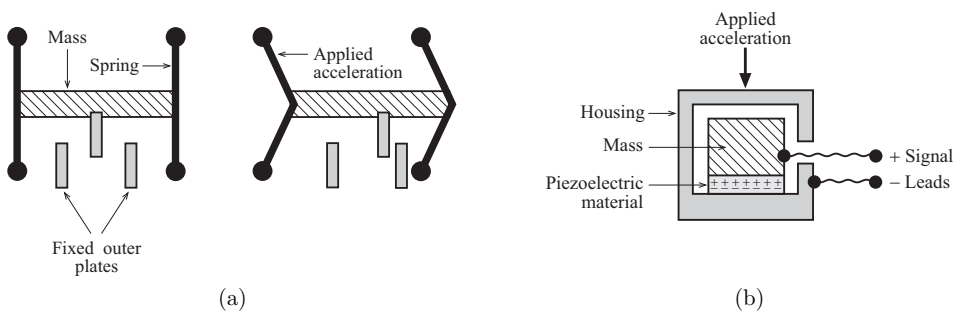

Fig. 2.2: Scheme of a MEMS accelerometer (a) and of piezoelectric accelerometer (b), (Negreira, 2013).

- **Piezoresistive:** also called strain gauge accelerometers. This type of accelerometers takes advantage of the resistance change of piezoresistive materials to covert mechanical strain to a DC output voltage. The resistors are normally configured into a Wheatstone bridge circuit, which provides a change in output voltage that is proportional to acceleration. They are often used for shock applications. They can sense accelerations down to 0 Hz; however, they are not very accurate for high frequencies.
- **Hall effect:** a magnet and a Hall effect sensor detecting changes in magnetic field values are placed in the seismic mass (proofmass) of the sensor. The output voltage sent by the Hall effect sensor is proportional to the acceleration the transducer is exposed to.
- **Heat transfer:** heat transfer accelerometers measure internal changes in heat transfer due to acceleration, and use thermoresistors to send out an electrical signal proportional to the acceleration detected.

Note that MEMS denotes the technology of very small devices, i.e. a technology that in its most general form can be defined as miniaturised mechanical and electro-mechanical elements (i.e., devices and structures) that are made using the techniques of microfabrication. Therefore, MEMS is not just associated to the capacitive accelerometers under investigation in this report, but also there can be MEMS piezoresistive accelerometers, for example, if this manufacturing technology is employed.

2.2.2 Parameters of accelerometers

The main parameters defining an accelerometer (and that could also be generalised for any type of transducer) are (Bishop, 2002; Bruel&Kjaer, 1978):

- **Sensitivity:** ratio of the accelerometer's electrical output to the mechanical input, expressed in terms of voltage per physical unit (e.g. $\mathrm{mV/ms^{-2}}$). In analog sensors, the sensitivity is given as the slope of the output and input signals. A special case (and also important in measurements) is the so-called transverse sensitivity, defined as the sensitivity to an acceleration applied at right angles to its main geometric axis.
- **Frequency response:** dependence of the charge or voltage sensitivity with frequency. It defines the useful frequency range with linear sensitivity. The upper frequency limit depends primarily upon the mounting resonance, whereas the bottom one is restricted mainly by the pre-amplifier used (Bruel&Kjaer, 1978). Accelerometers exposed to temperature variations will generate a low frequency response. Therefore, the pre-amplifiers can be set to have some cut-off frequency in the lower region to avoid it.
- **Phase response:** time delay between the mechanical input and the resulting electrical output. In general, this delay is not constant for all frequencies.
- **Transient response:** for shocks and transient vibrations. Two types can be distinguished:
  1. Zero shift: presence of phase non-linearities in the preamplifier, or accelerometers.
  2. Ringing: the transient contains high frequencies so that the resonance of the accelerometer is excited. It can be reduced by setting the mounting resonance to not less than 10/T, where T is the duration of the transient in seconds.
- **Resolution:** the smallest increment of input that can be reliably detected. In digitally operated sensors, the resolution is determined as the number of pulses per physical quantity. The analog sensors have, on the contrary, a resolution limit characterised by low-level electrical noise.
- **Weight:** in general, one could adhere to the following rule of thumb: the weight of the accelerometer should be at least ten times less than the effective weight of the vibration test specimen. A more precise relationship can also be calculated depending on the impedances and the so-called an added mass effect discussed in (Hopkins, 2007), according to:

$$v_m = v_a \frac{Z_{dp}}{Z_{dp} + i\omega m_{acc}}, \tag{2.1}$$

  with v_m and v_a being the measured and actual velocities respectively, Z_{dp} the driving point impedance of the structure and m_{acc} the mass of the transducer.
- **Dynamic range:** range over which the electrical output of the accelerometer is directly proportional to the acceleration at its base. The lower limit is a practical issue and is determined by the noise level of the measuring system. In general, the upper limit is higher with decreasing size of the accelerometer. The upper limit is of special interest for shock measurements.
- **Environmental characteristics:** the sensitivity of an accelerometer is influenced also by the environmental conditions, especially temperature, humidity, acoustic field, magnetic field or radiation. If measurements in severe conditions are to be performed, special accelerometers should be used.
- **Repeatability (reproducibility):** defined as the ability of the transducer to give identical outputs for the same input. The repeatability is influenced by e.g. electrical noise and hysteresis. To increase repeatability, averaging techniques or low-pass filtering can be used.
- **Linearity and accuracy:** ability to provide a direct (linear) relationship between the input and the output with minimal fluctuations. It is expressed as percentage of the full-scale.
- **Impedance:** ratio of the voltage and the current flow through the sensor. In general, a high input impedance is required to reduce current flowing from the source. As for output impedance, it is required to be low, as they behave as a source of current.
- **Eccentricity:** geometrical non-linearity.
- **Saturation:** defines the maximum output capability. When a sensor is saturated, its output remains constant even with increasing input signal.
- **Deadband:** a region of the input close to zero at which the output remains also zero. Once the input travels outside the deadband, then the output varies with the input accordingly. Occurs, for example, in thermostats or joysticks, so as to avoid small fluctuations.

2.2.3 Fixation of contact accelerometers

When performing measurements in general, and vibration measurements in particular, special attention must be paid to the way transducers are attached to the structure under investigation, as the results acquired could depend very much upon these fixations. An analysis prior to the measurements should be carried out to evaluate the most accurate possible way to affix the transducers onto the object to be measured. Typically, 9 types of fixations can be used (Bruel&Kjaer, 1982; ISO, 1998):

1. **Threaded stud:** the best fixation is to attach the accelerometer to the structure using a stud. It is recommended to use a thin layer of grease to increase the contact stiffness between both surfaces. It is necessary to make sure that the hole in the structure is perpendicular and that the contact surface is smooth. A drawback with this type of fixation is that the holes driven into the structure remain there after the measurements are performed, which is not always allowed depending on the object to be measured. Moreover and in particular for thin or fragile structures or materials, structural integrity could be affected when modifying the object to be measured by removing material and screwing studs into it.
2. **Beeswax:** to stick the accelerometer onto the structure, a thin layer of beeswax can also be used. Limitations of this type of attachment are its sensitivity to temperature (not feasible to use it for temperatures above 40°C), and to amplitude levels (when attaching them to clean surfaces, it can be used up to levels of about 100 m/s^2).
3. **Cement:** when drilling holes into the experimental structure is not possible, cement can also be used instead. It is recommended to use epoxy and cyanoacrylate types of cement.
4. **Isolated studs and mica washers:** recommended types of fixations when electrical isolation of the accelerometer from the object is required (i.e. in order to prevent ground loops).
5. **Permanent magnet:** applicable for flat magnetic surfaces. The magnet also electrically isolates the accelerometer. Even though the resonant frequency is reduced when using this type of fixation, it is still reasonably high even for accelerations up to 1000 or 2000 m/s^2.
6. **Hand held:** suitable for quick-look survey work. Due to its low stiffness, it introduces a lot of errors and is just suitable up to 1 kHz. According to (IEEE, 1999), this method is generally not recommended.
7. **Vacuum mounting:** it requires smooth surfaces and an external device to remove the air from the suction cup. Most of the times, it is practically difficult to perform.
8. **Double-sided adhesive disk:** suitable when the thickness as well as the material properties of the tape influence the transducer's operation region.
9. **Quick mount:** when an important issue is to experimentally determine the resonance and amplitude limits for the mount used.

The described mounting methods are shown in Fig. 2.4 and their performance is compared according to (ISO, 1998) in Fig. 2.5.

A discussion on the type and fixation of the transducers' cable is presented in the standard (ISO, 1998). According to the latter source, the cable should:

- Not be stiff, in order to avoid additional (unwanted) strain.
- Be properly fixed (e.g. using tape), since the loose cables may introduce tribo-electric effects (for piezoelectric type transducers), or also contribute to the acceleration recorded due to unwanted rebounds of the wires against the structure. A recommended clamping of the cables is shown in Fig. 2.3.

2.2.4 Calibration of accelerometers

According to the International Bureau of Weights and Measures (BIPM, 2008), calibration is the operation that, under specified conditions, in a first step, establishes a relation between the quantity values with measurement uncertainties provided by measurement standards and corresponding indications with associated measurement uncertainties (of the calibrated instrument or secondary standard) and, in a second step, uses this information to establish a relation for obtaining a measurement result from an indication. A calibration may be expressed by a statement, calibration function, calibration diagram, calibration curve, or calibration table. In some cases, it may consist of an additive or multiplicative correction of the indication with associated measurement uncertainty. It is also stated in the latter reference that calibration should not be confused with adjustment of a measuring system, often mistakenly called self-calibration, nor with verification of calibration. Matters related with calibration can be found in the

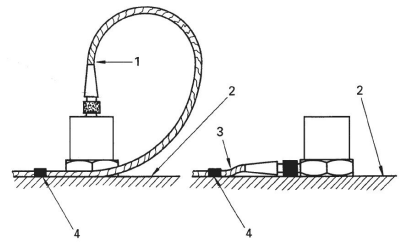

Fig. 2.3: Cable fixation for accelerometers with axial and radial connectors after (ISO, 1998). 1 and 3: transducer cable (not too tight so as to not influence the connection between cable and transducer), 2: structure to be measured, 4: fixation of cable to the surface to avoid rebounds.

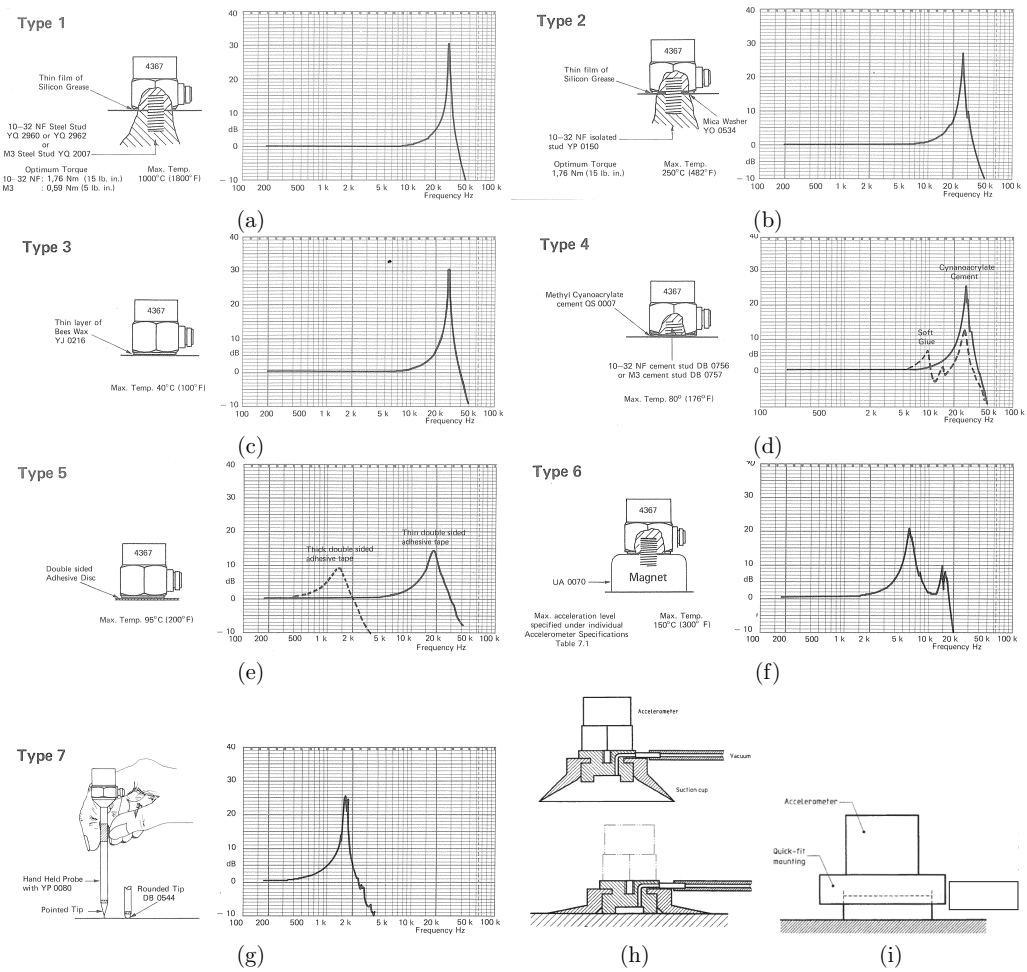

Fig. 2.4: Typical frequency responses for mountings using: (a) a threaded stud; (b) isolated threaded stud and mica washer; (c) thin even layer of bees wax; (d) methyl cyanoacrylate cement; (e) double sided adhesive disc; (f) permanent magnet; (g) hand-held probe (reproduced from (Bruel&Kjaer, 1978)); (h) vacuum mounting; and (i) quick mount discussed in (ISO, 1998).

	Resonance frequency	Temperature	Mass of transducer and stiffness of mounting	Resonance magnification factor Q	Importance of surface preparation
Stud	●	●	●	●	●
Methylcyano acrylate cement	●	●	●	●	◑
Beeswax	◑	○	◑	●	●
Double-sided tape	○	◑	○	○	●
Quick mount	◑	●	◑	◑	◑
Vacuum mounted	◑	●	●	◑	◑
Magnet	◑	●	○	○	●
Hand held	○	○*)	○	○	○

*) Depends entirely on distance between hand and measured surface.
Key: ● high ◑ average ○ poor

Fig. 2.5: Mounting methods criteria according to (ISO, 1998).

international standard (ISO, 2003).

In order words, and referred to the transducers dealt with in this report, calibration is performed in order to determine the correct sensitivity of a particular accelerometer, since, in general, each transducer has its own sensitivity (due to manufacturing, material variabilities, etc.). The sensitivity is normally frequency dependent. According to (Bruel&Kjaer, 1978), the following calibration procedures can be distinguished:

- **Use of calibration chart:** the so-called theoretical calibration, suitable for most general purpose measurements. The sensitivity value in the calibration chart is based on factory calibration. As stated in (Bruel&Kjaer, 1978), the accuracy of the factory calibration is better than $\pm 2\%$ and includes the influence of the connection cable supplied with the accelerometer.
- **Calibration using constant acceleration:** the sensitivity is determined from measurements of the peak output voltage by exciting the transducer with a known value. If an RMS indicating instrument is used, then the overall sensitivity corresponds to the RMS voltage measured multiplied by $\sqrt{2}$ (Bruel&Kjaer, 1978). In general, the input value employed is 10 ms^{-2}, e.g. using an accelerometer calibrator type B&K 4294, providing 10 ms^{-2} RMS at frequency 159.2 Hz (1000 rad/s). As noticed in (Bruel&Kjaer, 1978), the accuracy of the 10 ms^{-2} peak reference level of the B&K 4291 is $\pm 2\%$.
- **Back-to-back calibration:** the method can be described as a comparative method. It involves coupling the accelerometer to be calibrated as close as possible to a double-ended standard accelerometer for which its sensitivity over the frequency range in known; and driving the coupled pair with a shaker, carrying out a frequency sweep for the whole frequency response. Since they are tightly coupled together, they will both experience the same motion, thus the calibration being done by comparing both responses by measuring the output voltage and also taking into account that the ratio between their sensitivities is known:

$$S(f)_{\text{unknown}} = S(f)_{\text{ref}} \frac{V(f)_{\text{unknown}}}{V(f)_{\text{ref}}}, \tag{2.2}$$

where $S(f)$ is the frequency-dependent sensitivity and $V(f)$ the output voltage for each frequency of the accelerometer in question (unknown or reference). The calibration accuracy achieved can well be better than 2%. The method is described in (ISO, 2003). A discussion on uncertainties involved is presented in the standard as well. This is the method that was chosen to carry out the

calibration of the MEMS capacitive accelerometers developed in this report, thus a more precise description of it taken up later on.

The calibration process can also be classified according to the following criteria (Bruel&Kjaer, 1978):

- **Comparison method:** for example, the back-to-back calibration, where an unknown accelerometer is mounted as close as possible to a reference one, the vibration generator being carefully controlled. Accuracies better than 2% can be obtained.
- **Absolute method:** two methods can be distinguished, both having an accuracy of about 0.5% (Bruel&Kjaer, 1978):
  - Reciprocity calibration method: is based on the principle that reciprocal correspondence exists between transducers which are reversible, passive and linear.
  - Interference method: it uses laser interferometry, where the interference between two laser beams is used to determine the acceleration level. It is considered as a rapid and accurate calibration method (Bruel&Kjaer, 1978).

It must be noted that the accelerometer calibration should be done together with the pre-amplifier to be used. Although it is true that the pre-amplifier's uncertainty is usually low enough to not alter too much practical measurements, it has also its own uncertainty and should therefore be accounted for in order to increase accuracy.

2.2.5 MEMS calibrations methods

Some standardised ways to calibrate the MEMS accelerometers are presented in (IEEE, 1999) (Annex K and L) and in its updated version (IEEE, 2008). In general terms, two different methods for calibrating MEMS can be distinguished; one static and one dynamic.

Calibration using acceleration due to gravity

The widely applied method for MEMS calibration is to use gravitational acceleration. This method is also proposed by the manufacturers (Analog Devices, 2000, 2010).

Apart from some basic knowledge about calibration, acceleration due to gravity is also dealt with in (Carver and Looney, 2008). There, a two-axial sensor is fixed vertically and rotated $90°, 180°$ and $270°$ respectively, while recording the accelerations produced (Fig. 2.6a). When rotating, the output is sinusoidal with regard to the angle (Fig. 2.6b). In the figure, the ideal signal is shown with zero off-set and amplitude equal to 1 g. Comparing both measured and ideal results, the gain (sensitivity) and off-set (bias) can be determined. This method, however, is static and no frequency dependence is investigated (read-outs of the g-values are done after rotation at angles $90°, 180°$ and $270°$). As noticed in (Carver and Looney, 2008), perfect vertical alignment and precision in initial angle estimation is crucial to get correct results of sensitivity. A similar procedure to this one was used also in (Stein et al., 2007), where a tri-axial MEMS accelerometer was used instead. Discussions on this so-called "tumble test" are presented in (IEEE, 1999) (Annex K).

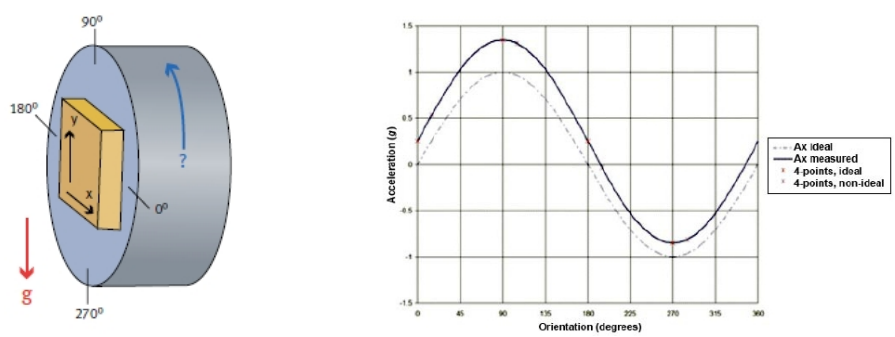

(a) (b)

Fig. 2.6: (a) Set-up used for calibration; (b) sinusoid (ideal and measured) fitted from 4 points measured (Carver and Looney, 2008).

Calibration in the frequency domain

Calibration in the frequency domain is analysed in e.g. (Badri et al., 2010), Fig. 2.7. In there, the back-to-back calibration (using a PCB integrated circuit piezoelectric accelerometer) is presented. An electrodynamic shaker was employed, with a sweep signal of rate 2.5 kHz/s. For verification, a pure sine signal was used as well (testing frequencies 20 Hz, 145 Hz and 377 Hz).

Some notes to frequency domain calibration of MEMS devices are summarised also in (IEEE, 1999) (Annex L), where the recommended sweep-rate to be used is 4 Hz/s.

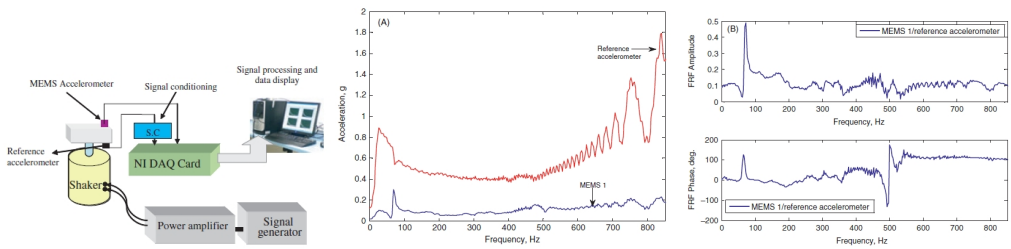

(a) (b) (c)

Fig. 2.7: (a) Set-up used for calibration; (b) acceleration measured; (c) corresponding frequency response function and phase plot (Badri et al., 2010).

3
MEMS accelerometers

In this chapter, an overview of the construction of the MEMS accelerometers developed is presented and the issues related to it discussed. Moreover, the principle and procedure of calibration is presented.

3.1 Introduction

In Fig. 3.1, a general capacitive accelerometer structure and its corresponding lumped mass model can be seen. Capacitive acceleration sensors have several attractive features: they have excellent sensitivity, the transduction mechanism is intrinsically insensitive to temperature and also independent of the base material. The lumped mass model in Fig. 3.1 depicts a typical MEMS accelerometer composed of a movable proof mass M with plates attached through a mechanical suspension system with stiffness K and damping D to a reference frame. As the external acceleration displaces the supporting frame, the internal stress in the suspension spring changes. The relative displacement $(y - z)$ can be measured as a change in capacitance (i.e. a change in the output voltage), giving a measure of the external acceleration.

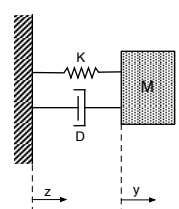

Fig. 3.1: General capacitive accelerometer structure and its corresponding lumped mass model.

3.2 Description of sensors

The MEMS accelerometers chosen for this study are the ADXL-202 and the ADXL-203 (Analog Devices, 2000, 2010). The sensor used in both types of MEMS is a dual-axis accelerometer with signal conditioned voltage outputs; the operating principle is capacitive measurement with a moving mass. A connection circuit diagram for the accelerometer ADXL-203 can be seen in Fig. 3.2. As aforementioned, the sensor measures acceleration by sensing changes in capacitance when the geometry of the capacitor is changing (either the area of the electrodes, the distance between them or the permittivity of the separating material) (Lyshevski, 2002). Table 3.1 shows some of the specifications of the two types of MEMS accelerometers utilised. Some additional notes on the accelerometers used are:

- The output signal is an analogue voltage signal (i.e. not a digital one).
- All the necessary electronics (condenser and the like) are packed within a small plastic casing.
- The power supply is 5 V DC, provided by an in-house built connection box (cf. Fig. 4.1r).
- For matters of fixation, two legs are built-in. In this way, the accelerometer can be attached to the host structure using screws. Also, wax can be used instead as mentioned in Section 2.2.3 if the structure to be measured cannot be damaged.
- The cable is rather thick as it needs to have 4 channels: two devoted to the $x-$ and $y-$signals and two for power supply.
- The cut-off frequency is determined by the choice of capacitor (C_X for measurement in the $x-$direction and C_Y in the $y-$direction), see Fig. 3.2.

Table 3.1: Specifications of the ADXL-202 and 203 accelerometers (Analog Devices, 2000, 2010).

	ADXL-202	**ADXL-203**
Measurement range	±2 g	±1.7 g
Sensitivity	312 mV/g	1000 mV/g
Noise density	500 $\mu g/\sqrt{Hz}$	110 $\mu g/\sqrt{Hz}$
Sensor resonant frequency	10 kHz	5.5 kHz

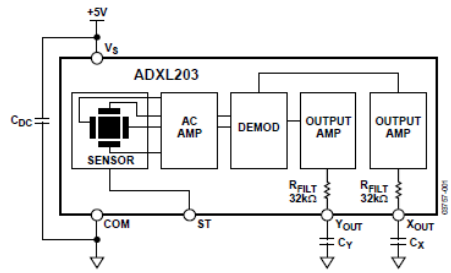

Fig. 3.2: Connection circuit diagram for MEMS accelerometer ADXL-203 (Analog Devices, 2010). The ADXL-202 has exactly the same layout and components, a different chip being used instead.

3.3 Construction

The ADXL-203 is factory packaged in a Ceramic Leadless Chip Carrier (LCC) package of size 5×5×2 mm^3. The package is mounted to a printed circuit board (PCB) as shown in Fig. 3.3b. On the PCB, capacitors determining the bandwidth of each channel are mounted. To amplify the signals, channels are connected to an STMicroelectronics TS922IN operational amplifier. A 4-lead cable is attached to the PCB and the complete setup is mounted in a casing which is filled with epoxy. The finished system can be seen in Fig. 3.3a, where also the mounting clips on each side of the capsule are shown. The PCB with the accelerometer chip is mounted sideways in the capsule; this way the orientation of the sensor will be x in the in-plane direction and y in the out-of-plane direction, as observed in Fig. 3.4a. The bandwidth selection, i.e. the capacitance of the capacitors C_x and C_y, influences the RMS noise of the transducer as shown in Fig. 3.4b. Note that to avoid aliasing effects, the maximum bandwidth is 2.5 kHz. To decouple the sensor from noise from the power supply, a 0.1 μF capacitor C_{DC} is mounted, as shown in Fig. 3.2.

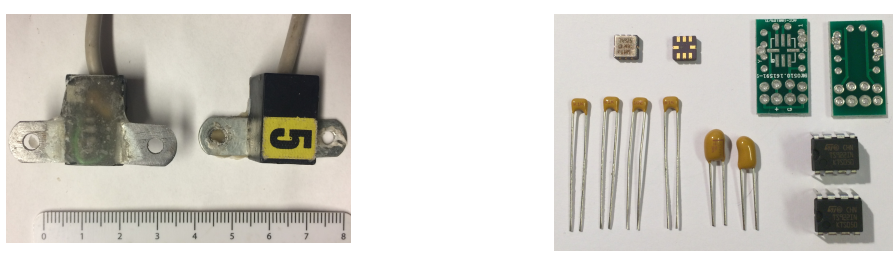

(a) (b)

Fig. 3.3: (a) Finished sensors. left: bottom side, right: top side. Note the PCB visible from the bottom; (b) parts required for building two sensors.

(a) (b)

Fig. 3.4: (a) Orientation of the sensor directions; (b) RMS noise as function of selected bandwidth for the ADXL-203.

4 Apparatus

During the report, different equipment (namely sensors, power supply, excitation sources, etc.) will be referred to. In this chapter, all the apparatus employed during the course of this work are listed below.

4.1 Apparatus used

The laboratory equipment used in the calibration process described in this report is:

MTS 810 (Fig. 4.1a): material testing machine used at LU.
- Versatile, multi-purpose servo-hydraulic testing system.
- Both for static and dynamic material and component testing.
- Waveforms available are: sine, square, triangle, ramp, or user-defined.
- The upper frequency limit is 50 Hz.
- A typical response curve is shown in Fig. 4.2a.

Spectrum computing M2i (Fig. 5.1b): data acquisition system.
- Input: only analog signals.
- 16 channels 250 kSamples/s 16-bit 125 kHz max bandwidth.
- Control and post processing is done in SBench 6 (Spectrum, 2015) with export possibilities into MATLAB.

Bruel & Kjaer PULSE (Fig. 4.1b): data acquisition system.
- Input: only analog signals (voltage signals up to 7 V peak input).
- Limit of PULSE license used at DMME AAU: 4 input and 2 output channels, FFT, CPB, Time data recorder.
- Control and post-processing of measurements can be done either in B&K PULSE LabShop or B&K PULSE REFLEX.
- Both LabShop and REFLEX allow to do post-processing/export also into MATLAB.

Bruel & Kjaer 7541 (Fig. 4.1c): vibration controller.
- Input: only analog signals (voltage signals up to 20 V peak).
- Limit of PULSE license used at DMME AAU: 2 input and 1 output channels.
- The PC interface using B&K Vibration control software.
- Random noise and sine/sweeped sine control up to 2 kHz.

Bruel & Kjaer 4809 (Fig. 4.1d): electrodynamic shaker at DMME AAU.
- Bottom frequency: 20 Hz.
- Maximum force: 44.5 N.
- Maximum acceleration: 75 g.
- Maximum displacement: 8 mm (peak-to-peak).
- Very low cross-motion (below 1% throughout the frequency range (Bruel&Kjaer, 1972)).
- A frequency response function (for a constant feeding voltage) is shown in Fig. 4.2f and load rating curves are presented in Fig. 4.2g.

Bruel & Kjaer 4808 (Fig. 4.1e): electrodynamic shaker at LU.
- Bottom frequency: 5 Hz.
- Maximum force: 112 N.
- Maximum acceleration: 71 g.
- Maximum displacement: 12.7 mm (peak-to-peak).

Bruel & Kjaer 4824 (Fig. 4.1f): electrodynamic shaker at LU.

- Bottom frequency: 2 Hz.
- Maximum force: 100 N.
- Maximum acceleration: 44 g.
- Maximum displacement: 25.4 mm (peak-to-peak).

Bruel & Kjaer 4291: vibration calibrator.

- Horizontal operating position.
- A correct weight of the calibrated transducer needs to be adjusted.
- Excitation with a single sine acceleration of frequency 79.4 Hz and amplitude 1 g.

Bruel & Kjaer 4294: vibration calibrator.

- Vertical operating position.
- No transducer weight adjustment is required (it is done automatically).
- Excitation with a single sine acceleration of frequency 159.2 Hz and RMS value 10 m/s^2.

Bruel & Kjaer 8305 (Fig. 4.1g): reference accelerometer.

- Flat frequency response (Fig. 4.2b).
- Not calibrated with a pre-amplifier (calibration just of the accelerometer). For more precise calibrations, it needs to be calibrated together with the pre-amplifier it is to be used with.

Bruel & Kjaer 4371 (Fig. 4.1j): a general purpose DeltaShear, uni-gain piezoelectric accelerometer.

- Its typical charge sensitivity is 1 pC/m s^{-2}.
- Side connector, i.e. another accelerometer can be attached on the top flat surface using e.g. glue or wax.
- A typical calibration curve is presented in Fig. 4.2c.

Bruel & Kjaer 4384V (Fig. 4.1k): a general purpose DeltaShear, Unigain piezoelectric accelerometer.

- Its typical charge sensitivity is 1 pC/m s^{-2}.
- Top connector.
- A typical calibration curve is presented in Fig. 4.2d.

Bruel & Kjaer 4374 (Fig. 4.1l): miniature charge accelerometer.

- The cable is permanently attached.
- Typical charge sensitivity is 0.15 pC/m s^{-2}.
- A typical calibration curve is presented in Fig. 4.2e.

Bruel & Kjaer 4507 001 (Fig. 4.1m): piezoelectric CCLD accelerometer.

- Built-in pre-amplifier.
- Typical sensitivity is 10 mV/g.

Bruel & Kjaer 4332 (Fig. 4.1n): charge accelerometer.

- Its typical charge sensitivity is 50 pC/g.
- Side connector.

Bruel & Kjaer 4524 B (Fig. 4.1o): triaxial CCLD accelerometer.

- Triaxial accelerometer with a built-in pre-amplifier.
- Typical sensitivity is 100 mV/g.

Bruel & Kjaer 2647A (Fig. 4.1h): charge to DeltaTron converter.

- Simple use (no settings required, just connected between the accelerometer and DAQ).
- CCLD: power supply provided directly from the B&K PULSE.
- Gain: 1 mV/pC.

Bruel & Kjaer 2626 (Fig. 4.1i): charge amplifier.

- Alternative to Bruel & Kjaer 2647A.
- The sensitivity is set in the amplifier, i.e. the output is unit voltage (or its multiples).
- In the past, the B&K 8305 was calibrated together with 2626 as a part of calibration set-up.
- The calibration sheet of B&K 8305 provides sensitivity without amplifier, so for more precise measurements, calibration of the reference accelerometer with the pre-amplifier is required.

Bruel & Kjaer 2706 (Fig. 4.1p): power amplifier for electrodynamic shaker Bruel & Kjaer 4809.

- Amplitude, damping control.
- Clipping (visualisation of distorted signal).

Bruel & Kjaer 2734 (Fig. 4.1q): power amplifier used at LU.

- A power amplifier used with shakers Bruel & Kjaer 4808 and 4824.

Connection box (Fig. 4.1r): in-house power supply/connection box built at LU.

- 5V DC supply to each accelerometer.
- 16 channels for dual axial accelerometers (32 channels).

Fig. 4.1: (a) Material testing system MTS 810; (b) Data acquisition system B&K PULSE; (c) Vibration controller B&K 7541; (d) Electrodynamic shaker B&K 4809; (e) Electrodynamic shaker B&K 4808; (f) Electrodynamic shaker B&K 4824; (g) Reference accelerometer B&K 8305; (h) Charge-to-DeltaTron Converter B&K 2647A; (i) Charge amplifier B&K 2626; (j) Accelerometer B&K 4371; (k) Accelerometer B&K 4384V; (l) Accelerometer B&K 4374; (m) Accelerometer B&K 4507 001; (n) Accelerometer B&K 4332; (o) Accelerometer B&K 4524B; (p) Power Amplifier B&K 2706; (q) Power Amplifier B&K 2734; (r) in-house made connection box for MEMS accelerometers (with built-in power supply).

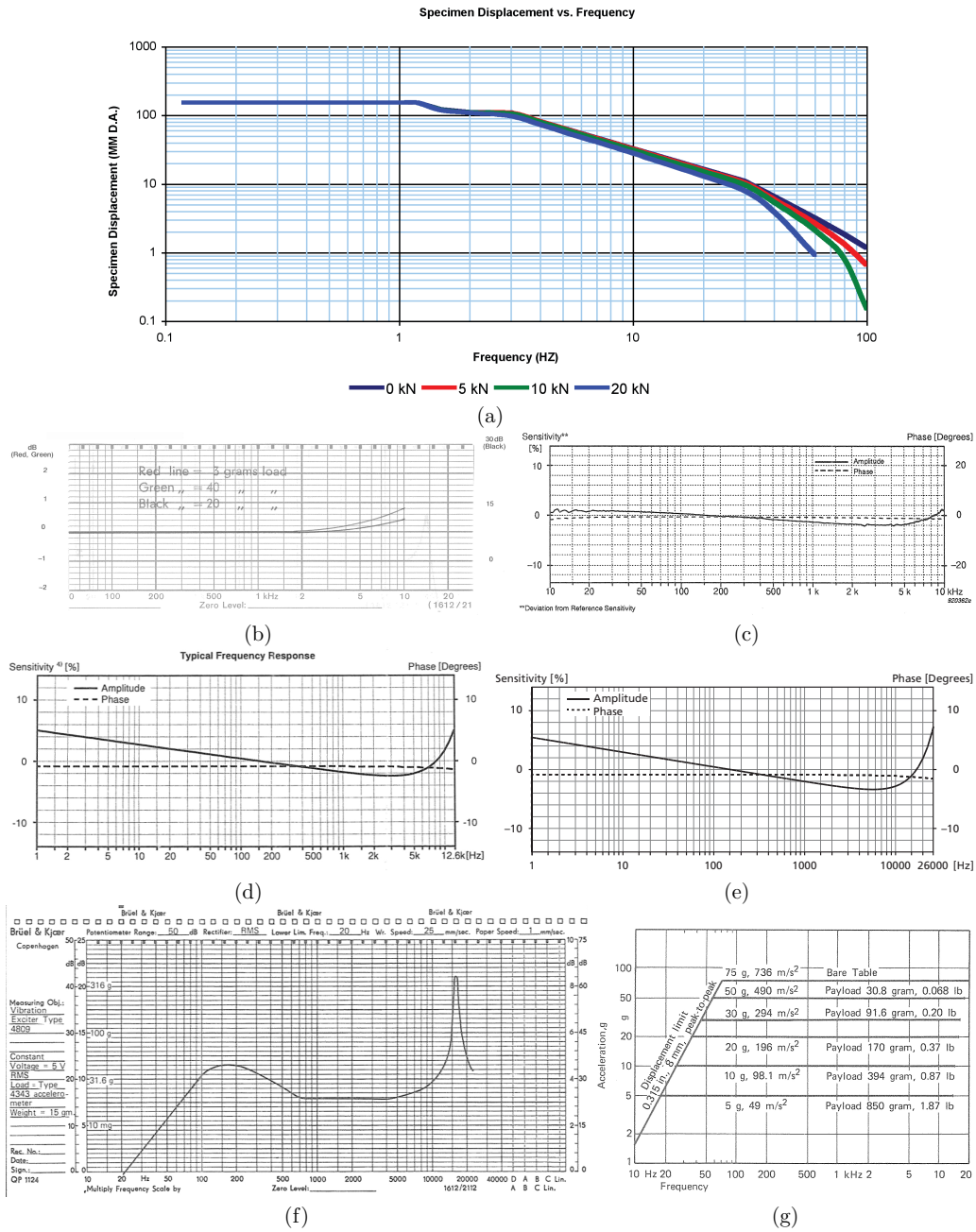

Fig. 4.2: (a) Frequency response curves of MTS 810 (MTS, 2006); Calibration curves for: (b) reference accelerometer B&K 8305; (c) multi-purpose accelerometer B&K 4371 and (d) B&K 4384V; (e) a miniature accelerometer B&K 4374; (f) and (g) a frequency response and load rating curves for a shaker B&K 4809 (Bruel&Kjaer, 1972).

5 Calibration using the MTS machine

The Material Testing System (MTS) is a versatile, calibrated multipurpose servo-hydraulic testing system for both static and dynamic material and component testing. The MTS 810, used in the first steps of these calibrations experiments, can be seen in Fig. 5.1a. The machine can easily be set up to perform any material test needed. Different materials such as plastic, aluminum, composites and even steel can be tested in different ways, namely tension, compression, fatigue, mechanical fracture and durability tests, for example (MTS, 2006).

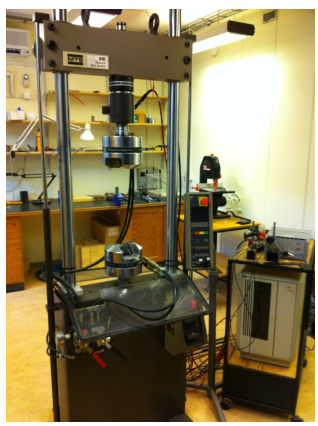

(a)

(b)

Fig. 5.1: (a) MTS 810 used at LU; (b) M2i4711 DAQ Card.

5.1 MTS Measurements

After the mounting of the transducers, the MTS was used to perform the very first calibration steps of the MEMS accelerometers under investigation here. The MTS machine, as a calibration device, is a very accurate but also a time consuming method, as the calibration has to be made with a constant sine excitation, which in turn needs to be repeated for various frequency values to obtain a frequency dependent calibration curve.

5.1.1 Equipment and measurement set-up

The equipment used for these first tests was the MTS 810 machine and the Spectrum computing M2i data acquisition card (DAQ) (see Section 4.1). A 20 mm thick steel plate was attached to the wedges of the MTS machine, which was driven vertically at a single (constant) frequency. The displacement of the plate is measured by the sensors built into the MTS machine. An array of 10 accelerometers was attached onto the aforementioned steel plate using nuts and bolts to ensure a fixed connection, all of them were connected to a computer with a DAQ (cf. Fig. 5.1b). The acceleration acquired by each accelerometer when driving the plate with the MTS machine were saved as MATLAB (.mat) files for post-analysis. As

the time history of the movement is registered by the MTS machine, the acceleration measured by the accelerometers can be calibrated against the movement as measured by the calibrated MTS machine. The software used for the acquisition was Spectrum SBench 6.1 from Spectrum computing (Spectrum, 2015). The acceleration and movement was recorded for 11 seconds with a sampling frequency of 5 kHz. A schematic of the setup can be seen in Fig. 5.2.

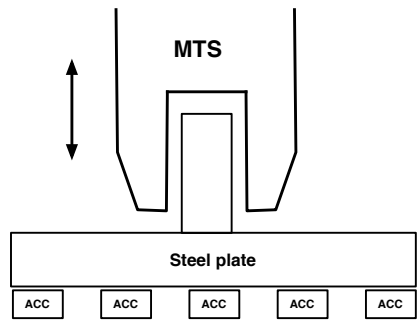

Fig. 5.2: Schematic of the measurement setup, the double arrow indicates the direction of travel.

5.1.2 Limitations

Using the MTS machine to perform calibrations proved to be a fairly accurate method. However, there are some drawbacks. The MTS machine can not be run above 50 Hz due to mechanical limitations in the system. This means that the calibration can only be performed for the very lowest frequencies. Moreover, the calibration is also very time consuming in the set-up of the accelerometers and the fact that the calibration must be performed for a single frequency per time.

5.2 Discussion on results

The signal-to-noise ratio of the data recorded was low. Thus, some sort of filtering was needed to reduce the amount of noise in the signals. The measured data were exported from MATLAB as `.wav` files (using the command `wavwrite(AI_Ch00,fs,'AI_Ch00');` f_s being the sampling frequency, 5 kHz in this case) and imported into B&K PULSE REFLEX to enable easy application of a filter. There, the simple band-pass filter was used setting the cut-off frequencies as close to the excitation frequency as possible, i.e. $f_{cL} = 9.99$ Hz and $f_{cH} = 10.01$ Hz for data measured at $f_e = 10$ Hz (cf. Fig. 5.3).

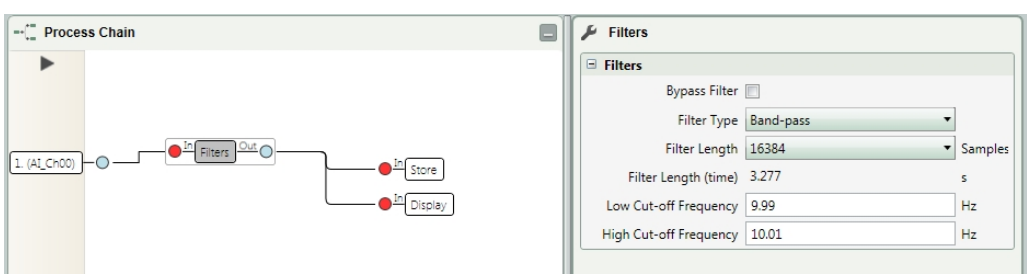

Fig. 5.3: Filter used in B&K PUSLE REFLEX environment.

The filtered data were processed back into MATLAB. As a first step, the amplitude at the excitation frequency (in the presented case 10 Hz) had to be found. This can be done in two principal ways:

- Analysis of peak-to-peak value: basically, minimum and maximum values are found in MATLAB and the amplitude is re-calculated. This method is not recommended, as small ripples (modulation of frequencies or filter error) are present in the signal even after filtering.

- Analysis of the amplitude in the FFT of the filtered signal: a crucial point in the FFT is the choice of the sample width and weighting (windowing) function. But when correct parameters are chosen, the FFT can be more precise and therefore decouple the ripples from the analysed signal.

The idea was to apply a rectangular window to the "ideal" signal, for which no distortion (attenuation) is introduced. However, as discussed in (Quach, 2011) and shown in Fig. 5.4, it is important that the sine wave analysed starts and ends in the same point, i.e. no discontinuities are introduced.

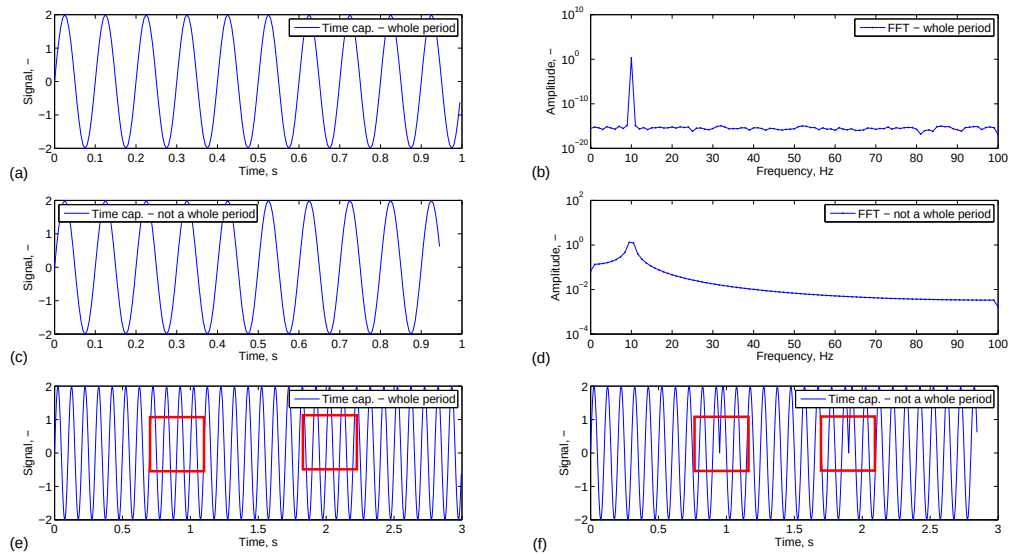

Fig. 5.4: Example of spectral leakage: (a)-(b) ideal sinusoid signal - whole period; (c)-(d) non-ideal sinusoid end (some delay); (e)-(f) comparison of three signals in a row, the rectangles show points where signals are merged. In the case (e) (ideal - whole period) no discontinuity is noticeable, but in (f) the discontinuity is obvious.

When analysing the filtered data, the signal was properly cropped in MATLAB so that a multiple number of periods were captured. Thus, ideally, no spectral leakage would occur after applying the rectangular window. As presented in Fig. 5.5, the FFT shows a purely tonal frequency at 10 Hz with minimal leakage around for a given analysed frequency, although some small ripples can, nevertheless, be noticed when zooming into the filtered signal. Comparing the maximum amplitude and the amplitude at 10 Hz of the FFT spectra:

- Peak value from the time signal: $A = 2.9063 \times 10^{-4}$.
- Amplitude from the FFT signal: $A = 2.884 \times 10^{-4}$.[1]

The error when comparing both methods is about 0.77%. To increase the accuracy of the FFT, one could possibly make the time signal longer, or also more samples of signal one on top of another could be stacked.

5.3 Conclusions

It can be concluded that even if accurate calibration results using the MTS could be achieved, it is not a practical method due to mainly four reasons:

- The MTS is a slow machine and can therefore not excite frequencies above 50 Hz. Even though the applications the MEMS are intended for will be low frequency vibrations in wood buildings (cf. Chapter 1) it is of interest that the upper frequency limit lies somewhere around 200 Hz to increase the reliability of the data acquired.

[1] When exporting into *.wav*-file, it was necessary to scale the measured data by 10^{-5}. The limitation of the *wavwrite()* function can be found in the MATLAB help (MathWorks, 2010).

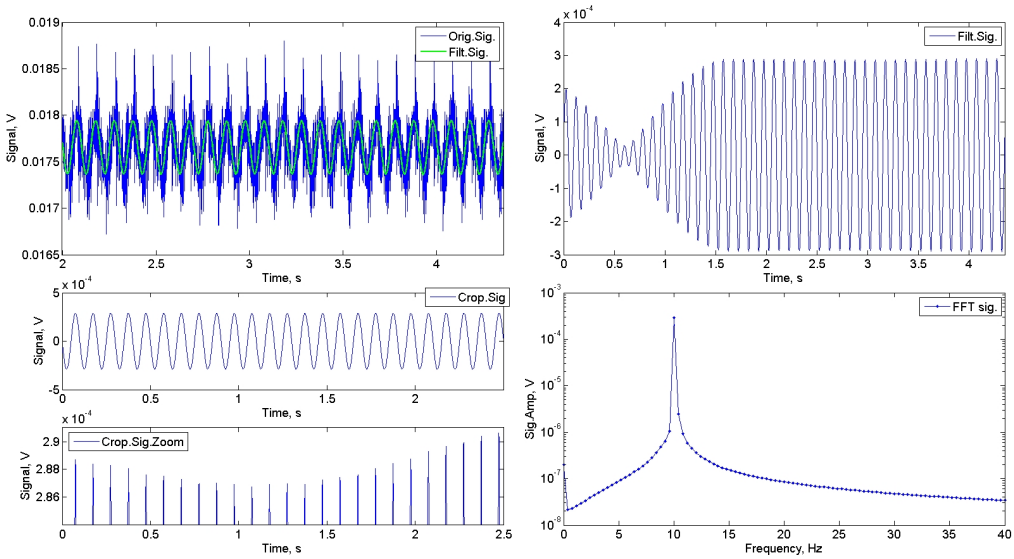

Fig. 5.5: Signal before and after filtration (Orig.Sig and Filt.Sig., respectively), cropped signal (Crop.Sig.) and zoom (Crop.Sig.Zoom) to show the ripples in amplitude and the FFT of the filtrated and cropped signal (FFT sig.).

- Furthermore, the method is not practical, since calibration based on single frequencies must be carried out.
- Filtration of signals is required due to the low signal-to-noise ratio of the data acquired, hence making the method even more time consuming.
- Lastly, one should perform some calculations addressing structural dynamic issues about the characteristics of the plate the array of accelerometers is attached to when performing the calibration. It should be assured that the fundamental mode of vibration of the plate is much higher than the upper frequency limit of calibration allowed by the MTS. Otherwise, the results could be affected by this dynamic unwanted behaviour.

6 Pre-measurements at AAU

In order to test the equipment at AAU and verify the settings of the apparatus involved, a set of preliminary measurements was carried out as described in this chapter.

6.1 Verification of the calibration procedure using a shaker

The aim here was to verify the methodology involved when using a swept sine excitation for the back-to-back calibration. Thus, no MEMS are being analysed thus far, but rather accredited calibrated accelerometers. A sweep sine signal from 50 Hz up to 1.6 kHz with a sweep rate of 4 Hz/s and linear variation was first applied to the electrodynamic shaker B&K 4809.

In Fig. 6.1, the results in form of an autospectra of both signals (the one from the reference accelerometer B&K 8305 and the one to be calibrated B&K 4371) are plotted. Moreover, the bottom plot in Fig. 6.1 presents the ratio between the two latter signals. Only the FFT license was used at this stage in B&K PULSE, i.e. no feedback loop control of the shaker was done. Therefore, the autospectra measured when the electrodynamic shaker was fed with a constant voltage (Fig. 6.1 up) follows the frequency response of the shaker provided by B&K (Fig. 4.2f). Since the response is not flat, the difference between the signals is not constant (Fig. 6.1 down). Hence, it is recommended to use some feedback loop control in order to idealise the excitation.

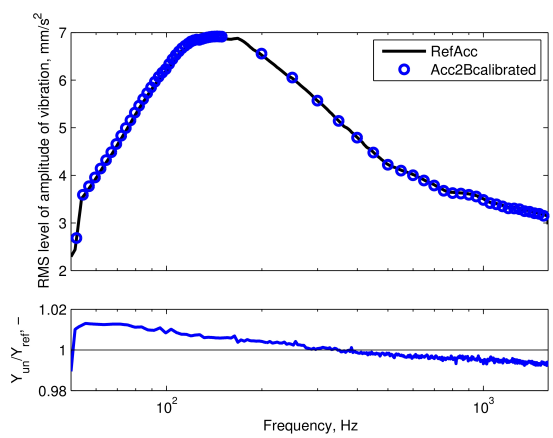

Fig. 6.1: Preliminary results measured with open-loop control (i.e. constant excitation voltage).

6.2 Calibration of the reference accelerometer B&K 8305

In order to see if the sensitivity of the accelerometer B&K 8305 (which will eventually be used as reference for the MEMS calibration using the back-to-back method) provided by the manufacturer in the calibration sheet had remained constant since it was performed, the accelerometer was calibrated using the accelerometer calibrator B&K 4291 (Fig. 6.2a-b). The operating position of this calibrator

(a) (b)

Fig. 6.2: (a) Set-up with B&K 4291 used for the B&K 8305 test calibration; (b) the calibrator B&K 4291.

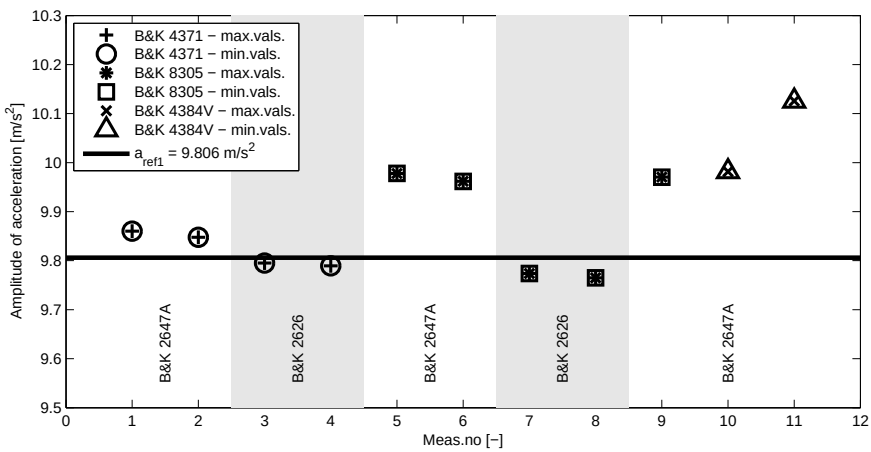

Fig. 6.3: Comparison of all amplitudes of the filtered signal measured for each combination of accelerometer/pre-amplifier. The accelerometer calibrator B&K 4291 was used.

is horizontal and it excites the accelerometer with a peak acceleration level of 1 g, i.e. 9.806 m/s^2, at 79.4 Hz. It is very important to adjust the weight of the accelerometer in the calibrator correctly to be sure that the reference level is indeed 1 g, since otherwise this could lead to additional errors.

The signal from the accelerometer was recorded in the time domain. To estimate the amplitude, minimum and maximum values of the waveform of the filtered signal are used for the calibration, as presented in Fig. 6.3. For the measurement procedure verification, two additional piezoelectric accelerometers (B&K 4371 and B&K 4384V) were used as well. The accelerometers were connected either to the Charge-to-DeltaTron Converters B&K 2647A (Fig. 4.1h), or to a Charge Amplifier B&K 2626 (Fig. 4.1i).

The results obtained and presented in Fig. 6.3 are not very consistent as well as are dependent on the accelerometer used (e.g. on the mass settings of the calibrator B&K 4291). Moreover, the B&K 4291 operates in a horizontal way, i.e. for heavier/larger accelerometers the influence of gravity could also be a reason for calibration errors. Instead, a calibrator with automatic adjustments would be preferred, i.e. one for which is not necessary to do the mass settings and hence subjective (i.e. human) errors when setting the mass scale (cf. Fig. 6.2b) would be removed. Along those lines, an accelerometer calibrator B&K 4294 could be used, for example.

6.3 Comparison of pre-amplifiers and calibrators

The influence of the pre-amplifier employed when calibrating the accelerometer B&K 8305 was also checked in this first studies in order to avoid potential errors stemming from this source. In Fig. 6.4, it can be seen that before filtering (solid lines), the signal is noisier and high frequency components are superimposed, especially when using the Charge-to-DeltaTron Converter B&K 2647A. However, after filtering using a band-pass filter with centre frequency 79.6 Hz and width 1 Hz, those high frequency components are successfully removed. Therefore, it is more recommended to use the Charge Pre-amplifier B&K 2626 in subsequent calibrations, due to the reason that it is more stable and does not introduce that much noise.

The latter statement is also strengthened if one looks back at the previous section. The accelerometers compared in Fig. 6.3 were connected there to two different pre-amplifiers, where, as indicated in the plot:

- A Charge-to-DeltaTron Converter B&K 2647A was used for measurements no. 1, 2, 5, 6, 9-11.
- The charge pre-amplifier B&K 2626 was employed for measurements no. 3, 4, 7, 8.

The results compared in that figure reveal that more consistent and precise data are obtained when the B&K 2626 is used (measurements no. 3, 4, 7, 8). On the other hand, for the accelerometers connected to the B&K 2647A, the amplitude measured was overestimated as the measured values were larger than 1 g, i.e larger than the value applied by the calibrator. Hence, again, the amplifier B&K 2626 seems to perform better and is therefore recommended.

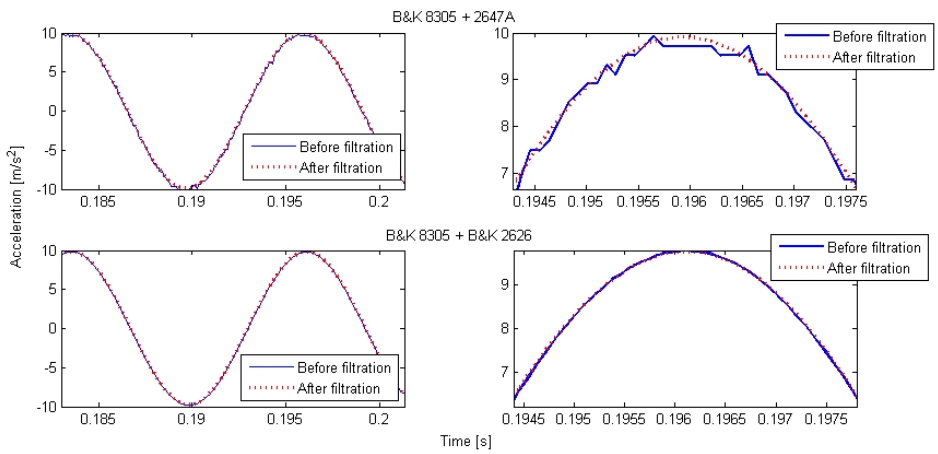

Fig. 6.4: Comparison of the measured and processed time signals using Charge to DeltaTron Converter B&K 2647A (up) and Charge pre-amplifier B&K 2626 (down).

6.3.1 Changing the accelerometer calibrator

To verify, if the calibrator B&K 4291 (cf. Fig. 6.2) works properly, a newer calibrator B&K 4294 (cf. Fig. 6.5a) was borrowed from GRUNDFOS. The advantage in using the B&K 4294 is that it has a built-in control of the vibration level. This means that it is not necessary to set manually the weight of the transducer to get the right level of excitation as well as the fact that it operates in vertical position, i.e. the transversal vibration of large and bulky transducers is minimised.

The previous calibrations using the calibrator B&K 4291 pointed out that the pre-amplifier B&K 2626 seems to be a better option than using the Charge-to-DeltaTron Converter 2647A. Another aim of this set of calibrations was also to double check this assumption and test the two B&K 2626 available at AAU. The results, presented in Fig. 6.6, show that for the calibration of the transducer B&K 8305, more precise measurements were obtained with use of the pre-amplifier B&K 2626_u1 (i.e. the first unit available in the laboratory), while the second B&K 2626 (i.e. the so-called u2) and the B&K 2647A are both at the upper limit of available calibration error. The same measurements as for the B&K 8305 were performed again for a second piezoelectric accelerometer B&K 4371. The difference between the pre-amplifiers is

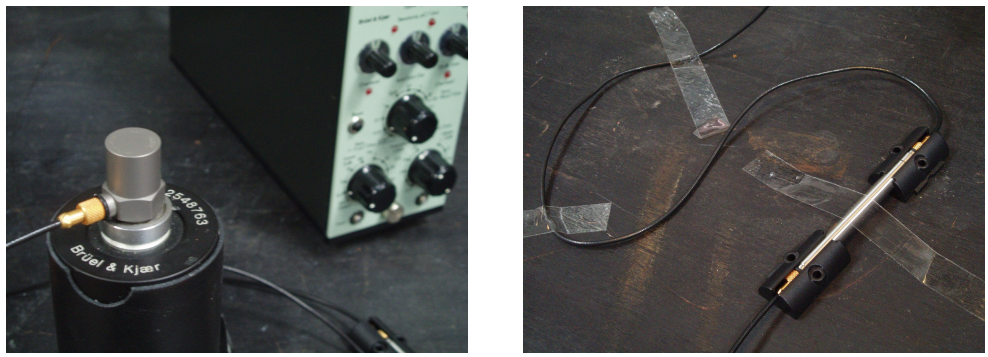

(a) (b)

Fig. 6.5: (a) The accelerometer B&K 4371 fixed onto the calibrator B&K 4294, with the pre-amplifier B&K 2626 shown in the background; (b) the Charge-to-DeltaTron Converter B&K 2647A.

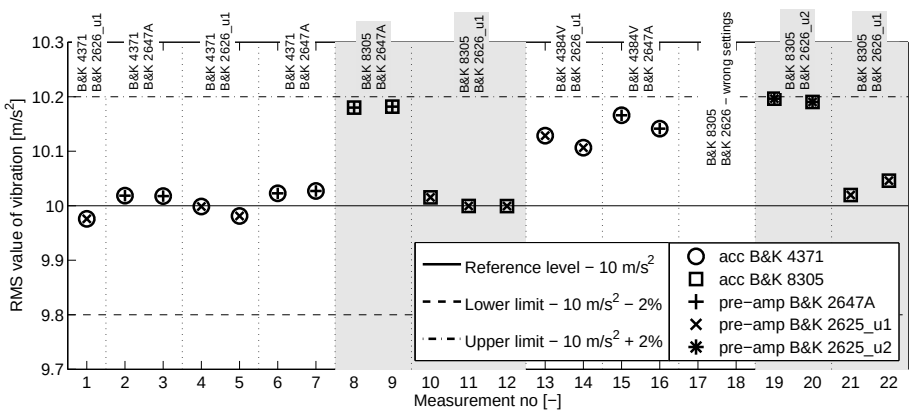

Fig. 6.6: Comparison of the amplitudes measured for each combination of accelerometer/pre-amplifier obtained using a calibrator B&K 4294. Highlighted are measurements using the reference accelerometer B&K 8305 (disregarding the measurements with wrong settings no. 17 and 18). Two pre-amplifiers B&K 2626 (labelled as B&K 2626_u1 and B&K 2626_u2 respectively) are compared as well.

in this case not so dominant. Finally, a last transducer (B&K 4384V) was tested, yielding somewhat imprecise results, i.e. it needs to be properly re-calibrated (i.e. the gain must be adjusted).

The calibrator B&K 4294 was working properly, consistently and the calibration procedure is faster, since no weight adjustments are needed (as required using B&K 4391). Also using the B&K 4294, the tests with the pre-amplifier B&K 2626 were more precise and it is less noisy than the Charge-to-DeltaTron Converter 2647A, which confirms the previous observations.

6.3.2 Comparison of the calibrators

During the tests, one extra B&K 4294 calibrator was found at AAU's laboratory. To verify, that the it still worked properly and to check if the batteries were not dying out[1], new sets of measurements were performed. Thus both the old (B&K 4291) as well as new (B&K 4294) calibrators were compared for a series of calibrations, the results obtained for the B&K 4294 being shown in Fig. 6.7a and for the B&K 4291 in Fig. 6.7b.

[1]As discussed with Dr. Sørensen (Sørensen, T., 2011), the level of acceleration should be constant even when the batteries are dying out. The only thing that could be affected is the time the calibrator is operated after switching it on. Therefore, one can rely on the data measured for all times.

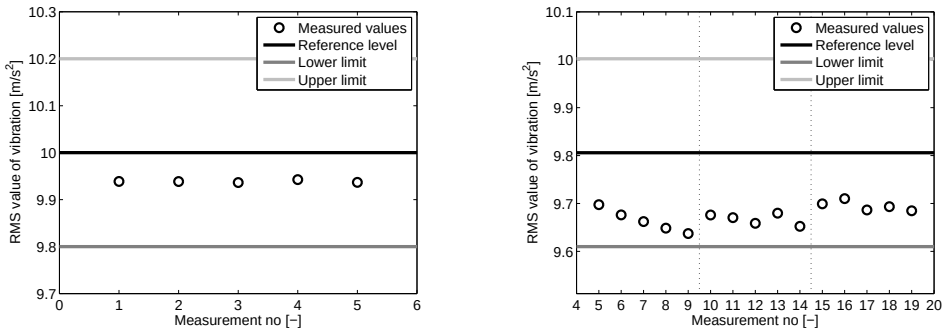

Fig. 6.7: Calibration using (a) B&K 4294 (with fixed accelerometer at all times); (b) using B&K 4291 twice adjusted the mass of accelerometer (some drifting analysed).

It can be seen that the amplitudes obtained are within the limits prescribed by B&K, i.e. they fall within the tolerances marked as upper and lower limits in Fig. 6.7. The gain analysed from B&K 4294 is 1.0061, whereas the one from B&K 4291 is 1.0099. Using the default PULSE LabShop calibration for the B&K 4291, the gain obtained was 1.007 instead.

As already stressed, before each calibration, the B&K 4291 requires to set the correct weight of the accelerometer, which introduces a potential source for additional errors. This can be observed in Fig. 6.7b, where the results have larger variation than the ones obtained for the B&K 4294 (Fig. 6.7a) and even some drifting of the weight set was observed in the first 5 measurements (no. 5-9). After those measurements, the weight value was re-adjusted. Due to this potential additional sources of errors, it is recommended to use the calibrator B&K 4294 instead of the B&K 4291 in subsequent measurements.

6.4 Conclusions

From the preliminary measurements described in the chapter, it can be concluded that the reference accelerometer B&K 8305 can be used for calibration and, together with the pre-amplifier B&K 2626, promising results are obtained, i.e. the amplitudes measured were very close to the one provided by the calibrator. Moreover, there were some inconsistency using the horizontally operated calibrator (B&K 4291), thus the vertically operated one (B&K 4294) should be used instead in subsequent calibrations.

7

Steady State Response Measurements

In order to solve the problem with having a frequency dependent excitation level when the shaker is supplied with a constant voltage input signal (i.e. open-loop control strategy), a license for Steady State Response (SSR) Analysis Type 7772 was used. The SSR analyser uses stepped sine excitation to measure steady state response. The response can be measured as a function of the excitation frequency or excitation level. The measurement system can use an adaptive scan algorithm or linear averaging, ensuring that the steady state response is measured to a user-specified accuracy in the minimum possible time (Bruel&Kjaer, 2015). All the measurements performed with the SSR license were performed using an electrodynamic shaker B&K 4809 with various SSR settings.

7.1 Multi-buffer vs. Steady-State Response

For measurements using a sine sweep type of signal as excitation, the frequency response functions (FRF) were obtained using a multi-buffer to continuously record the responses. The contour plot of such measurements, where each slice represents the frequency response at certain time period defined by multi-buffer, is shown in Fig. 7.1a. The diagonal lines represent the excitation frequency (and its harmonics/orders), from which the total frequency response was extracted. The response measured was extracted exporting contour plots to MATLAB and picking up the amplitudes of the main diagonal (the one with the largest amplitudes). The precision of the method was dependent on the time the slices were saved and sweep rate used. It was not the most ideal approach, but it provided the data needed.

The latter a approach is not very precise and thus after some discussions (Sørensen, T., 2011), an SSR license was used instead and series of measurements were carried out. SSR is used in electroacoustics; and with a stepped sine as excitation, the steady state response is measured (Fig. 7.1b). It provides relatively precise response functions. However, a full feedback loop control would still be more beneficial, since the SSR does not provide the "true" control loop function. Instead, an inverse of the frequency response measured during equalisation is used to provide the signal to the vibration exciter. The latter implies that any random external vibration which was not captured during the equalisation process, can still influence the measurements. On the other hand, in the case of full feedback control, the controller

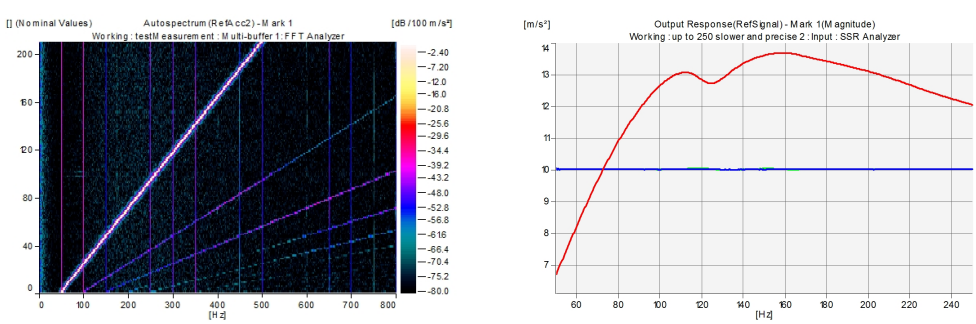

(a) (b)

Fig. 7.1: (a) The FFT analysis using a multi-buffer; (b) Frequency response obtained using SSR.

senses the current vibration of the exciter and adjusts it on-line according to the requirement. Thus it is capable (up to the limits of the control theory used) to handle also the random external vibration and so the measurements are more idealised.

7.2 Tests of MEMS accelerometers

7.2.1 Accelerometer type

In the preliminary tests presented here, two types of MEMS accelerometers, each with different typical sensitivity (namely ADXL-202 and 203, described in Table 3.1), were assessed seeking for differences in their performances. For the measurements, both of the tested accelerometers were glued to the reference accelerometer B&K 8305, which was, in turn, connected to the pre-amplifier B&K 2626 (keeping in mind that back-to-back calibration method was decided to be used, see Section 2.2.4). The coupled pair of transducers was driven by the shaker B&K 4809 (with a power amplifier B&K 2706) fed with a stepped sine excitation up to 500 Hz and a excitation level of 4.4 m/s^2. The response functions from the tests are plotted in Fig. 7.2.

The responses for both MEMS accelerometers (no.8 using an ADXL-202 chip and no.40 with an ADXL-203) are similar in any direction measured ($x-$ as shown in Fig. 7.2a,c,e,g or $y-$ presented in Fig. 7.2b,d,f,h). From the zoomed plots (Fig. 7.2c-h) it can be noticed, that their responses are just being shifted in the frequency domain. Also, as shown in Fig. 7.2h, the transducer no.40 seems to be more sensitive to the excitation at 280 Hz, which will be analysed more thoroughly later on in the report.

7.2.2 Measurement direction

Both MEMS ADXL-202 and 203 were excited in both y- and $x-$directions (cf. Fig. 7.3), the responses being compared for both accelerometers (no.8 and no.40) as shown in the results presented in Fig. 7.4. It can be seen that the behaviour at 280 Hz occurs regardless of the measurement direction. Therefore, it is not linked to the measurement direction and needs, still, to be further analysed to understand its origin.

From Fig. 7.4, it can also be noticed that the MEMS no.8 (the one with an ADXL-202 chip, i.e. with lower characteristic sensitivity) seems to have different sensitivities in the x- and y-directions (i.e. the responses, shown in Fig. 7.4e, do not overlap each other), whereas for the MEMS no.40 (ADXL-203, with higher sensitivity) the sensitivities are fairly similar (Fig. 7.4f). On the other hand, the change of sensitivities can also be caused by a not correct alignment of the chip inside of the capsule. It hence needs to be eventually analysed.

7.2.3 Type of fixation

Another thing that could have an influence in the measurements when performing the back-to-back calibrations was that of the type of fixation of the MEMS accelerometer to the reference one. Hence, investigations aiming at clarify this were performed; the out-of plane direction (i.e. y-direction) being excited according to Fig. 7.5.

Two types of fixations were studied (cf. Fig. 7.5): wax and glue, whose results are plotted in Fig. 7.6. Again, a level of 4.4 m/s^2 was used as excitation for the stepped sine excitation up to 500 Hz employed. Since only a single equalisation procedure of SSR was done, the output response is not perfectly flat. However, the FRFs seem to be sufficiently smooth.

As can be seen from Fig. 7.6, there is a small change in behaviour at around 280 Hz between the two analysed cases (wax and glue) for the directly excited signal (i.e. in the y-direction), which is dependent on the fixation type. As discussed (Larsen, J.B., 2011), the excitation of both x- and y-directions (Fig. 7.6c-d), especially around 280 Hz, could be caused also due to fixation onto the shaker as such. All in all, these strange resonant phenomena should be analysed deeper to get to the cause of it.

7.2.4 Amount of wax

As discussed in Section 7.2.3, the type of fixation of the MEMS to the reference accelerometer on top of the shaker could have an influence when performing measurements. In order to further investigate the

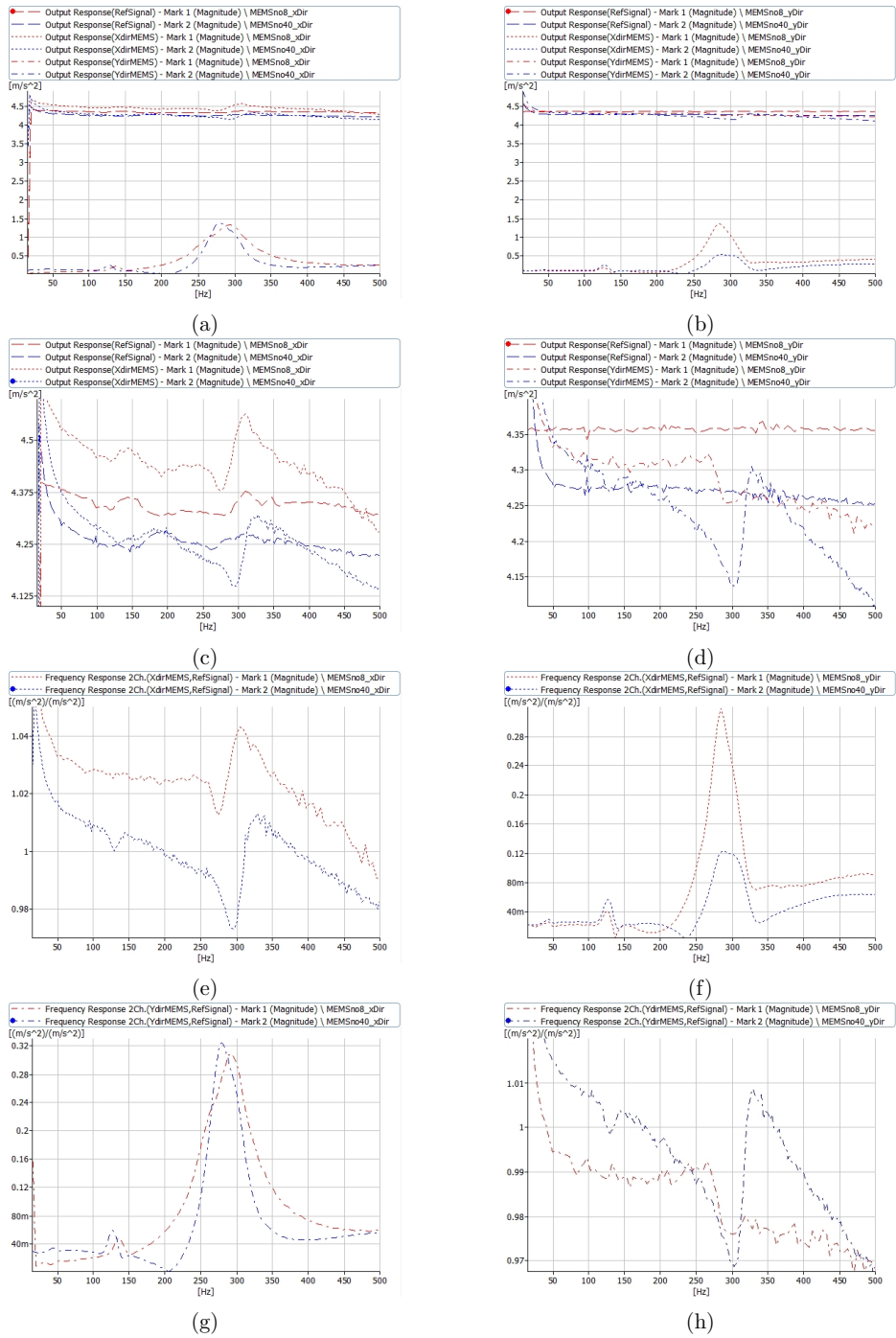

Fig. 7.2: Comparison of the ADXL-202 (MEMS no.8) and ADXL-203 (MEMS no.40) measured either for excitation in x-direction -(a),(c),(e),(g)- and y-direction -(b),(d),(f),(h). In (a)-(b), the output responses are plotted, their zoomed-in version into the excitation level being shown in (c)-(d). In (e)-(h) the FRFs are presented. Colour plots online.

latter statement, studies aiming at determining if the amount of wax (beeswax was used) can influence the response of the accelerometers, were performed. Three different cases were compared (cf. Table. 7.1). It should be noted that the exact amount of wax (defined in here as "normal", "minimum" and "much") was difficult to quantify thoroughly. The purpose of this study was, however, to check whether the wax layer thickness influences the response seen in the previous subsections, where "normal" amount of was was used. Wax behaves as a spring (a non-ideal one, and sometimes even as a damper), so it was our belief that the amount of wax could have some impact on the dynamical response measured. In general, it is recommended to use just a "thin evenly distributed layer" of wax for fixation (Bruel&Kjaer, 1978). The MEMS accelerometer no.40 (the one with higher sensitivity) was used for this set of measurements.

In the previous tests the level of acceleration was taken as 4.4 m/s^2. However, to replicate the calibration used for piezo accelerometers, the amplitude was increased to 10 m/s^2.

The results are presented in Fig. 7.7. Again, it can be seen that the problem with the resonant behaviour at 280 Hz is still not solved, hence the amount of wax not being responsible for that. Further-

(a) (b)

Fig. 7.3: Fixation of the MEMS accelerometer in (a) $y-$ and (b) $x-$direction.

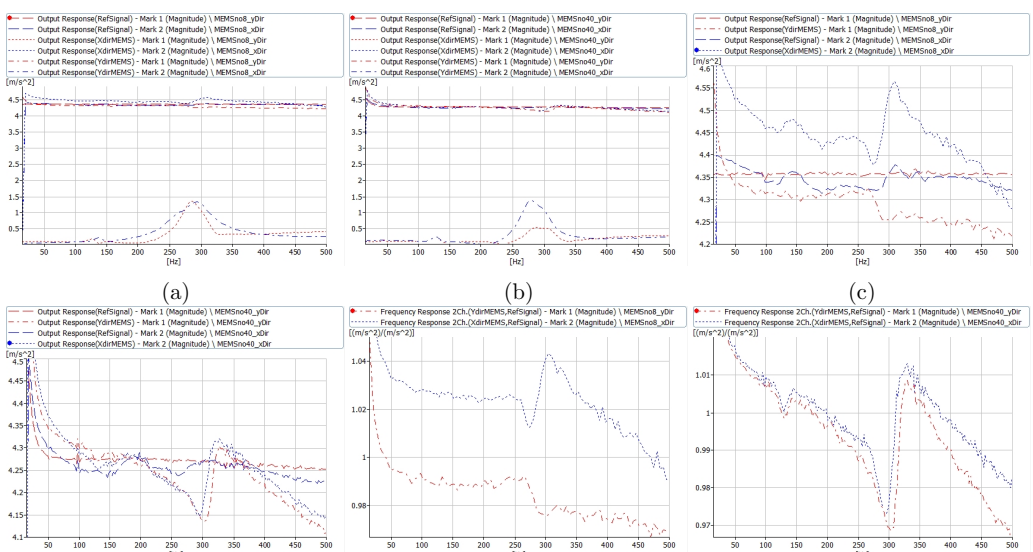

(a) (b) (c)

(d) (e) (f)

Fig. 7.4: Comparison of the measurement directions for ADXL-202 (MEMS no.8) -(a),(c),(e)-, and ADXL-203 (MEMS no.40) -(b),(d),(f). In (a)-(b), the output responses of all signals are plotted with (c)-(d) zoomed into only the excitation direction. The corresponding FRFs are presented in (e)-(f). Colour plots online.

(a) (b)

Fig. 7.5: Fixation of accelerometer: (a) using wax; (b) using cyanoacrylate glue.

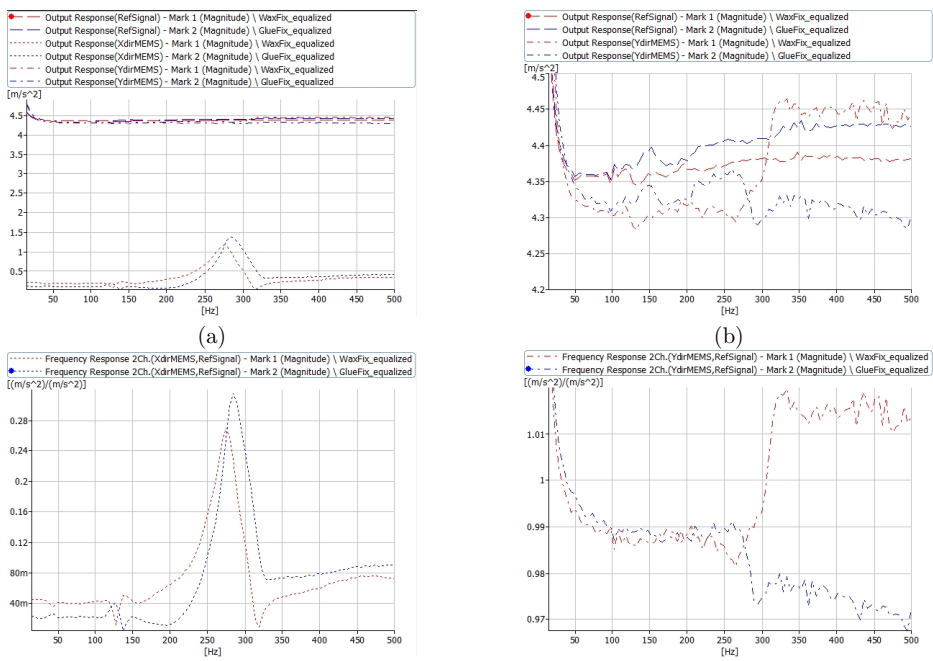

(a) (b) (c) (d)

Fig. 7.6: (a) Output response for all the measured signals; (b) zoom of the output response on the excitation level; (c) frequency response of the signal measured in the MEMS' x-direction; (d) frequency response of the signal measured in the MEMS' y-direction. Red curves corresponds to wax fixation whereas blue represent the glued connection. Colour plots online.

Table 7.1: List of set-ups studied to verify the influence of the amount of wax employed.

Case	Fixation of Ref. Acc.	Acc. to be calibrated	Fixation of MEMS
MEMS with normal wax on B&K 8305	Screwed to shaker	MEMS no.40	Normal wax onto 8305
MEMS with minimum wax on B&K 8305	Screwed to shaker	MEMS no.40	Minimum wax onto 8305
MEMS with much wax on B&K 8305	Screwed to shaker	MEMS no.40	Much wax onto 8305

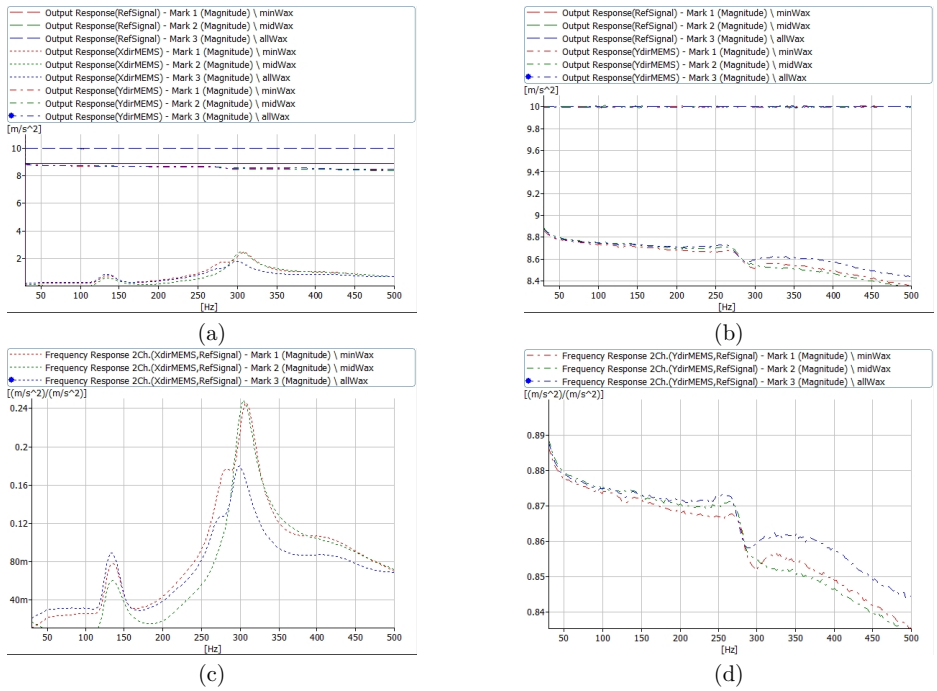

Fig. 7.7: (a) Output response for all the measured signals; (b) zoom of output response on excitation level; (c) frequency response of measured signals in the MEMS' x-direction; (d) frequency response of measured signals measured in the MEMS' y-direction. Red curves corresponds to thin ("minimum") wax layer thickness, green to medium ("normal") and blue to thick ("much") layer. Colour plots online.

more, assuming that wax behaves as a spring element, modifying the amount of wax should modify the local resonance (since the stiffness is changed). However, as it can be seen from Fig. 7.7d, the position of that local resonance is not detuned for the various wax layer thicknesses investigated.

7.2.5 Fixation to reference accelerometer / fixing directly on shaker

After observing that the local resonant behaviour remained the same despite of the type of fixation (glue and wax) and the amount of wax used between the reference and the MEMS accelerometer, it was decided to check whether or not this response came from the fixation of the B&K 8305 reference accelerometer to the vibration exciter as such. To that end, the MEMS was attached directly to the shaker using wax and analysed by comparing its response to the one of a smaller accelerometer B&K 4374. As a reference, the B&K 4374 was taken instead of the so far used B&K 8305 in order to check if its bulky shape and high weight could have been the reason for that local resonance at 280 Hz. The case just described where the MEMS accelerometer was attached directly onto the shaker and compared with a smaller reference accelerometer was also correlated with two already investigated cases (where the MEMS was attached either using wax or glue to the B&K 8305 reference accelerometer), see Fig. 7.8. The coupled pair of transducers was driven by a sine excitation up to 500 Hz and a excitation level of 10 m/s^2. The results obtained are shown in Fig. 7.9. The responses measured for MEMS waxed/glued onto the reference B&K 8305 showed again the local resonance occurring at around 280 Hz, as analysed in the previous measurements. Likewise, the some resonant behaviour is observed even for the small accelerometer B&K 4374 used instead of the B&K 8305, however it is shifted to frequencies above 500 Hz (i.e. out of measurement range).

From the shaker's data sheet (Bruel&Kjaer, 1972) (Fig. 4.2f), one can see that the shaker should have a resonance at around 160 Hz, which should not be responsible for the problems occurring at 280 Hz. For the cases where the MEMS accelerometer was fixed (using wax) directly on the shaker (Fig. 7.8b), one

(a) (b)

Fig. 7.8: Fixation of MEMS and small B&K 4374 on (a) reference one 8305; (b) directly on shaker.

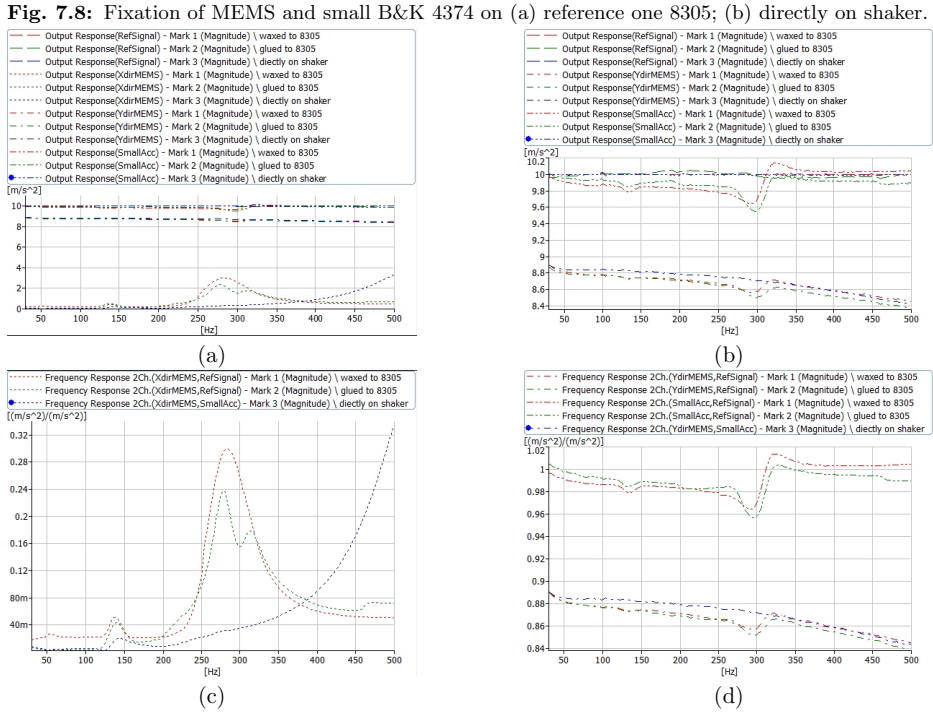

Fig. 7.9: (a) Output response for all the signals measured; (b) zoom of output response on excitation level; (c) frequency response of measured signals in the MEMS' x-direction; (d) frequency response of measured signals in the MEMS' y-direction. Red curves correspond to measurement with the MEMS waxed onto the B&K 8305, green ones to the glued MEMS onto the B&K 8305 and blue lines depict the response of the MEMS directly fixated onto the shaker (wax being used). Colour plots online.

can see that the resultant response (blue curves in Fig. 7.9b and d) are smooth up to 500 Hz. However, looking into the response in the $x-$direction (Fig. 7.9c), it seems that the local resonance is just detuned to the region above 500 Hz. This could point out at a problem having to do with the cable, since fixing the MEMS directly on the shaker made us change the cable fixation. Nevertheless, this needs to be investigated further[1].

All in all and at this stage, if calibration of the MEMS up to just 500 Hz is of interest, then fixation of the MEMS accelerometer directly onto the shaker could solve the problem with the resonant behaviour

[1]Actually, the "detuning of the local resonance" to 500 Hz can be partially observed in Fig. 7.12, where the local resonance is noticeable especially in the x-direction (non-directly excited). In the y-direction, there is some change in response noticeable around 500 Hz, but it is not so significant as for the measurements using the B&K 8305. In fact, it could be caused by also the cable of the MEMS. When the MEMS is fixed to the B&K 8305, the influence of the cable (which could also behave as a stiffness element) is larger. On the other hand, it does not answer the question of why the same behaviour is observed for the small accelerometer B&K 4374.

at 280 Hz. On the other hand, knowledge of what exactly causes this problem to assure why it happens would be beneficial so as to not run into such phenomena when eventually performing measurements.

7.2.6 Relative position of the MEMS with respect to the reference one

In order to investigate if the position of the centre of gravity of the MEMS accelerometer with respect to the reference accelerometer's position can have an influence on the resonant behaviour at 280 Hz, its location was varied, as shown in Fig. 7.10. Wax was used for fixation, as it was faster and simpler in order modify the set-up. The electrodynamic shaker was used for excitation in form of a stepped sine up to 500 Hz.

As shown in the results of Fig. 7.11b, i.e. for the position 3, (Fig. 7.10c), the amplitude at 280 Hz is the largest. All in all and comparing all results in Fig. 7.11, the behaviour at 280 Hz is still present for all cases. The resonant behaviour is lessened for position 1, where the MEMS chip should be aligned with the axis of the B&K 8305 (Fig. 7.10a). Nevertheless, it can be concluded that the location of the MEMS accelerometer with respect to the reference accelerometer is not directly responsible for the resonant behaviour at 280 Hz either. However, it does to some extent affect the response of the MEMS transducer, position 1 being the recommended option.

(a) (b) (c)

Fig. 7.10: Relative position of the MEMS accelerometer with respect to the reference one (B&K 8305): (a) position 1; (b) position 2; (c) position 3.

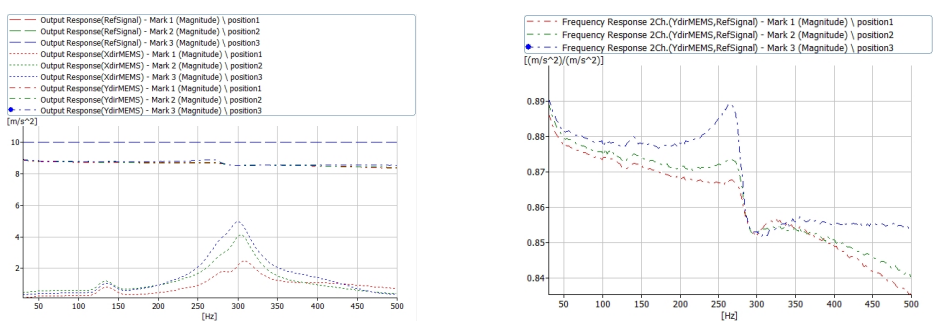

(a) (b)

Fig. 7.11: (a) Output response of all 3 channels (reference signal, MEMS' x- and MEMS' y-direction) and (b) frequency response in the y-direction for the three different positions shown in Fig 7.10. Colour plots online.

7.2.7 Influence of vibration amplitude

The aim of the studies presented in this section is to see to which extent the response of the MEMS transducers is linear. To that end, the variation on vibration amplitudes was assessed. The excitation levels coming out from the shaker were varied from 1 m/s^2 to 10 m/s^2 (set as the "calibration level") in steps of 1 m/s^2. The bandwidth was increased from 50 Hz to 1.5 kHz in order to see the behaviour also at higher frequencies.

The results for the MEMS transducer no.40 are shown in Fig. 7.12, the reference accelerometer used being the B&K 4374. In an ideal case (a linear behaviour of the transducers), the FRFs would be independent of the "calibration level". However, as seen from Fig. 7.12, this is not the case here, i.e. there is some source of this non-linear behaviour present in the measurement chain. According to the data sheet (Analog Devices, 2010), the measuring range is up to 1.7 g (i.e. approx. 16.7 m/s^2), which is way above the maximum level used in tests presented here (10 m/s^2). Thus, the fixation of the MEMS transducer, the casing or cabling could possibly be the responsible for these variations. On the other hand, as discussed earlier, the MEMS' fixation could be ruled-out, since neither the type (wax/glue) nor their amount or a position of the transducer would indicate that is responsible for the local resonance.

From the results obtained for the indirectly excited direction (Fig. 7.12b), a resonant behaviour can still be noticed at around 550 Hz. This could be explained by the stiffness of the support being modified.

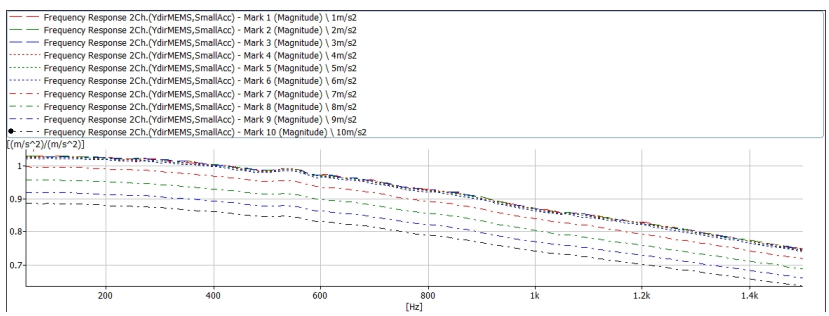

(a)

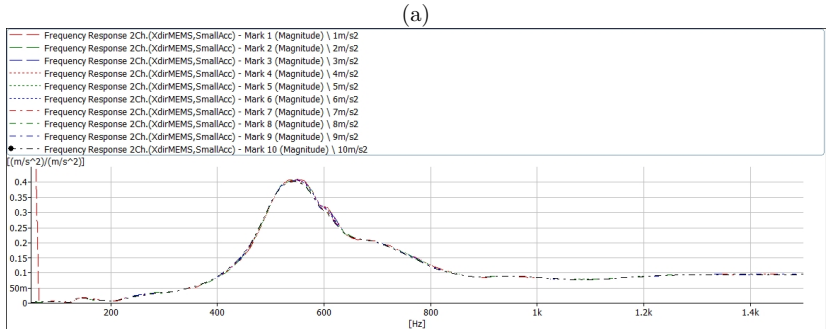

(b)

Fig. 7.12: Frequency response of the signal measured in the MEMS' y-direction, where a small accelerometer B&K 4374 is taken as reference: (a) for $y-$direction (excitation direction); (b) for $x-$direction. Colour plots online.

7.3 Calibration of piezo accelerometers

In order to figure out if the problem with the local resonance at 280 Hz is related to the MEMS accelerometer or to other apparatus used, piezoelectric sensors were used instead of the MEMS in this section; the back-to-back calibration being carried out in the same fashion as in the previous tests between combinations of reference and test accelerometers as explained in the subsequent sections.

7.3.1 Accelerometer B&K 4374 to be calibrated using B&K 8305 as reference

First, a small accelerometer B&K 4374 is studied as the accelerometer to be calibrated. As shown in Fig. 7.13 and listed in Table 7.2, three different arrangements are compared. The results are presented in Fig. 7.14. The FRFs (Fig. 7.14b) reveal that at around 280 Hz there is still a significant change of the response, i.e. the curve is not smooth throughout the whole frequency bandwidth analysed. It seems that the fixation is not stiff enough to avoid problems at 280 Hz, even when not using the MEMS accelerometer. Furthermore, the wax seems to perform worse, which could turn into fixation problems.

Table 7.2: List of compared set-ups with B&K 4374.

Case	Fixation of Ref. Acc.	Acc. to be calibrated	Fixation of acc.
B&K 4374 waxed to B&K 8305	screwed to shaker	B&K 4374	Waxed to B&K 8305
B&K 4374 glued to B&K 8305's stud	screwed to shaker	B&K 4374	Glued to stud B&K 8305
B&K 4374 glued to B&K 8305's washer	screwed to shaker	B&K 4374	Waxed to B&K 8305

(a) (b) (c)

Fig. 7.13: Fixation of the B&K 4374 to B&K 8305 using: (a) wax; (b) glued to stud; (c) glued to plate.

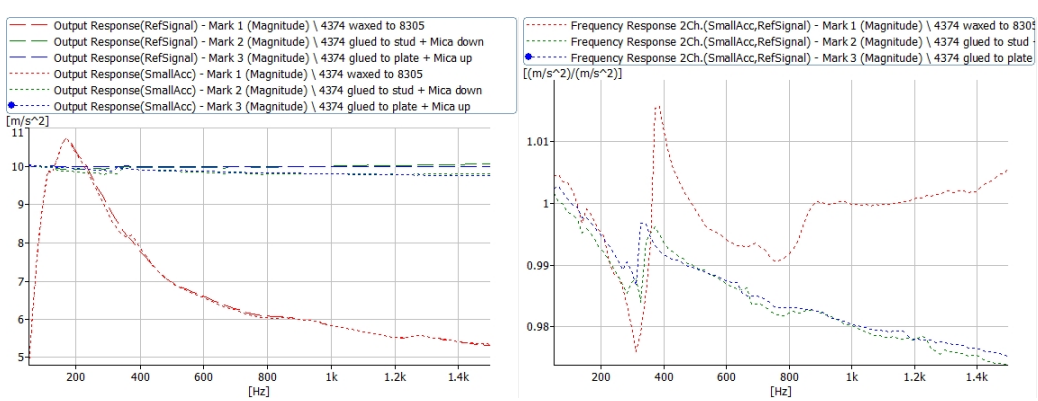

(a) (b)

Fig. 7.14: Output response (a) and FRF (b) measured for the B&K 4374, waxed or glued to the B&K 8305.

7.3.2 Accelerometer B&K 4371 calibrated with B&K 8305 and a mica washer

In order to check if any difference in the behaviours could be detected, the accelerometer B&K 4371 was attached to the reference one (B&K 8305 in this case). Furthermore, a different contact type between the reference and the investigated accelerometer was checked to see if it does influences the response. To that end, a mica washer was introduced in between both transducers (Fig. 7.15a). In Table 7.3, the different measurements performed are listed.

The results presented in Fig. 7.16 depict that the mica washer is not helping to solve the problem with the response at 280 Hz. In fact, its influence is counterproductive, i.e. it introduces a non-ideal surface and thus the problem at 280 Hz is enhanced. Thus, the use of mica washers is not recommended at all to perform this type of calibrations.

(a) (b)

Fig. 7.15: (a) Disk plate and a mica washer; (b) B&K 4371 on the top of B&K 8305.

Table 7.3: List of set-ups with the accelerometer B&K 4371 and a mica washer.

Case	Fixation of Ref. Acc.	Acc. to be calibrated	Fixation of acc.
B&K 4371 screwed to B&K 8305	screwed to shaker	B&K 4371	Waxed to B&K8305
B&K 4371 screwed to B&K 8305 one mica washer	screwed to shaker (mica washer in-between)	B&K 4371	Screwed to B&K 8305
B&K4371 screwed to 8305 two mica washers	screwed to shaker (mica washer in-between)	B&K 4371	Screwed to B&K 8305 (mica washer in-between)

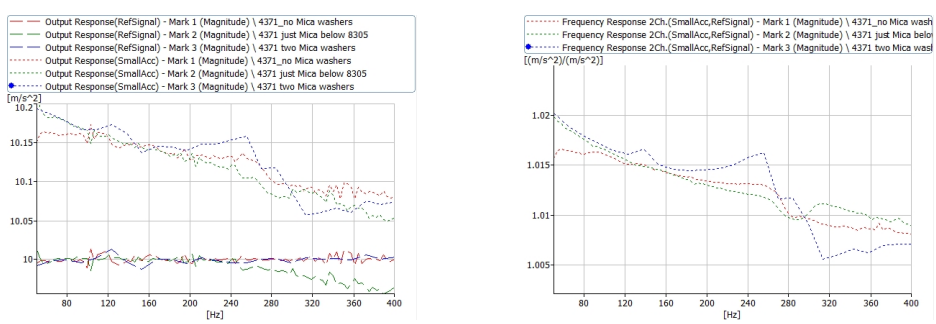

(a) (b)

Fig. 7.16: Output function (a) and frequency response (b) measured for the B&K 4371 and the B&K 8305, with or without mica washers. Colour plots online.

7.3.3 Accelerometer B&K 4374 calibrated using B&K 4371 as reference

Further tests were performed to analyse if the fixation of the accelerometer to the previously used as reference B&K 8305 is the cause of the local resonance. In the test performed here, the B&K 4371 was used as reference against the B&K 4374, two fixation types being compared: (a) using wax and (b) employing glue (cf. Fig. 7.17 and Table 7.4).

The results are presented in Fig. 7.18. It can be seen, that the local resonance around 280 Hz is still present (similarly as when the B&K 8305 was used as the reference accelerometer); the latter implying that the issue investigated here is not the cause of it.

Table 7.4: Studied set-ups with the accelerometer B&K 4371 as a reference.

Case	Fixation of Ref. Acc.	Acc. to be calibrated	Fixation of acc.
B&K 4374 waxed to B&K 4371	screwed to shaker	B&K 4374	Waxed to B&K 4371
B&K 4374 glued to B&K 4371	screwed to shaker	B&K 4374	Glued to B&K 4371

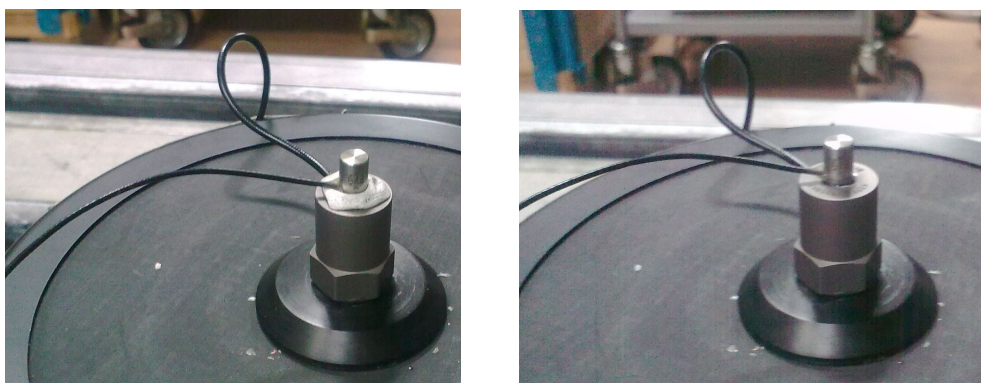

(a) (b)

Fig. 7.17: A small accelerometer B&K 4374 attached to B&K 4371, used as reference, with: (a) wax; (b) glue.

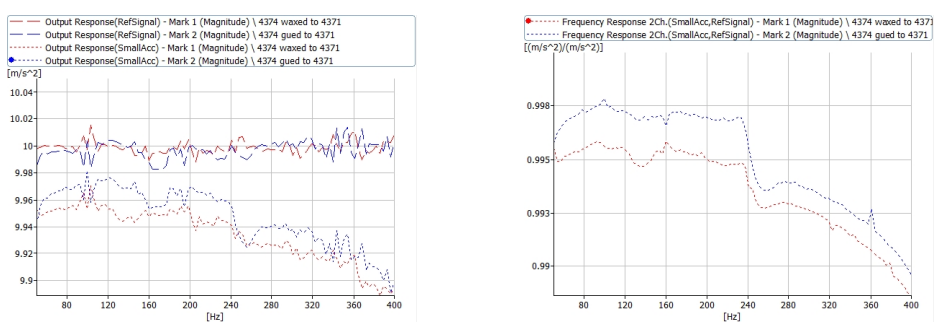

(a) (b)

Fig. 7.18: Output function (a) and frequency response (b) measured for wax (red) and glue (blue) fixation. Colour plots online.

7.4 Cable fixation

As noted in Section 2.2.3, the cable should be correctly attached to the shaker in order to avoid unwanted influences on the measurements. Thus various arrangements were tested, the results being summarised in the subsequent sections.

7.4.1 Piezo accelerometer

With the piezo accelerometer B&K 4371 fixed on the reference one (B&K 8305), three cases are compared Fig. 7.19: (a) old measurement set-up with free attachment of the cables and location of the shaker on the concrete block; (b) cables fixed using a wax and (c) cable fixations performed using a hot glue gun, which should ensure firm attachment. As can be seen in Fig. 7.19b, the fixation type of cables as such does not have any marked influence on the outputs recorded. On the other hand, together with the different fixation, the shaker as such was moved between the measurements from the concrete block to the floor. And the latter alternation does have a bigger impact, as will be discussed later in Section 7.5.1.

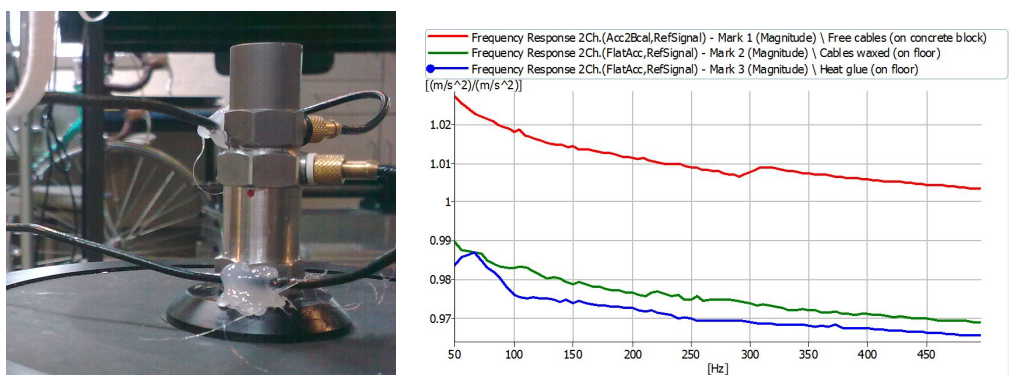

(a) (b)

Fig. 7.19: (a) Fixation of cables using a hot glue gun; (b) measured FRFs. Colour plots online.

7.4.2 MEMS accelerometer

The same type of tests as in the previous section were performed, this time attaching the MEMS accelerometer instead of the piezo on top of the reference one (B&K 8305). Again, three cases are compared (Fig. 7.20): (a) cables are hanging freely; (b) cables being taped to the reference accelerometer using a duct tape and (c) cables glued (as recommended in the standard (ISO, 1998)), hot glue being used.

The results (cf. Fig. 7.21) point out that the problem could lie in the balancing of the MEMS accelerometer and/or in the thickness of the cable involved, since neither of the cable fixation methods used is solving the problem with the unwanted response around 280 Hz. Even the firmer attachment did not help to solve the problem. Therefore, it could be interesting to test the MEMS with a thin cable in order to lessen the effect of the cable thickness (i.e. cable stiffness).

7.5 Verification of shakers

It was our belief that the measurement results can be influenced also by the electrodynamic shaker involved in the tests, and especially by its inherent dynamic characteristics or location during the test. The aim here is to investigate issues related to the shakers used.

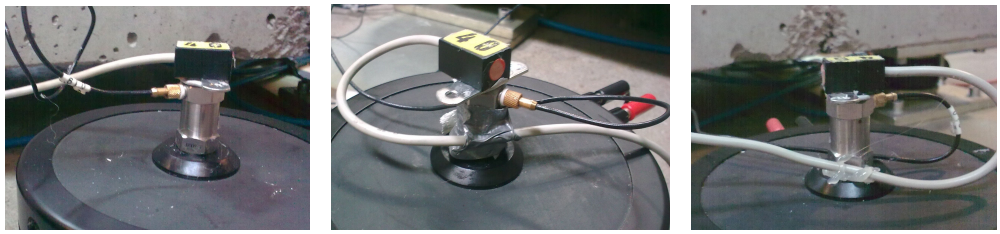

(a) (b) (c)

Fig. 7.20: (a) Cables freely hanging; (b) cables taped using duct tape; (c) cables glued using a hot glue gun.

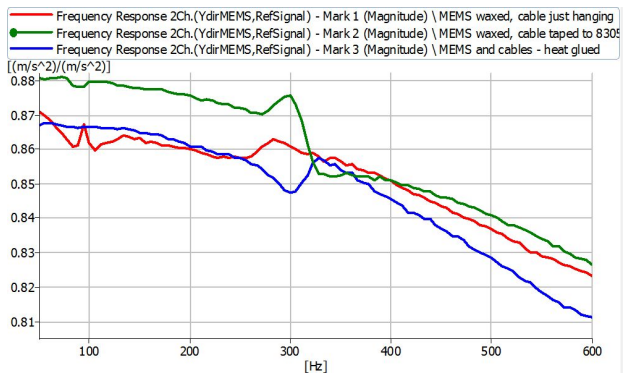

Fig. 7.21: Resultant FRFs for all three analysed cases. Colour plots online.

7.5.1 Shaker's location

In most of the calibrations performed thus far, some non-ideal behaviours were observed at around 280 Hz and the cause of it must be investigated. Therefore, two cases were compared here: (a) a shaker located on top of a concrete block laying on air-springs, which in principle was supposed to eliminate the environmental vibration and (b) the shaker being place directly on the laboratory floor. The results are shown in Fig. 7.22d. Based on those results, it is recommended not to use a concrete block on air springs, but rather just to put the shaker directly on the rigid concrete floor. Possible rocking motion is then not emphasised, which can be the case when locating the shaker on the concrete block.

7.5.2 Shaker used

At AAU's laboratory, two shakers were available at the time of the measurements. As it can be seen in Fig. 7.23, the two responses are not equivalent. One shaker experiences an "additional resonance", even though the same set-up and boundary conditions (cable fixations) were used. After contacting B&K regarding this issue, their response on shakers' comparison was the following (Plechinger, P.L., 2011):

```
The response from our expert team to your shaker comparison is the following:
This resonance is due to the combination of the table head mass and the stiffness
of the spring suspending the mass. If the spring and the table (which are circular)
were fully symmetrical without any eccentricity, there would theoretically be
a single resonance peak. Because of non-symmetry in the production process,
this is to be expected. However, if one was using a
control loop, this would not make any difference.
```

Thus no other action was taken at this stage and the difference was taken as an inherent problem, a feedback loop control being recommended if possible.

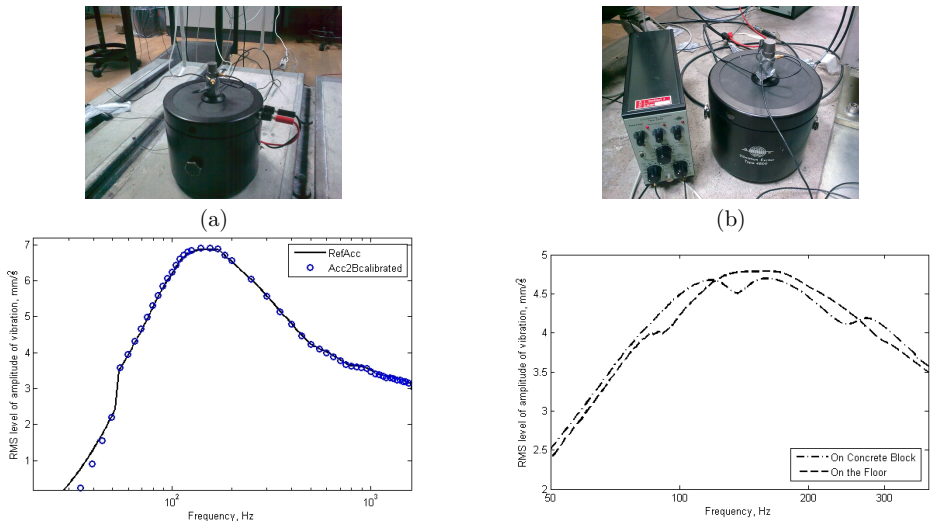

Fig. 7.22: Location of the shaker (a) on the concrete block; (b) on the floor; (c) first results from shaker calibration test located on the table (Section 6.1); (d) comparison of shaker calibration tests located on a concrete block and floor.

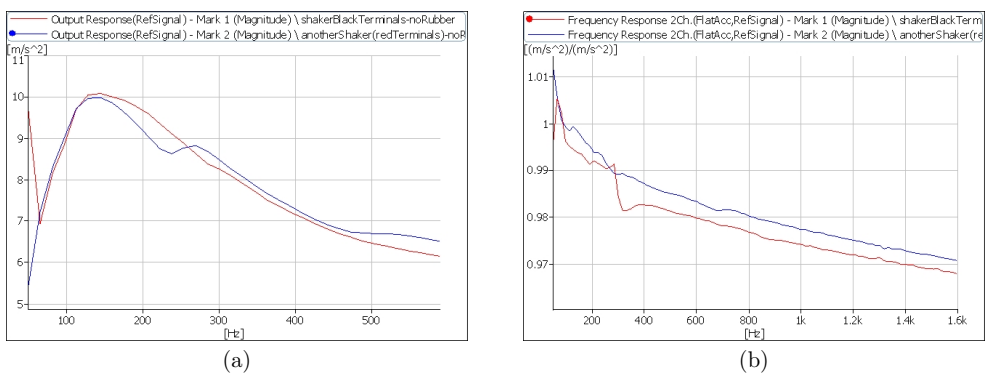

Fig. 7.23: Comparisons of responses measured at two different shakers. Colour plots online.

7.6 Signal clipping

It was also observed that at amplitudes above approximately 8 m/s^2, the time signal is "clipped" at the top (Fig. 7.24a). On the other hand, for low acceleration levels (Fig. 7.24b) clipping does not occur. The latter could be caused by the fact that the amplitude of static and dynamic components exceed the maximum voltage to be sent to PULSE. However, PULSE is capable to accept 7.071 V_{peak} (Bruel & Kjær, 2008) and the clipping 43.323 m/s^2 corresponds to 4.4195 V_{peak}, which is way below the PULSE limit input peak voltage. The reason for the latter issue could be that the accelerometer no.40 has a measurement range only up to 1.7 g (cf. Table 3.1), and since we measure in the horizontal direction, the signal to be measured is superimposed over the constant acceleration due to gravity (of value 1 g). Thus, in the next tests, the accelerometer no.40 was not used and only the one with lower sensitivity (no.8) was tested so as to lessen this effect.

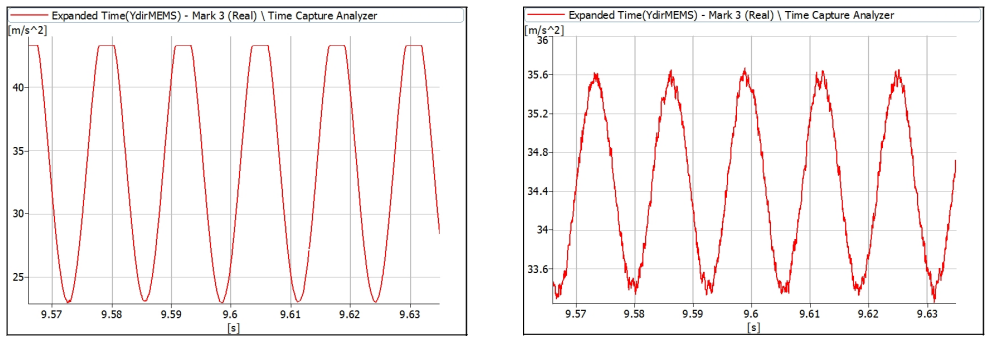

(a) (b)

Fig. 7.24: Time capture of the non-filtered time signal from the MEMS accelerometer for excitation level: (a) 10 m/s^2 and (b) 1 m/s^2.

7.7 Linearity of the MEMS transducer

After figuring out that the MEMS accelerometer no.40 experiences some clipping at higher accelerations, the MEMS accelerometer no.8 was employed instead (the one with no clipping observed). Then, the linearity in terms of response at different amplitudes of acceleration was re-analysed[2]. The MEMS was directly glued onto the shaker (hot glue being used) and the small B&K 4374 accelerometer was used as the reference (also being attached on the top of the MEMS using a hot glue gun, as shown in Fig. 7.25a). A stepped sine excitation up to 1.5 kHz was sent out from the shaker to perform the calibration.

As can be seen from Fig. 7.25b, the behaviour at different excitation levels is approximately the same. The ripples at very low level (3 m/s^2) were caused by combination of low precision of the SSR and the lower signal to noise ratio (the dynamic range was not tuned after each change of level, in order to speed up the measurements). These results are in contradiction with the tests analysed in Section 7.2.7. However, as previously pointed out in Section 7.6, the MEMS no.40 used in Section 7.2.7 exhibited some signal clipping, which could be responsible for the non-linear behaviour.

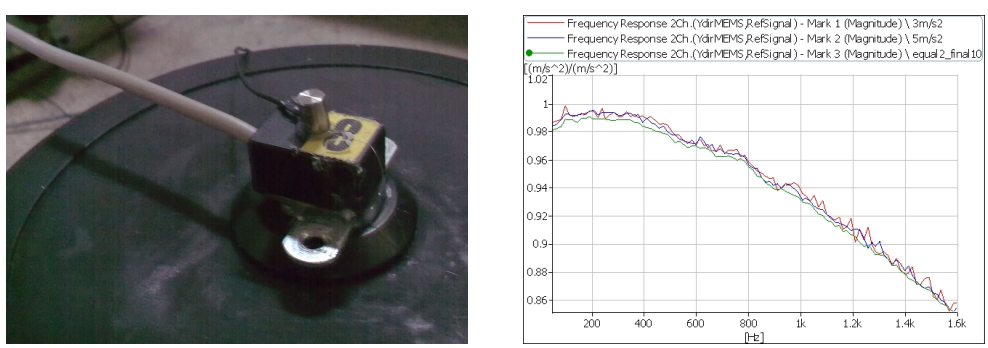

(a) (b)

Fig. 7.25: (a) Reference accelerometer B&K 4374 glued to the top of the MEMS to be calibrated; (b) FRFs measured. Colour plots online.

[2]The measurements presented in Section 7.2.7 were carried out using the transducer no.40, for which clipping occurred. Thus, the re-measurement was performed.

7.8 Reproducibility of measurements

Even when using the same set-up, the same responses had not been recorded throughout the report thus far in some cases. This points at some potential problems concerning reproducibility. Simply by playing with the position of the string support of the cable, some improvement was achieved, however still the re-measurements did not lead to the same responses (cf. Fig. 7.26). The problems could be caused by the fact that the cable is rather thick and stiff, embedded and clamped into the accelerometer's body. There were some attempts to fix the cabling as recommended (discussed in Section 7.4), but the string was too stiff and the glue too soft so it would not hold firmly. The problem with cabling, a potential cause for the resonant behaviour as well as for lack of reproducibility will be addressed later on by using a bare MEMS chip with thin and flexible cables (i.e. with no casing).

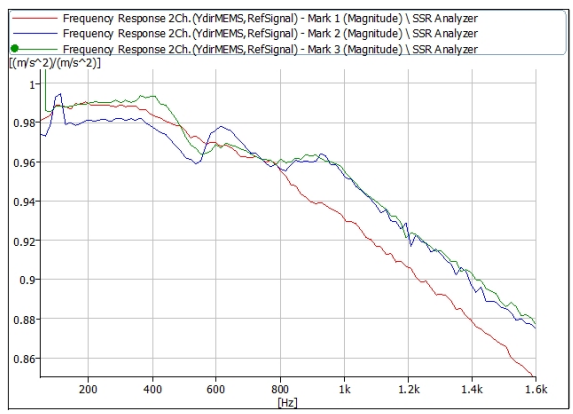

Fig. 7.26: Checking reproducibility: Mark 1 - measurements on shaker with black terminals; Mark 2 - using shaker with red terminals; Mark 3 - returning to the shaker with black terminals. Colour plots online.

7.9 Steady-state response vs. Sine sweep excitation

Further measurements comparing the SSR approach and the sine sweep one were done in order to see if the excitation method used could influence the results obtained. The tests were done with the reference accelerometer calibrated (where for the sine sweep measurements the gain was set in the post-processing, since it was forgotten to be set during measurements).

For the first set of tests done (Fig. 7.27) the responses obtained from SSR correspond with the data measured for sine sweep excitation. When the sine sweep test was re-measured, some differences were observed, as presented in Fig. 7.28. This can be caused by a pre-amplifier drift (the B&K 2635 was used) or some environmental conditions which would cause the change of calibration constant used. However, it is recommended to re-run the measurement with properly calibrated reference accelerometer (using calibrator) and/or try another pre-amplifier (e.g. more noisy but probably stable Charge-to-DeltaTrons).

7.9.1 Sine sweep settings

Using sine sweep measurements and FFT analyser recording the data into the multi-buffer for each period of time, some ripples were present in the autospectra measured. Thus, some verification was carried out as well. As shown in Fig. 7.29a-c, the effect is independent of the shakers, accelerometer or pre-amplifier used; however it was found, as presented in Fig. 7.29d, that using averaging, the problem is solved. Moreover, it was recommended to use peak averaging instead of the multi-buffer analysis for future tests.

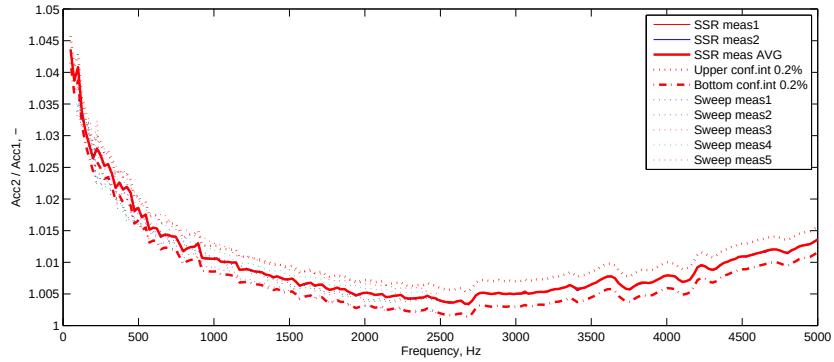

(a)

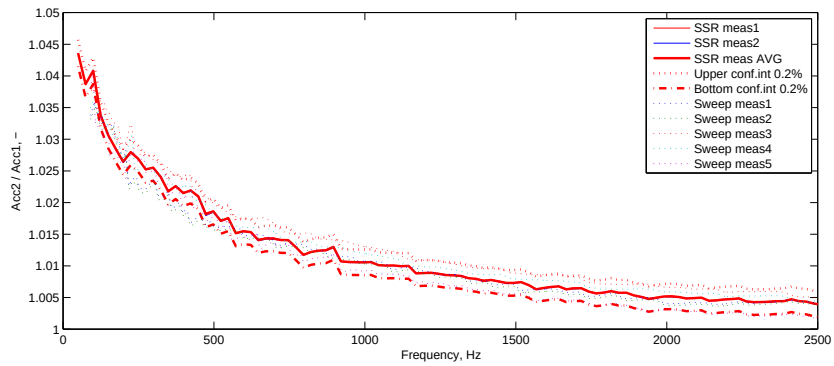

(b)

Fig. 7.27: Comparison of SSR and sweep results: (a) up to 5 kHz; (b) zoom to 2.5 kHz. Colour plots online.

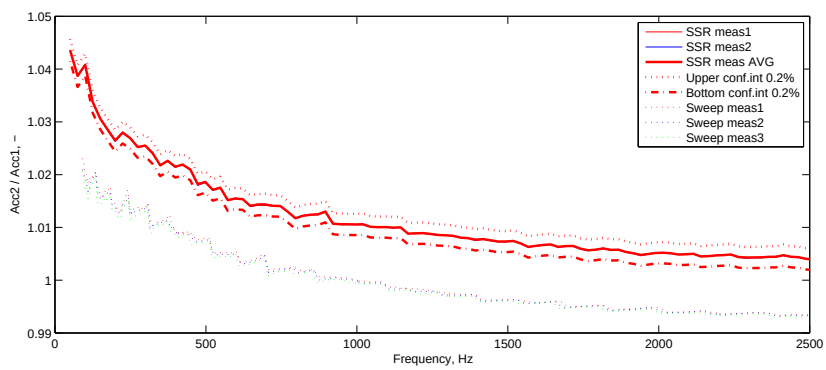

Fig. 7.28: Comparison of SSR measurements (old set) and re-measuring the sine sweep measurements (new set). Colour plots online.

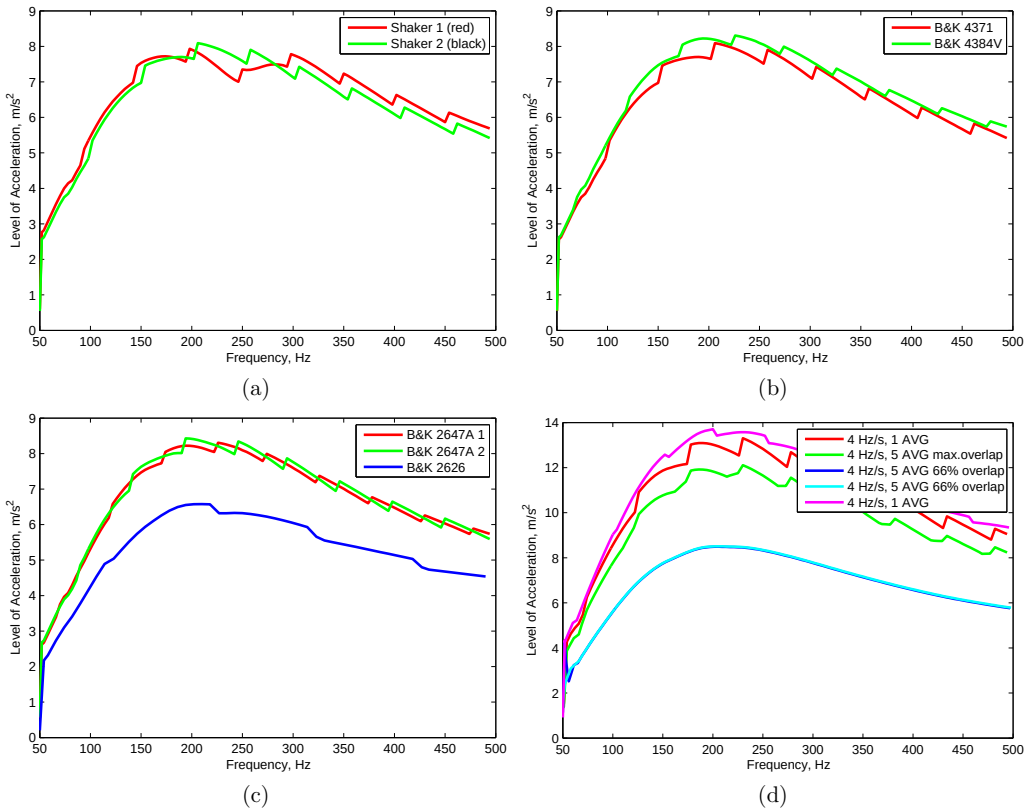

Fig. 7.29: Autospectra measured changing (a) the shaker; (b) accelerometers; (c) accelerometer's pre-amplifiers; (d) varying the averaging. Colour plots online.

7.10 Conclusions

In order to idealise the excitation, an SSR license was used. It did not ensure the full feedback loop control, yet the stepped sine excitation was providing (more or less) constant excitation level during the test. Thus, the two MEMS accelerometers were tested, the problem with the resonant response at 280 Hz being still observed and tracked when altering the position, type of fixation or even the type of reference transducer. The direct cause of this misbehaviour was not identified in this chapter; however, it was recommended to locate the shaker on the floor as well as changing the cabling for the MEMS accelerometer due to its thickness. Furthermore, the traducer no.40 should not be used due to clipping problems.

8

Sine Sweep Measurements using a vibration controller

After the purchase of the vibration controller B&K VC-LAN 7541 (Fig. 4.1c) by AAU, measurements were performed using a closed feedback loop control, which was supposed to idealise the measurement scenario and therefore improve the results. The controller is capable to adjust the amplitude of vibration on-line, which was not possible using the SSR employed in the previous chapter (it relied on the response recorded during the equalisation process). Also the measurement process is faster comparing to the SSR, since no equalisations are required. The test carried out alongside their results are presented in this chapter.

8.1 Sine sweep settings

Firstly, a set of back-to-back calibration measurements with a fixed acceleration amplitude were performed, two different types of sweep rate being compared:

- Linear sweep at a rate of 10 Hz/s and 20 Hz/s.
- Logarithmic sweep at a rate of 2.5 oct/min and 5 oct/min.

In B&K PULSE LabShop, the FFT analyser was set to Peak averaging in order to capture just the response at the excitation and thus avoiding problems with the multi-buffer discussed in Section 7.9.1. Moreover, in order to reduce the noise in the measured responses, overlap was chosen as "Max" when the curves were smooth. Zero overlap was not tested, but for 66.6% as well as for 75%, the signal was still noisy.

The FRFs (H1[1] being the one plotted) are presented in Fig. 8.1. It can be seen that except for the case `linSweep20Hz/s` (i.e. linear sweep at rate 20 Hz/s), good agreement between the FRFs is obtained. The 20 Hz/s case needs to be re-measured.

From the FRFs, it can also be noticed that there are no longer troubles at 280 Hz as observed in the previous tests. The response curve is relatively smooth for all cases. The frequency dependence of the FRF (ideally the response of the accelerometers should be independent of the frequency) can be caused by the reference accelerometer's response (B&K 4371 was used as the reference, its response being presented in Fig. 4.2c), or due to the accelerometer to be calibrated. With the reference accelerometer B&K 8305, the possible frequency dependence will be caused purely by the calibrated accelerometer.

The autospectrum is the representation of the signal's energy during the measurement period. Thus, as shown in Fig. 8.2, it is dependent on the sweep rate, since for slower sweeping more energy is "collected" within the measurement period than for the faster one. Also, the type of sweep influences the autospectrum. Using the FFT (frequency bands of constant frequency width), the logarithmic sweeping will cause exponential shape of the autospectra (it is slower at low and faster at higher frequencies)[2]. On the other hand, the FRFs are independent of the type of excitation, since it takes the ratio of the two signals which are exposed to the same excitation at each frequency (and so it does not see the sweep type).

[1] As a reminder, an FRF is defined as the ratio between the output Y(f) and input X(f) of a system in the frequency domain. In situations where the output of the system is expected to be noisier than the input, an FRF H1, defined as the ratio of the cross spectral density in the frequency domain of the input X(t) and the output Y(t) -denoted as S_{xy}- by the auto spectral density in the frequency domain of the input X(t) -denoted as S_{xx},is used instead.

[2] The peaks around 1 kHz visible in Fig. 8.2a-b are caused by some troubles with the finish of sweeping, which after reaching 2 kHz continued down to 1kHz when stopped. This problem was solved in future tests.

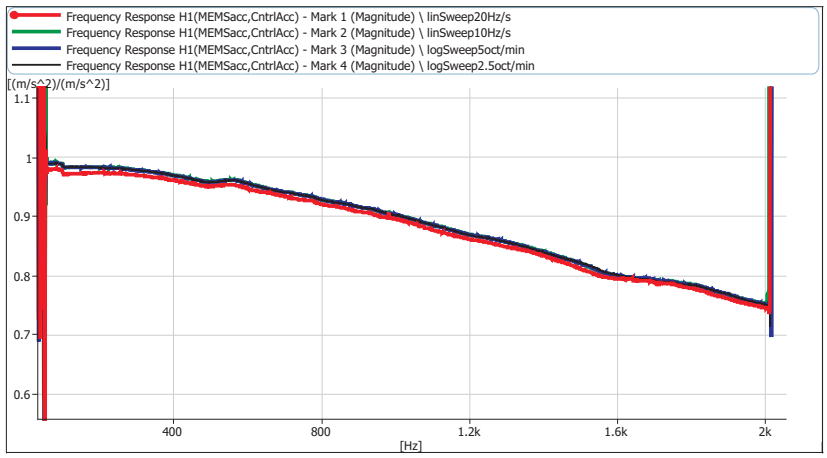

Fig. 8.1: Comparisons of all measured FRFs H1. Colour plots online.

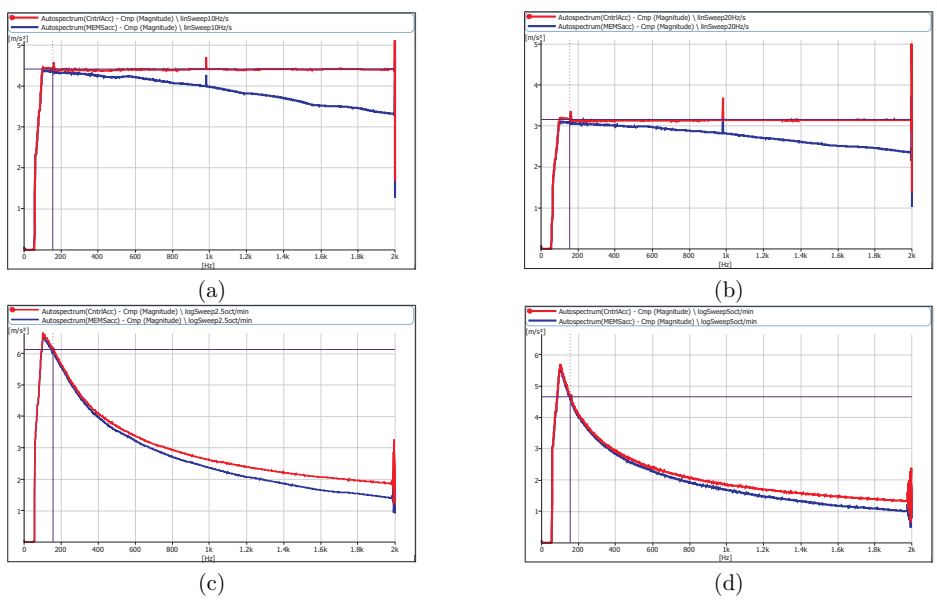

Fig. 8.2: Autospectra functions for control and MEMS accelerometers: (a) linear frequency sweep at rate 10 Hz/s; (b) linear frequency sweep at 20 Hz/s; (c) logarithmic frequency sweep at 2.5 oct/min; (d) logarithmic frequency sweep at 5 oct/min. Colour plots online.

8.2 Sine sweep vs. single sine excitation

To verify whether or not sine sweep measurements can provide the same results as single frequency measurements, and hence prove that sine sweep can be used instead of the sine excitation, four different types of sweep excitations were compared with the excitation at single frequencies. As for the sine sweep, the sweep rates as well as the sweep types (both linear and logarithmic), were varied.

As shown in Fig. 8.3, neither the sweep rate nor the sweep type affects the frequency response (FRF H1 estimate is of interest here). Also and more importantly, the responses obtained for the single frequency excitation agree with the sine sweeps, i.e. the sweep measurement can be used instead of series of pure sine excitations. In doing so, the calibration process can be markedly sped up.

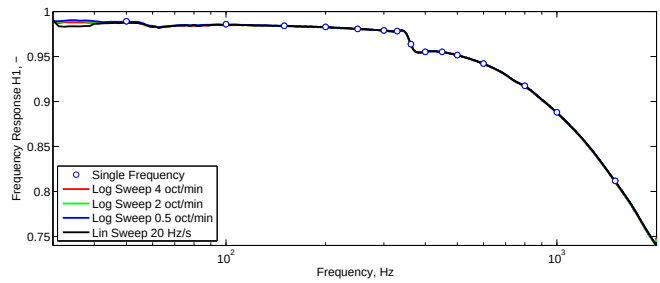

Fig. 8.3: Frequency response function H1 for the different sweeps under study (Log - logarithmic, Lin - linear) and a single frequency excitations. Colour plots online.

8.3 Conclusions

Using the vibration controller, it was proved that it can substitute (and even improve) the vibration excitation and so enhance the tests as such. From the comparison of the sine sweep and single sine excitation, a very good agreement of the two methods was obtained, so further on the controller with the electrodynamic shaker will be used for excitation.

The comparison of the linear and logarithmic sweep revealed that they excite the system in equal manner. Hence, if the constant frequency step is not required, a logarithmic one of around 5 oct/min can be used to save time of measurement, since it is faster than the linear one.

9 Sine sweep measurement at LU

In order to avoid a potential rocking motion, which could occur when using the small shaker B&K 4809 as excitation (as done during tests at AAU), new series of measurements were carried out at LU, involving here the use of bigger shakers as well as a vibration controller.

Thus, some of the measurements already performed thus far and presented in the previous chapter were re-done to look for improved results when involving a bigger shaker together with the vibration controller.

9.1 Fixation of the shaker

Before the tests with the MEMS accelerometers were performed, an investigation regarding the influence of the type of shaker employed and their fixation was done first. To that end, two different shakers (B&K 4808 and B&K 4507) were investigated. The shaker B&K 4808 was fixed in two ways: (i) mounted on top of a wooden plate and the latter being bolted to a metal table (Fig. 9.1b) or (ii) directly bolted to a heavy metal table (Fig. 9.1c); whereas the B&K 4507 was only fixed by bolting it to the metal plate (Fig. 9.1d). For each shaker, different accelerometers were placed on the shaker itself as well as around, as shown in Fig. 9.1, their response being recorded when the shaker was fed with a random noise signal (except of `B&K 4808_meas2`, which was done with a sine sweep).

The FRFs for the table-shaker and wood-shaker attachment measurements are presented in Fig. 9.2. The accelerometer denoted as "Table" was always fixed to the steel table (Fig. 9.1), whereas the one denoted as "Wood" represented either the accelerometer fixed onto the wooden support (when present for the B&K 4808, Fig 9.1b) or to the base of the shaker (for later measurements, Fig. 9.1c,d). The frequency responses between the wood and table are shown in Fig. 9.3.

As presented in Fig. 9.2 and 9.3, the shaker B&K 4808 (measurements denoted as `B&K 4808_meas1` and `B&K 4808_meas2`) does not possess any significant resonance peaks within the measured bandwidth, just some noise being measured. On the other hand, the responses from the shaker B&K 4824 (denoted as `B&K 4824_meas1` and `B&K 4824_meas2` in the plots) do present some significant high frequency responses (above 500 Hz in all measurements). The latter was actually perceived when carrying out the measurements in the lab using the B&K 4824, as some high frequency noise coming from the shaker was heard. Hence, the shaker B&K 4824 was not used in order to avoid potential problems with it,

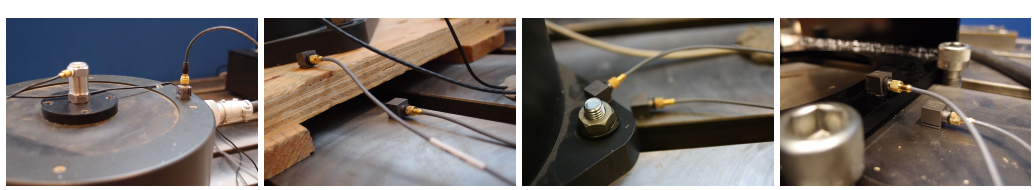

(a) (b) (c) (d)

Fig. 9.1: Location of the table, wood and shaker accelerometers: (a) top of the shaker (shaker accelerometer fixation); (b) Table and Wood accelerometers when the shaker B&K 4808 was fixed on the wooden plate; (c) Table and Wood accelerometers when the shaker B&K 4808 was fixed directly on the steel table; (d) Table and Wood accelerometers when the shaker B&K 4824 was fixed directly on the steel table.

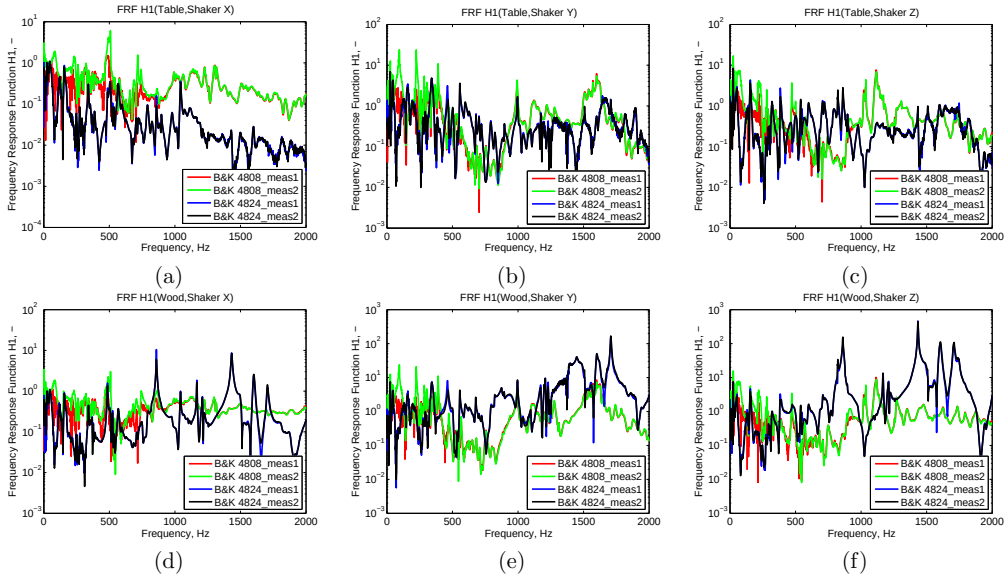

Fig. 9.2: FRFs for shaker-wood-table measurements: (a)-(c) table-shaker X,Y,Z; (d)-(f) wood-shaker X,Y,Z, for all four test measurements (the curves denoted as B&K 4808_meas1 and B&K 4808_meas2 were done using the shaker B&K 4808 and the ones named as B&K 4824_meas1 as well as B&K 4824_meas2 on the B&K 4824).

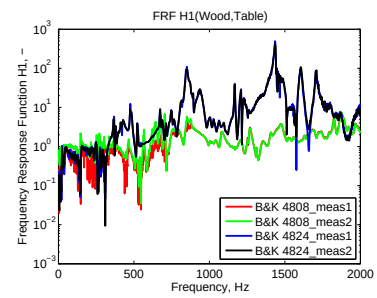

Fig. 9.3: FRFs for wood-table measurements (the curves denoted as B&K 4808_meas1 and B&K 4808_meas2 were done using the shaker B&K 4808 and the ones named as B&K 4824_meas1 as well as B&K 4824_meas2 on the B&K 4824). Colour plots online.

and thus the B&K 4808 fixed directly on the steel table (no wood plank used) was utilised in further measurements.

9.2 Sweep rate investigation

Together with the verification of the shakers' fixation, the chosen sweep rate 4 oct/min (as seen in the previous chapter, a logarithmic sweep of around 5 oct/min is recommended) was analysed if it is suitable also for the bigger shakers. The MEMS inner-chip accelerometer was fixed to the reference B&K 8305 by using wax and the FRFs recorded. A comparison with random noise as well as with a slower sweep (2 oct/min) was done, the results being presented in Fig. 9.4. Since the slower sweep rate provided exactly the same response as the one chosen 4 oct/min, a sweep rate 4 oct/min was considered as optimal for further measurements (this conclusion is coherent with the one drawn in the previous chapter, but it was considered that it should be double checked for the different shakers too). However, the results from random noise measurements presented in Fig. 9.4 do not yield to the same response as obtained for the sine sweep. Nevertheless, analysing a later set of measurements using two dual axial MEMS accelerometers (no.06 and 17), one can notice that both types of excitation are indeed equivalent (cf. Fig. 9.5). The problems depicted in Fig. 9.4 could have be caused by, for example, insufficient or wrong FFT analyser settings.

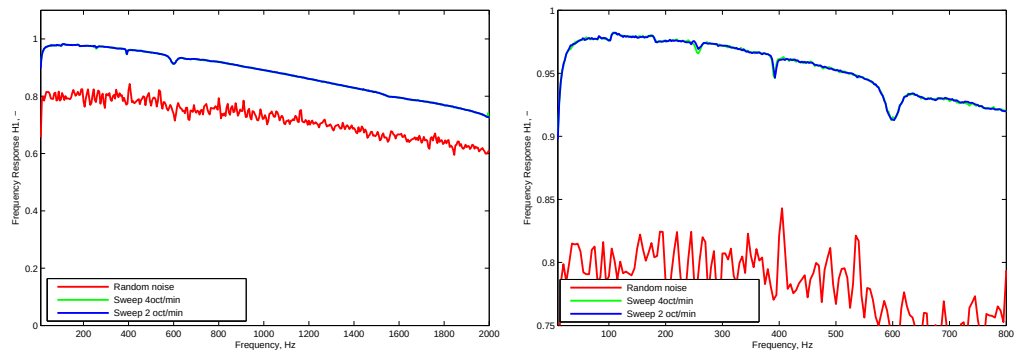

(a) (b)

Fig. 9.4: Frequency response of the sine sweep measurements with different sweep rates as well as random noise: (a) an overall view; (b) zoom to signals measured. Colour plots online.

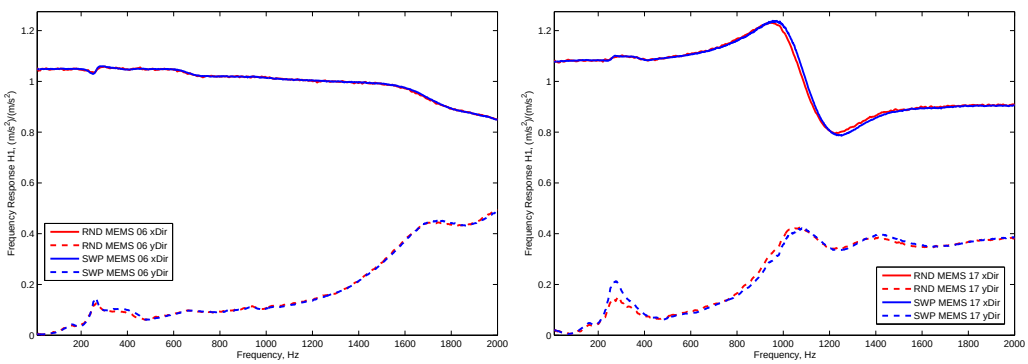

(a) (b)

Fig. 9.5: Comparison of random noise (RND) and sine sweep (SWP) excitation for dual-axial measurements on: (a) MEMS 06 and (b) MEMS 17. Colour plots online.

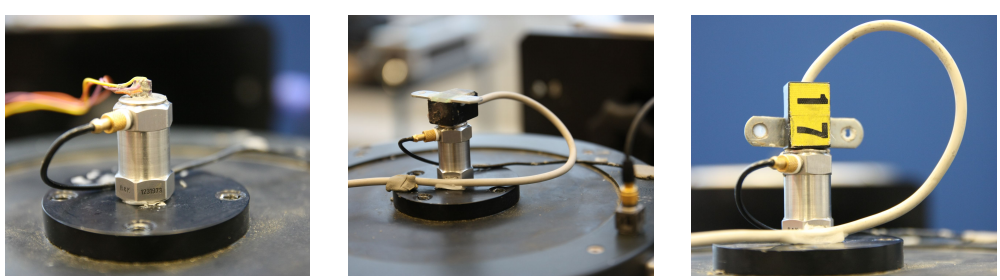

(a) (b) (c)

Fig. 9.6: Fixation of: (a) naked MEMS; (b) encapsulated MEMS, y-direction; (c) encapsulated MEMS, x-direction. The B&K 8305 is used as reference when calculating the FRFs.

9.3 Comparison of MEMS transducers

In the measurements performed in this section, five different MEMS transducers of the ones developed at LU have been used, either encapsulated or as a pure chip with thin cables (the henceforth so-called "naked MEMS", see Fig. 9.6). All of these MEMS are equipped with the chip ADXL-202 (due to the signal clipping problem present in the ADXL-203 chip mentioned in Section 7.6). The comparison of FRFs is shown in Fig. 9.7, using the accelerometer B&K 8305 as the reference for calibration. The estimated calibration constants for 159.2 Hz[1] are listed in Table 9.1. It can be seen that a quite substantial variation in calibration constants is present for the MEMS transducers tested. However, their response is relatively flat within the bandwidth up to 250 Hz, which indicates that after a correct calibration, the transducers could be potentially used for low frequency acceleration measurements as they are intended to.

To verify if the estimated calibration constants given in Table 9.1 work properly, the time data recordings previously acquired for the MEMS no.06 in its x-direction were multiplied by a reversed value of the corresponding constant listed in Tab. 9.1 (i.e. for MEMS 06 xDir by 1/1.0481), the results being plotted in Fig. 9.8. In Fig. 9.8b, it can be seen that not only the amplitude, but also a phase shift should be considered in order to achieve a precise calibration. The corresponding FRFs (before and after calibration) are compared in Fig. 9.8c, where a small difference is still present. The latter calls for further verification of the usage of the calibration constant.

Table 9.1: List of estimated calibration constants (FRF H1 at 159.2 Hz.)

	MEMS 06	MEMS 08	MEMS 17	MEMS 43	naked MEMS
xDir	1.0481	1.0069	1.0792	0.9965	0.9750
yDir	1.0190	1.0558	1.0734	0.9980	-

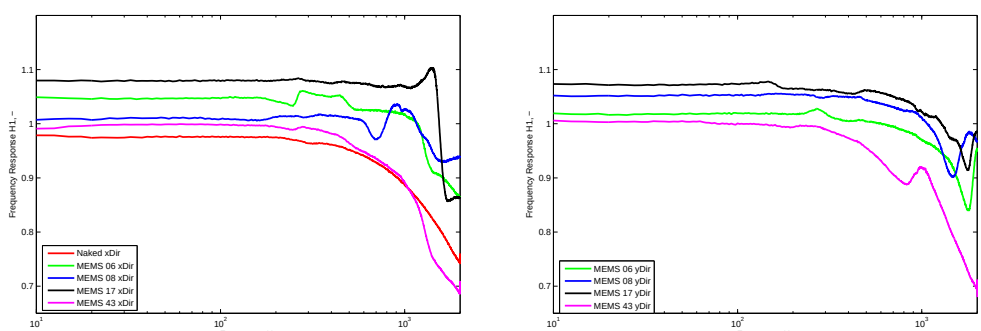

(a) (b)

Fig. 9.7: FRFs for all the MEMS transducers excited in: (a) x-direction; (b) y-direction. Colour plots online.

9.4 MEMS position onto the reference accelerometer

The relative position of the MEMS accelerometer with respect to the reference one was analysed using the SSR approach in Section 7.2.6. The offset caused by the location of the MEMS transducer could cause some transversal vibrations. Therefore, the MEMS transducer was fixed to the reference one using beeswax re-trying different positions and measured again, this time employing the bigger shaker (B&K 4808, instead of the B&K 4809 utilised in Section 7.2.6). The vibration controller was used to improve the excitation as such.

[1]The calibrator B&K 4294 provides a vibration excitation level of 10 m/s^2 at 159.2 Hz (or 1000 rad/s). To be able to compare the results from B&K 4294 with the ones gathered from the sweep calibration, the read-out at 159.2 Hz was taken.

The comparison of the FRFs for different off-set positions and cabling arrangements (shown in Fig. 9.9) is presented in Fig. 9.10. From those, it can be concluded that the off-set location is responsible for excitation of frequencies above 200 Hz. However, what is noticeable is that the response below 100 Hz seems to be unchanged, thus for low frequency measurements it can be stated that the correct alignment is not so important.

9.5 Capsule fixation onto the reference

During the previous tests, it was observed that when abundant amount of wax was used, that created a gap between the reference accelerometer and the MEMS' capsule (Fig. 9.11b). Therefore, three cases were compared in this section: a centered capsule with "normal" amount of wax (i.e. sort of an ideal condition) as well as two cases where different amounts of beeswax were used, see Fig. 9.11a. Similarly to the previous test, the low frequency content up to approximately 200 Hz seems to be unaffected. However, for frequencies above 200 Hz, both the amount of wax as well as the relative position of the MEMS on top of the reference one influences the responses significantly. All in all, the fixation during calibrations needs to be done properly.

9.6 MEMS vs. piezo accelerometer

To verify if the problem with the response at 280 Hz is only related to the MEMS transducers, or if it can be detected also using piezoelectric transducers, both types were compared. Some analysis has already been presented in Section 7.3, however the results were questionable. In the test performed

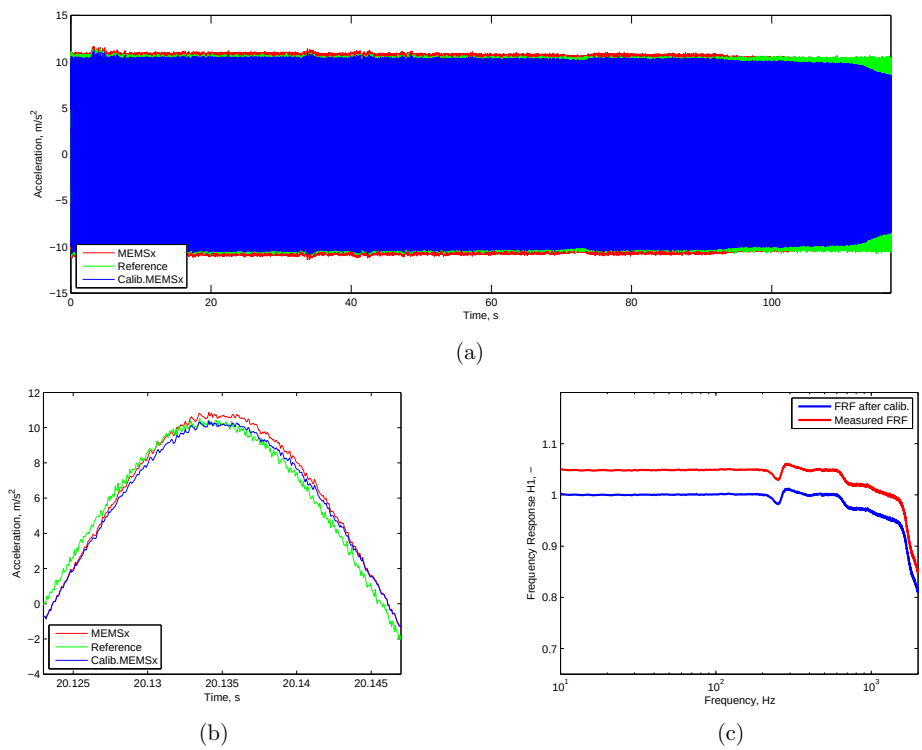

Fig. 9.8: (a) Whole time capture for MEMS 06 x-direction measurement; (b) Zoom to half-period of time capture; (c) Comparison of FRFs before and after calibration (i.e. after application of the calibration constants given in Table 9.1). Colour plots online.

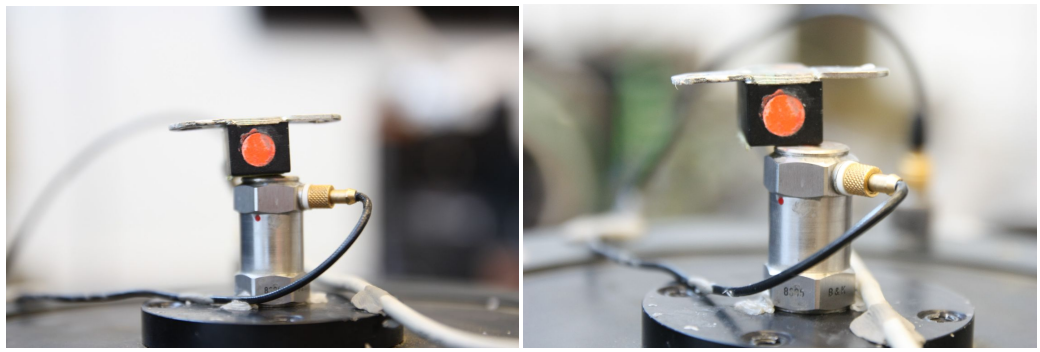

(a) (b)

Fig. 9.9: Accelerometer with MEMS chip in: (a) centered position; (b) off-set.

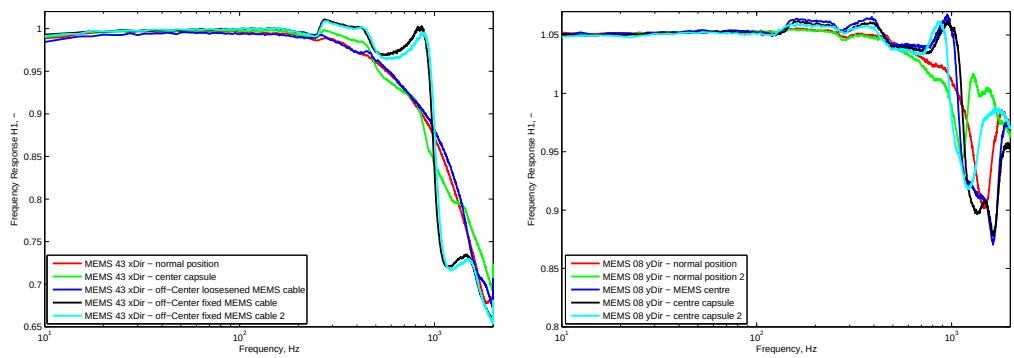

(a) (b)

Fig. 9.10: Comparison of different off-set positions of MEMS transducers for (a) x-direction measurements; (b) y-direction measurements. The normal position was the one before paying attention with a specific alignment (it was close to having capsule centered). For MEMS 43 also the cable of the MEMS transducer was either fixed to the shaker's table (as in Fig. 9.9) or not. Colour plots online.

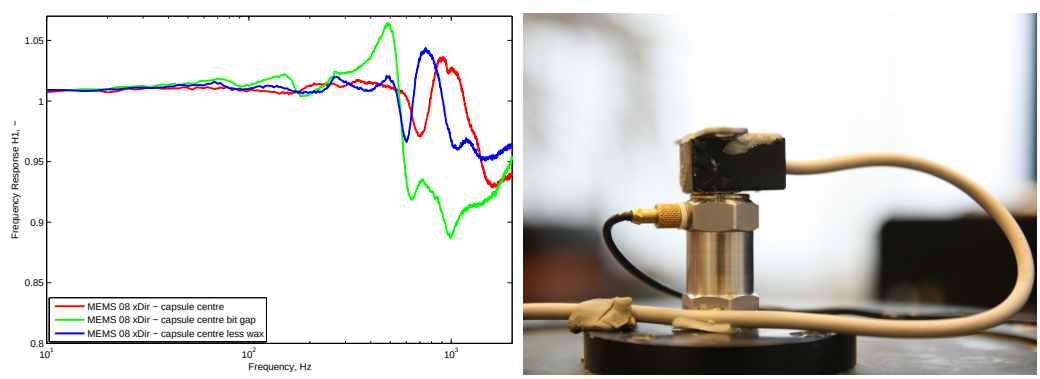

(a) (b)

Fig. 9.11: (a) Comparison of the influence of the gap and wax layer; (b) visualisation of the gap between the reference accelerometer and the MEMS capsule. Colour plots online.

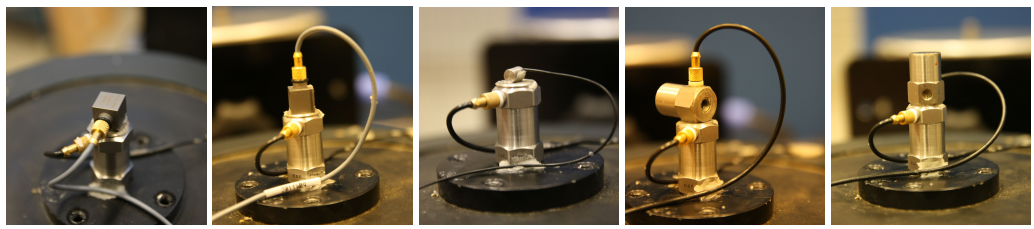

(a) (b) (c) (d) (e)

Fig. 9.12: Piezo accelerometers used: (a) B&K 4507-001, direct measurement; (b) B&K 4507 001, reverse (indirect) measurement; (c) B&K 4374, reverse (indirect) measurement; (d) B&K 4332, direct measurement; (d) B&K 4332, reverse (indirect) measurement.

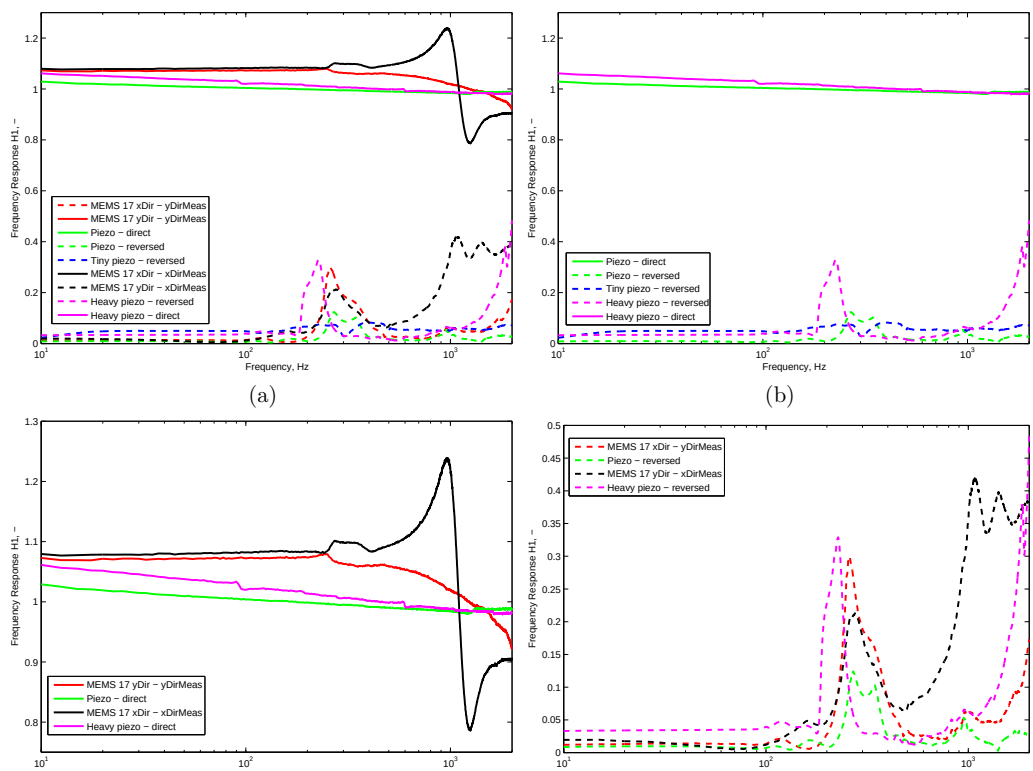

Fig. 9.13: FRFs for: (a) both piezo as well as MEMS transducers (MEMS for both measurement directions); (b) comparison for direct and reversed excitation of piezo transducers; (c) comparison of direct excitation of both piezo as well as MEMS transducers; (d) comparison of indirect (reverse) excitation of the transducers. The so-called "Tiny piezo" relates to the B&K 4374, "Piezo" denotes the B&K 4507-001 and "Heavy piezo" the B&K 4332. Colour plots online.

here, the vibration controller was hooked up to the big shaker. Furthermore, the number of piezo accelerometers tested was increased. Five piezo accelerometers arrangements shown in Fig. 9.12 were compared. The transducers B&K 4507-001 and 4374 (Fig. 9.12a-c) were fixed by means of beeswax, whereas the B&K 4332 (accelerometer in Fig. 9.12d-e) has a side thread to fix the transducer turned 90°, i.e. a stud was employed to assure a firmer fixation.

The FRFs measured are presented in Fig. 9.13. Taking only the piezo accelerometers (Fig. 9.13b), the transducers were excited also in the indirect way and some resonant response at around 250 Hz was captured. It is our belief that this could be caused by the fixation, or even by the reference transducer. A bit unclear is why the heavy piezo accelerometer B&K 4332 fixed by a stud does not provide a firm fixation and also transverse motion is detected. Thus, even when using a big shaker and a vibration controller, no definite results using piezo transducers were obtained and they should be checked further.

9.7 Two channel recordings

In the case of the two-axial MEMS accelerometers, the two signals (for each direction) are logged simultaneously. Therefore, to see how (and if) the responses are interconnected, various excitation directions (either $x-$ or $y-$direction) were applied. The responses recorded are presented in Fig. 9.14. It can be observed that some response is measured also indirectly (in the transversal direction). It is also noticeable that the frequencies excited indirectly (around 300 Hz and 1 kHz) are the frequencies where the problematic response in the directly excited direction is observed, i.e. they are linked each other. This can point out that the alignment of the chip can contribute to the response at 280 Hz.

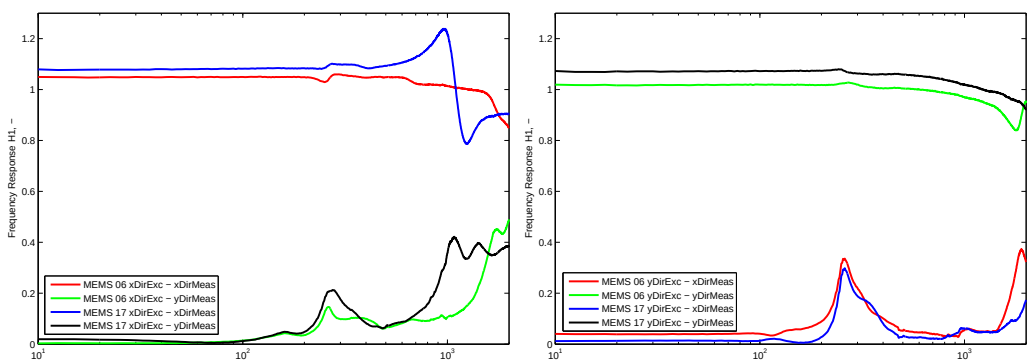

Fig. 9.14: Comparison of measurements with both channels logged for MEMS 06 and 17 excited in: (a) x-direction; (b) y-direction. Colour plots online.

9.8 Conclusions

To eliminate the possible transversal vibration which can occur on the smaller shaker, bigger shakers were tested together with the vibration controller in a way creating a more ideal excitation. Some of the previous tests were re-measured, but the cause of the resonant response at 280 Hz could still not been identified. Yet using smaller amount of wax and centering the capsule, the FRFs obtained were less distorted than the ones obtained in previous chapters (i.e. using a smaller shaker and SSR excitation method). Thus, a bigger shaker together with the vibration controller are recommended for calibration.

10 Additional characterisations

As seen in previous chapters, the chip alignment could be a potential cause of the resonant behaviour observed at 280 Hz. Thus, the last set of measurements performed with the chip set-up and thin cables (i.e. naked MEMS) focused on checking the influence of the chip alignment within the capsule. Moreover, focus was put into the measurement bandwidth and the calibration methodology as such.

10.1 Gain evaluation

Up to now, it was assumed that during the measurements performed, the noise is present at the output signal (in our case, the signal from the accelerometer to be calibrated). Thus, the FRF H1 estimate was used. However, to verify that this assumption is correct, all three types of FRFs which can be found in the B&K PULSE software to evaluate the results, namely the FRFs H1, H2 and H3, were compared in Fig. 10.1. From the figures, it can be noted that the FRFs for all three types are identical, i.e. they overlap each other, the latter implying that no influence in the results is observed regardless of

Table 10.1: Comparison of FRFs values at 159.2 Hz and corresponding gain value extracted from sweep sine measurements.

Measurement name	FRF H1	FRF H2	FRF H3	Gain (1/FRF)
Calibration using B&K 4294	-	-	-	**0.9116**
20120401piezoCalibTest1_withCalibConst_with159.2Hz	1.0019	1.0019	1.0019	0.998104≈**1**
20120401piezoCalibTest1_withNoCalibConst_with159.2Hz	1.0992	1.0992	1.0992	**0.909753**

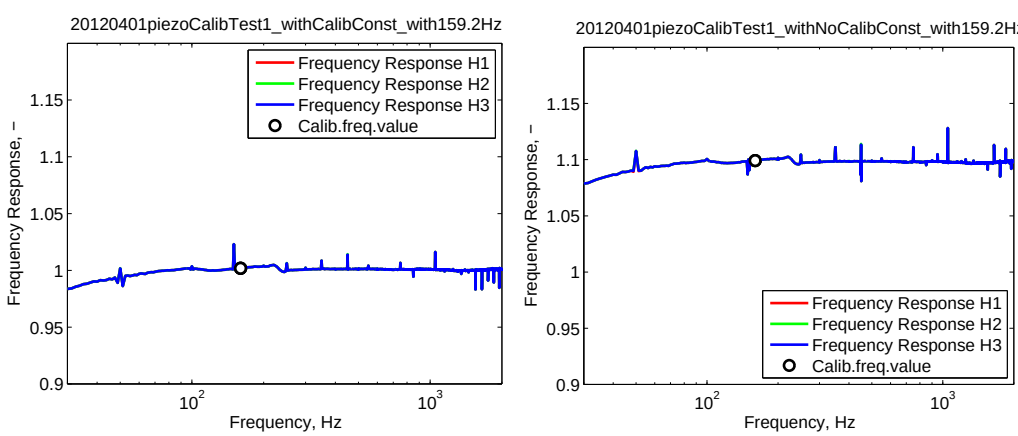

Fig. 10.1: Comparison of the frequency response functions H1, H2, H3 for the two measurements listed in Table 10.1. Colour plots online.

the function chosen for evaluation.[1]

Firstly, the calibration of the piezo transducer (for the test, a B&K 4332 was taken) was done with the B&K 4294, a gain of 0.9116 (Table 10.1) being found. Subsequently, this factor was used in PULSE to calibrate the accelerometer signal. Performing the sine-sweep measurements, the FRFs are plotted in Fig. 10.1a. Reading the value of the FRF at 159.2 Hz, the gain was found to be very close to 1 (Tab. 10.1).

The sine-sweep test were performed again, this time with no gain inserted in the PUSLE system (i.e. just the sensor sensitivity is used), the FRFs obtained being plotted in Fig. 10.1b. Reading-out the value at 159.2 Hz, the gain was found as 0.9097, which is close to the one found using the calibrator B&K 4294, i.e. close to 0.9116. Thus, the calibration procedure using a reference accelerometer and a sine-sweep control approach of the shaker seems to be sufficiently precise for the purposes under investigation here.

10.2 Tilting of the MEMS' chip using a rubber isolator

Due to the fact that the MEMS' chips are glued to the sensor's casing in a way that the alignment is not necessarily ideal, i.e. x-, y- and z-axis do not necessarily coincide with the edges of the casing, the influence of the chip's tilting (i.e. deviation from the ideal position, as shown in Fig. 10.2) was investigated here. As shown in Fig. 10.3, seven different tilting angles were assessed. Furthermore, the influence of a rubber isolator being placed between the shaker and the reference accelerometer was also analysed, which should help to avoid transversal motion on the calibration, as discussed in (Licht and Salbøl, 2010). Another parameter investigated in this set of measurements was also the influence of amount of beeswax, just to prove that the measurements carried out are not influenced by that factor. The coordinate system of the MEMS transducer is shown in Fig. 10.2. For measurements, a logarithmic sine sweep (4 oct/min) with a closed feedback control was chosen. As concluded in Chapter 8, the linear and logarithmic control strategies with the parameters used yielded to similar results and since logarithmic seeps are faster, they were used in these tests.

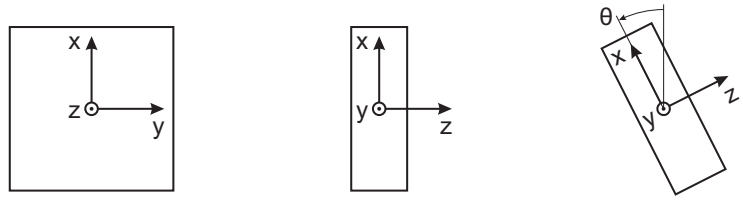

Fig. 10.2: Sketch of a naked MEMS accelerometer ADXL-202/ADXL-203. θ indicates the tilting angle.

10.2.1 Influence of tilting

As shown in Fig. 10.4, the orientation of the transducer has a significant influence on its dynamic response. Even the problematic response around 200 Hz seems to be caused by tilting the transducer. When the chip is correctly installed (i.e. at zero tilting angle), the FRF is smooth and close to 1. However, as the chip is tilted, the response lies below 1 and some local resonance around 200 Hz starts to emerge[2].

Even when comparing the responses at 159.2 Hz (i.e. the calibration frequency) for various tilting angles, one can see from Fig. 10.5 that there is some tendency, which can be properly fitted with a second order polynomial function. Thus it can be concluded, that the tilting (caused by improper alignment

[1] In Fig. 10.1 some peaks occur. The source of those peaks have not been identified, but it is assumed that combination of the sweep and single sine control strategy used could have caused it. However, at the frequency of interest (i.e. 159.2 Hz) the FRFs are smooth, i.e. the evaluation of the gain is unaffected.

[2] Note that the local resonance has shifted down from the previous value of 280 Hz to 200 Hz. This could be due to the fact that e.g. the MEMS' capsule is not present. All in all and regardless of the frequency value, the local resonance is still present and must therefore be addressed properly so as to properly calibrate the MEMS.

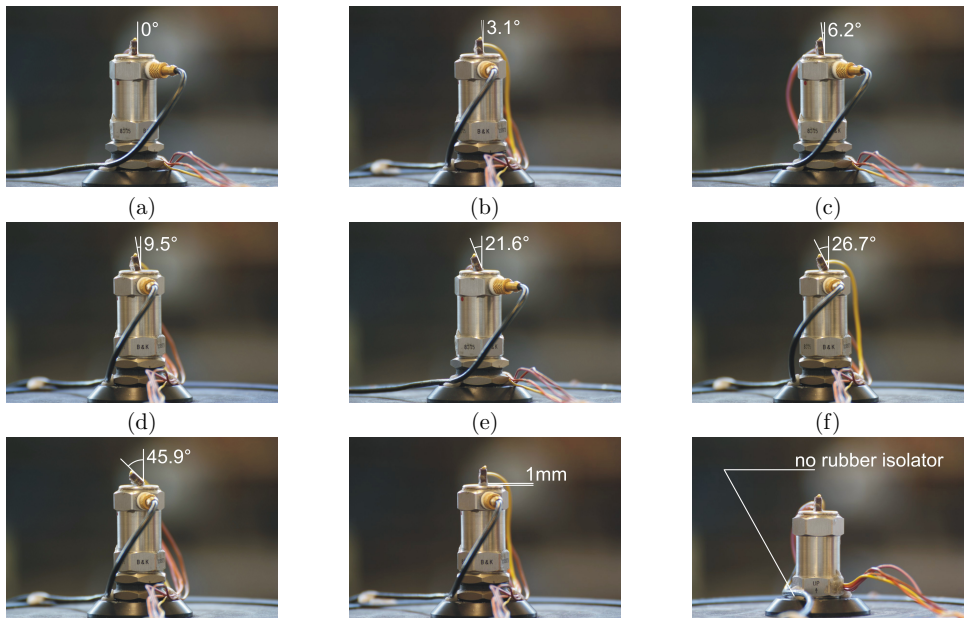

Fig. 10.3: Fixation of the naked MEMS accelerometer on a top of the reference accelerometer B&K 8305; (a) - (g) variation in tilting angle (rubber isolator present); (h) increasing the amount of beeswax (rubber isolator present); (i) removing the rubber isolator between the shaker table and reference accelerometer.

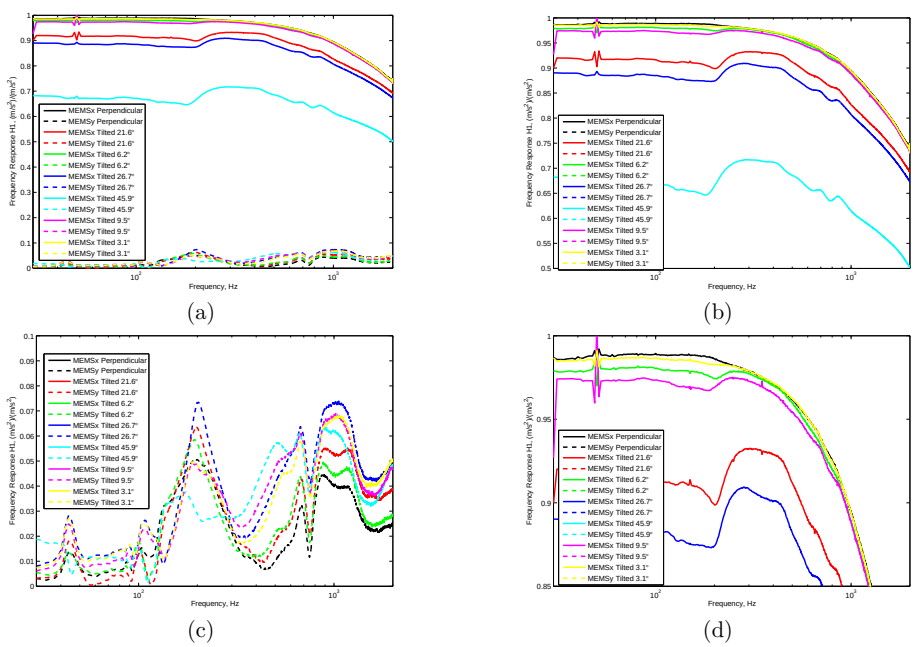

Fig. 10.4: FRFs for different tilting angles: (a) both x- and y-direction measurements; (b) zoom to x-direction measurements; (c) zoom to y-direction measurements; (d) zoom to x-direction measurements with focus on the "correct" response curve (i.e. for perpendicular, 0° tilting angle). Colour plots online.

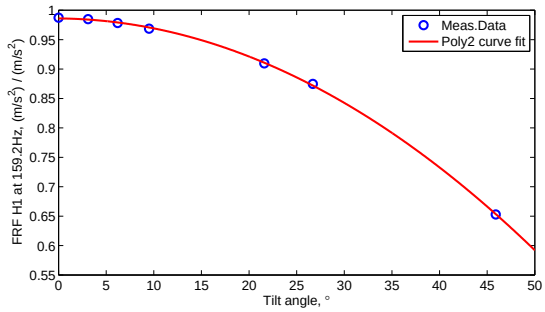

Fig. 10.5: Frequency response at 159.2 Hz (calibration frequency) for different tilting angles. The points were fitted with a second order polynomial function.

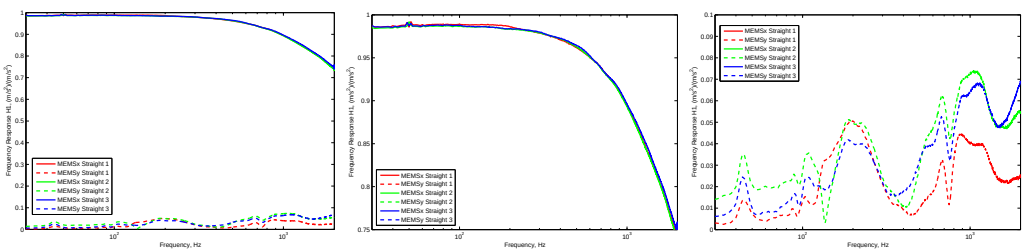

(a) (b) (c)

Fig. 10.6: Repeatability test: FRFs for the three measurements considering a straight position of MEMS accelerometer: (a) all measurements; (b) zoom to x-direction; (c) zoom to y-direction. Colour plots online.

inside of the casing) can cause the erroneous results with problematic response around 200 Hz, which was observed from the beginning of the project.

To check if the same responses could be reproduced for the straight position, the MEMS transducer was removed, re-installed and remeasured three times. As summarised in Fig. 10.6, a good reproducibility was achieved.

10.2.2 Using a rubber isolator

The influence of transversal vibration on the calibration process is discussed in (Licht and Salbøl, 2010). In there, they managed to reduce the transversal vibration of the accelerometer to be calibrated at higher frequencies (around 4 and 21 kHz) by using a mechanical filter B&K UA-0559 between the shaker and the reference accelerometer. In the investigations presented here, a different rubber isolator was found in the accelerometer set B&K 4370 and installed between the shaker and the reference accelerometer (instead of a B&K UA-0559 as they did in the previous reference), cf. Fig. 10.3.

When no isolator is used (Fig. 10.3i), some problems at 280 Hz are still present (cf. Fig. 10.7). On the other hand, using the isolator, however, the response is improved and the unwanted response around 280 Hz reduced. Hence, it seems that the use of an isolator can improve the quality of the measurements performed.

10.2.3 Influence of beeswax layer

The third parameter that was checked was the amount of beeswax applied for fixation (the wax B&K YJ-0216 was used). As presented in Fig. 10.9, the thickness of the beeswax layer does not significantly affect the FRFs. The problems around 200 Hz are not present, since the rubber isolator is used and the MEMS sensor was placed in the theoretically ideal straight position.

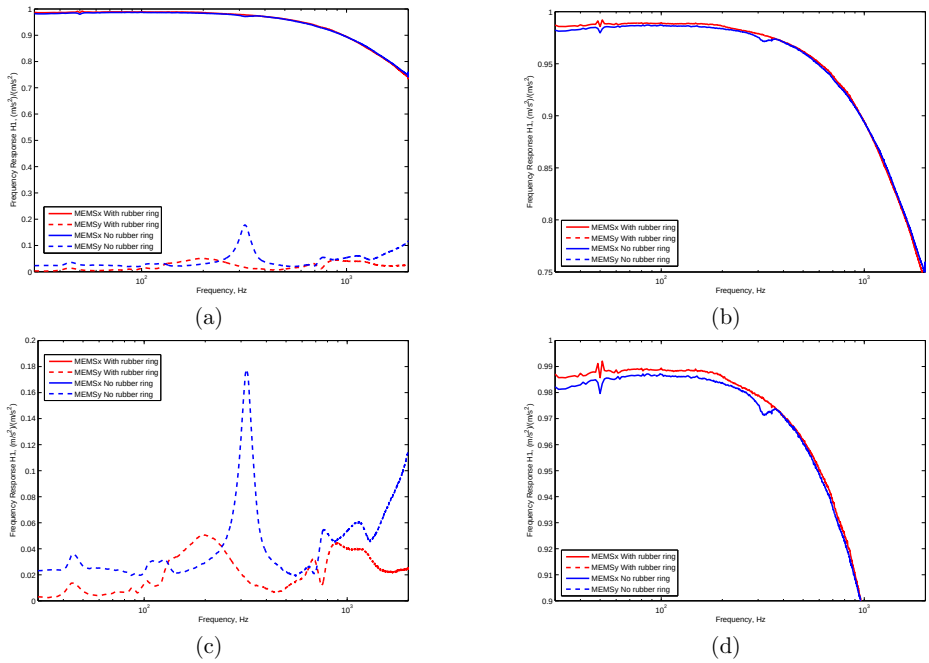

Fig. 10.7: FRFs for the cases with and without a rubber ring (Fig. 10.3a and Fig. 10.3i, respectively): (a) both x- and y-direction measurements; (b) zoom to x-direction measurements; (c) zoom to y-direction measurements; (d) zoom to x-direction measurements with focus problem on the non-smooth part of the curve around 200 Hz. Colour plots online.

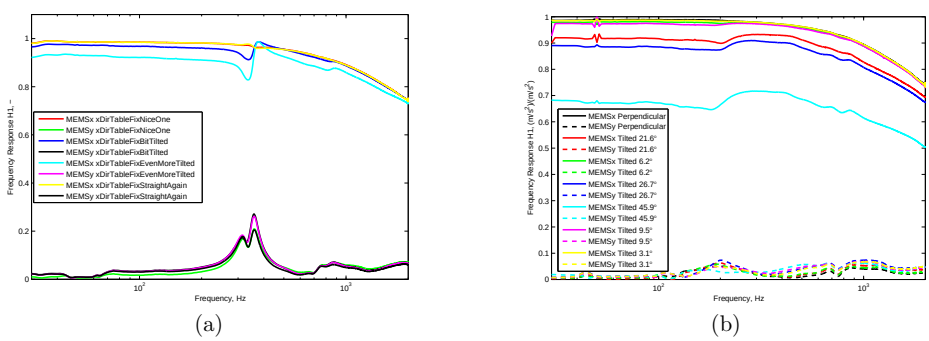

Fig. 10.8: FRFs for different tilting angles: (a) old measurements with no rubber isolator (Darula, 2013); (b) measurements with the rubber isolator used. Colour plots online.

10.3 Bandwidth settings by a capacitance value

According to the MEMS accelerometers' data sheets (Analog Devices, 2010), the bandwidth of the transducer can be controlled by the value of the capacitance used, where the limit values are 0.002 μF and 10 μF. Its exact value is then calculated from (Analog Devices, 2010):

$$F_{-3dB} = \frac{5\ \mu F}{C_{(X,Y)}} = \frac{1}{2\pi(32\ \mathrm{k\Omega}) \times C_{(X,Y)}} \tag{10.1}$$

which leads to bandwidths (at -3 dB) from 0.5 Hz to 2.5 kHz.

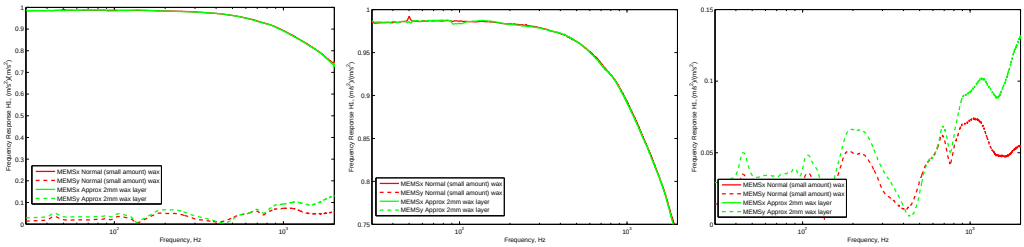

(a) (b) (c)

Fig. 10.9: FRF for the straight position of the MEMS accelerometer with "normal" (i.e. small amount) of wax layer (Fig. 10.3a) and approximately 2 mm layer wax (Fig. 10.3h): (a) all measurements; (b) zoom to x-direction; (c) zoom to y-direction. Colour plots online.

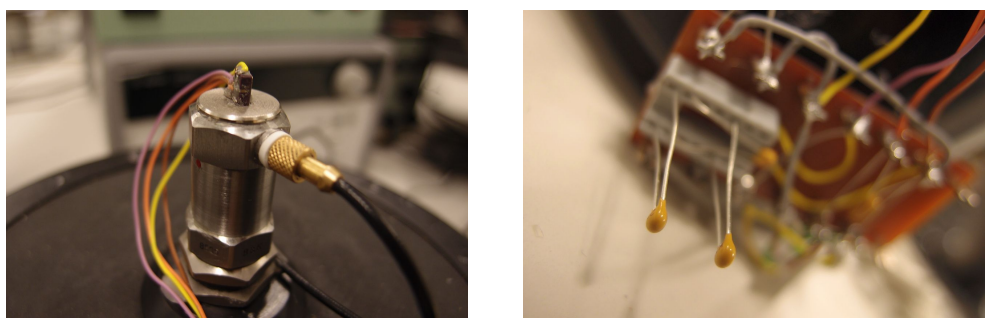

(a) (b)

Fig. 10.10: (a) A naked MEMS fixed to the reference accelerometer by means of beeswax. The reference accelerometer is isolated from the shaker using a rubber element to improve the performance at 300 Hz. (b) fixation of two additional capacitors into the compartment (all together three capacitors C_x were used at that measurement).

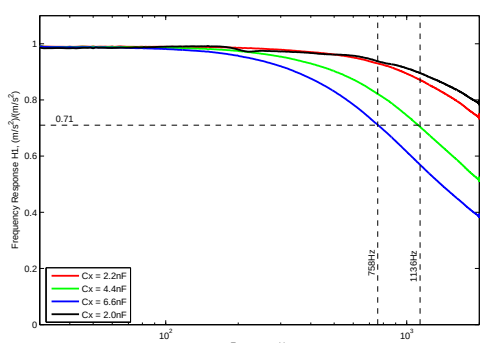

Fig. 10.11: FRFs for different values of the capacitance C_x. Colour plots online.

Table 10.2: Bandwidth values for different capacitances.

Capacitance C_x	Bandwidth
2.0 nF	2500 Hz
2.2 nF	2273 Hz
4.4 nF	1136 Hz
6.6 nF	758 Hz

To verify the latter, the MEMS transducer was fitted to the reference one (the B&K 8305) as straight as possible (following Fig. 10.10a) and equipped with a board, where the capacitance can be varied (Fig. 10.10b). The FRFs for different values of the capacitance used and their corresponding bandwidths marked are shown in Fig. 10.11, the resultant upper limits being listed in Table 10.2. As expected from Eq.(10.1), by increasing the capacitance C_x, the bandwidth is reduced. Thus, the choice of capacitance

can be effectively used to optimise the performance of the transducers. Moreover, it needs to be kept in mind that the capacitance affects the calibration curve (FRF) to an extent where the transducer can be just used within the limits governed by the $C_{(X,Y)}$ value.

On the other hand, as can be noticed from the Fig. 10.11, the change of capacitance does not influence the response in low frequencies. Thus, if that region is of interest (as it is the case for us), the choice of capacitance is not so important.

10.4 Sweep parameters

The sine sweep was assessed in Chapter 8, i.e. when the vibration controller was firstly used for tests. However, and ultimately aiming at sorting out the problem with the response around 280 Hz to obtain the correct smooth calibration curves using a naked MEMS; the potential influence of the sweep settings on the calibration results was re-tested.

Different sine-sweep types (linear and logarithmic) are here assessed comparing the autospectra measured (Fig. 10.12-10.13). As seen in Fig. 10.12, the FRFs obtained are independent of the type of sine sweep used. Furthermore, as can also be seen in Fig. 10.13, different sweep rates excite the transducer at different levels in the frequency domain. However, using the vibration controller implies that the level of the acceleration applied during the sweep is preserved constant (Fig. 10.14), i.e. 10 m/s^2 (except of some deviations caused by a sudden change of the system). Also, as proved in the previous section (and as it is shown in Fig. 8.3 as well as in Fig. 10.12), using the FRF, the frequency responses are similar. The latter means that within the levels analysed, the MEMS transducers can be treated as linear, i.e. independent of the excitation.

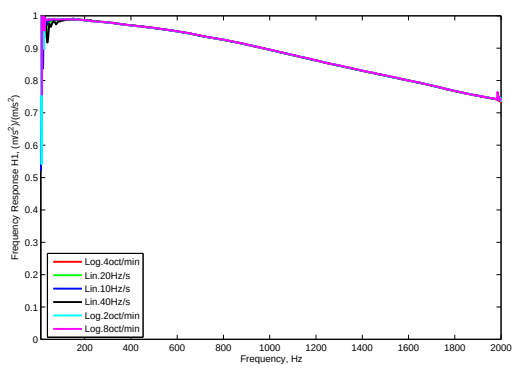

Fig. 10.12: FRFs for all types of sine sweeps compared. Colour plots online.

10.5 Conclusions

In the final set of measurements, only the inner chip with thin cables was investigated so as to eliminate the influence of the thick cable used with capsules. The assessment of the chip tilting revealed that a correct (straight) arrangement leads to the smooth FRFs, i.e. the problematic response around 280 Hz is not present. Thus, it is recommended to align the chip in the capsule as straight as possible.

Also it was observed that a rubber isolator between the reference accelerometer and the shaker helps to suppress the unwanted response around 280 Hz as well. Therefore it should be used also in further calibrations.

In this chapter, the influence of the capacitors controlling the measurement bandwidth was also assessed, the results obtained coinciding with the manufacturer's data provided. Moreover, it was shown that any of the capacitors used in the test influenced the low frequency response.

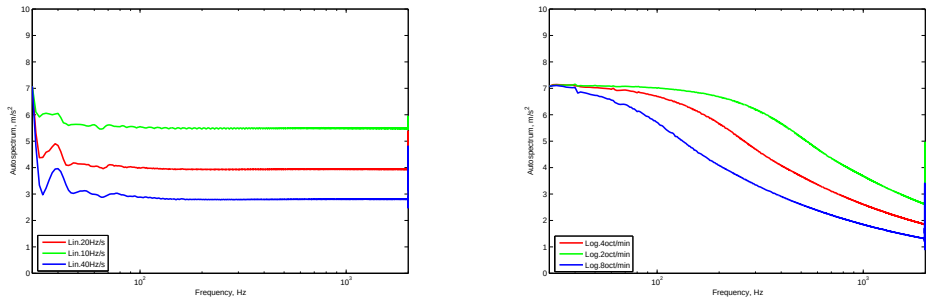

(a) (b)

Fig. 10.13: Measured autospectra for different sine sweeps (a) linear; (b) logarithmic. Colour plots online.

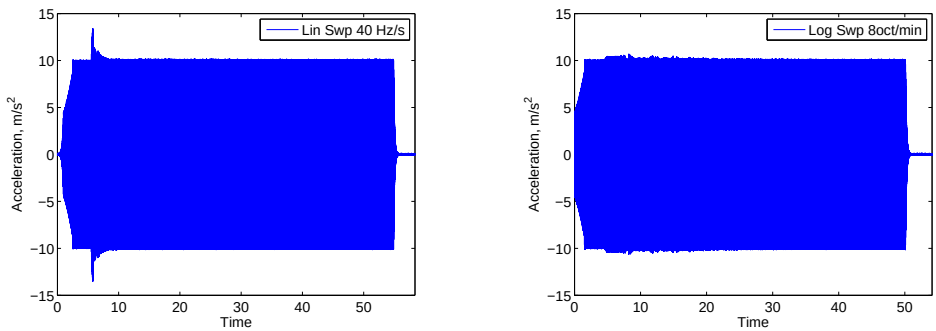

(a) (b)

Fig. 10.14: Time captures (a) linear; (b) logarithmic.

11 Conclusions

The report summarises the construction as well as calibration of MEMS-based vibration transducers. The MEMS chips are placed within the capsules together with the corresponding PCBs, capacitors and operational amplifiers. The sensitivity of the constructed transducers was assumed using the chip manufacturers' data-sheets, but also a more precise method was searched. More specifically, the latter was investigated through performing back-to-back calibration tests, using the transducer B&K 8305 as reference and several electrodynamic shakers. Firstly, a set of simple tests (using the MTS machine, and an open-loop shaker set-up) proved the feasibility of the method. Later on, using the SSR license, the excitation was more idealised (constant in the frequency domain). However, an unwanted response of the MEMS transducers around 280 Hz was observed. One of the ways to identify the problem was to substitute the SSR license with a proper feedback loop control and so to idealise the excitation even more. However, it did not solve the problems with the unwanted resonant responses. With further series of test and changing the elements in the measurement chain, it was finally found, using a set-up with a naked MEMS (i.e. no casing involved), that the alignment of the inner-chip needs to be set properly, since it strongly affects the sensitivity of the transducers. Moreover, the cables should not be too stiff to avoid transverse motion of the casing.

It was also found that the MTS method can potentially be used, since the FRFs are constant in the lower frequency region. However, it is too time consuming due to the calibration procedure being based on single frequencies, and also because of the need of performing filtering after the signals are acquired, due to the noise present. Furthermore, it can only be used (due to MTS limitations) up to 50 Hz, and the plate the accelerometers are attached to must be analysed dynamically prior to the calibration so as to avoid excitation of its modes of vibration within the frequency range analysed.

11.1 Guidelines for development of MEMS accelerometers

All in all, it was also shown that the MEMS accelerometers developed are suitable for the applications dealt with in our research (i.e. vibrations of small amplitude and up to approximately 300 Hz). This will enable acquisition of rich data as input for calibration and development of vibroacoustic computer prediction tools of wooden buildings.

However, for the accelerometers to be reliable and accurate, several aspects must be kept in mind when constructing and calibrating these transducers:

1. Initially and during their construction and mounting, special attention must be paid to the following aspects:
   - When introducing and assuring the chip into the casing, if a misalignment of the chip respect to the edges takes place, non-smooth FRFs (i.e. resonant behaviours) in the frequency range of interest for us could occur. The mounting should, hence, be as straight as possible.
   - The cables of the accelerometers should be compliant enough not to cause transversal motion of the accelerometers, which could lead to erroneous readings.
   - The MEMS chip ADXL-203 should be used with care (i.e. with lower excitation levels), due to possible signal clipping taking place. It is desired, hence, to use the ADXL-202, with lower sensitivity, to avoid those problems. If higher sensitivity is required for the problem at hand, saturation issues of the ADXL-203 should be addressed thoroughly beforehand.
2. Calibration using the MTS machine, despite of it being accurate, should be, when possible, avoided, since no calibration above 50 Hz is possible.

3. A back-to-back calibration method proved to be accurate and fairly simple to perform calibrations. The following aspects were found:
   - Use of an electrodynamic shaker (the big one B&K 4808 tried being the preferred one) together with a vibration controller (proper feedback loop control) is the recommended method to be used.
   - The shaker should preferably be placed, when measuring, on the lab floor or solid object fixed to the floor. In this manner, possible rocking motion which could be present when putting the shaker, e.g. on top of a concrete block on air cushions, is avoided.
   - Regarding the shaker excitation, a logarithmic sweep could be employed when no constant frequency step is required, since it is faster. Moreover, a rate of around 5 oct/min could be used to further speed up the process, since it was proved that it yielded the same FRFs than slower rates.
   - For fixation of the MEMS accelerometer onto the reference one (B&K 8305 behaving good to that end), it is sufficient to use a beeswax for the frequencies of interest here (i.e. up to a couple of hundred Hertz).
   - Likewise, it is recommended to use a rubber isolator between the reference transducer and the shaker to reduce potential small transversal vibrations.

The report presents the results obtained during the course of the project. However there are still fields of potential continuation, e.g.:

- Long-term stability with respect to calibration.
- Compensation of the misalignment of the chip inside of the capsule (to be able to use current transducers with some possible inherent misalignments).
- Automation or further simplification and speeding-up of the calibration procedure.

Bibliography

Analog Devices (2000). *Low-Cost ± 2g Dual-Axis Accelerometer with Duty Cycle Output.* Norwood, USA: Analog Devices.

Analog Devices (2010). *Precision ± 1.7g Single-/Dual-Axis iMEMS Accelerometer ADXL103/ADXL203.* Norwood, USA: Analog Devices.

Badri, A., J. K. Sinha, and A. Albarbar (2010). A method to calibrate the measured responses by mems accelerometers. *Strain 47*(Supplement s2), 242–257.

BIPM (2008). International vocabulary of metrology (VIM) – Basic and general concepts and associated terms.

Bishop, R. H. (2002). *The Mechatronics Handbook* (1 ed.). Boca Raton, USA: CRC Press.

Bruel & Kjær (2008). IDAe Hardware Configurations for PULSE - Types 3560-B, 3560-C, 3560-D and 3560-E. System Data. Available online: `http://www.bksv.jp/doc/bu0228.pdf` (last access: 8.12.2015).

Bruel&Kjaer (1972). *PM Vibration Exciter Type 4809. Instruction Manual.* Naerum, DK: Bruel&Kjaer.

Bruel&Kjaer (1978). *Piezoelectric Accelerometers and Vibration Preamplifiers. Theory and Application Handbook.* Naerum, DK: Bruel&Kjaer.

Bruel&Kjaer (1982). *Measuring Vibration. Primer.* Naerum, DK: Bruel&Kjaer.

Bruel&Kjaer (2015). *PULSE Electroacoustics Type 7907-S1. PULSE Basic Electroacoustics Type 7797. Product data.* Naerum, DK: Bruel&Kjaer.

Carver, R. and M. Looney (2008). Calibrate accelerometers for industrial apps. *EE Times-Asia March 16-31*, 1–4.

Darula, R. (2013). Mems calibration - check influence of tilting. report from measurements (18.3.2013). Aalborg, DK: DMME AAU.

Hopkins, C. (2007). *Sound Insulation.* Oxford, UK: Elsevier / Butterworth-Heinemann.

IEEE (1999). IEEE 1293-1998: IEEE Standard Specification Format Guide and Test Procedure for Linear, Single-Axis, Non-gyroscopic Accelerometers. The Institute of Electrical and Electronics Engineers, New York, USA. i.

IEEE (2008). IEEE 1293-1998/Cor 1-2008: IEEE Standard Specification Format Guide and Test Procedure for Linear, Single-Axis, Nongyroscopic Accelerometers Corrigendum 1: Changes to Annex K and Annex L. (Corrigendum to IEEE 1293-1998). The Institute of Electrical and Electronics Engineers, New York, USA. C1 -3.

ISO (1998). ISO 5348: Mechanical vibration and shock – Mechanical mounting of accelerometers. International Organization for Standardisation, Geneva, CH.

ISO (2003). ISO 16063-21: Methods for the calibration of vibration and shock transducers - part 21: Vibration calibration by comparison to a reference transducer. International Organization for Standardisation, Geneva, CH.

ISO (2013a). ISO 717-1: Acoustics – Rating of sound insulation in buildings and of building elements – Part 1: Airborne sound insulation. International Organization for Standardisation, Geneva, CH.

ISO (2013b). ISO 717-2: Acoustics – Rating of sound insulation in buildings and of building elements – Part 2: Impact sound insulation. International Organization for Standardisation, Geneva, CH.

Larsen, J.B. (2011). Personal communication, 2011.

Licht, T. and S. Salbøl (2010). ISO 16063-11: Uncertainities in Primary Vibration Calibration by laser Interferometry - Reference Planes and Transverse Motion. Bruel & Kjær Technical Review, No.1/2010. Naerum, DK: Bruel&Kjaer.

Ljunggren, F., C. Simmons, and K. Hagberg (2014). Correlation between sound insulation and occupants perception – proposal of alternative single number rating of impact sound. *Applied Acoustics 85*, 57 – 68.

Lyshevski, S. (2002). *MEMS and NEMS – Systems, Devices, and Structures.* CRC Press LLC.

MathWorks (2010). Matlab r2010b help.

MTS (2006). *MTS 810 & 858 Material Testing Systems.* Eden Prairie, USA: MTS SYSTEMS CORPORATION.

Negreira, J. (2013). *Vibrations in Lightweight Buildings – Perception and Prediction.* Department of Construction Sciences, Division of Engineering Acoustics, Lund University, Sweden.

Plechinger, P.L. (2011). Personal communication, november 2011.

Quach, Q. (2011). Matlab - windowing part 1. `http://blinkdagger.com/matlab/matlab-windowing-part-1/` (last access: 13.7.2011).

Randall, R. B. (2011). *Vibration-based Condition Monitoring: Industrial, Aerospace and Automotive Applications* (1 ed.). Chichester, UK: Wiley.

Sørensen, T. (2011). Personal communication.

Spectrum (2015). *SBench 6.2.12 Data Acquisition Software for Windows and Linux.* Spectrum Systementwicklung Microelectronic GmbH. Manual. Available online: `http://spectrum-instrumentation.com/sites/default/files/download/sbench6_manual_english.pdf` (last access: 10.12.2015).

Stein, G., R. Chmurny, and V. Rosik (2007). Measurement and analysis of low frequency vibration. *Measurement Science Review 7.3*(3), 47 – 50.

A
Laboratory journals

To track the whole process of the measurements reported on this technical publication, solving the partial problems and verifying how some apparatus/parameters influenced the responses of the MEMS sensors, a number of small reports (laboratory journals) were prepared, their being listed below together with a small description of their content.

Each laboratory journal related to the measurements contains a list of apparatus (with serial numbers of the items used), description of the measurement parameters envolved as well as a list of the measurements themselves, in order to be able to replicate the measurements, if ever needed.

All the journals are archived and they are available upon request at the authors.

Calibration of MEMS accelerometers (9.5.2011)
The report presents a brief literature review on MEMS calibration, lists of available apparatus which can be used for calibration and presents the preliminary measurements done at AAU on June 2nd, 2011.

MEMS Calibration (18.7.2011)
The report summarises the first results from the MEMS calibration and points out at some questionable areas, which should eventually be investigated. Calibration was executed AAU on June 29th, 2011. The additional measurements were done at AAU afterwards (1-3.7.2011).

MEMS Calibration #2 (27.7.2011)
The report presents a quick analysis of results done on the MEMS set-up until July 27th, 2011. The main attention is paid on eliminating the non-ideal behaviour of the MEMS accelerometer's response at around 280 Hz observed during the previous measurements.

MEMS Calibration #3 (2.8.2011)
The report summarises a comparison of the two shakers available at AAU and discusses linearity of the MEMS accelerometers as well as the reproducibility of the measurements performed.

MEMS Calibration #4 (30.8.2011)
Comparison of two methods; an SSR (steady state response) and sweep (rate 4 Hz/s) are presented and discussed. The reference accelerometer B&K 8503 and piezo accelerometer B&K 4331 with the pre-amplifier B&K 2635, borrowed from LU were used in the test.

Sine Sweep and Ripples (28.9.2011)
The report summarises a quick discussion on the setting of the sweep function in B&K PULSE LabShop. Especially focus is paid on ripple phenomena observed when the shaker was run immediately after one run was terminated.

Add-on Measurements / Calibrations (23.2.2012)
A discussion on add-on measurements for the MEMS calibration is summarised.

MEMS calibration with Bruel&Kjaer PULSE and Bruel&Kjaer VC-LAN (22.1.2013)
Test the MEMS calibration using a constant amplitude at sine sweep excitation. To that end, the shaker control strategy using the vibration controller B&K VC-LAN. To make more advance signal processing of the transducer signals, they are recorded and processed in B&K PULSE (LabShop v17 was used).

MEMS calibration – Big shaker (7.3.2013)
The aim of the measurements was to do additional MEMS calibration using a bigger shaker(s) and thus avoid possible rocking motion of the shaker's table. During the measurements, also piezo accelerometers were used in order to compare directly the responses of the MEMS and piezos.

MEMS calibration – Check influence of tilting (18.3.2013)
The aim of the quick check was to find if also "naked" MEMS accelerometers have a response in the non-directly excited direction with a peak around 300 Hz. It was observed that the tilting around the non-excited axis introduces some non-smooth behaviour.

MEMS calibration – Sine Sweep Test (24.3.2013)
The aim of the measurements performed was to compare different sine sweep rates as well as single frequency excitation to prove that the chosen 4 oct/min is safe and that no transients occur.

MEMS calibration – Check the Gain evaluation (1.4.2013)
The main aim was to check if the FRF H1 can be used to extract the calibration constant at 159.2 Hz. The "real" calibration in PULSE LabShop is done first, and then also using a controller sweep and a pure sine excitation to double check the procedure. Moreover, three different FRF estimates (H1, H2 and H3) are compared.

MEMS calibration – Check the influence of tilting and modify the shaker fixation (13.4.2013)
The main purpose of the measurements carried out was to see the behaviour of the FRF curves for different tilting angles of the naked MEMS accelerometer. Furthermore, a rubber isolator was used to improve contact between the shaker and the reference accelerometer, similarly as it was done in B&K Tech.Rev. (Licht and Salbøl, 2010) using mechanical filters (B&K UA-0559). A comparison of the case with and without the isolator is provided as well.

MEMS calibration – Bandwidth and Sine Sweep Test (17.4.2013)
Measurements performed so as to test the capacitance C_X (used to set the bandwidth of the x-direction measured signal). Also, the linear and logarithmic sweep rates are compared from autospectra plots.

B

MATLAB GUI for data comparison

To speed up comparisons of the measured data and easily generate figures for the reports, a graphical user interface (GUI) function was created in MATLAB. Its main window is shown in Fig. B.1.

B.1 Features

- The main feature of the GUI is to load data and to sort them into a table on the left. There is an option to load the "MAT data" (stored under `\auxFiles\MathDataFile.mat`), or the PULSE ASCII files stored under `\data`.
- To identify the measurement number, additional information is loaded from the PULSE ASCII file and listed into the table (using the bottom slider under the table, additional information can be accessed).
- From the left table, the measurements can be plotted and compared with one another.
- To tweak the legend, it is allowed to change the name of the measurement, by just clicking the field in the table. The same holds for the transducer, channel name as well as for the type of analyser.
- In the bottom left, it is allowed to choose what will be listed in the legend (transducer, channel name, analyser and/or name of the measurement).
- Also the plot ranges and plot scales (linear/logarithmic) can be adjusted to get the best visualisation.
- If a specific data are to be plotted all, the "plot all" box can be ticked.
- Choosing the top menu `File` one can reset the plots (un-tick all ticked plots), re-load data (re-set all the names), or close the GUI.
- Choosing the top menu `Evaluate->Calib.constant`, a window with calibration constants evaluated at 159.2 Hz for all chosen (plotted) measurements appears (Fig. B.1b).
- Choosing the top menu `Export->Export Fig`, the window for figure export appears (Fig. B.1c).

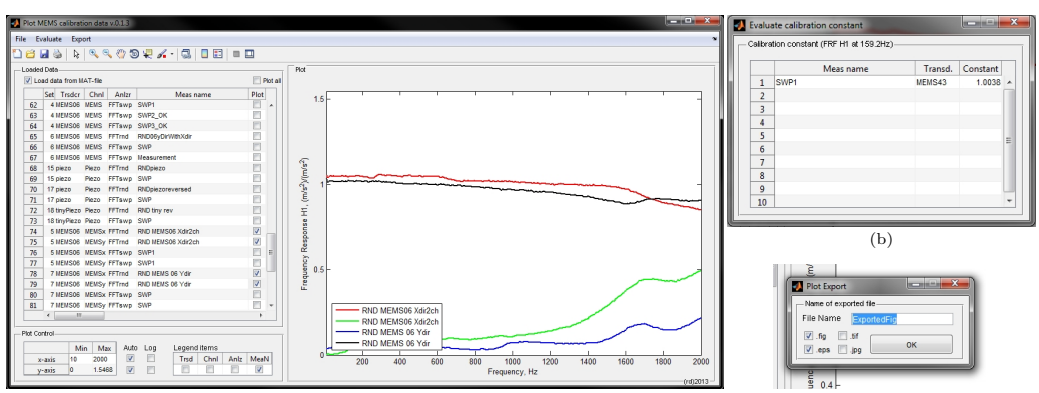

(a) (b) (c)

Fig. B.1: MATLAB GUI v.0.1.3: (a) overview on the main window; (b) window with evaluation of the calibration constant; (c) export window.

One can choose what type is to be saved (.fig, .eps, .jpg, .tif) and the name can be changed as well. The figures are saved by default to the folder `\figs`.

B.2 Restrictions

- Due to the loading of the PULSE ASCII file and using the B&K file `GetPulseAsciiFile.dll` to process them, the 32-bit version of MATLAB needs to be used. At this stage, no .uff file support has been added.
- No double y-axis feature has been implemented yet. The latter means that only one physical quantity can be compared, either FRFs or Autospectra, not FRF with Autospectra.
- No size of the exported plot can be defined yet, just a fixed default one is used.